PROTEIN-BASED NANOPARTICLES FOR DRUG DELIVERY APPLICATIONS

JOHANNES GUTENBERG UNIVERSITÄT MAINZ

DISSERTATION

zur Erlangung des akademischen Grades
„Doktor der Naturwissenschaften“
im Promotionsfach Chemie
am Fachbereich Chemie, Pharmazie und Geowissenschaften
der Johannes Gutenberg-Universität in Mainz

Eingereicht von
Lars Matthias Fach, Master of Science
geboren in Groß-Gerau / Deutschland
Mainz, 2016

– D77 –

Mainzer Dissertation

Dekan:	not available in electronical version
Erstgutachter:	not available in electronical version
Zweitgutachter:	not available in electronical version
Tag der Einreichung:	28. November 2016
Tag der Mündlichen Prüfung:	20. Dezember 2016

DANKSAGUNG

not available in electronical version

EIDESSTATTLICHE VERSICHERUNG

Hiermit erkläre ich an Eides statt, dass ich die vorliegende Dissertationsschrift selbstständig und nur mit den angegebenen Hilfsmitteln ausgeführt habe. Diese Dissertation wurde noch nicht als Prüfungsarbeit für eine andere Prüfung eingereicht. Zudem wurden bisher weder die gleiche, noch Teile der Abhandlung als Dissertation bei einer anderen Fakultät oder einem anderen Fachbereich eingereicht.

Mainz, …… ……

L. Matthias Fach

ZUSAMMENFASSUNG

Für das Jahr 2030 wird von der Weltgesundheitsorganisation ein Anstieg der Anzahl neuer Krebserkrankungen auf 21.7 Millionen erwartet. Bereits heute wird jeder siebte Tod durch Krebs verursacht. Nanopartikel die in ihrer Größe und Form biologischen Nanostrukturen gleichen haben bereits viel versprechende Ergebnisse als Wirkstofftransporter in der Tumortherapie gezeigt. Sie erhöhen die Löslichkeit sowie die Bioverfügbarkeit von Wirkstoffen und verringern zudem Nebenwirkungen, die häufig während der Chemotherapie auftreten, da sie sich durch eine erhöhte Permeabilität und Retention im Tumorgewebe anlagern. Proteine sind eine wertvolle Quelle hoch definierter Biomaterialien für die Nanopartikelherstellung da sie eine geringe Toxizität und hohe Bioabbaubarkeit aufweisen.

In dieser Arbeit wird ein neuartiges Konzept für die Herstellung von Nanopartikeln gezeigt, das auf der Anlagerung oberflächenmodifizierter Proteine basiert, nachdem diese in organische Lösungsmittel überführt wurden. Für hydrophobe Wirkstoffe wird hierbei eine Öl-in-Wasser Nanoemulsionstechnik verwendet die keine zusätzlichen Denaturierungs- oder Quervernetzungsschritte für die Stabilisierung der Partikel benötigt. Der notwendige Wechsel des Löslichkeitsverhaltens wird dabei durch eine hohe PEGylierung der Oberfläche hervorgerufen bei der die natürliche Struktur der Proteine erhalten bleibt. Diese Methode wird zunächst anhand des Modellproteins Lysozym und dem Krebswirkstoff Doxorubicin detailliert gezeigt. Im Anschluss an eine umfassende Untersuchung der erhaltenen Protein-Polymerkonjugate wurden leere und Doxorubicin beladene Nanopartikel mit einer Größe von etwa 100 nm hergestellt, die noch immer eine enzymatische Aktivität des natürlichen Proteins aufweisen. Die Partikel sind in physiologischen Puffersystemen stabil und eine Freisetzung des Wirkstoffes ist erst nach einer zeitabhängigen Zellaufnahme zu beobachten. Daraufhin werden Proteine mit einer großen Spannweite an Molekulargewichten als Ausgangsmaterial verwendet, um zu zeigen, dass diese Methode das Potential besitzt auf jedes Protein der Wahl übertragen zu werden. Durch den Einschluss von Curcumin wird zudem der hydrophobe Wirkstoff variiert und Partikel einer Größe unterhalb von 200 nm hergestellt. Des Weiteren wird eine Wasser-in-Öl-in-Wasser Nanoemulsionstechnik gezeigt, mit der Partikel mit eingeschlossenem hydrophilem Wirkstoff hergestellt werden können. Dies zeigt, dass dieses System ein hohes Potential für den Transport von hydrophilen Wirkstoffen, wie z.B. Nucleinsäuren aufweist.

ABSTRACT

By the year 2030, the World Health Organization expects the total number of new cancer cases will grow to 21.7 million worldwide. Today, almost every seventh death is caused by cancer. Nanocarriers are very similar in size and shape to biological nanostructures and have already shown very promising results for drug delivery in cancer therapy. They increase drug solubility as well as bioavailability and reduce toxic side effects that often occur during chemotherapy as they selectively accumulate in the tumor tissue by an enhanced permeability and retention effect. Proteins show low toxicity and high biodegradability. Therefore, they can be a valuable source for highly defined biomaterials for the preparation of nanocarriers.

In this work, a novel method for the preparation of nanoparticles based on the assembly of surface modified proteins that are soluble in organic solvents is presented. Particle preparation for hydrophobic payloads is carried out by an oil-in-water nanoemulsion technique without the need of additional cross-linking steps or denaturation for stabilization. The necessary lipophilic switch of the protein material is obtained by high surface PEGylation whilst preserving the native structure of the proteins. This system is first presented in detail for lysozyme, as model protein and doxorubicin as hydrophobic model drug. After a comprehensive analysis of the obtained protein-polymer conjugate, empty and doxorubicin-loaded nanoparticles are prepared with a diameter around 100 nm that still present the enzymatic activity of the native protein. The particles are stable in physiological buffers and a release of the therapeutic payload into cancer cells is only observed after a time dependent cellular uptake.

Later, proteins in a broad range of molecular weights are used as starting material to exemplify that this preparation procedure has the potential to be transferred to any protein of choice. Here, also the influence of the polymer chain length on the solubility in organic solvents for the different protein sizes is presented. Additionally, the hydrophobic payload of the particles is exchanged by curcumin to present the high variability of this carrier system leading to particles with diameters below 200 nm.

Furthermore, a water-in-oil-in-water nanoemulsion technique is used to prepare protein-based nanoparticles with an entrapped hydrophilic payload. This shows that the presented nanocarrier system has also high potential for the delivery of hydrophilic payloads, e.g. nucleic acids.

TABLE OF CONTENTS

1 INTRODUCTION

In 2016, almost every sevenths death worldwide is caused by cancer. This means, cancer causes more deaths than AIDS, tuberculosis and malaria combined.[1] Overweight, obesity, smoking, physical inactivity, and poor nutrition – about one out of four to five cases of cancer in developed countries is caused by an unhealthy lifestyle. For the year 2012, the International Agency for Research on Cancer reported 14.1 million new cancer cases worldwide, of which 6.1 million occurred in economically developed countries, which contain only approx. 18% of the world's population. The corresponding estimates for total deaths caused by cancer are 8.2 million (approx. 2.9 million in developed countries). By the year 2030 this amount is expected to grow to 21.7 million for new cancer cases and 13 million for cancer deaths. This is mainly reasoned by the aging of the population and its increasing life expectancy but also adopting the lifestyle of developed countries by developing countries.[2] Despite therapies of some cancer types already show high five-year net survival rates (e.g. 85% for female breast cancer in Germany) others are rarely cured (e.g. 14% of patients with liver cancer in Germany).[3] Besides surgical operations, current cancer therapies are based on radiation or chemotherapeutics. A major drawback in cancer therapy is the poor solubility and chemical stability of many potential anti-cancer drugs. This heavily limits the bioavailability of the compound and additionally might impede the development of novel anti-cancer agents as they fail in early state drug screenings.[4] Additionally, the administration of small molecules increases the risk of toxic side effects in the body. For example paclitaxel, an anti-cancer drug that is used very successfully in the treatment of several types of cancer (e.g. ovarian, skin, esophageal and lung) shows a very poor solubility in water. For clinical application this drug is most commonly dissolved in ethanol (Taxol®) and administrated together with polyoxyethylated castor oil (Cremophor EL) as solvent. Especially the co-administration leads to toxic side effects including hypersensitivity that additionally require the administration of steroids and anti-histamines.[5, 6] But also highly soluble anti-cancer drugs lead to unwanted toxic side effects. Doxorubicin represents a highly potent anti-cancer drug in the class of anthracyclines. These are known to address a broad number of cancer types like acute leukemia, breast, or lung cancer.[7] This drug is highly water soluble as hydrochloride salt but shows a very unspecific cellular uptake by passive diffusion. This results in serious side effects like hematologic and cardiac toxicity as the drug is also accumulated in healthy tissues.[8]

1.1 Nanocarriers in Cancer Therapy

The entrapment of drugs into nano-dimensional carriers has the potential to meet the two main requirements for a successful cancer treatment – preventing the drug from degradation on one hand and preserving the healthy tissue from the drug on the other. Among several applications of nanoparticles in different areas, drug delivery is one of the most advanced.[9] This is mainly driven by the success of polymeric and liposome-based drug delivery systems of that many are used in daily clinical practice (see Table 1). According to the number of clinical trials registered at the database 'clinicaltrials.gov', a total number of 2157 nanomedicine formulations had been registered for clinical trials by October 2016 (search terms: 'liposome', 'nanoparticle' and 'micelle').[10] Hereof, 1793 are placed in the field of cancer therapy. Despite many of these trials focus on new applications or combinations of already marked products like liposomal doxorubicin or albumin bound paclitaxel with other anti-cancer agents. These numbers represent the upcoming interest in nanomedicine nowadays.

Table 1. Nanoparticles-based therapeutics that are currently approved for clinical cancer treatment.

Trade Name	Type of Nanocarrier	Drug	Application
Abraxane®	albumin-bound nanoparticle	paclitaxel	metastatic breast cancer[11]
Caelyx®	PEGylated liposome	doxorubicin	metastatic breast and ovarian cancer, Kaposi sarcoma[12]
DaunoXome®	liposome	daunorubicin	Kaposi sarcoma[13]
DepoCyt®	liposome	cytarabine	lymphoma[14]
Doxil®	liposome	doxorubicin	Kaposi sarcoma[15]
Genexol-PM®	polymeric micelle	paclitaxel	lymphoblastic leukemia[16]
Marquibo®	liposome	vincristine sulfate	metastatic breast cancer[17]
Myocet®	liposome	doxorubicin	acute lymphoblastic leukemia[18]
Oncaspar®	PEGylated aspariginase	aspariginase	acute lymphoblastic leukemia[19]
Zinostatin stimalamer®	poly(styrene-co-maleic-acid)-conjugated neocarzinostatin	neocarzinostatin	hepatocellular carcinoma[20]

1.1.1 Types of Nanocarriers

Nanocarrier in modern medicine can be obtained from various materials (Figure 1). A general distinction can be made between inorganic- and organic-based nanoparticles. Inorganic particles are often used for imaging techniques like optical imaging or magnet resonance imaging, whereas organic-based nanocarriers are often used for drug delivery applications. The group of organic particles can be further divided in the two major groups of lipid-based and polymer-based nanoparticles. Here, the class of polymer-based nanoparticles includes synthetic as well as natural polymers.

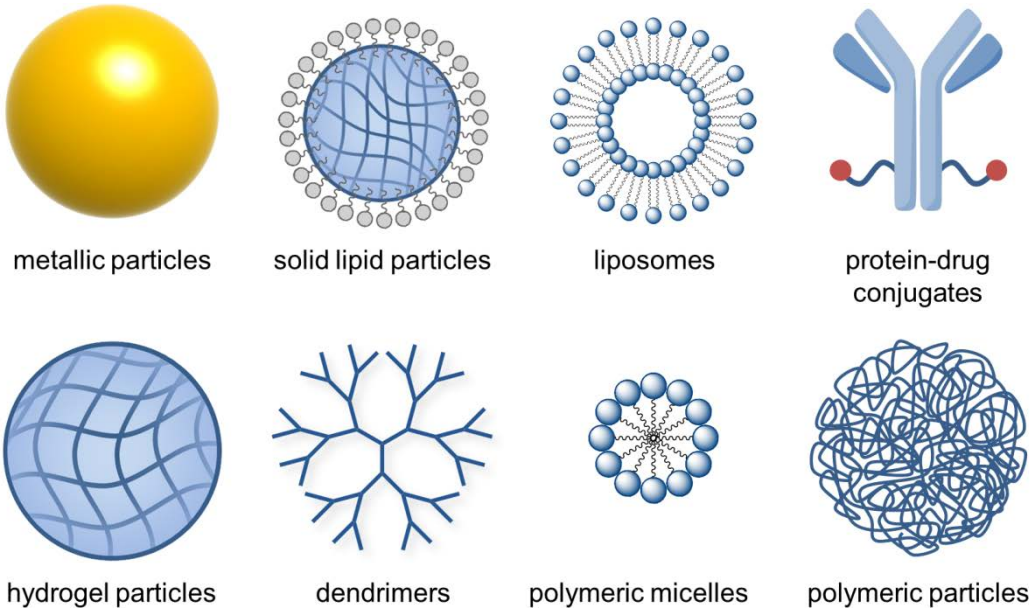

Figure 1. Nanocarrier systems used in medicinal applications and research. Redrawn from Sun *et al.*[21]

Nanocarriers are defined as colloidal particles ranging in their size from 1 to 1000 nm.[22, 23] Figure 2 shows the different sizes used in nano-research by the example of polymeric and lipid-based nanocarriers. Drug-polymer conjugates are considered as nanoparticles because of their size in the lower nanometer range. They often consist of pharmaceutically active drugs, linked to targeted antibodies, peptides or polymers.[24, 25] These conjugates are typically in the size range of 5–20 nm. Here the conjugation of the drug to a polymer leads to a change in the pharmacokinetics of the drug mainly by an increase in circulation time.

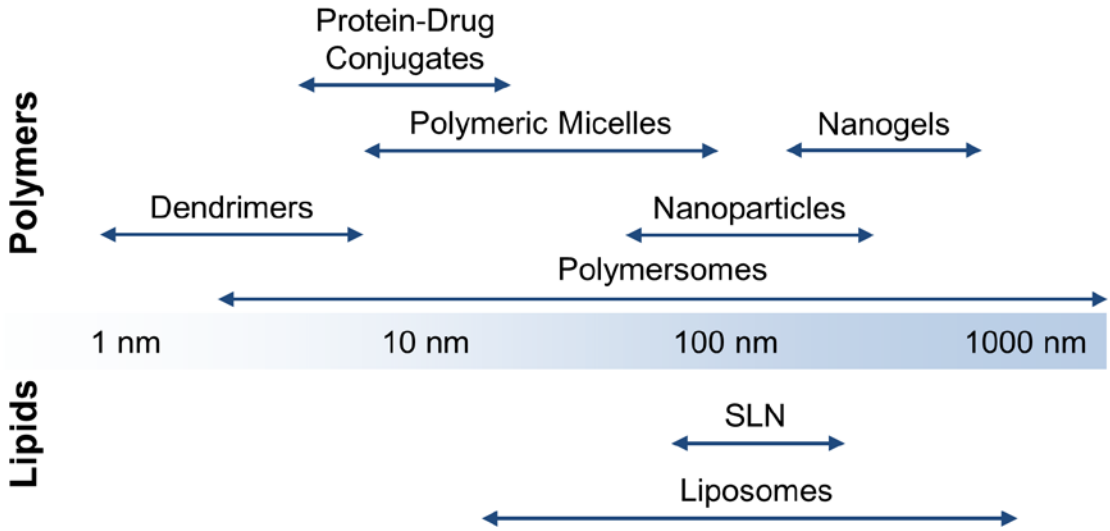

Figure 2. Overview on the size distribution of lipid and polymer-based nanocarries systems used for drug delivery applications. Redrawn from Nicolas *et al.*[22]

Currently, many of these drug-polymer conjugates show promising results in clinical trials but none of them has made it to clinical approval so far.[9, 24, 26] Among the clinically approved nanocarrier systems more than the half is based on lipid nanocarriers (Table 1). Here, the most investigated systems are the liposomal formulation and solid lipid nanoparticles (SLN). PEGylated liposomes for the delivery of doxorubicin (Doxil®) were the first nanoparticular system being approved by the US Food and Drug Administration (FDA) in 1995.[15, 27] So far, five more lipid-based nanocarrier systems are approved for the clinical use. None of these liposomal systems is targeted for the improvement of cellular uptake, but all of them are reported to prolong the half-life of their therapeutic payload and improve their toxicity profile.

With Abraxane®, only one protein based nanocarrier system has made its way from bench to bedside until now. Here, the anti-cancer drug paclitaxel is bound to albumin in a high pressure emulsification procedure.[28, 29] By this method, the solubility of the drug is increased and the use of the castor oil for co- administration can be avoided. After application of Abraxane® into the blood stream, the particles disassemble into the single albumins carrying the anti-cancer drug. Paclitaxel is non-covalently bound to the hydrophobic surface patches of albumin. By this, the protein mediates transcytosis as the protein addresses the gp60 receptor on the endothelium and thereby enhances the uptake of the associated drug.

1.1.2 Biodistribution

Why are nanocarriers so interesting for tumor therapy? The answer is given by their special biodistribution. First noticed by Maeda *et al.*, the enhanced permeability and retention (EPR) effect is the main reason for passive accumulation of nanocarrier systems in tumor tissues.[30] By further providing experimental data, Matsumura and Maeda substantiated a concept of tumor targeting for the first time.[31] The penetration of healthy tissue is normally limited to the size below 1–2 nm.[32-34] In contrast, solid tumors are surrounded by angiogenic blood vessels with abnormally large vascular openings in the size of 100 to 800 nm and impaired lymphatic drainage, depending on tumor type and stage.[30, 35, 36] Particles smaller than this size can extravasate from the blood stream into the tumor interstitium (Figure 3). Tests with liposomes have shown that a typical cut off size for extravasation was around 400 nm.[37] The best results were obtained from particles below a size of 200 nm. For this reason nanocarriers in therapeutic approaches are typically in the size range from 10 to 200 nm.[35, 38-40] Therefore, the targeting properties of macromolecular drugs and nanocarriers are enhanced over small molecules. Additionally, the selectivity of tumor tissue over healthy tissues is increased.

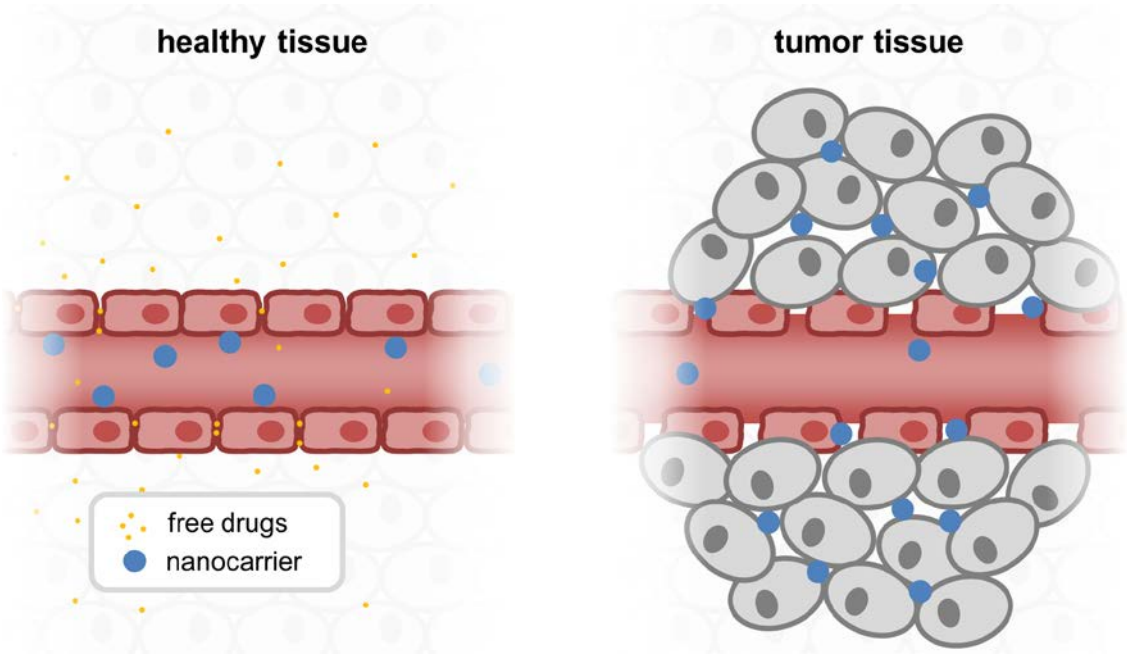

Figure 3. Passive targeting of nanoparticles towards the tumor tissue. Small molecular drugs can penetrate healthy tissues, whereas nanocarriers are too large to exit the blood stream (left). Nanocarriers benefit from the expanded vascular openings and accumulate in tumor tissues (right). Redrawn from Noble *et al.* and Gullotti *et al.*[41, 42]

1.1.3 Cellular Uptake

Before a nanocarrier system can be further investigated in animal studies or clinical trials, the uptake and the effects on a cellular level need to be investigated. When a nanocarrier encounters a cell it will be internalized via endocytosis. After the uptake, the carrier will be transferred into various organelles, like or endosomes. Endocytosis can be mediated by either binding between a ligand on the carrier surface with a receptor on the cell surface or by nonselective binding to the cell membrane by hydrophobic or electrostatic interactions. The five major internalization pathways have been identified, depending on the size and surface properties of the nanocarrier.[43-45] An overview of these internalization pathways is presented in Figure 4.

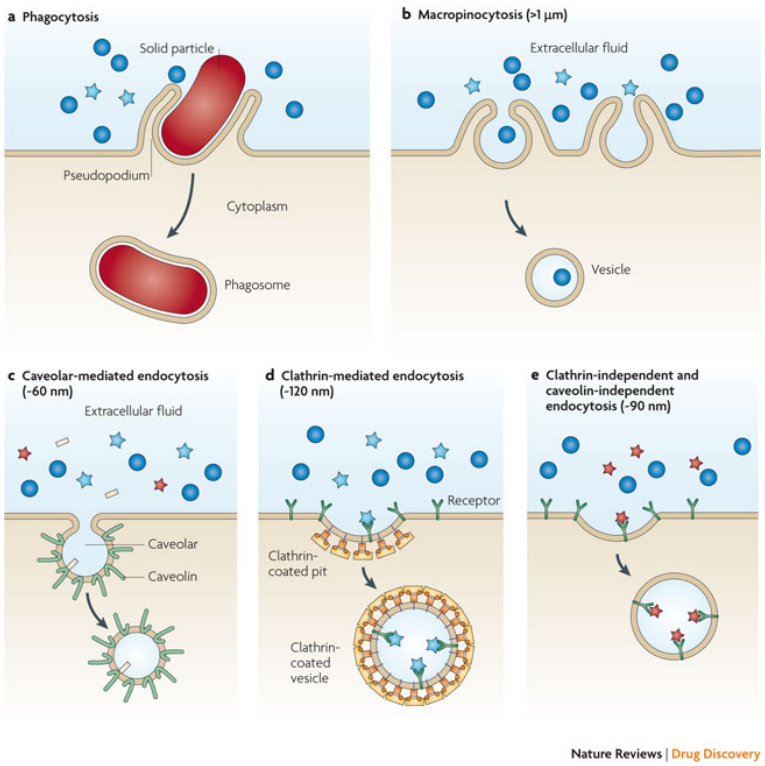

Figure 4. Internalization of large particles is facilitated by phagocytosis (a). Nonspecific internalization of smaller particles (>1 μm) can occur through macropinocytosis (b). Smaller nanoparticles can be internalized through several pathways, including caveolar-mediated endocytosis (c), clathrin-mediated endocytosis (d) and clathrin-independent and caveolin-independent endocytosis (e), with each being subject to slightly different size constraints. Nanoparticles are represented by blue circles (> 1 μm), blue stars (about 120 nm), red stars (about 90 nm) and yellow rods (about 60 nm). Reprinted by permission from Macmillan Publishers Ltd: Nature Reviews Drug Discovery Petros *et al.*,[39] copyright 2010.

Clathrin-mediated endocytosis is driven by vesicles with a coating made up of proteins that are associated with the cytosolic protein clathrin. These clathrin-coated pits can locate various extracellular receptors like antibodies that are responsible for receptor-mediated endocytosis. In caveolae-mediated endocytoses extracellular molecules and particles are internalized after binding to specific receptors in the caveolae. These are 50–100 nm sized invaginations of the plasma membrane that are present in many but not all cell types. Pinocytosis is also described as cell drinking. This internalization process starts with the formation of an invagination of the cell membrane. These pockets are detached from the membrane and form small vesicles with diameters ranging from 0.5 to 5 μm. These vesicles, filled with extracellular fluid, later fuse with lysosomes. In phagocytosis, the cell binds actively to particles with a diameter larger than 250 nm. This includes cell debris, microorganisms like bacteria and apoptotic cells. In comparison to clathrin- and caveolae-mediated endocytosis, in pinocytosis and phagocytosis much larger areas of the surface of the cellular membrane are involved. In contrast to phagocytosis, that is only occurring in specialized mammalian cells like macrophages or monocytes, pinocytosis takes place in all cell types.[46] From this, it can be concluded that large particles depend on phagocytosis and pinocytosis for internalization whereas smaller particles are taken up by clathrin- and caveolae-mediated endocytosis.

1.1.4 Drugs in Nanomedicine

Many hydrophobic drugs are currently used for cancer treatment.[9, 47] As presented in Table 1, many different drugs are also used in nanocarrier systems.The drugs paclitaxel and vincristine inhibit normal breakdown of microtubules during cell division of tumor cells. [11, 16, 17] Cytarabine, neocarzinostatin, daunomycin, and doxorubicin cause a different mechanism of action. Here, the drugs interact with the cellular DNA inducing cell death. [12-15, 18, 20, 47] Besides, many other drugs are currently under investigation for clinical applications in nanocarrier systems.[48] In this section, two different hydrophobic drugs that are frequently used in nanocarrier research are presented in detail. The well-established anti-cancer drug doxorubicin and the promising therapeutic agent curcumin.[49, 50]

Doxorubicin (DOX) is broadly used as hydrophobic model drug in nanocarrier research and represents the family of anthracyclines.[7] The red-colored antibiotic is produced from the bacteria *streptomyces peucetius* and structurally similar to the natural product daunomycine.[49] The

drug is regularly used in chemotherapy and listed on the WHO list of essential medicines, that presents the most important medications in the basic health system.[51] The therapeutic effect of DOX is mainly caused by intercalation in the DNA causing breakage of double strands and inhibition of macromolecular biosynthesis.[49, 52, 53] The occurrence of toxic side effects – especially regarding the cardiac system – is the main drawback in medication with DOX. Three liposomal formulations of doxorubicin Caelyx®, Doxil®, and Myocet® are already approved by the FDA for the treatment of metastatic breast and ovarian cancer, Kaposi sarcoma and acute lymphoblastic leukemia (see Table 1).

Curcumin (CUR) is a yellow crystalline drug isolated from the rhizome of turmeric (*curcuma longa*). Tumeric has been used as spice and coloring agent but also as therapeutic agent in Asia for centuries. For this reason, curcumin has been recently an emerging interest in pharmaceutical science.[54] Curcumin has been found to possess antibacterial, antiprotozoan, antiviral, hypolipemic, hypoglycemic, anti-coagulant, anti-oxidant, anti-tumour and anti-carcinogenic effects.[54] It suppresses symptoms associated with Alzheimer's disease, type II diabetes, rheumatoid arthritis and multiple sclerosis.[55] Additionally, curcumin blocks transformation, proliferation and invasion of tumor cells.[55] Animal studies have shown, that curcumin has chemopreventative activity against a broad variety of tumors.[56] It also suppresses the activation of transcription factors that are implicated in carcinogenesis.[57] However, the potential of curcumin in therapeutic applications is limited by its low oral bioavailability, poor solubility in aqueous media and rapid degradation at physiological pH.[58, 59] Entrapment of curcumin in nanoparticles has been shown to overcome some of the drawbacks of curcumin-based therapeutic approaches.[60, 61]

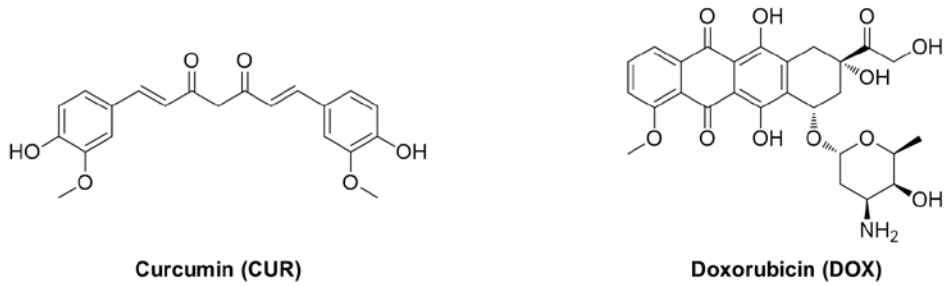

Figure 5. Chemical structures of the potential anti-cancer drug curcumin (CUR) and the clinically established drug doxorubicin (DOX).

1.1.5 Drug Release

After reaching the targeted tissue and the cellular uptake, the entrapped payload needs to be released from the nanocarriers (to become therapeutically active). Nanocarriers mainly release their payload by two different mechanisms (Figure 6). In a diffusion controlled release, the drug is evenly distributed in a matrix of water insoluble polymers like polyurethane or poly(methyl methacrylate) (PMMA).[21] In this process drug molecules need to diffuse through the particle matrix for a release in the tissue. Mathematical modeling has presented that this is a main drawback as the number of available drug molecules decreases with increased particle sizes.[62] Particular systems that rely on this mechanism often show only weak release of the drug. For example, a particular system of polyurethane showed a release of doxorubicin of only 40% of the encapsulated drug within 6 days.[63]

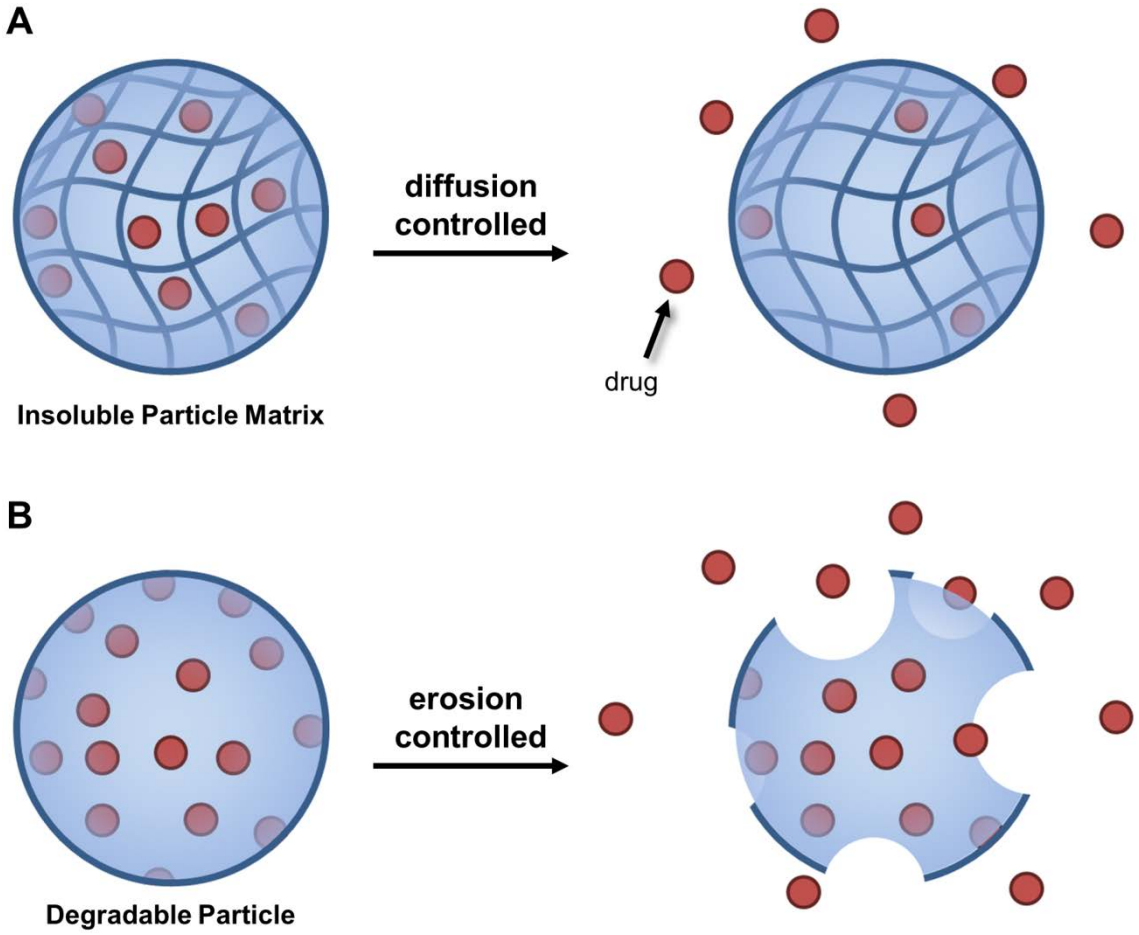

Figure 6. Different methods of drug release from nanocarriers. The release from insoluble particles is controlled by diffusion (A). Degradation of the particle material leads to an erosion controlled drug release.

Nanocarriers prepared from degradable materials show a more effective way of drug release. Disruption of the particle into smaller parts enhances the release of encapsulated drugs. Additionally the particle material can easily cleared from the body after successful drug release.[64] A various number of polymers have been used for the preparation of erodible nanoparticles. Synthetic polymers can be fine-tuned to benefit from the degradation mechanisms present in the human body (e.g. a reductive or acidic environment or proteins like esterases and proteases).

The stabilization of micellar structures with cross-linking agents bearing a disulfide bond has been reported to cause disruption of the micelles when exposed to a reductive environment, as present in the cytosols of cells.[65] The ester bonds of poly(lactid acid) (PLA), poly(glycolic acid) (PGA) and poly(lactic-*co*-glycolic acid) (PLGA) can be cleaved through the hydrolytic action of esterases. The degradation products, lactid or glycolic acid can be easily metabolized by the body.[66] The group of Fréchet established a dextran based nanocarrier system where the particle material consists of acetalated dextran. By acetalation, the polysaccharide becomes water insoluble and stable particles can be formed. After lowering the pH of the surrounding environment, e.g. after cellular uptake in lysosomes, the acetals are cleaved and the water soluble dextran is retained. By this the carrier is degraded and thereby releases encapsulated drugs.[67-70] Proteins as biodegradable nanoparticle material are a promising material for the preparation of degradable nanoparticles. Intramolecular disulfide bonds can be cleaved under reductive conditions and additionally proteases lead to a degradation of the protein after a cellular uptake. These mechanisms are regarded as beneficial for an enhanced release of drugs from a nanocarrier.[71]

1.2 Protein-based Nanocarrier

Nanocarriers based on polymers provide a high diversity in their design as various polymers can be easily chemically modified making them an interesting material for nanocarrier preparation. A major drawback for many synthetic polymers is that they lack in biocompability and degradability.[72] Nature's biopolymers like carbohydrates, polypeptides, and proteins are promising alternatives to overcome these issues. They trigger in most cases only a low immunoreactivity, are structurally well-defined, and readily accessible.[73]

Especially proteins represent natural polymers that have unique functionalities for potential applications in medicinal and material science.[74] They show an amphiphilic behavior which is ideal for nanocarrier development as they can interact with both the solvent and the drug.[71] They can be categorized in three types: fibrous proteins, globular proteins and membrane proteins. Hereof, only fibrous and globular proteins are frequently used in nanocarrier research as they are readily accessible in high amounts – in many cases at low cost of the protein material. Nanocarriers obtained from proteins are often biodegradable and metabolizable. Additionally, as proteins typically consist of a high variation of amino acids, multiple functional groups on the protein surface are accessible for further modification (e.g. cysteine [-SH], lysine [-NH_2] and aspartic/glutamic acids [-COOH]). Nanocarriers consisting of proteins are expected to present the same functionalities their surface.

Nature offers a wide range of fibrous proteins like elastin, gelatin, resilin or silk. These proteins exhibit elastic mechanical properties and are capable to store mechanical energy. Their primary sequence mostly consists of alternating building blocks with diverse functionalities making their 3D structure highly flexible. Self-assembly of these proteins into multifunctional materials through modular protein engineering have been reviewed intensively.[75] With the origin sequence these proteins can serve as matrix material for nanomaterials.

More than fibrous proteins, globular proteins are very interesting for the pharmaceutical research – especially for the developement of nanocarriers. They already occur naturally in human secrets and the blood stream. Figure 7 shows high variety in size and shape of globular proteins that are used in current nanocarrier research. The most prominent representative of this group is human serum albumin (HSA, 66.5 kDa) as well as the structurally alike bovine

serum albumin (BSA, see supplemental information Figure 67, Table 24 and Table 26). HSA is the main transport protein in the human body and known to be extremely robust over a broad pH- and temperature range.[76-78] Additionally, it is preferential taken up by tumor cells by addressing the gp60 receptor.[79] The smaller spherical protein ovalbumin (OVA, 42.8 kDa), a widely used food protein, has high potential for controlled drug release due to its pH- and temperature sensitive properties.[80] Besides albumines also other spherical model proteins are used in nanocarrier research. Lysozyme (LYZ, 14.3 kDa) – for research purposes mainly isolated from chicken hen egg white – is a bacteriolytic enzyme frequently found in human body fluids and a frequently used food preservative.[81] Additionally it is reported to inhibit tumor metastasis in mice.[82-84] β-Lactoglobulin (BLG, 18.3 kDa) the major whey protein found in cow milk is known to be stable at low pH values making it highly resistant to proteolytic degradation in the stomach.[85, 86] Ferritin (FER, 485 kDa) is a supramolecular assembly of 24 subunits forming an inner core that naturally entraps iron ions.[87] Here, therapeutic agents can additionally replace the iron core of the protein.[87, 88] Until now, these proteins play an important role in the preparation of nanomaterials.[86-92]

Synthetic protein-based nanoparticles can be formed either by the use of unmodified proteins of by the use of protein-polymer conjugates. Unmodified proteins need to be denaturated to induce hydrophobic interactions whereas protein-polymer conjugates assemble after the attachment of hydrophobic polymers. Different approaches of particle preparation will be presented in the following sections.

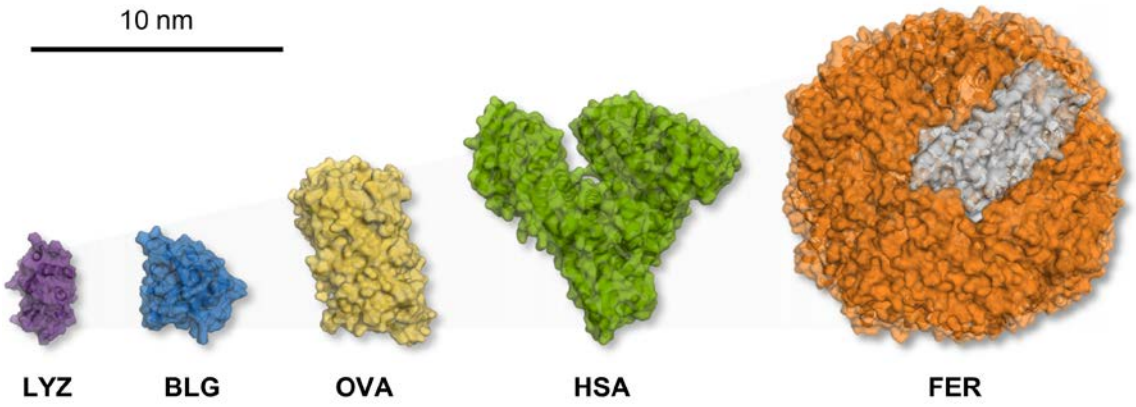

Figure 7. 3-Dimensional structures of the globular proteins lysozyme (LYZ, purple, pdb: 1lyz), β-lactoglobulin (BLG, blue, pdb: 1beb), ovalbumin (OVA, yellow, pdb: 1ova), human serum albumin (HSA, green, pdb: 1e7i) and the 24-mer ferritin (FER, orange with a subunit highlighted in grey, 1ier). Scale bar: 10 nm.

1.2.1 Preparation of Nanoparticles by Protein Denaturation

The preparation of protein-based nanoparticles by denaturation can be divided in three major types of preparation: desolvation, coacervation, and emulsification (Figure 8). Another, but less frequently used procedure is spray drying[93]

Protein Desolvation

The desolvation method was originally introduced by Marty *et al.*[74] in 1978 and further developed by Langer *et al.*[94] as they optimized the desolvation method for HSA in 2003 by forming NPs in a size range from 150 to 280 nm.[94, 95] Today, this is a frequently used method to obtain protein-based nanoparticles. Here, the proteins are dissolved in an aqueous environment and a slow addition of salt or water miscible solvent like alcohol, acetone or DMSO leads to the formation of protein agglomerates.[71, 96] This addition of a certain degree of organic solvent is altering the protein structure causing the start of aggregation. For further stability, the aggregates need to be cross-linked by highly reactive agents like the dialdehydes glutaraldehyde or glyoxal. Here, the aldehydes react with amino groups of lysines on the surface of the proteins and form imine bonds. When a dialdehyde reacts with two different proteins, intermolecular linkages between the aggregated proteins are formed. In a similar manner BLG was used to produce nanoparticles with a diameter of ~130 nm. Additionally, it was observed that preheating of the protein solution to 60° before solvent addition decreases the diameter of the particles to ~60 nm.[85] Other examples include silk proteins, that can be precipitated with acetone to induce an assembly into nanoparticles. In this method the amorphous regions of silk are progressively degraded in shorter silk fragments while sparing the crystalline regions. This likely facilitates the formation of nanoparticles in the size of ~100 nm.[97] Clinically established and emerging anti-cancer drugs can be encapsulated in the silk matrix.[98] In a different approach, salting out of spider silk from an aqueous solution to mimic the natural spinning process formed protein-microspheres. Herein, the high salt concentration induces a phase separation between salt- and protein-rich water. Nucleus formation in the protein rich phase induces the growth of microspheres – followed by a structural transition in the associated protein.[99] By this method a broad range of hydrophobic drugs can be encapsulated with encapsulation efficiencies of up to 98% with a size distribution from 170 to 700 nm.[100] Whereas desolvation is usually performed by adding an organic

solvent to an aqueous phase, gelatin was used to present a reverse desolvation method to produce nanoparticles. Herein, the protein is dissolved in water and added dropwise to an organic solution containing a stabilizer. Using gelatin as protein and ethanol as organic solvent, nanoparticles were obtained in the range from 200 to 300 nm after cross-linking with glutaraldehyde. This procedure enables the entrapment of FITC-labeled dextran as a hydrophilic model drug into the particles.[101] Besides the denaturation of the protein by cross-linking, another disadvantage is the loss in chemically active groups – mostly amines – on the surface of the particle. This limits further conjugation (e.g. with active targeting groups or PEG chains) to the surface of the NPs. Therefore, one strategy is protecting the amines of the protein with dimethylmaleic anhydride (DMMA) first reduces the amount of aldehyde reactive group prior cross-linking. After the cross-linking, detaching DMMA regains free amino groups on the surface of the particle, making it to be more favorable for further modifications.[102] Without doubt, cross-linking of multiple proteins enhances stability of protein nanoparticles but besides concerns about the toxicity of cross-linking agents also the effectiveness of the nanoparticles is decreased by high degrees of cross-linking as the increased stability was shown to obstruct a sufficient drug release.[103] Langer *et al.* successfully encapsulated plasmid DNA into glutaraldehyde cross-linked HSA nanoparticles. The group attached RGD and Tat peptides for targeting to the surface of particles with high and low degrees of substitution. In this manner it was shown that high cross-linking degrees decrease the transfection potential of the particles significantly as the gained particle stability limits an efficient intracellular plasmid release is.[104] The breakage of intramolecular disulfide bonds of HSA prior desolvation offers a new approach of intermolecular cross-linking. The resulting multiple free thiol groups on the denatured proteins can now form new disulfide bonds between different proteins. In another example, partially denaturation of HSA induced by low pH levels increases the exposure of the hydrophobic surface area by conformational changes of the protein. This drives self-assembly of the protein in a hydrogel via change in pH to 3.5 at 37 °C within 10 min or at pH 7.4 heating the protein to 80 °C allowing to entrap all-trans retinoic acid, inhibiting smooth muscle cell migration.[105] These methods avoid the loss of amino groups on the particle surface and toxic cross-linker; However, these methods irreversibly unfold the proteins.[106]

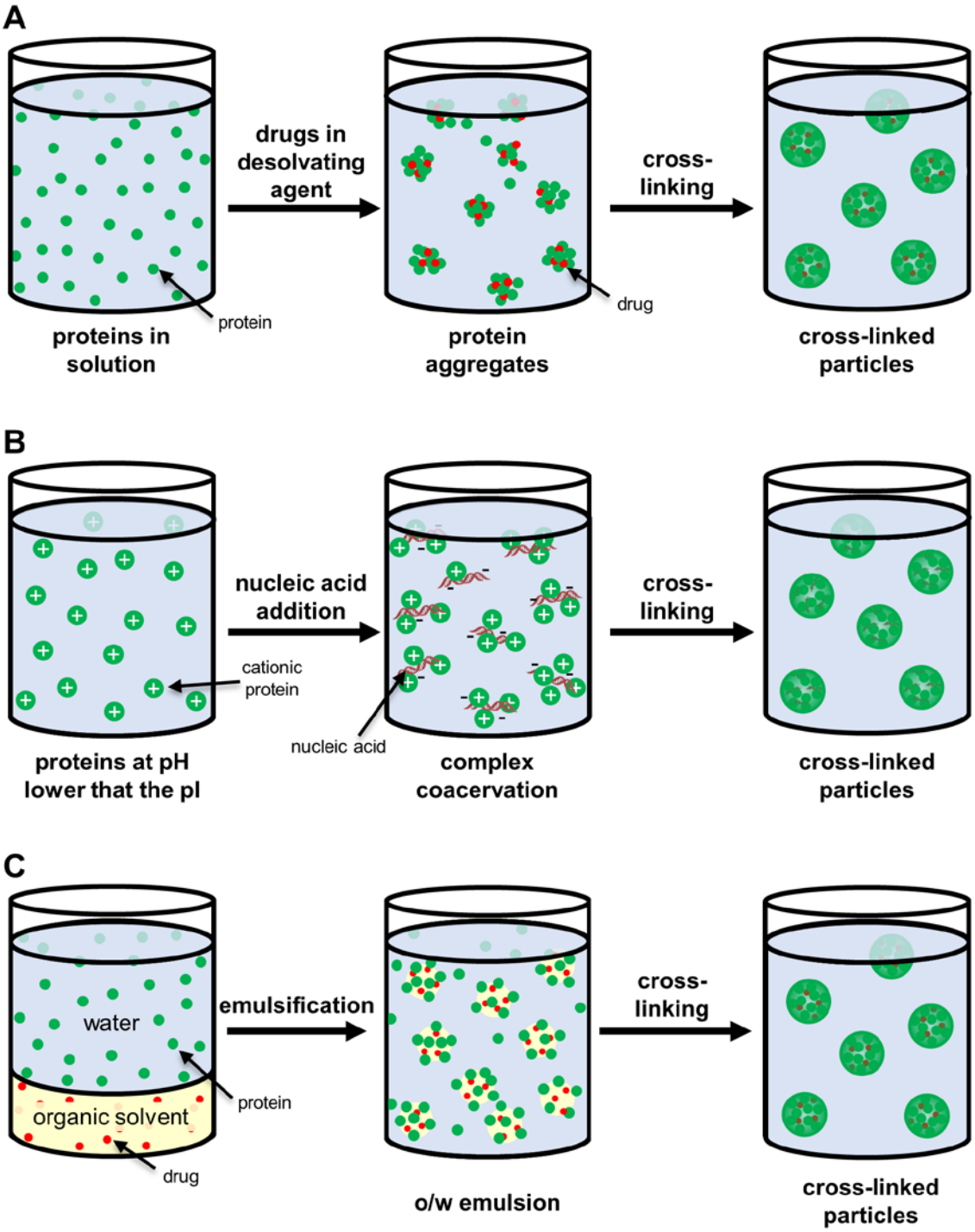

Figure 8. Procedures for the preparation of protein-based nanoparticles. Desolvation (A), coacervation (B) and emulsification (C).

The main use of the desolvation method is the preparation of nanoparticles from unmodified proteins. Furthermore, the attachment of a polymer to the protein – forming a protein-polymer conjugate – prior a desolvation step leads to nanoparticles that present the attached polymer also on their surface. By this, the resulting nanoparticle can benefit from the polymer features. For example, poly(amidoamine) or poly(thioetheranudeo acid) with PEG as copolymer (PAA-PEG and PTAAC-PEG) can be attached to the protein surface prior to a desolvation step. The resulting NPs then also represent these polymers on their surface. Desolvation with acetone and a following cross-linking step with glutaraldehyde leads to nanospheres with a diameter of around 100 to 130 nm. These particles showed a reduced plasma adsorbtion in comparison to particles from unmodified proteins.[107] More effects and benefits of protein-polymer conjugates and their role in nanocarrier formation will be presented later in detail (Section 1.2.2).

Coacervation

Coacervation is a procedure that is ideal for the entrapment of polyelectrolytes like nucleic acid that are of broad interest for gene delivery e.g. in immunotherapy. This technique benefits from the amphoteric character of proteins that present many charged functional groups on their surface but also from hydrophobic intermolecular interactions. After adjustment of the pH below the isoelectric point (pI) a protein becomes positively charged. By this, the protein can form electrostatic interactions with other, oppositely charged, polyelectrolytes like oligonucleotides or nucleic acids by complex coacervation. After complex formation, the proteins need to be cross-linked to obtain long term stability. A sub-form of coacervation is the so called thermal gelation. Here a heat-induced unfolding leads to protein-protein interactions. This includes hydrogen bonding, hydrophobic, and electrostatic interactions as well as disulfide-sulfhydryl interchange reactions.[90, 108] In addition, biodegradable cross-linkers can be used to stabilize protein NPs. Exemplary, the conjugation of dextran via a Maillard reaction to BSA allows the entrapment of doxorubicin into the conjugates. Heating of an aqueous solution of the modified protein to 80 °C for 1 h leads to nanoparticles with a diameter about 180 nm by a gelation process.[109] The two oppositely charged proteins OVA (negatively) and LYZ (positively) can be used to obtain narrowly distributed nanogels. The heat treatment of a protein mixture (80 °C for 90 min) forces denaturation of the proteins.

This procedure leads to particles with a hydrodynamic diameter of about 100 nm that consist of a lysozyme core with the ovalbumin mainly distributed in the shell.[90] A pre-coordination of the proteins – by the formation of protein containing liposomes – can also be performed prior thermal gelation to control the particle size In an approach by Papi *et al.,* collagen is pre-coordinated in a multi-step approach into liposomes. Heating of the liposomal dispersion to 37°C for 2 h afterwards leads to gelation of the proteins inside the liposomes. Dissolving the liposomal layer releases particles in a size of ~340 nm.[110]

Emulsification

In the emulsification technique, commonly an aqueous solution of the protein is emulsified with a water immiscible organic solvent like dichloromethane or hexane by using sonication or high-speed homogenization. This forms an oil-in-water emulsion and the amphiphilic proteins form nano-sized particles on the interface of oil and water. Surfactants like Span 80, that stabilize the oil droplets, are frequently added to the aqueous phase.[111] Depending on the further application of the particles, the organic solvent often remains inside of the particles, for example when olive oil or castor oil is used to form the emulsion.[112, 113] This preparation procedure also requires the use of cross-linking agents or thermal cross-linking to stabilize the nanoparticles. Casein, the major protein in milk, shows an open protein sequence like fibrous proteins. It consists of hydrophobic and hydrophilic building blocks but lacks in a distinctive secondary or tertiary structure. An oil-in-water (o/w) emulsion technique was used to encapsulate hydrophobic drugs in a casein matrix. With the protein in the aqueous and a hydrophobic drug in the organic phase (methylene chloride), emulsification followed by solvent evaporation leads to particles with a drug core and a protein shell. The proteins are afterwards cross-linked ionically by a polyanionic tripolyphosphate.This method was used to produce particles below 100 nm for the delivery of the anti-cancer drug flutamide.[114] Encapsulation of hydrophilic drugs into nano-sized capsules is often a problem if not impossible in desolvation steps as the payload needs to be entrapped in the protein matrix during the hydrophobic assembly. Emulsions of water droplets in oil is a very promising method to encapsulate hydrophilic payloads into nano-sized protein materials. The preparation of nanoparticles mediated by a water-in-oil nanoemulsion, where the hydrophilic payload is dissolved together with the protein in water was used by Piradashvili *et al.*[115] A hydrophilic

drug – fluorescently labeled DQ™ OVA or oligonucleotides – was dissolved together with the BSA in the aqueous phase. The hydrophobic cross-linker 2,4-toluene diisocyanate is used in the organic phase to cross-link the proteins in the interface between the aqueous and the organic solution. In this manner nanocapsules with a diameter of 170 nm were formed that entrap the hydrophilic payload.

1.2.2 Assembly of Protein-Polymer Conjugates

Synthetic protein-polymer conjugates are used to modify the physical properties of the protein by adding specific properties of a polymer to the resulting conjugate. For example, the attachment of hydrophobic polymers can change the behavior of the hybrid material drastically in comparison to the natural protein.[116] This can be used to induce a self-assembly of the protein-polymer conjugates into nano-sized particles.[60, 91] Furthermore conjugates of proteins and polymers provide the opportunity of combining properties of both materials – for example the solubility in organic solvents – whilst preserving the natural protein structure.[117]

The main two methods of creating a protein-polymer hybrid materials are the "grafting to", and the "grafting from" method. A third but less relevant method is the "grafting through" procedure (Figure 9). In the "grafting to" method polymer strands are bond covalently to the surface of proteins. This method takes advantage of the naturally occurring reactive groups of amino acids on the surface of the protein. Additionally, non-natural amino acids can be introduced to express unnatural functionalities such as alkynyl or azido groups.[118] In the "grafting from" method, the protein serves as macromolecular initiator molecule for the polymerization of a synthetic polymer. High control over molecular weight and dispersity of the polymer attached to the protein can be achieved via controlled radical polymerization techniques such as reverse addition-fragmentation chain transfer (RAFT) or reverse addition-fragmentation chain transfer (ATRP). This requires the attachment of initiating moieties on the surface of the protein (e.g. double bonds[119] or halogens[120]) first. These methods meanwhile avoid harsh reaction conditions and toxic catalysts and are suitable to retain the protein structure.[121] In the "grafting through" method, proteins are attached to a polymer that presents multiple protein reactive groups.

The most prominent protein conjugation is PEGylation. This has been widely used to enhance circulation time of proteins in blood, reduce plasma and protein adsorption and has been reviewed intensively.[122] It is the gold standard of protein-polymer conjugates and does not only enhance circulation time and half-life of proteins but additionally can reinforce proteins against mechanical unfolding.[123] Currently, 10 PEG-protein conjugates are currently on the market.[124] A major drawback of PEG is that this polymer is not biodegradable, nevertheless it is generally regarded as save by the FDA. Improvement of the attached polymer is one of the main topics in current research. n addition to the half-life extension, it is reported that the conjugation of polymers to proteins induces assembly of the protein to fibrillary and micellar structures.[125] Besides PEG, many other synthetic polymers are used for the conjugation to the protein surface to obtain similar effects.

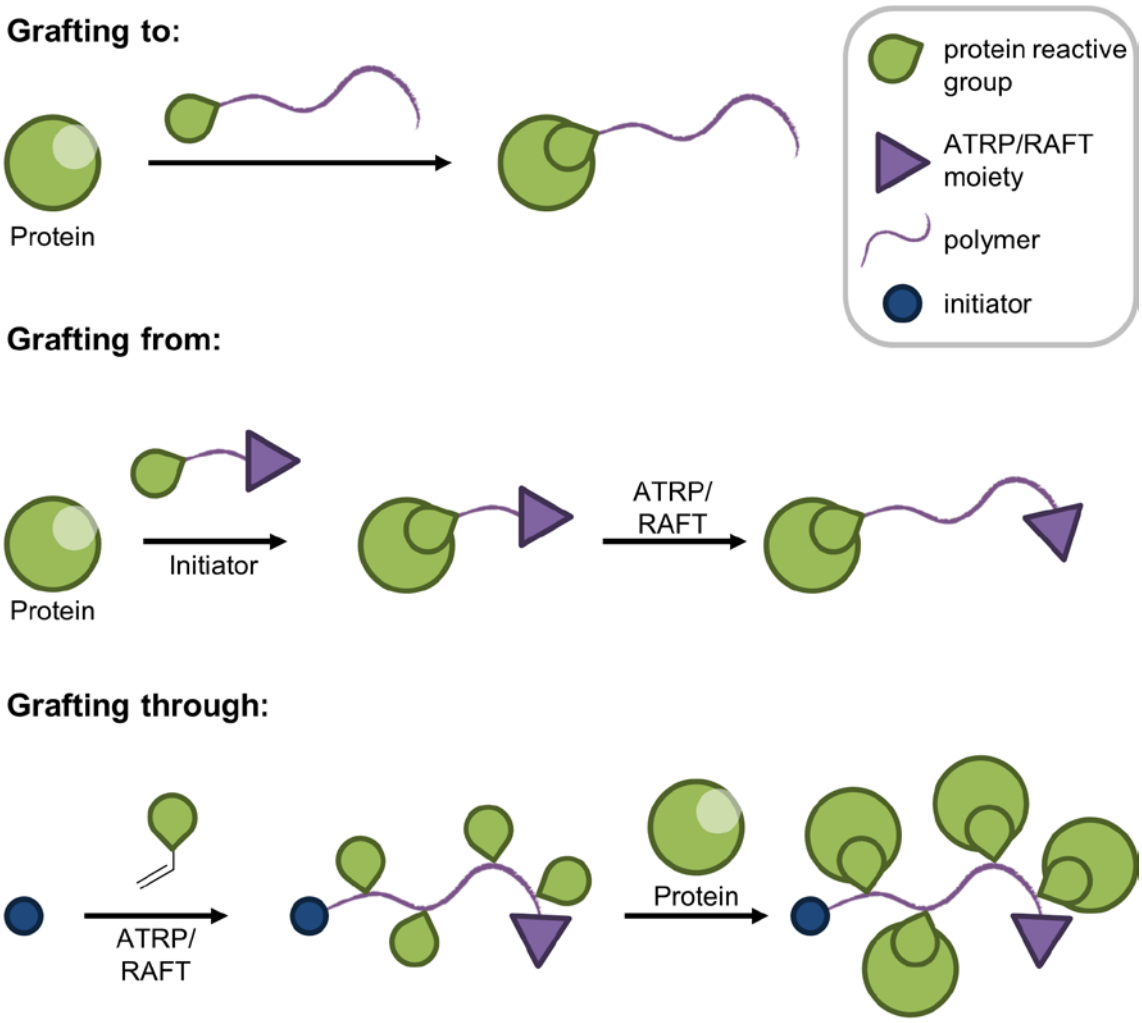

Figure 9. Different approaches for the preparation of protein-polymer conjugates. Redrawn from Grover *et al.*[126]

This is mainly to form an amphiphilic conjugate that leads to the self-assembly of the material into nano-sized structures like micelles. Here, the protein structure remains mostly intact. This is in contrast to the previously described methods where the proteins need to be denaturated for either the formation or later stabilization of the nanoparticles. Not only the type of polymer but also the amount of polymers attached to the proteins plays a key role for the further behavior of the protein-polymer conjugates.

Therefore, the preparation principles of protein-polymer conjugates can be separated in two basic ideas: 1) site-specific polymer conjugation on proteins to introduce one or only a small amount of polymer chains, and 2) the introduction of multiple polymer chains that cover the entire surface of the protein.

Site-specific Polymer Conjugation

The most common method for site-specific conjugation of proteins is the maleimide mediated Michael addition of polymers to the thiol of cysteine. This amino acid is often only present in a small amount on the surface of proteins. Boyer *et al.* presented a site-specific conjugation of *N*-isopropylacrylamide (NIPAAM) to cys34 of albumin (BSA) that leads to the formation of spherical particles with a size of 250-300 nm above the lower critical solution temperature (LCST) of the conjugates.[127] Almost ten years later, the Stenzel group presented a similar site-specific conjugation of maleimide-terminated PMMA to cys34 of BSA. The introduced hydrophobic PMMA block leads to a self-assembly into nanoparticles in the size range from 50 to 220 nm (Figure 10). The drug was successfully entrapped into the self-assembling micelles by addition of the hydrophobic drug curcumin to the polymer feed solution.[91] In a similar manner poly(oligo (ethylene glycol) methyl ether methacrylate) (PPEGMA) with a molecular weight of 26 kDa was attached to cys34 of albumin leading to a conjugate with a hydrophobic polymer tail and a negatively charged protein head. This protein-polymer conjugate forms stable complexes with positively charged proteins such as lysozyme or sprouty 1, a protein that plays a key role in cancer development.[128] This complexation leads to particles between 15 and 25 nm depending on the ratio of BSA to LYZ or sprouty 1. The proteins complexes were successfully transported into MDA-MB-231 and MCF-7 cells without losing the activity of the encapsulated protein sprouty 1.[92]

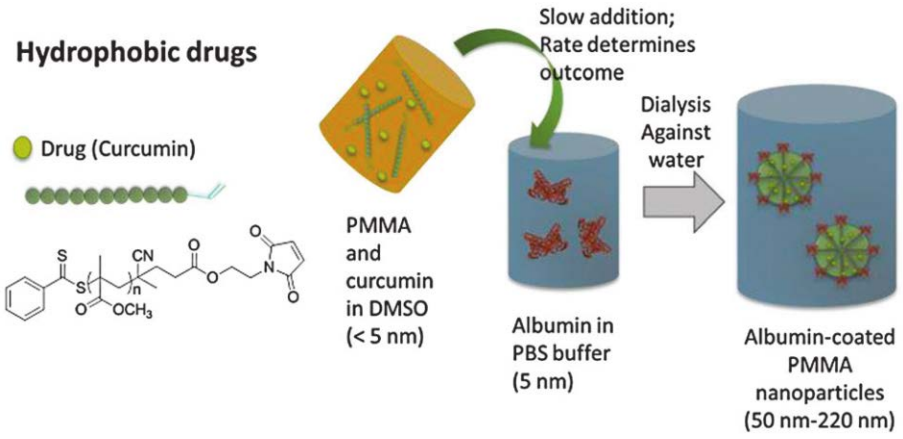

Figure 10. Slow addition of a hydrophobic polymer (PMMA) that is highly reactive towards cys34 of BSA and the drug curcumin leads to the formation of stable micelles in the size range from 50 to 220 nm. Reprinted from Jiang *et al.*[91] This article is licensed under a Creative Commons Attribution 3.0 Unported Licence.

Not all proteins are alike in their amino acid sequence and not every protein offers the possibility of a site-specific attachment of polymers by a lack of a sole amino acid such as cysteine on the surface. For a site selective polymer conjugation, this issue has to be overcome first. Under optimized reaction conditions, it is possible to introduce a single thiol functionality – by attaching *N*-succinimidyl-*S*-acetylthiopropionate to only one lysine – on the surface of lysozyme. Naturally, this protein does not exhibit a free cys on its surface. By this method can be used to conjugate only one maleimide functionalized PPEGMA to a protein that naturally does not offer an isolated amino acid on the surface.[129] This technique has the potential to apply specific conjugation using cysteine selective chemistry to any protein of choice.

I a different approach, the site-specific introduction of an either linear or Y-shaped poly(dimethylacryl-amide) co poly(*N*-isopropylacrylamide) (PDMA-PNIPAM), and PPEGMA block polymer leads to the formation of micelles with diameters from 25 to 31 nm with the protein hidden in the core or exposed on the surface, depending on the form of the attached copolymer (Figure 11).[118]

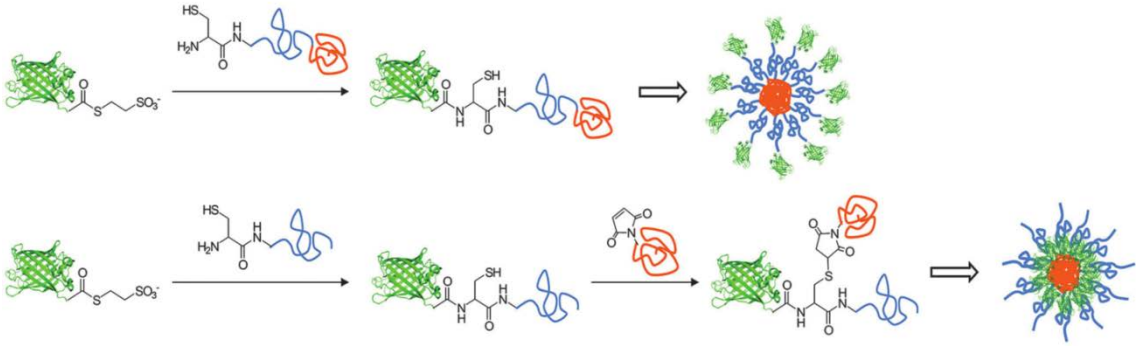

Figure 11. Synthesis of linear (top) and Y-shaped (bottom) GFP–block copolymer conjugates and their proposed micellar assembly with different protein location in respective micelles. Reprinted from Xia *et al.*[118] with permission of The Royal Society of Chemistry.

Natural protein cages – similar to ferritin or viruses – are promising transport vehicles by themselves.[130] However, their size is limited by the highly defined structure of the individual proteins. An approach to increase the size is the controlled assembly of multiple protein cages after the formation of protein cage-polymer conjugates. As an example, a PNIPAM chain was attached to the surface of human metapneumovirus (hMPV). This led to a change in the thermal properties of the protein cage. The conjugate does not respond to temperature changes at pH 7 but forms reversibly particles in the size of 300 nm by thermal changes at pH 6. Neither the hMVP vault nor the conjugate were damaged despite the heat cycling.[131]

As mentioned previously, not only naturally rarely occurring amino acids can be used for the site-specific attachment of polymers. Further, point mutations on proteins allow expressing unnatural functionalities on the protein surface. The incooperation of *p*-azidophenylalanine to the sequence of superfolder green fluorescent protein (sfGFP) offered the possibility to attach PPEGMA polymers site selectively by copper catalyzed "click" chemistry. The protein-conjugate becomes temperature-responsive due to the nature of the attached polymer and forms agglomerates in the range from 100 to 500 nm upon heating. The conjugation to different sites of the protein does not affect the shape of bioconjugate but leads to an apparent difference in thermal properties (Figure 12).[132]

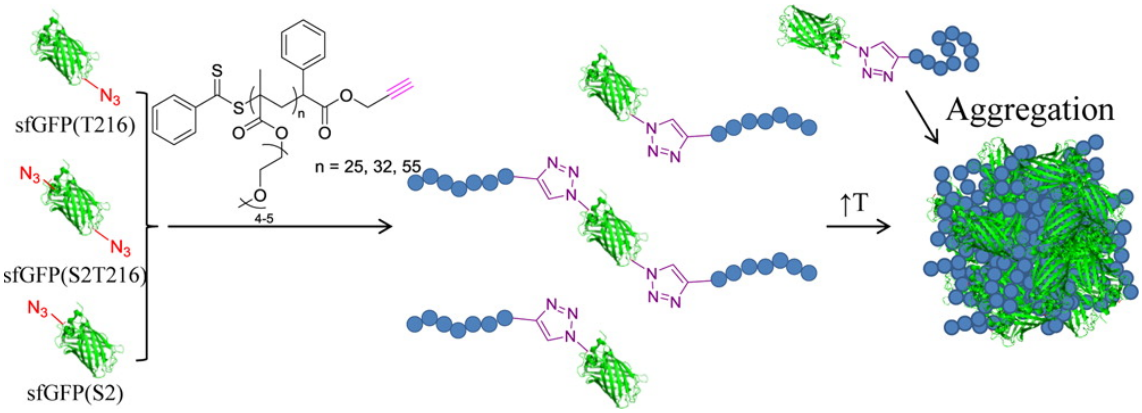

Figure 12. Strategy for the synthesis of sfGFP-PEGMA bioconjugates via the engineering of three sfGFP analogues with T216, S2T216, and S2 site modification with pAzF before the CuAAc of alkyne-functional PEGMA (three different molecular weights). Upon an increase of the solution temperature, all bioconjugates were found to aggregate. Reprinted. Reprinted from Moatsou *et al.*[132] This Article is licensed by a Creative Commons Attribution (CC-BY) Licence.

Polymer Conjugation in High Ratios

The attachment of multiple polymers to the protein surface allows not only to introduce the polymer properties to the conjugate but also to mask the entire protein without losing its initial function.[133] High degrees of modification of proteins with a polymer can be achieved by the "grafting to" method via electrophilic activated polymers. These are highly reactive to the primary amino group of lysine, which is present in high amounts on most proteins. These reactions can be performed under mild conditions in an aqueous environment without the need of metallic catalysts.

For example, the co-attachment of the anti-cancer drug doxorubicin (DOX) and PEG to the surface of human serum albumin forms – along with additional free drug – micelles with a diameter of approximately 30 nm (Figure 13). PEG with a mol. wt. of 5 kDa was introduced via NHS active esters. The thiolated drug (DOX-SH) was conjugated in a second step via a sulfo-LC-SPDP linker on the remaining free amines on the protein surface. The attachment of the drug enhances the surface hydrophobicity of the protein. This, and the incoperation of additional "free" doxorubicin drives the formation of stable micelles, where the drug is covalently attached to the protein as well was physically entrapped in the micelle.[134]

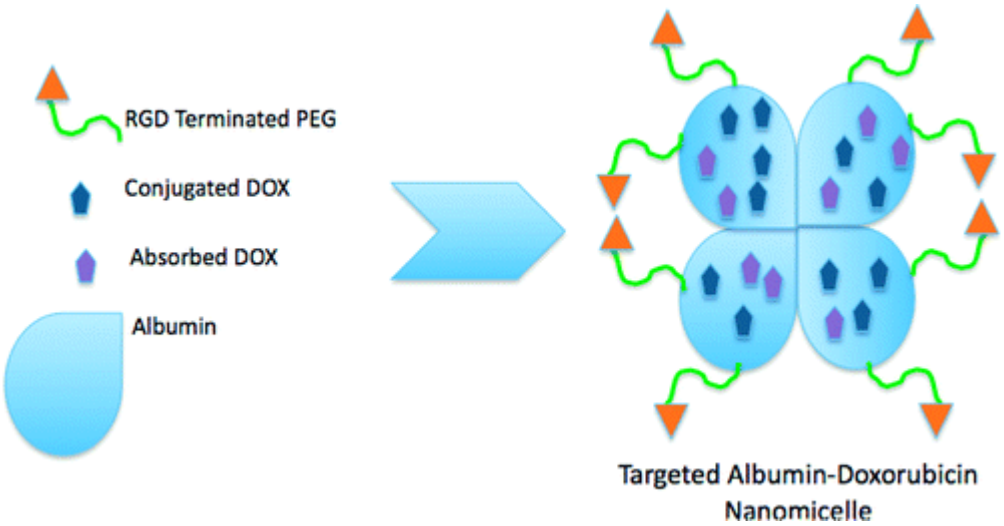

Figure 13. Multiple poly(ethylene glycol)s were used to form a hydrophilic outer layer, with the inner core formed by albumin conjugated with doxorubicin attached via disulfide bonds. Additionally doxorubicin was physically adsorbed into the protein core allowing a high drug loading capacity, where each albumin was associated with about 50 doxorubicin molecules in total. Reprinted with permission from *Xu et al.*[134] Copyright (2011) American Chemical Society.

For the "grafting from" method in a high ratio, multiple initiator groups for polymer polymerization need to be attached to the protein surface. In an approach by Vanparijs *et al.* the attachment of five poly [(2,2-dimethyl-1,3-dioxolane)methyl]acrylamide chains to the BSA surface leads to an assembly of the proteins above the clouding point of the polymer. This forms micellar nanoparticles with a size of ~190 nm. As the polymer contains acid-labile ketal groups its hydrophobic character is highly sensitive to pH changes. After a decrease of the pH, ketal groups of the polymer chains are cleaved and present the hydroxyl groups on the polymer. This hydrophilic switch leads to a disassembly of the micelle.[135]

In a different approach, the introduction of double bonds on the surface of BSA allows the use of the protein as a macroscopic initiator for the polymerization of PMMA. By this method Ge *et al.* were able to form micellar structures with a nanoprecipitation procedure of the protein-PMMA conjugate – together with BSA in free form – wherein the hydrophobic polymer is forming the core of the particle and BSA forms the shell. Here the size of the resulting nanoparticles is tunable and depends on BSA:PMMA weight ratio ranging from 63 nm (1.6 : 1) to 452 nm (0.04 : 1).[119]

In another example, the conjugation of a natural polymeric structure to a protein surface was not only used to enhance the uptake of the protein but also the attached macromolecule itself. The cellular uptake of oligonucleotides was enhanced by ~280-fold trough functionalization of the surface of the hydrolytic enzyme *β*-galactosidase with ~25 DNA strands (spherical nucleic acid). A short bifunctional (NHS-PEG_4-azide) spacer was attached to lysines on the protein surface. The DNA was then linked to the introduced azide groups via copper free "click" chemistry. The mild reaction conditions lead to a complete preservation of the protein structure maintaining the initial protein activity.[117]

Introduction of halogens by the attachment of 2-bromoisobutyryl bromide on the surface of BSA converts the albumins to a macro initiator with reported ~15 initiator groups on the protein surface. 2-(Dimethylamino)ethyl methacrylate was polymerized directly from the BSA surface in a ATRP mechanism afterwards forming nanoparticular BSA (nBSA). The conjugate increased its weight from 65 to 220 kDa under reaction conditions that are suitable to preserve the protein structure. In combination with pDNA, the positively charged nBSA-conjugate forms polyplexes with tunable sizes with an average diameter of 50 nm (Figure 14).[120]

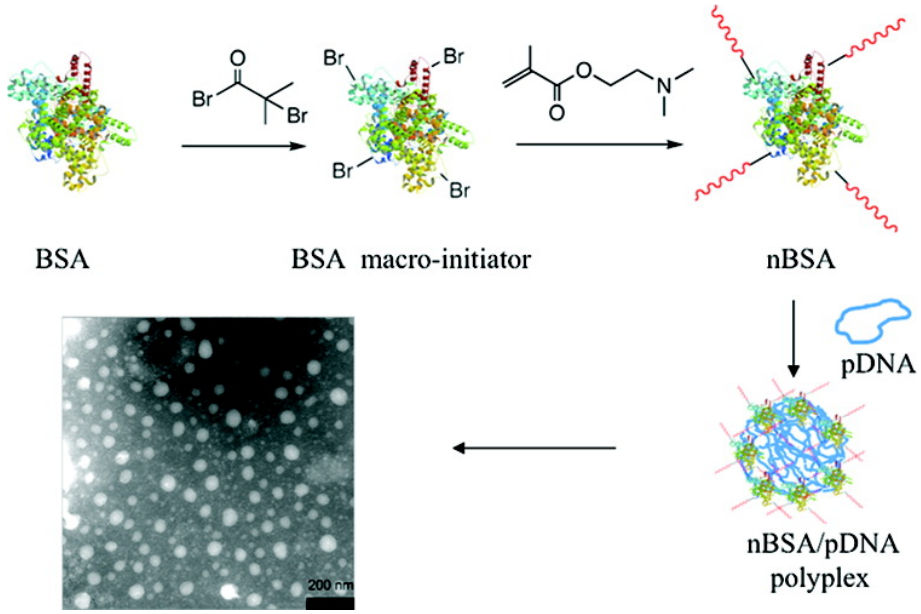

Figure 14. Polymerization of PDMA from the protein surface in a high ratio leads to nanoparticular BSA (nBSA) in a size range from 5 to 15 nm. Formation of a complex of nBSA with pDNA leads to particles with an average diameter of 50 nm. Reprinted with permission from Zhang *et al.*[136] Copyright (2011) American Chemical Society.

These examples show that the formation of protein-polymer conjugates is a promising approach to obtain nanoparticles with preserved protein structure. This has been efficient for both site-specific and high ratio conjugation. The major drawback of these systems is a lack in a general applicability. All approaches have only shown promising results with a specific protein or specific payloads. None of these systems shows enough versatility for a broad use of different proteins or the transport of both hydrophobic and hydrophilic payloads. Further, the benefit of an intact protein structure is hardly exploited by these systems as they are mainly based on albumin that only serves as material without further function. In fact, there is no assembled protein-based particle system, that still presents a catalytic activity. These circumstances lead to the motivation of this PhD-work.

2 AIM OF THE WORK

Aim of this work is to develop a protein-based nanocarrier system wherein the natural protein structure and functionality is preserved (Figure 15). If successful, this would represent the first protein-based nanoparticles system that allows the entrapment of hydrophobic and hydrophilic payloads using the same protein-polymer conjugate. Moreover, this system is aimed to be potentially applicable to any protein or enzyme of choice to form nanoparticles. The intension is to apply an emulsification method – originally established for polysaccharides by the group of Jean M. J. Fréchet at the University of California, Berkeley – to proteins. In the original approach, nanoparticles are formed by a mild emulsification method where the particle matrix material is dissolved in the organic phase. This was applied to encapsulate hydrophobic as well as hydrophilic cargos.[67-70, 137, 138] The particle size ranges in diameters below 200 nm, a size that is ideal for passively targeting tumor tissues.[30] The major challenge in transferring this system is that proteins are naturally insoluble in volatile organic solvents like dichloromethane. This aspect in particular is required for the emulsification procedure where the formation of stable particles is achieved by solvent evaporation. To overcome this issue, a method described in the 1980s by Inada and Abuchowski has shown promising results to transfer proteins into organic solvents. [133, 139-146] PEGylation of proteins in high ratios acquired the necessary solubility in organic solvents whilst preserving the activity of the protein to preform catalytic reactions. The aim of this PhD work is to combine these previous literature known approaches to obtain a protein material that is suitable for a particle preparation by emulsification using surface PEGylated proteins.

The first challenge of this work is to evaluate the best method of protein modification to obtain a protein-based material that is suitable for particle preparation. It also has to be ensured that the protein structure remains unaffected and retains its initial activity (when applicable). After a successful transfer of the protein to organic solvents, a single emulsification procedure shall be applied for the preparation of nanoparticles, preferably with a size below 200 nm and no requirements of cross-linking steps for stabilization. The *in vitro* behavior of these particles shall be analyzed in regards of cellular association, uptake and viability. Here, this will be investigated in detail for the model enzyme lysozyme and doxorubicin as model payload/drug.

To demonstrate, that this particle preparation method is transferable to any protein of choice a broad variety of proteins needs be used as starting material. In addition, the payload should to be varied, e.g. using alternative drugs to substantiate the versatility of this system. In addition, it is aimed to expand the preparation system to the entrapment hydrophilic payloads. For this, the protein-polymer conjugates shall be applied in a double emulsion technique. This should allow the entrapment of hydrophilic cargos, e.g. fluorescent labeled dextran that can act as model drugs of similar weight and charge as nucleic acids.

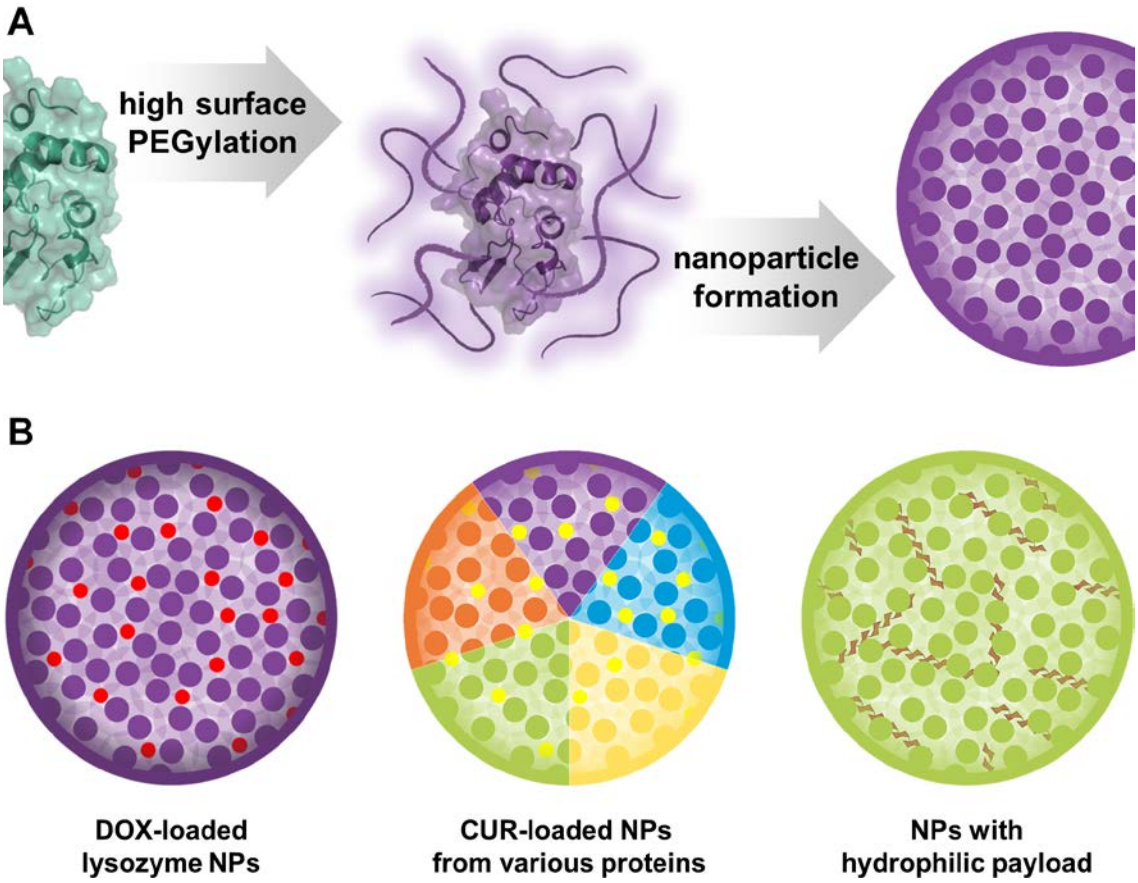

Figure 15. Graphical illustration of the aimed nanoparticle preparation. Surface PEGylation in a high ratio is supposed to obtain a lipophilic protein-polymer conjugate, followed by different types of emulsification techniques to obtain protein-based nanoparticles (A). Lysozyme-based nanoparticles for the entrapment of doxorubicin intend to provide the proof of the principle of the presented system. Curcumin-loaded nanoparticles obtained from a variation of proteins shall substantiate the general applicability of this particle preparation method to various types of proteins and hydrophobic drugs. Entrapment of hydrophilic payloads expands the system for further applications e.g. in immunotherapy (B).

3 RESULTS AND DISCUSSION

3.1 Lysozyme Nanoparticles for Doxorubicin-Delivery

The majority of the data in this section has already been published briefly as communication in the Journal of the American Chemical Society (Fach *et al.*[147]) and is discussed here more detailed.

3.1.1 PEGylation of Lysozyme

Activation of mPEG

Due to the low reactivity of the hydroxyl terminus, the attachment of mPEG to the surface of proteins is difficult – if not impossible – especially in high ratios. For this reason, the hydroxyl terminus needs to be substituted to generate a more reactive species. By attaching the highly reactive linker trichloro-*s*-triazine (TsT) to the –OH terminus of mPEG, the now "activated" polymer becomes highly reactive towards nucleophilic groups on protein surfaces like $–NH_2$ of lysine, –OH of tyrosine, or –SH of cysteine. The attachment of TsT to the polymer follows an addition-elimination mechanism of an aromatic substitution (S_NAr). TsT has the potential to react stepwise with multiple substituents. The first chlorine substituent is replaced between 0–5 °C, the second at 30–50 °C and the third at 70–100 °C.[148] Nevertheless, under mild alkaline conditions with Na_2CO_3 as base, in benzene at room temperature with a 3-fold excess of linker molecule, the substitution of only one mPEG to the TsT linker is observed (Scheme 1).[145] The same reaction was performed with mPEG2k and mPEG5k.

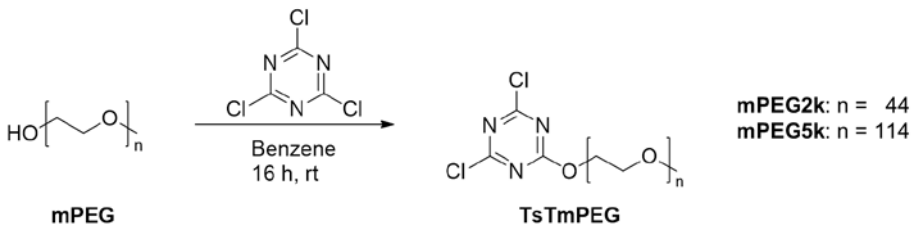

Scheme 1. Activation of the hydroxyl group of *a*-methoxy-*ω*-hydroxy polyethylene glycol (mPEG) with trichloro-*s*-triazine (TsT) to the activated TsTmPEG conjugate.

Elemental analysis was performed to determine the substitution efficiency of the activation step. For mPEG2k, 65% of the chains carry a TsT-linker. For mPEG5k, 62% of the PEG chains are activated. Despite a relatively low activation efficiency of around two thirds, the reaction conditions were not further changes. Increasing the amount of TsT linker would lead to a more difficult purification of the final product and residual linker raises concerns about its toxicity. Additionally, free reactive linker preferably reacts with nucleophilic groups (e.g. on the protein surface) and impurities would compete with the TsT-activated mPEG. Increasing the alkalinity and/or the reaction temperature is reported to result in homo bi-functionalized TsT with two polymers attached to a single linker molecule.[144] This would impede the attachment of the activated mPEG to the protein surface due to the resulting low reactivity of the third chlorine substituent.

The attachment of only one mPEG chain to the linker molecule was confirmed by size exclusion chromatography (SEC, Figure 16). The elugrams of activated TsTmPEG samples were compared to the hydroxyl-terminated mPEG. The attachment of a single TsT linker molecule is not expected to change the elution volume (V_e) of the polymer sample as the change in the length of the polymer is only marginal (~2% for mPEG2k and below 1% for mPEG5k). On the contrary, the multiple attachment of a second mPEG chain to TsT leads to a size increase by 100%. This increase is expected to be clearly visible in the elution pattern of the polymer sample. Both activated samples (TsTmPEG2k and TsTmPEG5k) correspond with the references of unmodified mPEG. From these results, the attachment of multiple mPEG chains for a single TsT linker can be excluded for both mPEG2k and mPEG5k.

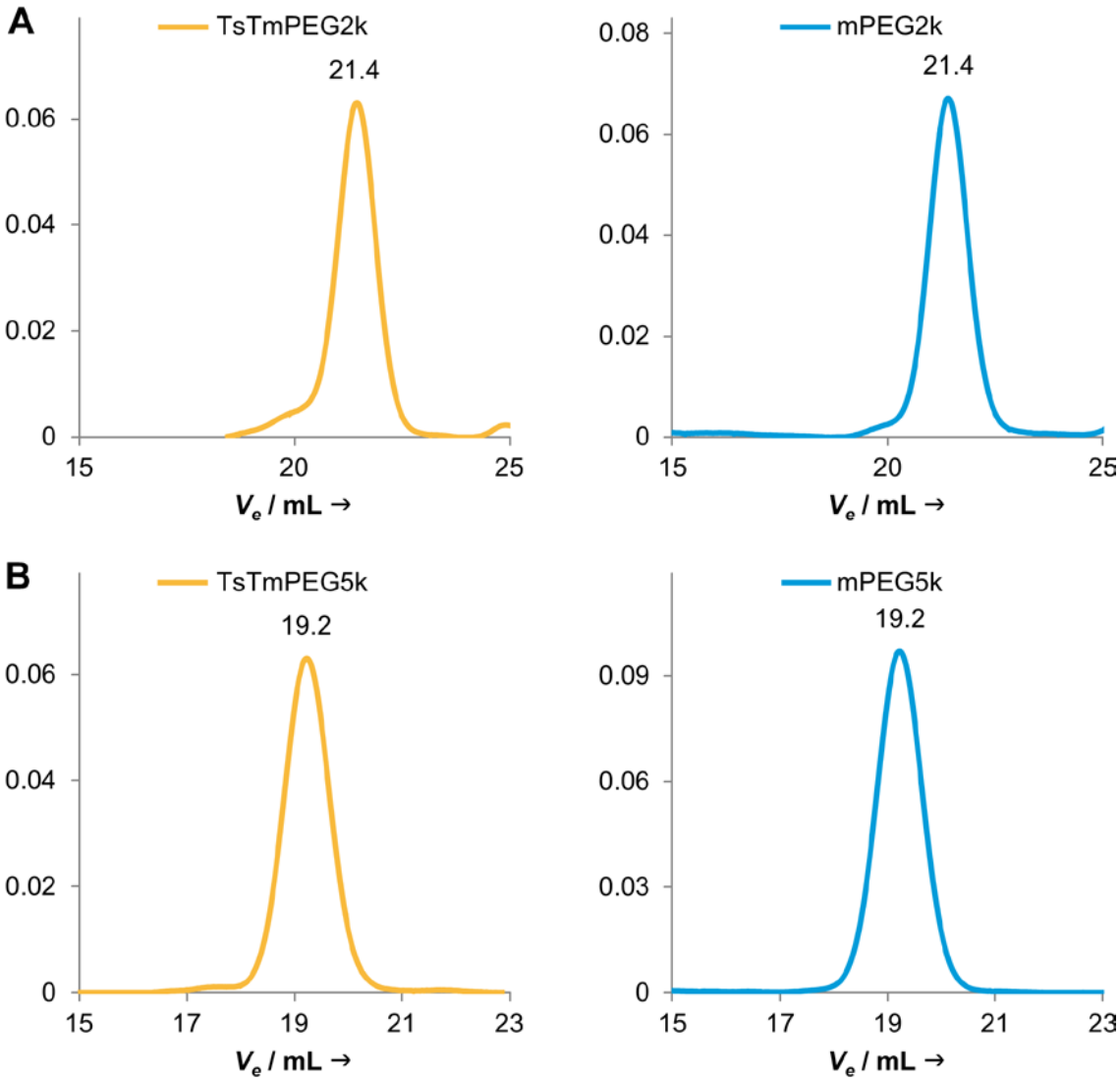

Figure 16. SEC elugrams of TsTactivated mPEG (yellow, left) in comparison unmodified mPEG (blue, right). The elugram of activated Cl-TsT-mPEG2k shows the same eluation pattern as the elugram of reference mPEG (mol.wt.: 2000 g/mol) with an eluation volume of 21.4 mL (A). The elugram of activated Cl-TsT-mPEG5k shows the same eluation pattern as the elugram of reference mPEG (mol.wt.: 5000 g/mol) with an eluation volume of 19.2 mL (B). In parts adapted from Fach *et al.*[147] Copyright (2016) American Chemical Society.

Protein PEGylation

High surface PEGylation is achieved by the reaction of the activated TsTmPEG with nucleophilic amino acids on the protein surface. The most dominant amino acid is thereby lysine. With a pK_a of 10.5 for the primary *ε*-amino group and a typically high amount on the protein surface, this amino acid is the most prevalent nucleophile on the surface of proteins. Additionally, the hydroxylic group of tyrosine (pK_a: 10.9), the secondary amine of histidine (pK_a 6-7) and the N-terminal amine of a protein (pK_a 8.0) can take place in reactions with electrophiles. With 6 lysines, three tyrosines and the N-terminal amine on the protein surface, lysozyme bears 10 nucleophilic amino acids on the protein surface available for modification.

The surface conjugation is carried out under basic (pH 10) aqueous conditions and mild heating of the sample (40 °C) for two hours (Scheme 2). These conditions are required for the substitution of the second chlorine of TsT by the surface amino acids. To achieve a high surface PEGylation of LYZ a 20-fold excess of TsTmPEG per lysine group on the surface of the protein was used. Lowering the excess of TsTmPEG did not lead to a full modification and also not to a solubility of the protein conjugate in organic solvents.

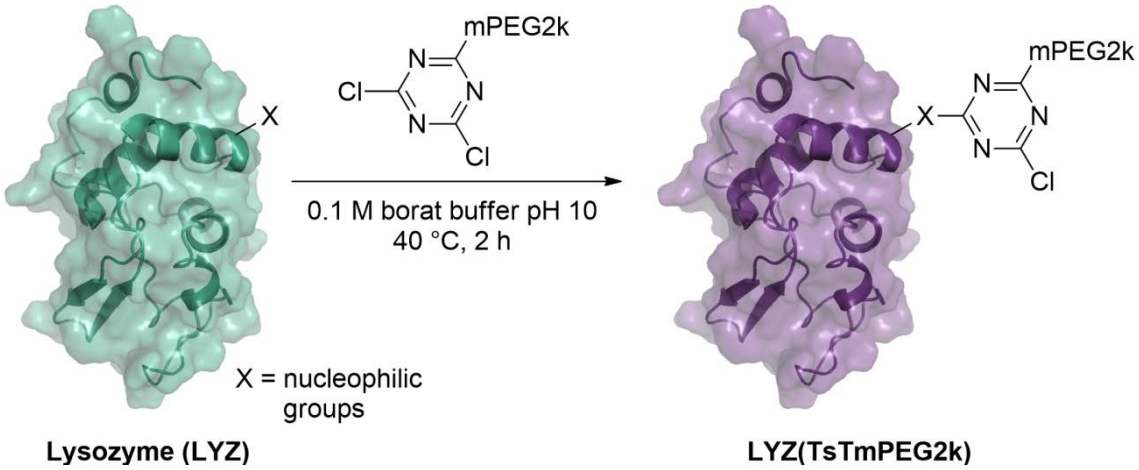

Scheme 2. Surface PEGylation of lysozyme (LYZ) with TsT-activated mPEG under slightly basic conditions (pH 10). Seven amines (6 × lysine and 1 × N-terminal -NH_2) and three hydroxyl (3 × tyrosine) groups are accessible on the surface of LYZ for substitution with TsT-activated mPEG. Reprinted from Fach *et al.*[147] Copyright (2016) American Chemical Society.

The excess amount of polymer was removed by ultrafiltration using centrifugal filter devices with a molecular weight cutoff (MWCO) of 30 kDa. This method was preferred over dialysis as the reaction mixture is – due to the polymer – to viscous for a sole diffusion mediated solvent exchange. After freeze-drying, the protein-PEG conjugate was obtained as a colorless solid. The effects of surface PEGylation towards the protein are described in the next sections. In the following, lysozyme-PEG conjugates are shortened as the three letter abbreviation of the protein and indexed with the size of the attached mPEG chain e.g. LYZ^{2k} for lysozyme with mPEG chains with a mol. wt. of 2 kDa attached to its surface.

Molecular Weight Analysis by Gel Electrophoresis

Sodium dodecyl sulfate polyacrylamide gel electrophoresis (SDS-PAGE) is widely used for the determination of the molecular weight of protein samples. In this analysis technique, denaturation by heat and addition of mercaptoethanol (2-thioethanol) forms a complex of the protein with sodium dodecylsufate (SDS). For unmodified proteins, the formed complex is proportional to the mass of the protein. This complex is applied on a porous polyacrylamide gel with defined pore sizes and is moved through the gel matrix by an applied electrical field. Small proteins move hereby faster through the PA-matrix than larger samples. Figure 17 shows the PEGylated proteins LYZ^{2k} and LYZ^{5k} in comparison to the native lysozyme (lane LYZ). A marker (lane M) with proteins in different sizes from 10 to 170 kDa is used as reference. The native LYZ shows a sharp protein band at a size slightly below the 15 kDa band of the protein marker corresponding to the molecular weight of 14.3 kDa. However, the two PEGylated proteins LYZ^{2k} and LYZ^{5k} show broad distributed protein bands. Both samples do not show traces of native protein indicating a complete conversion to the highly PEGylated conjugate. The band of LYZ^{2k} is distributed from around 35 kDa up to the detection limit of 170 kDa with the highest intensity between 40 and 70 kDa. The band of LYZ^{5k} is distributed from around 70 kDa to 170 kDa. From the running behavior of the samples in the SDS-PAGE, it can be concluded that an amount of 13 to 28 mPEG2k chains is attached to the surface of LYZ. For LYZ^{5k} an amount of 11 to 31 mPEG5k chains on the protein surface can be assumed. As described previously,[149] PEGylated proteins tend to interact differently with SDS and form more complex conjugates then native proteins. This results in smearing behavior in

the gel electrophoresis implying higher molecular weights and broader size distributions of the sample so the sample is not represented correctly.

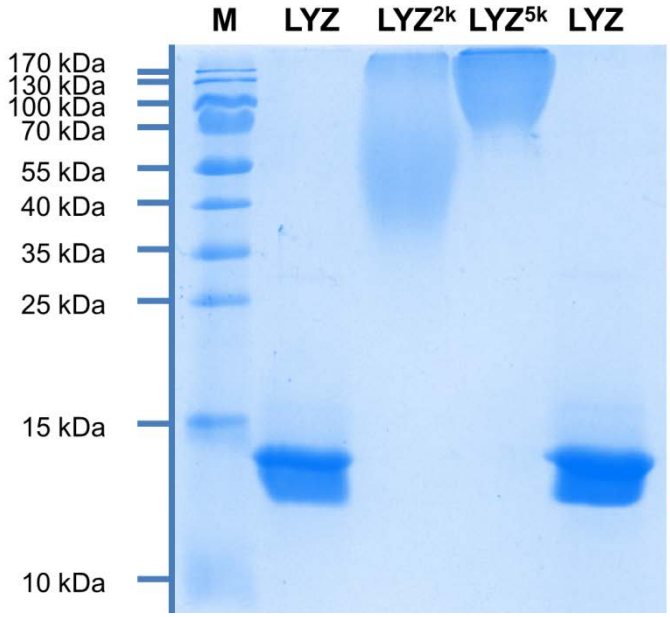

Figure 17. SDS-PAGE of the reference marker (lane M, 5 μL), unmodified lysozyme (lane LYZ, 15 μg), LYZ(TsTmPEG2k) (lane LYZ^{2k}, 30 μg) and LYZ(TsTmPEG5k) (lane LYZ^{5k}, 30 μg). The polyacrylamide content was 15% with a thickness of 0.75 mm (first 90 V, 60 min; then 200 V, 30 min). The gels show no trace of unmodified lysozyme after PEGylation for both, the LYZ^{2k} and LYZ^{5k} conjugate.

Size Increase Analysis by Fast Protein Liquid Chromatography (FPLC)

Attaching a high amount of mPEG chains to the surface changes the hydrodynamic diameter (d_{hyd}) of the protein. For determination of a qualitative shift in d_{hyd}, fast protein liquid chromatography (FPLC) was used. The separation principle is based on a size exclusion chromatography where the sample passes a column with porous matrix material. Large samples show less interaction with the pores and eluate faster than small samples that highly interact with the pores of the matrix material. Native LYZ shows a V_e of 20.2 mL. For LYZ^{2k} the V_e shifts to 12.5 mL, for LYZ^{5k} a shift to 10.6 mL is observed. From these results, a defined shift in d_{hyd} is observed. In Addition, as already presented in SDS-PAGE, no traces of unmodified LYZ is determined. It is remarkable, that LYZ^{5k} shows a relatively broad peak whereas the peaks of LYZ and LYZ^{2k} are quite narrow. This indicates that the sample contains protein conjugates with different amounts of mPEG attached to the surface.

Using FPLC, a quantitative estimation of the amount of mPEG chains on the protein surface is not possible for this protein-polymer conjugate system. Despite size standard samples are commercially available for native proteins; these are not applicable for the presented protein-polymer conjugate system. Size standards for FPLC consist of proteins with defined molecular weights. However, the separation principle of SEC is depending on the d_{hyd} and not the actual molecular weight. This difference can be neglected when comparing unmodified proteins with the standard as most proteins show similar densities due to their compact 3-dimensinal structure. But attaching a flexible polymer to the protein surface changes the d_{hyd} in a higher ratio than the mol. wt. is affected. Additionally the PEG-shell around the protein core is very soft and flexible and interactions of this conjugate with the pores of the column matrix are hardly comparable to the interactions observed by commercial protein standards.

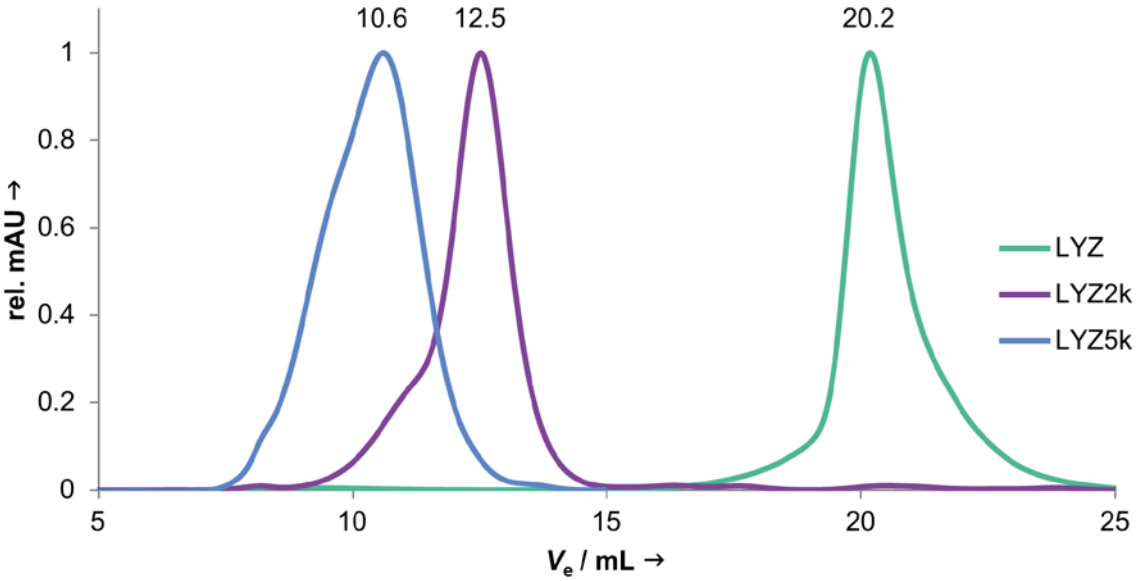

Figure 18. FPLC elugram of LYZ^{2k} (purple) LYZ^{5k} (blue) and native lysozyme (green). LYZ(TsT-mPEG)$_{10}$ shows a shift of the elution volume V_e in comparison with native lysozyme from 20.14 mL to 12.51 mL. This shift increases to a V_e of 10.6 mL for LYZ^{5k}. In parts adapted from Fach *et al.*[147] Copyright (2016) American Chemical Society.

Molecular Weight Analysis of Lysozyme Conjugates by MALDI-ToF MS

Matrix-assisted laser desorption/ionization time of flight mass spectrometry (MALDI-ToF MS) was used to determine the molecular weight of the protein-polymer conjugates LYZ^{2k} and LYZ^{5k}. In contrast to other methods, it is regarded as mild In this analysis method the sample is co-precipitated with a laser absorbing matrix. From this surface, molecules are expelled by the flash of a laser. The molecules capture electrons as they exit the matrix and leave as negatively charged ions. The ions are afterwards accelerated in an electric field towards a detector. Small molecules are accelerated more, move faster and arrive the detector prior large molecules. In contrast to other mass determination methods like electrospray ionization, MALDI-ToF MS is a mild method that does not destroy the sample. Therefore it is ideal for the determination of biopolymers.[150] This method allows determining the exact mass of a protein-sample and is hence used for determination of the amount of mPEG chains attached to the protein.

Figure 19 shows the Maldi-ToF spectra of LYZ^{2k} and LYZ^{5k} in comparison to the native protein LYZ. The LYZ^{2k} sample shows three distinct mass peaks at 17.5 m/z, 34.9 m/z and 70 m/z. As the samples are detected as mass by charge, the signal at 17.5 m/z is assigned to the double charged (M^{2+}) protein-PEG conjugate. The signal at 70 m/z represents the dimer of the sample. The most dominant signal is observed at 34.9 m/z and represents a single protein-PEG conjugate. According to the single charge of the sample the mass of LYZ^{2k} is 34.9 kDa. For PEGylation with TsTmPEG5k a similar pattern of the protein with M^{2+}, M^{+} and dimer peak is observed. Here the M^{+} peak of the LYZ5k is not as defined as observed for LYZ^{2k}. The main peak is observed at 46.2 kDa but additionally, mass peaks in the distance of 5 kDa are observed ranging from 41 to 56 kDa around the maximum. The 5 kDa step represents the mass of a single mPEG chain, showing that the sample contains a mixture of conjugates with different degrees of surface modification.

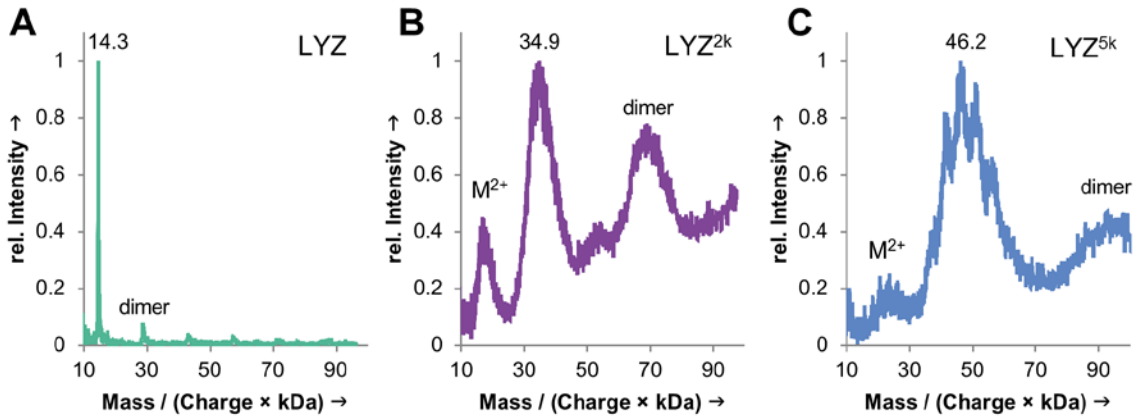

Figure 19. MALDI-ToF MS spectra of LYZ (A) in comparison to the protein-PEG conjugates LYZ^{2k} (B) and LYZ^{5k} (C). The molecular weight of lysozyme increases from 14.3 kDa to 34.9 kDa by PEGylation with mPEG2k and to 41–56 kDa by PEGylation with mPEG5k. In parts adapted from Fach *et al.*[147] Copyright (2016) American Chemical Society.

From this measurement method, it is possible to calculate the amount of mPEG (x_{mPEG}) on the protein surface by Equation 1 with the mol. wt. of LYZ of 14.3 kDa ($M_{Protein}$) and the mol.wt. of the attached mPEG ($M_{TsTmPEG}$) of around 2.1 kDa and 5.1 kDa respectively. The detected mass of 34.9 kDa ($M_{Protein\text{-}PEG\ Conjugate}$) of LYZ^{2k} represents a lysozyme with around 10 mPEG2k chains attached to the surface. For LYZ^{5k} (41 to 56 kDa), the amount of mPEG5k chains on the surface ranges from 5 to 8 with a maximal population bearing 6 mPEG chains on the surface.

$$x_{mPEG} = \frac{M_{Protein-PEG\ Conjugate} - M_{Protein}}{M_{TSTmPEG}} \qquad \text{Equation 1}$$

Table 2. Amount of mPEG chains attached to the surface of LYZ for the conjugates LYZ^{2k} and LYZ^{5k}.

Sample	mass/z	z	mol. wt.	n_{PEG} / protein	Chemical Structure
LYZ^{2k}	~34.9	1	34.9 kDa	10	LYZ(TsTmPEG2k)$_{10}$
LYZ^{5k}	~41-56	1	41-56 kDa	5 to 8	LYZ(TsTmPEG5k)$_{5\text{-}8}$

Lysozyme Activity after PEGylation

By PEGylation of the protein, the surface of the enzyme is highly changed. To investigate how this change on the surface affects the enzymatic activity of the protein, an activity assay was performed (Figure 20) where the native protein LYZ is compared to LYZ^{2k} and LYZ^{5k}. The assay is based on the ability of LYZ to cleave 1,4-β-linkages in peptidoglycan. A 4-metylumbelliferone-labeled triacetylchitotrioside was used as substrate for the activity assay (Scheme 6, Page 127). As the cleaved 4-metylumbelliferone is fluorescent, the amount of cleaved molecules from the triacetylchitotrioside by the enzyme is determined spectrometrically (λ_{EX}: 380 nm / λ_{EM}: 460 nm). The release of fluorophore is associated with the activity of the protein. By comparison of the increase of the fluorescence over time, a statement over the enzymatic activity of the protein after PEGylation can be made (

Table 3). The native protein LYZ shows an activity of 15.93 U/min. This growth rate is lowered to 3.00 U/min after PEGylation with mPEG2k (leading to LYZ^{2k}). This means, that 19% of the initial protein activity is remained even after high surface PEGylation. The main influence for the lowered protein activity is probably the dense brush-like structure of the PEG corona around the protein core of the conjugate. This-mPEG corona has a thickness of 3.6 nm (determined by DLS, described later in this section) and leads to a high shielding of the catalytic center of LYZ. For this reason, a lower amount of substrate can be converted. This is supported by the effect of the PEGylation with TsTmPEG5k. Hereby, the activity of LYZ^{5k} is even lowered to 1.17 U/min of the initial activity showing that a longer PEG chain leads to a higher decrease in activity. From this point, only the more active conjugate LYZ^{2k} was further investigated.

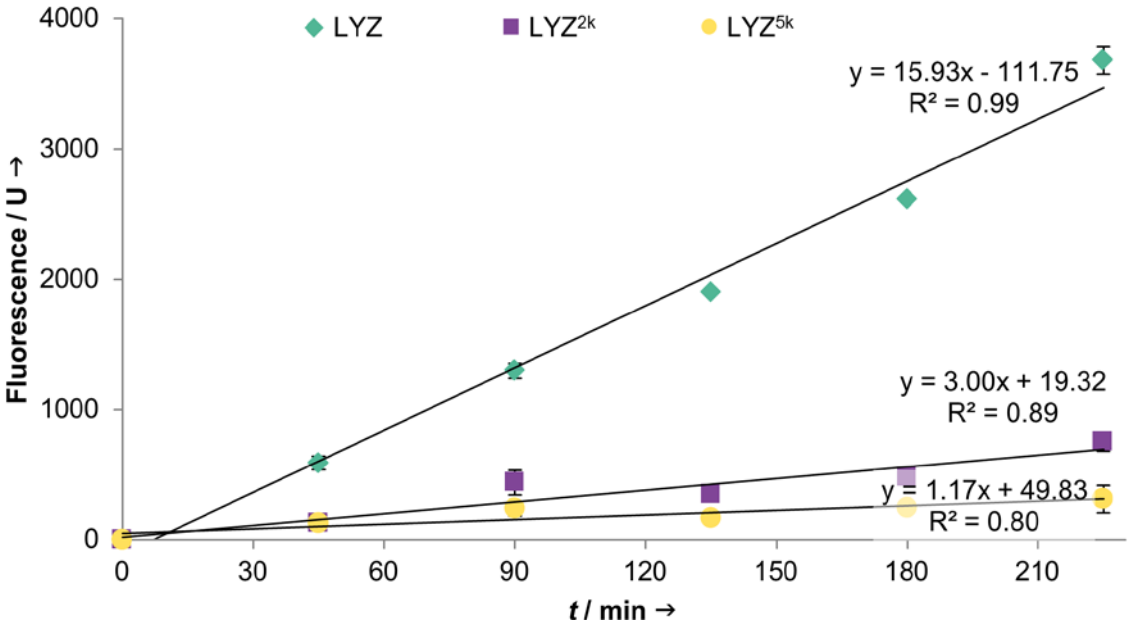

Figure 20. Activity assay of LYZ^{2k} (■) and LYZ^{5k} (●) in comparison with native lysozyme (◆). The remaining activity of the PEGylated protein is 19% compared to the original protein activity for LYZ^{2k} and even to 7% for LYZ^{5k}. In parts adapted from Fach *et al.*[147] Copyright (2016) American Chemical Society.

Table 3. Relative activity of LYZ-PEG conjugates with different chain lengths compared to the native protein.

Sample	**Slope / U min^{-1}**	**rel. Activity / %**
LYZ	15.93	100
LYZ^{2k}	3.00	19
LYZ^{5k}	1.17	7

Structural Integrity Lysozyme after PEGylation

Proteins consist of highly ordered secondary structure elements. To ensure that the loss of activity does not origin from a structural disintegration of lysozyme, the protein structure was investigated during the PEGylation process via circular dichroism (CD) spectroscopy. It is used to determinate and to observe changes in these structural segments. CD is defined as the unequal absorption of left-handed and right-handed circularly polarized light. When asymmetric molecules interact with light, they may absorb right- and left-handed circularly polarized light to different extents and also have different indices of refraction for the two waves.[151] For the special case of proteins, the chromophores of the amides of the polypeptide backbone are aligned in arrays; their optical transitions are shifted or split into multiple transitions. As a result, different structural elements show characteristic CD-spectra.[152] The two major structure elements are the *α*-helix and the *β*-sheet. *α*-helices have a positive band at 193 nm and negative bands at 222 nm and 218 nm.[153] Proteins with *β*-sheets have a positive band at 195 nm and a negative band at 218 nm.[151, 154] Disordered proteins have negative bands near 195 nm and low ellipticity near 210 nm.[155]

The CD-pattern is individual for each protein based on its structural segments. The loss in secondary structural elements is expected to lead to a decrease of the initial signals of the structural segments (*α*-helix and *β*-sheet) and an increased amount of unordered segments. The CD spectra of the PEGylated LYZ^{2k} is shown in Figure 21. A procedure as described for the protein PEGylation was performed and the influence of the reaction conditions on the protein structure was observed. Activated mPEG (A, so simulate the reaction conditions), *ω*-hydroxyl-mPEG (B, to observe the signal of unattached polymer in solution) or only buffer (C, to investigate the influence of heat treatment and the alkaline environment) were added to the protein solution and incubated. Additionally a solution containing LYZ only without heating (D, for the representation of native protein) and with heating to 80 °C (E, for heat induced denaturation) was used as reference. From the observed spectra, no significant change in the protein structure is observed for all samples, with the exception of the denaturated sample.

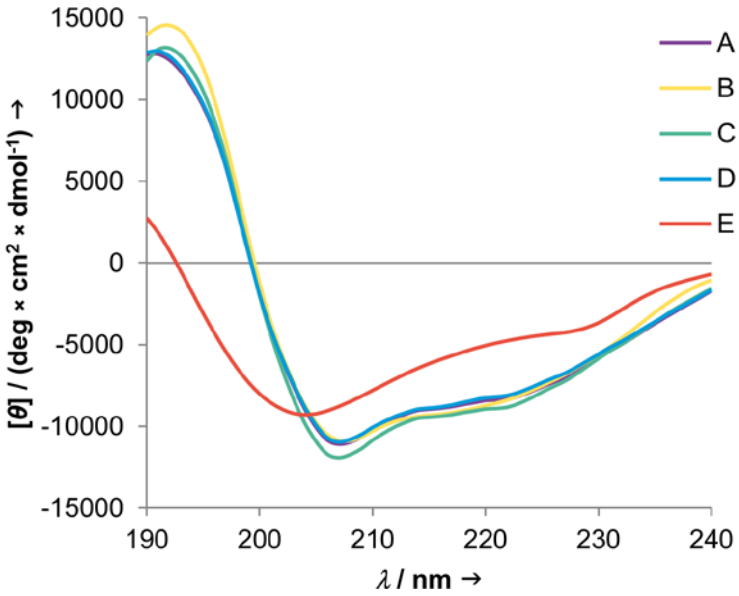

Figure 21. CD-Spectra of PEGylated protein (A, purple), mixture of LYZ and mPEG-OH (B, yellow) and LYZ only (C, green) incubated for 2 h under reaction conditions. For comparison, an untreated LYZ sample (D, blue) and an untreated sample measured at 80 °C (E, red) causing thermal denaturation. The spectra show that the protein retains its native structure after PEGylation. Reprinted from Fach *et al.*[147] Copyright (2016) American Chemical Society.

This result is additionally confirmed by the calculation of the secondary structure elements using DICHROWEB[156, 157] (Table 4). For calculation, the CONTIN-LL method was used with reference set 7[152]. The amount of observed *α*-helices slightly decreases (< 1.5%) whereas the total amount of *β*-sheets is minimally increased by 2%. More importantly, the amount of unordered structures remains unaffected. According to these results it can be assumed that no significant change of the secondary structure occurs during the surface PEGylation.

Table 4. Results summary of structural elements calculated with DICROWEB using the CONTIN-LL method (reference set 7[152]).

Sample	$\alpha_{regular}$	$\alpha_{disordered}$	α_{total}	$\beta_{regular}$	$\beta_{disordered}$	β_{total}	Turns	Unordered	Total
A	0.176	0.131	0.307	0.091	0.052	0.143	0.137	0.414	1.001
B	0.179	0.128	0.307	0.098	0.055	0.153	0.147	0.394	1.001
C	0.184	0.137	0.321	0.073	0.049	0.122	0.142	0.413	0.998
D	0.173	0.129	0.302	0.085	0.053	0.138	0.143	0.417	1.000
E	0.065	0.082	0.147	0.112	0.073	0.185	0.153	0.515	1.000

Besides the surface modification of the protein with heating under alkaline conditions, sonication of the PEGylated protein is used to form nanoparticles. Sonication produces high shear forces and local heat, when ultrasound is generated. Despite sonication is used for the cell lysis to isolate proteins from cells, it has to be secured, that this step does not affect the secondary structure of the protein-PEG conjugate. For this reason, the effect of the sonication conditions as used for particle preparation was investigated. The CD-spectra of LYZ^{2k} prior (solid line) and after sonication (dashed line) are presented in Figure 22. As previously seen for the surface PEGylation, no change in the CD-spectra is observed after sonication of a protein sample for 45 s. Therefore, also an influence of sonication on the secondary structure of the protein-PEG conjugate can be excluded.

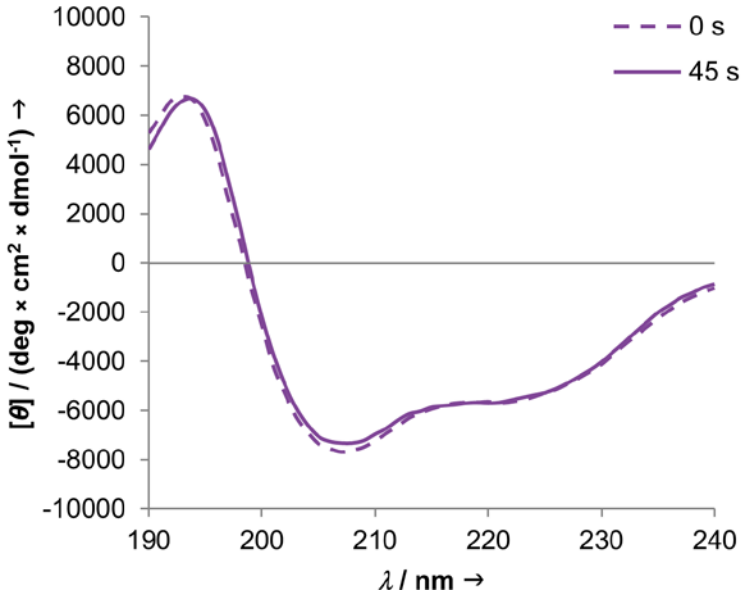

Figure 22. CD-Spectra of LYZ^{2k} prior sonication (dashed line) and after sonication for 45 s (solid line). Reprinted from *Fach et al.*[147] Copyright (2016) American Chemical Society.

Determination of Primary Amines on the Protein Surface

The loss of primary amines on the protein surface provides an additional insight in the extend of surface modification and can be analyzed by a 2,4,6-trinitrobenzenesulfonic acid (TNBS) assay.[158] Herein, the primary amines of lysines on the protein surface and the N-terminus react with the sulfonic acid group of TNBS and form a yellow-colored conjugate. The Amount of TNBS attached to the protein is determined by measuring the absorbance (λ = 405 nm) of the protein sample and comparing this result to a standard curve of free glycine in defined concentrations (Figure 62). Seven free amines were determined on the surface of unmodified lysozyme, what corresponds to the theoretic amount of six lysine residues on the protein surface and the additional N-terminus. After PEGylation of the protein with TsT-activated mPEG2k, no free amines were detected on the protein surface. Due to the high steric demands of the mPEG2k chain, it is possible that the polymer shields remaining free amines on the surface. Furthermore, TsT-activated mPEG is known to react not only with the NH_2-bearing lysines but also with the nucleophilic amino acids tyrosine and histidine on the protein surface (not detectable by TNBS assay). For this reason – despite its wide use in protein PEGylation[144, 159] – the TNBS assay gives only a good insight on the loss of amines on the surface but not the exact amount of mPEG2k chains on the protein surface.

Change of Lysozyme Surface Charge by PEGylation

The successful modification of the nucleophilic amino acids on the protein surface is also provided by a shift in the isoelectric point (pI) of the protein. The pI represents the pH value at which a protein carries no electrical charge in the statistical mean. A change in the amount of positively or negatively charged groups on the protein surface results in a shift of the pI value. The applied protein surface modification is based on the reaction of nucleophilic groups, for example primary amines on the protein surface with TsT-activated mPEG. After a successful conjugation of the protein, the amount of free amines on the surface is reduced and the remaining carboxylic groups dominate the surface charge. This loss in positively charged groups results in a decrease of the pI as the negatively charged carboxylic groups remain unaffected. The surface charge of a macromolecule at a desired pH value is represented by its zeta potential.[160] Consequently, the pI of a macromolecule can be estimated by measuring the zeta potential of a sample over a broad pH range (Figure 23). From this method, the pI of the

protein shifts from 5.8 for the native, unmodified protein to 2.1 of the PEGylated protein. By these results it is expected, that a high modification of the protein surface occurred during the PEGylation step.

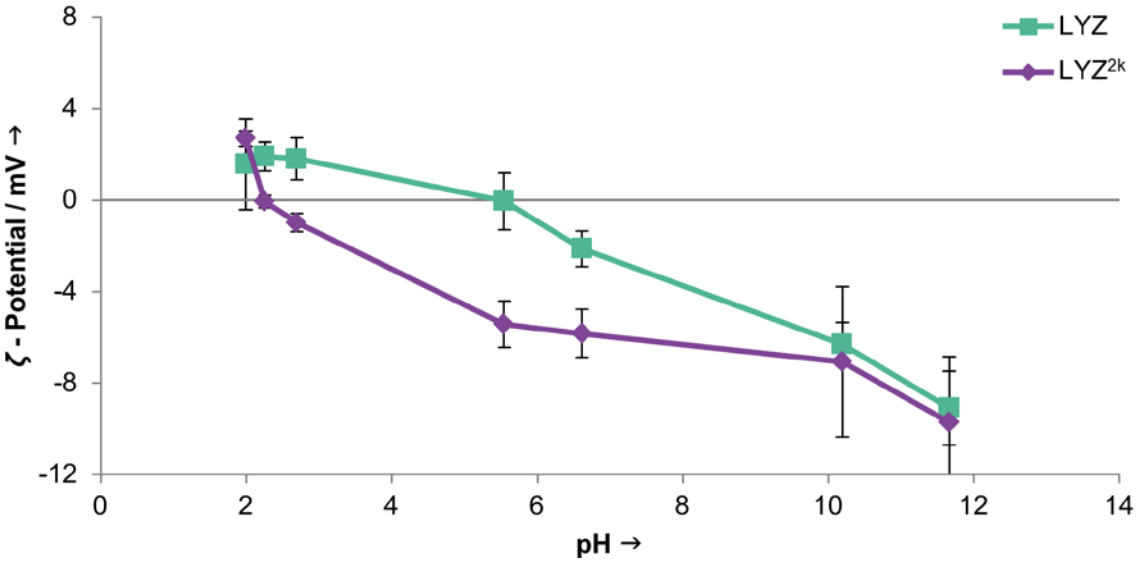

Figure 23. Change in the zeta potential of LYZ (■) and LYZ(TsTmPEG2k) (◆) over a pH range from pH 2 to pH 12. The pH value at which the sample shows no electrical potential represents the isoelectric point and shifts by surface modification of the amines present on the protein surface from 5 of unmodified protein to 2.1 of PEGylated protein.

Hydrodynamic Diameter Increase after PEGylation

Dynamic light scattering (DLS) was used to determine the increase of the hydrodynamic diameter of LYZ after PEGylation. For the native protein, a d_{hyd} of 3.6 nm was detected. This corresponds well to the reported lysozyme size of 4.5 × 3.0 × 3.0 nm.[161] With a monomer length of 0.35 nm,[162] the maximal length of a fully extended mPEG2k-chain (~44 repetition units) attached to the protein surface is 15.4 nm. It is not expected for the conjugate to show an increased diameter by 30 nm as polymers are highly unordered in solution due to entropic effects. The PEGylated sample of LYZ^{2k} shows an increased diameter in the mean of 10.8 nm. Accordingly, LYZ is surrounded by an mPEG-layer with a thickness of around 3.6 nm

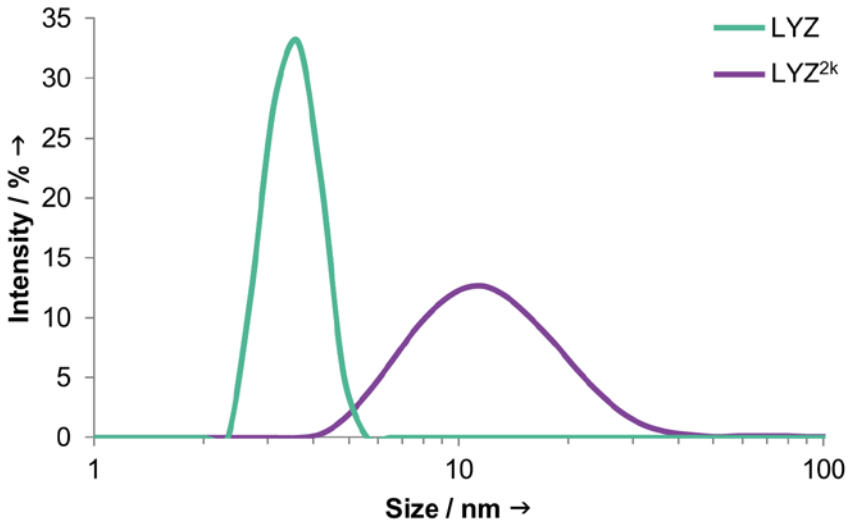

Figure 24. Size distribution determined by dynamic light scattering (DLS) shows a hydrodynamic diameter for native LYZ of 3.60 ± 0.16 nm (green) and for LYZ^{2k} a hydrodynamic diameter of 10.80 ± 0.17 nm (purple). Reprinted from Fach *et al.*[147] Copyright (2016) American Chemical Society.

Polymer Arrangement on the Protein Surface

From the amount of mPEG on the protein surface and the d_{hyd} of the protein, the shape of the attached polymers on the protein surface can be estimated. Generally, polymers can form two different shapes upon attachment to a surface. The 'mushroom' structure represents a polymer expansion similar to the polymer in solution. The 'brush'-like structure represents a stretched formation of the Polymer.[162, 163]. The conformation depends on the grafting density of the polymer to the surface. A graphical illustration of the polymer conformations is presented in Figure 68 as supplemental data (Section 6.2). By the diameter of the native lysozyme of 3.6 nm and the assumption of a spherical shape, the surface area of the protein is 40.7 nm^2. With the amount of mPEG chains on the surface (10), one mPEG chain is grafted per 4.07 nm^2 (0.25 mPEG chains per nm^2). Hence the distance between two mPEG chains is approx. 2.3 nm. From this distance, the conformation of the polymer on the surface of the protein surface can be estimated. The minimal distance required between grafted polymers on a surface to form a mushroom conformation is defined as the Flory radius (*R*). Polymers with less space than *R* have lower conformational freedom and a brush conformation is obtained. Equation 2 is used to calculate R with the polymer chain length (*n*), monomer length (α) and solvent type (ν).

$$R = \alpha n^{\nu} \qquad \text{Equation 2}$$

For the used mPEG2k chain in water, *R* is 3.4 nm (α =0.35 nm, n = 44, ν = 3/5)[162]. This means, for a brush-like structure, the polymers have to be grafted with a maximum of 6.8 nm apart (one mPEG chain per 11.6 nm^2, 0.086 mPEG2k chains per nm^2).As the distance between two neighboring mPEG chains grafted to the protein surface is 35% of *R*, it is considered that a brush like structure of the mPEG chains is present.

When mPEG5k is regarded, *R* increases to 6.0 nm (α =0.35 nm, n = 114, ν = 3/5)[162]. Accordingly, for a brush-like structure, the polymers have to be grafted with a maximum of 12 nm apart (one mPEG chain per 36 nm^2, 0.028 mPEG5k chains per nm^2). It was observed by MALDI-ToF MS that 5–8 mPEG chains are attached to the LYZ surface area (40.7 nm^2). This means that on mPEG chain is grafted per 5.1 to 8.1 nm^2. This means that the distance between two mPEG5k chains ranges from 14 to 22% of *R*. This shows – despite a lower total amount of mPEG chains – a higher mPEG density for mPEG5k than for mPEG2k. This might be an additional explanation for the decreased protein activity of LYZ^{5k} compared to LYZ^{2k}.

Solubility of PEGylated Lysozyme in Organic Solvents

To consider the protein-PEG conjugate as suitable for the striven nanoparticle preparation procedure, it needs to be soluble in a water immiscible organic solvent. For most native proteins, this is not the case. To the best of my knowledge only surface modification can lead to a full solubility in organic solvents e.g. by alkylation[164, 165] or PEGylation.[160] The enhanced solubility of the protein-PEG conjugate LYZ^{2k} is shown in Figure 25. A complete solubility is observed for $CHCl_3$ (A), CH_2Cl_2 (B) and toluene (F). LYZ^{2k} remains insoluble in EtOAc (C), EtOH (D) and hexane (E). This solubility behavior corresponds to the solubility of the conjugated polymer PEG. Therefore it can be concluded that its solubility behavior of PEG was successfully transferred to the protein. DCM was chosen for further investigation of the solubility behavior of LYZ^{2k} as the use of chloroform raises concerns about its higher toxicity and the low vapor pressure of toluene makes it unsuitable for an evaporation based NP-preparation method.

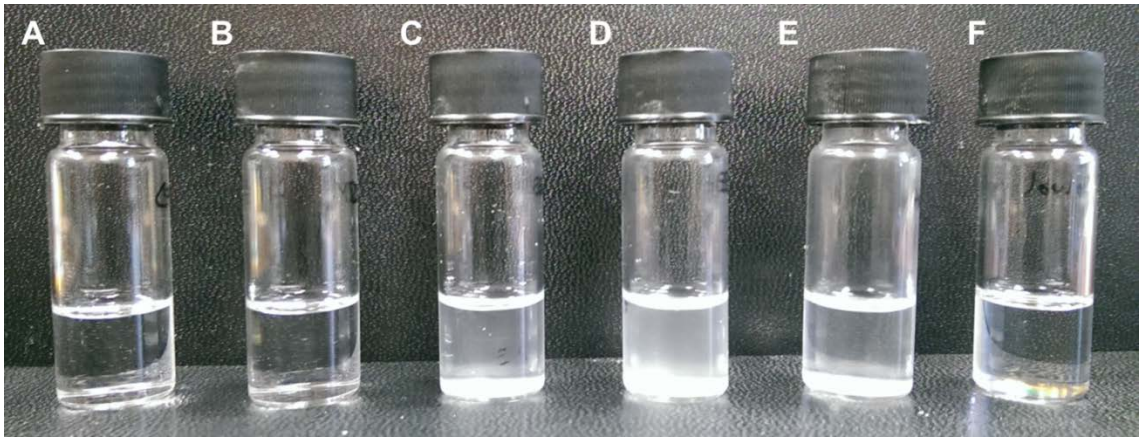

Figure 25. Solubility of LYZ^{2k} in $CHCl_3$ (A), CH_2Cl_2 (B), EtOAc (C), EtOH (D), hexane (E) and toluene (F). The modified protein is insoluble in EtOAc, EtOH, hexane and soluble in $CHCl_3$, CH_2Cl_2, toluene. Reprinted from Fach *et al.*[147] Copyright (2016) American Chemical Society.

Preference of Solubility after PEGylation

More important than the solubility of the protein-PEG conjugate in DCM is the effect that an organic environment should be preferred over an aqueous. The lipophilic preference is highly important as it must be secured that the protein-polymer conjugate remains in the DCM droplet and is not transitioning into the aqueous phase during the planned emulsion based particle preparation. For this, a solvent extraction experiment was performed. The highly PEGylated LYZ^{2k} was dissolved in DCM and layered with the same amount of water. After 24 h the two solvents were separated and absorption spectra from λ = 250 to 400 nm were recorded. The aromatic amino acids of the protein absorb light at a wavelength of around 280 nm. Accordingly a detected absorption signal in this area indicates the presence of the protein conjugate. After 24 h of vigorous mixing, no protein signal is detected in the aqueous layer whereas the DCM-layer shows an intense protein signal. This demonstrates that native protein undergoes a lipophilic switch by PEGylation in a high ratio from the hydrophilic native state to a rather hydrophobic one and cannot be extracted back from a DCM phase by water.

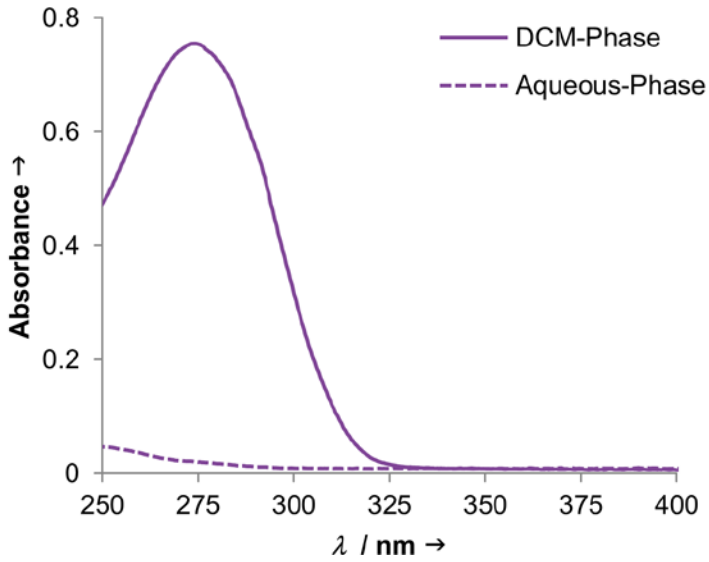

Figure 26. Comparison of LYZ^{2k} absorbance after vigorous mixing of the two layers for 24 h. The broad peak at 280 nm indicates the presence of LYZ^{2k} in the organic phase (solid line) after phase separation. The aqueous phase (dashed line) does not show any protein signal. Reprinted from Fach *et al.*[147] Copyright (2016) American Chemical Society.

3.1.2 Fluorescence Labeling of PEGylated Lysozyme

Fluorescence labeling of the protein-PEG conjugate allows tracking of the protein material in various *in vitro* and *in viv*o applications. The fluorescence has to be chosen carefully depending on the desired application. Each fluorophore has a defined combination of excitation and emission wavelengths. For a differentiation of two or more fluorescent samples at least one parameter needs to be different. If the emission of the dyes is similar, the dyes can be excited separately by using different wavelengths. On the other hand, if the excitation wavelength of two fluorophores is similar, the dyes can be distinguished by their emitted light. In this case the fluorophore fluorescein was chosen for tracking the protein material. With an excitation wavelength of 490 nm, the fluorescent excitation is similar to the wavelength for the excitation (λ_{EX}) of doxorubicin (λ = 490 nm) that will be used to establish the particle system. Therefore, an excitation of fluorescein is always linked with an excitation of DOX. The separation of the dye and DOX is performed by their difference in the emitted light. Fluorescein has an emission maximum (λ_{EM}) of λ = 520 nm whereas the emission of DOX has its maximum at λ = 590 nm with shoulders at λ = 560 nm and λ = 630 nm. By the selection of a suitable filter system, the emitted light from these two fluorophores can be determined separately.

Fluorescein is thus suitable as dye for the labeling of the protein NP-matrix to track the matrix isolated from the encapsulated drug.

Coupling of 6-Aminoflurescein to PEGylated LYZ

The fluorescent dye was attached to the surface of the protein via a carbodiimide (EDC) mediated amide coupling reaction (Scheme 3). First, the carboxylic group on the protein gets activated by EDC and forms an active ester intermediate that is highly reactive towards primary amines. Excess dye was removed via centrifugal filter devices as this provides high purification rates in very low time. The labeling of the protein-PEG conjugate was carried out after successful surface modification to avoid cross-linking between two individual proteins. Due to the high PEGylation, the surface amines of the proteins are saturated with mPEG chains and not available for further reactions. The shielding effect of the PEG chains might affect the labeling efficiency but only a minimal fluorescence labeling is sufficient for most *in vitro* applications like cell sorting or confocal microscopy. Additionally, labeling in a low ratio avoids that the fluorescent dye changes the surface properties the initial material.

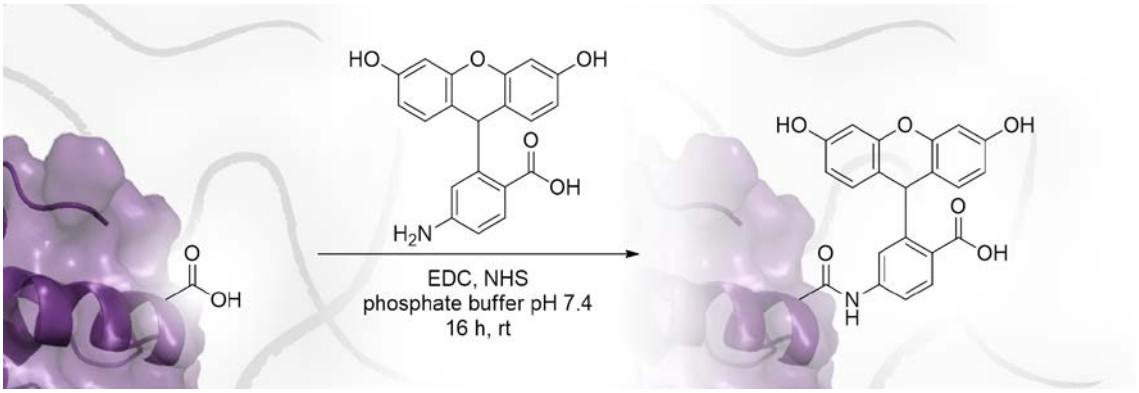

Scheme 3. Carbodiimide mediated attachment of 6-aminofluorescen to carboxylic amino acids on the surface of the protein. Carboxylic groups are activated by *N*-(3-dimethylaminopropyl)-*N*′-ethylcarbodiimide hydrochloride (EDC) and NHS catalytically forms a more stable intermediate that is highly reactive towards the nucleophilic amine of 6-aminofluorescein. The reaction is performed in phosphate buffer (0.1 M, pH 7.4) at room temperature for 16 h.

Figure 27 shows the successful fluorescence labeling of LYZ^{2k} to F_ LYZ^{2k} in a SDS-PAGE gel. The left side of the image shows the coomassie blue staining of the gel with the marker (lane M), native LYZ (lane 1), LYZ^{2k} (lane 2) and F_LYZ^{2k} (lane 3). By this staining method, no difference between the protein bands of the PEGylated samples is observed prior and after

labeling. The right side of Figure 27 shows a fluorescence image of the gel. Here, only the marker band and the fluorescently labeled sample of F_LYZ^{2k} are visible. Additionally, no free dye is visible in the gel. This shows that 6-aminofluorescein was successfully attached to the protein surface.

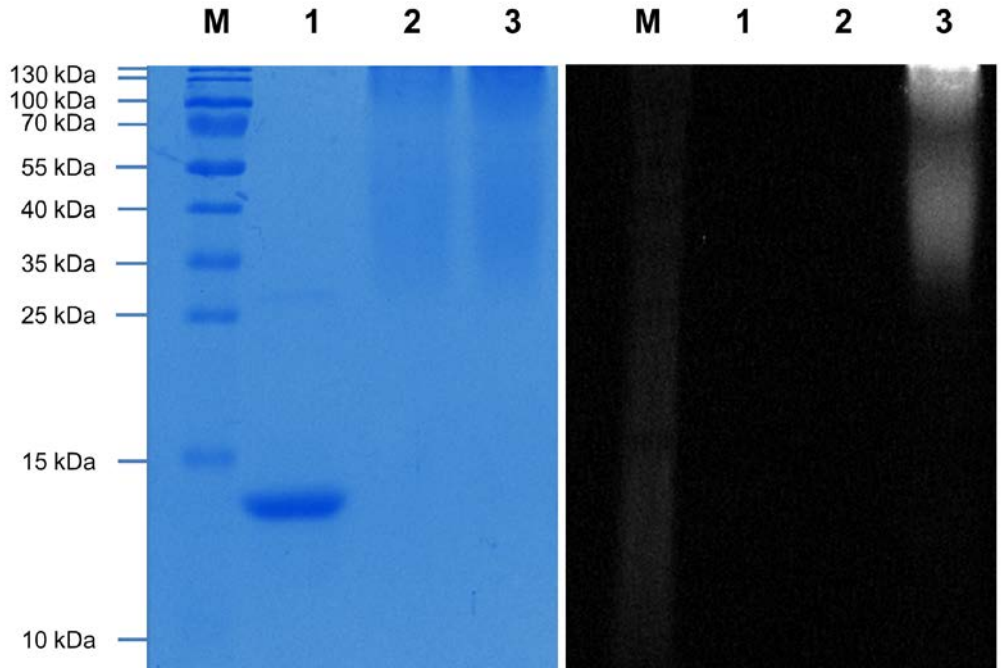

Figure 27. SDS-PAGE of the reference marker (lane M, 5 μL), unmodified lysozyme (lane 1, 15 μg), LYZ^{2k} (lane 2, 30 μg) and fluorescence labeled protein F_ LYZ^{2k} (lane 3, 30 μg). The polyacrylamide content was 15% with a thickness of 0.75 mm (first 90 V, 60 min; then 200 V, 30 min). The gels show no trace of unmodified lysozyme after PEGylation (lane 2) and the successful attachment of fluorescein to the PEGylated protein (lane 3, right). Reprinted from Fach *et al.*[147] Copyright (2016) American Chemical Society.

Amount of Fluorescein Attached to the Protein Surface

The amount of fluorescein on the protein surface was determined by comparing the fluorescence of the protein to an external standard dilution of the dye. The protein was dissolved in a concentration of 573 nM and the fluorescence was compared to a standard dilution ranging from 200 to 12 nM of free fluorescein. The fluorescence signal of the protein sample corresponds to a fluorescein concentration of 64.5 nM. As the concentration of the protein sample is known to be 573 nM, the ratio of fluorescein per protein is 0.11. This means, that approximately every ninth protein carries a fluorescent dye. This amount of dye is sufficient for the intended *in vitro* analysis methods. Furthermore, as only every ninth protein

conjugate bears a fluorophore, a change of the physical behavior of the sample due to fluorescence labeling can be excluded.

3.1.3 Preparation of Empty and Doxorubicin-loaded Nanoparticles

The lipophilic lysozyme-PEG conjugate is now suitable to serve as material for a single emulsion-based nanoparticle preparation. It can now be dissolved alone or with a hydrophobic drug in DCM. Formation of an emulsion then leads to stable nanoparticles. Here, doxorubicin is used as hydrophobic model drug since it has been well studied *in vitro* and *in vivo*.

Desalting of Doxorubicin

As the commercially available form of doxorubicin (DOX) is in a protonated ammonium state forming a hydrochloride salt Hence this salt (DOX × HCl) is only hardly soluble in DCM the drug has to be transferred in its neutral form (DOX) to obtain a high solubility in DCM since this is required for the later particle preparation. The primary amine on the 4-position of the tetrahydropyran ring has a pK_a value of 8.2.[166] Thus, the ammonium form can be easily deprotonated to the free amine under mild basic conditions. For this method the DOX × HCl was dissolved in water and triethylamine (pK_a 10.8) was added. The desalted DOX was extracted from the aqueous phase with DCM with a yield of 80%.

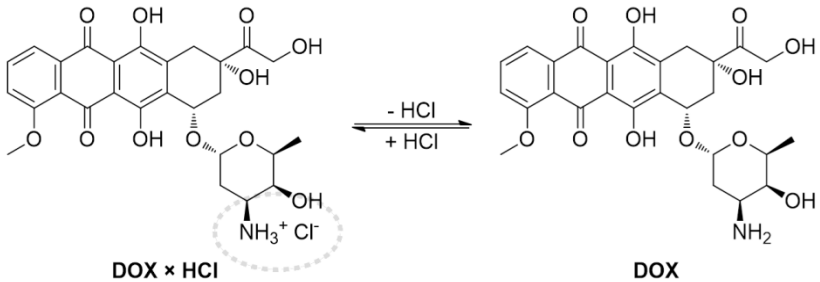

Scheme 4. Desalting of the ammonium hydrochloride salt (framed in grey) of doxorubicin (DOX × HCl) leads to the amine form of the drug (DOX).

Preparation of Lysozyme-based Nanoparticles by an Emulsion Technique

Nanoparticles are prepared by a nanoemulsion technique, where evaporation of the organic solvent leads to a stable NP suspension in an aqueous solution (Figure 28). This method is described in a similar manner for synthetic polymers[167, 168] or other lipophilic biopolymers like polysaccharides.[169] In the first step, the NP material is dissolved in the highly volatile organic solvent DCM and layered with a five-fold excess of PBS buffer. Sonication with an ultrasonic homogenizatior forms a stable oil-in-water (o/w) emulsion. Nano-sized oil droplets are evenly distributed in the aqueous environment. As presented earlier, the protein-PEG conjugates remain in the oil droplets and take up a spherical preorganized state. Surprisingly, due to the amphiphilic character of PEG, no additional stabilizing agent such as polyvinyl alcohol is needed to stabilize the nano-emulsion. Since DCM is used as oil component, the organic layer evaporates at room temperature due to the high vapor pressure of the solvent. By this, the nano-sized droplets become increasingly smaller and the encapsulated material in the droplets self-assembles into a particle matrix of tightly packed individual proteins. Now, the proteins prefer the hydrophobic intermolecular interactions and form stable particles without additional cross linking of the material. This method allows the preparation of both, empty and drug-loaded nanoparticles. Encapsulation of hydrophobic drugs can be performed by adding the drug molecule to the DCM layer along with the PEGylated protein. Based on the hydrophobic properties of the drug, it remains in the DCM layer whilst the preparation steps in the same manner as the PEGylated protein. The drug is entrapped in between the protein-matrix when DCM evaporates from the organic nano-droplets. The preparation of drug-loaded NPs is presented step-by-step in Figure 29. The protein-PEG conjugate is dissolved in DCM and covered with a layer of PBS (A). In the next step, a sonicator tip is placed slightly above the DCM layer (B). Emulsification creates an oil-in-water nano-emulsion (C). Evaporation of DCM (D), followed by dialysis, leads to a stable suspension of nanoparticles.

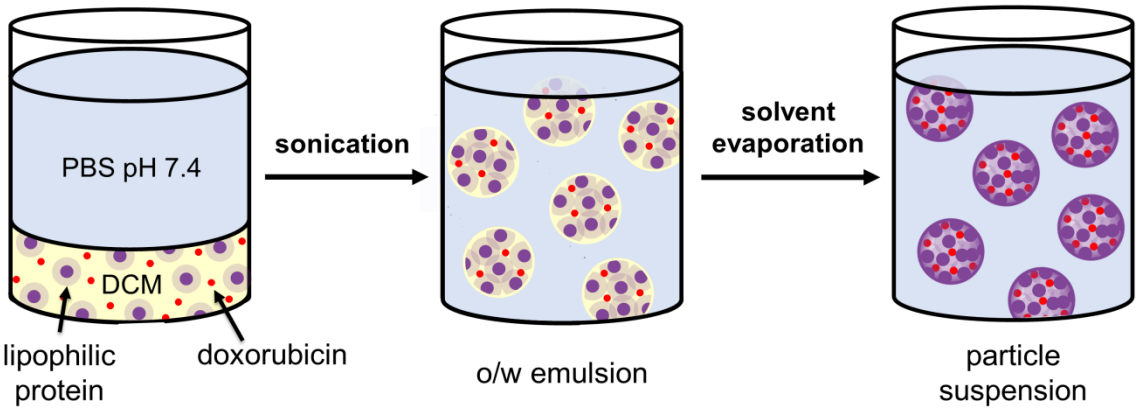

Figure 28. Protein-based nanoparticles are prepared by sonification of the PEGylated proteins and the drug dissolved in DCM with an aqueous buffer phase. Sonication forms a stable oil-in-water emulsion. Evaporation of the volatile organic solvent and purification by dialysis leads to a suspension of stable nanoparticles. Partially adapted from Fach *et al.*[147] Copyright (2016) American Chemical Society.

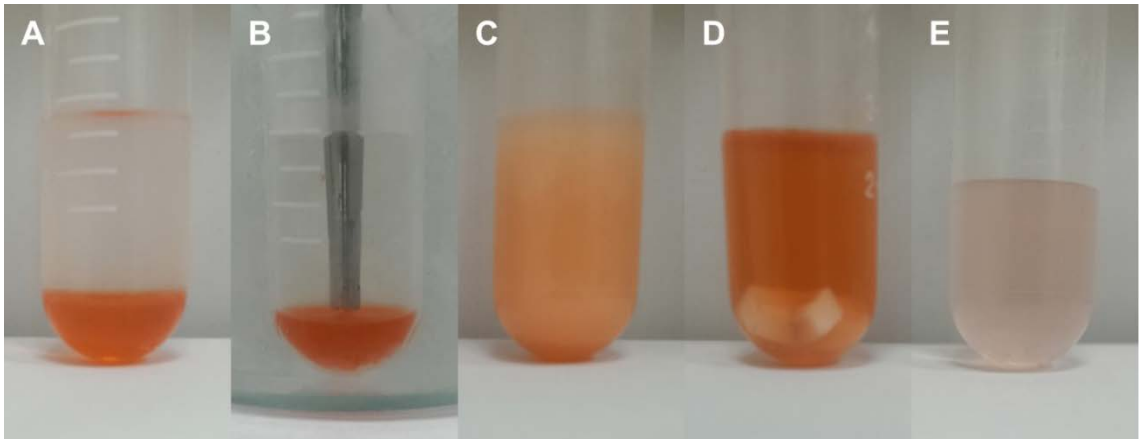

Figure 29. Step by step particle preparation procedure (A to E). Doxorubicin and LYZ^{2k} are dissolved in DCM and covered with PBS (A). Sonication (B) forms a stable oil/water emulsion (C). Evaporation of DCM (D) and dialysis leads to a stable protein nanoparticle suspension (E). Reprinted from Fach *et al.*[147] Copyright (2016) American Chemical Society.

The scattering effect of a nanoparticle suspension for light in the range from λ = 40 to 900 nm is known as the Tyndall-effect. Figure 30 shows suspensions of DOX-loaded and empty NPs in comparison to a solution without NPs. The colloidal character of the nano-suspension is visualized by the scattering of a green laser beam.

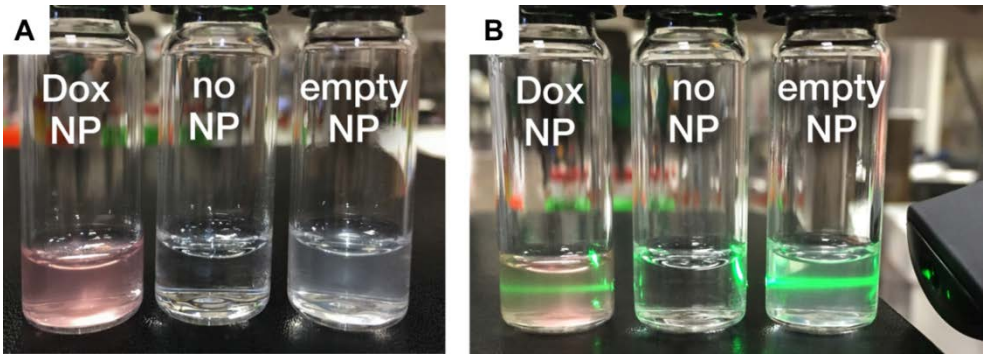

Figure 30. DOX-loaded (left) and empty nanoparticles in PBS solution (right) in comparison to a solution without nanoparticles in the middle (A). The scattering beam of green laser light (caused by the Tyndall effect) visualizes the colloidal character of the nano suspensions (B). Reprinted from Fach *et al.*[147] Copyright (2016) American Chemical Society.

Size Determination by Nanoparticle Tracking Analysis (NTA)

The size of the nanoparticles after purification was determined using various methods. Nanoparticle tracking analysis is a relatively newly developed method by Malvern instruments. The measurement is based on the Brownian motion of the particles in liquid. Here, a laser illuminates the particle sample and a video camera is used to capture the scattered light. The particle movement is calculated by the Stokes-Einstein equation. Depending on the particle type the range of sie determination by this method is from 10 to 1000 nm.[170] Particles are diluted in water to a final concentration of 2 μg/mL. Each measurement represents the mean of five individual runs over a time of 30 s. An automatic syringe pump was used for a user-independent change of the measured particle frame.

The size distribution determined by NTA is presented in Figure 31. The statistical details of representing the size distribution of the particles are presented in Table 5. The mean particle diameter d_{mean} represents the average diameter of all measured particles in the suspension with the standard deviation stated as SD. The size of the highest population present in the NP

suspension is presented as the modal diameter (d_{mode}). D_{90}, D_{50} and D_{10} describe that 90%, 50% or 10% respectively are below this size.

Both NP-samples show a mean size of the particles around 100 nm. Empty NPs are thereby with a mean diameter of 94.6 nm slightly smaller than DOX-loaded NPs that have a size of 101.9 nm. The standard deviation of the nanoparticles is similar for both samples (38.2 ± 2.4 nm for empty and 38.6 ± 2.7 nm for drug-loaded NPs). These results show, that encapsulation of DOX into NPs has no significant effect on the particle size.

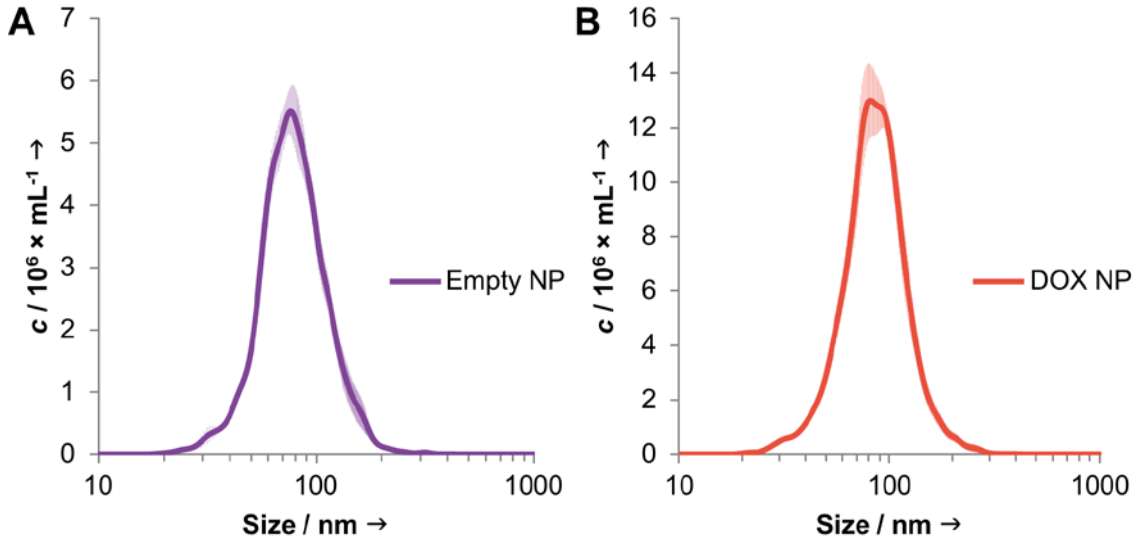

Figure 31. Nanoparticle tracking analysis shows for empty particles (A) a mean diameter of 94.6 ± 1.9 nm (mode: 75.5 ± 2.0 nm) and for DOX-loaded particles (B) a mean diameter of 101.9 ± 2.7 nm (mode: 89.1 ± 5.0 nm). Adapted from Fach *et al.*[147] Copyright (2016) American Chemical Society.

Table 5. Detailed particle size and statistical parameters of empty and DOX-loaded NPs. Mean size and SD (standard deviation) correspond to the arithmetic values calculated based on the sizes of all particles detected in the NTA measurement. Mode values describe the average size of the main particle population. D_{90} (D_{50}, D_{10}) value describes that 90% (50%, 10%) of particles in the sample are below this size.

Sample	d_{mean} /nm	d_{mode} /nm	SD /nm	D_{90} /nm	D_{50} /nm	D_{10} /nm
Empty NP	94.6 ± 1.9	75.5 ± 2.0	38.2 ± 2.4	136.3± 5.8	85.8 ± 1.0	56.8 ± 0.4
DOX NP	101.9 ± 2.7	89.1 ± 5.0	38.6 ± 2.7	148.1 ± 4.8	93.8 ± 4.8	62.3 ± 1.7

Size Determination by Dynamic Light Scattering (DLS)

Additionally, the size of the obtained NPs was determined by dynamic light scattering (DLS) with a Zetasizer Nano ZS by Malvern Instruments. This method is also based on the Brownian movement of the particles in liquid and particle size is calculated by the Stokes-Einstein correlation. In contrast to NTA, DLS does not visualize the particles individually. Here the time dependent scattering intensity fluctuation – caused by the Brownian movement of the particles – is analyzed. An exponential autocorrelation is then used to calculate the particle parameter.[171] The mean particle size in diameter is described by the Z-average. The number represents the diameter of the highest NP-population in the suspension. The polydispersity index (PDI) describes the polydispersity of the sample. Usually, a PDI of 0 characterizes a monodisperse particle sample whereas a PDI of 1 reflects a high polydispersity of the sample. The size distribution of empty and DOX-loaded NPs is presented in Figure 32A directly after NP preparation and in Figure 32B after storage for 6 months at +4 °C. The detailed information of the NP size is presented in Table 6. The hydrodynamic diameter and ζ-potential of the particles was measured in aqueous buffer using a Malvern Zetasizer Nano ZS and dynamic light scattering (DLS) technology.

Table 6. Detailed size determination by DLS for empty and DOX-loaded nanoparticles. The size directly after particle preparation is compared to a sample stored for 6 month at +4 °C in the dark.

Sample	Z-Average /nm	PDI /nm
Empty NP	115.0 ± 0.17	0.250
Empty NP after 6 months	115.8 ± 1.12	0.243
DOX NP	104.3 ± 5.05	0.321
DOX NP after 6 months	99.0 ± 0.65	0.293

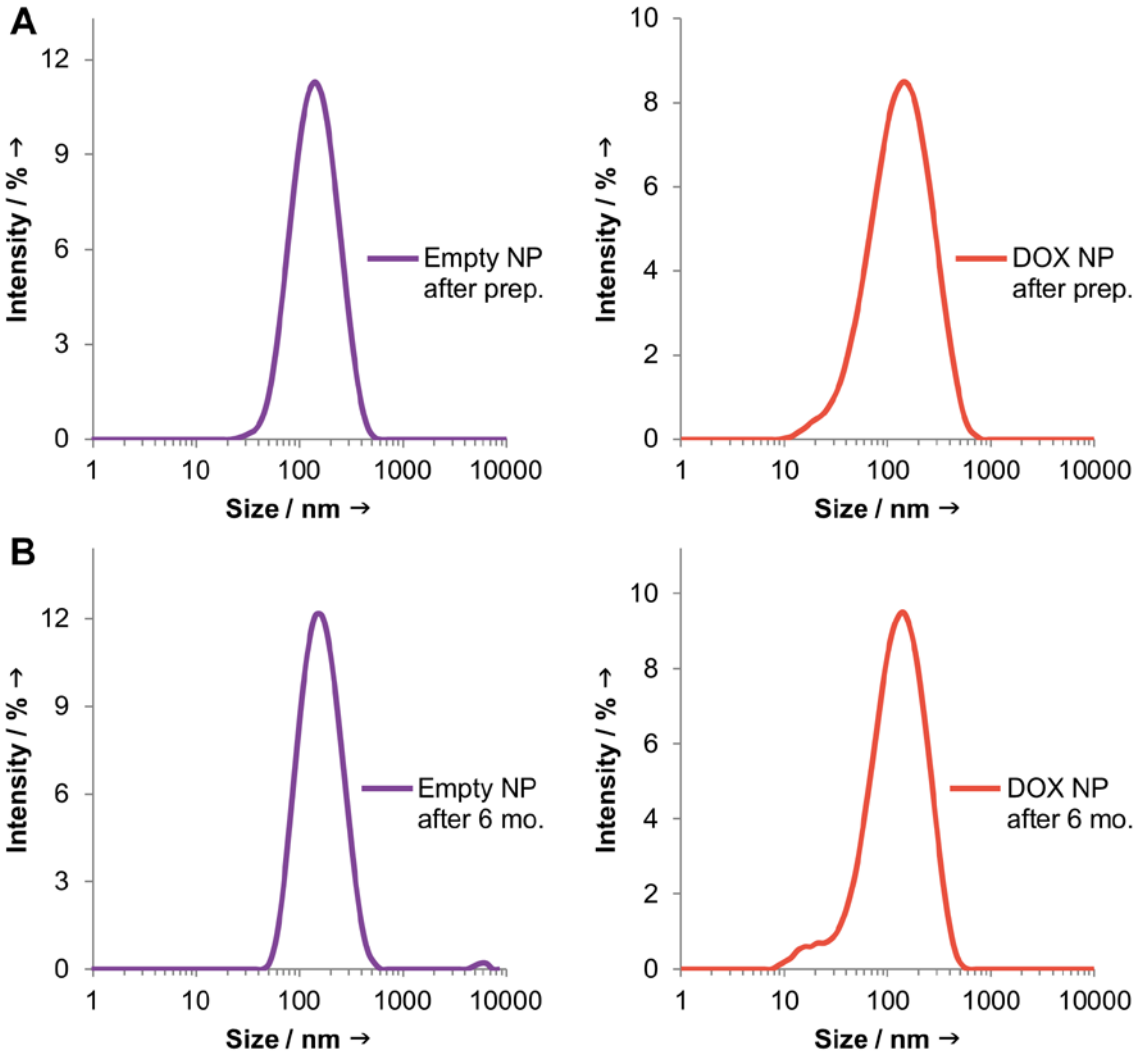

Figure 32. Size distribution determined by dynamic light scattering (DLS) shows a hydrodynamic diameter (Z-average) directly after nanoparticle preparation (A) for empty NPs of 115.0 ± 0.17 nm (PDI: 0.250) and for DOX-loaded NPs of 104.3 ± 5.05 nm (PDI: 0.321). To test long-term stability, size distribution was measured again after 6 month (B) and shows a Z-average for empty NPs of 115.8 ± 1.12 nm (PDI: 0.243) and for DOX-loaded NPs of 99.0 ± 0.65 nm (PDI: 0.293). Adapted from Fach *et al.*[147] Copyright (2016) American Chemical Society.

Surface Charge of Empty and Drug-loaded Nanoparticles

As described previously for the surface modification of LYZ, the ζ-potential represents the surface charge of the nanoparticle. The measurement was performed with a Zetasizer directly after particle purification in PBS buffer. This buffer was chosen, as its osmolality and ion concentration represent those of the human body. DOX-loaded as well as empty NPs were investigated. Since the ζ-potential is highly depending on the buffer conditions, the unmodified protein LYZ and the PEGylated LYZ conjugate LYZ^{2k} were used as reference under the same buffer conditions as the nanoparticles for a better comparison. Empty NPs consist completely of LYZ^{2k}. Therefore, the same surface charge as for the single proteins is expected from the nanoparticle. This is also the expected case for DOX-loaded NPs since the drug is entrapped inside of the NP-matrix and not presented on the surface. The ζ-potential of the samples is presented in Table 7. As expected from the shift in the pI of the protein (see previous section, Figure 23), the ζ-potential is decreased by the surface PEGylation from + 3.77 ± 0.44 mV for LYZ to – 3.03 ± 1.18 mV of LYZ^{2k}. The surface charge of the resulting nanoparticles for both, empty (– 3.12 ± 0.56 mV) and DOX-loaded NPs (– 2.89 ± 0.75 mV) corresponds precisely to the surface charge of the sample of single proteins.

Table 7. ζ-potential of native lysozyme, $LYZ(TsT\text{-}mPEG)_{10}$, empty particles and DOX-loaded particles.

Sample	**ζ-Potential / mV**
Lysozyme	+ 3.77 ± 0.44
LYZ(TsTmPEG2k)	– 3.03 ± 1.18
Empty LYZ NPs	– 3.12 ± 0.56
DOX-loaded LYZ NPs	– 2.89 ± 0.75

Transmission Electron Microscopy (TEM)

Transmission Electron Microscopy (TEM) was used to visualize the process of the nanoparticle preparation from the surface modification to the final particle. In this method an image is formed by detection of electrons passing a thin sample. The density difference by different thickness and composition of the specimen is thereby the responsible for the contrast of the image. The PEGylation step of the protein is shown in Figure 33. After surface PEGylation, a faint halo of the soft polymer is formed around the more dense protein core (Figure 33B). This corresponds to the previous results where PEG forms a soft corona around the protein and thereby increases its size.

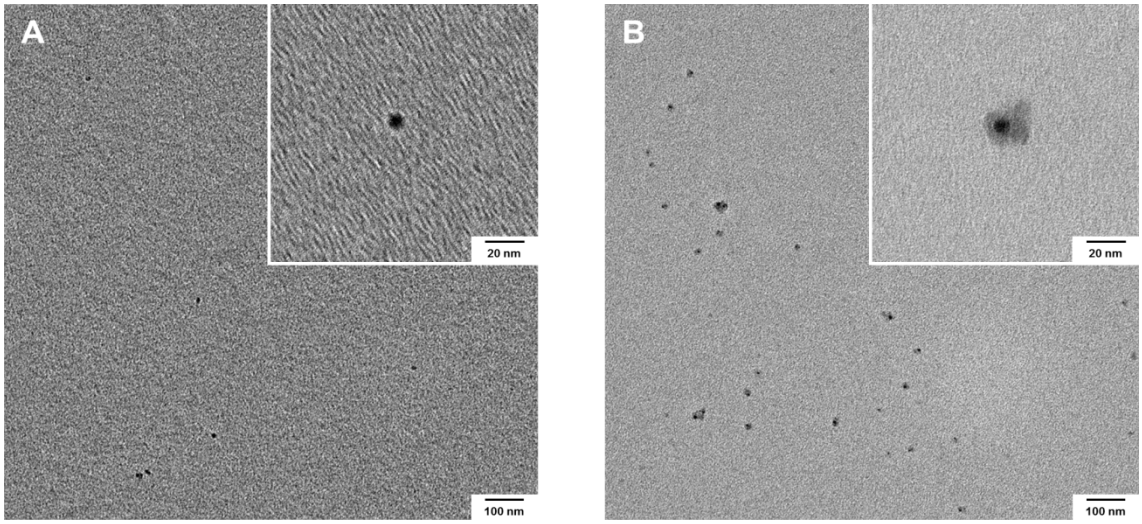

Figure 33. TEM images of native lysozyme (A) and LYZ^{2k} (B). A faint halo around the more dense protein core indicates the successful covalent attachment of PEG to the surface of the lysozyme (B). Reprinted from Fach *et al.*[147] Copyright (2016) American Chemical Society.

TEM images also provide a visual idea about the possible morphology and composition of the nanoparticle systemFigure 34. The magnification of empty particles in Figure 34A confirms the assembly of multiple proteins into single particles. Here it is visible, that the particles consist of multiple PEGylated proteins (as presented in the magnification of Figure 33B). The drug-loaded NPs show a more dense structure that most likely results from the DOX entrapment. However, due to the type of measurements (particles are measured in a dry state) and the nature of the rather soft material of the NP a size determination from TEM is not appropriate. In a dry state, the attached PEG starts to shrink and the size of the protein-conjugate and the NP is expected to change and does not represent the size of the sample in solution.

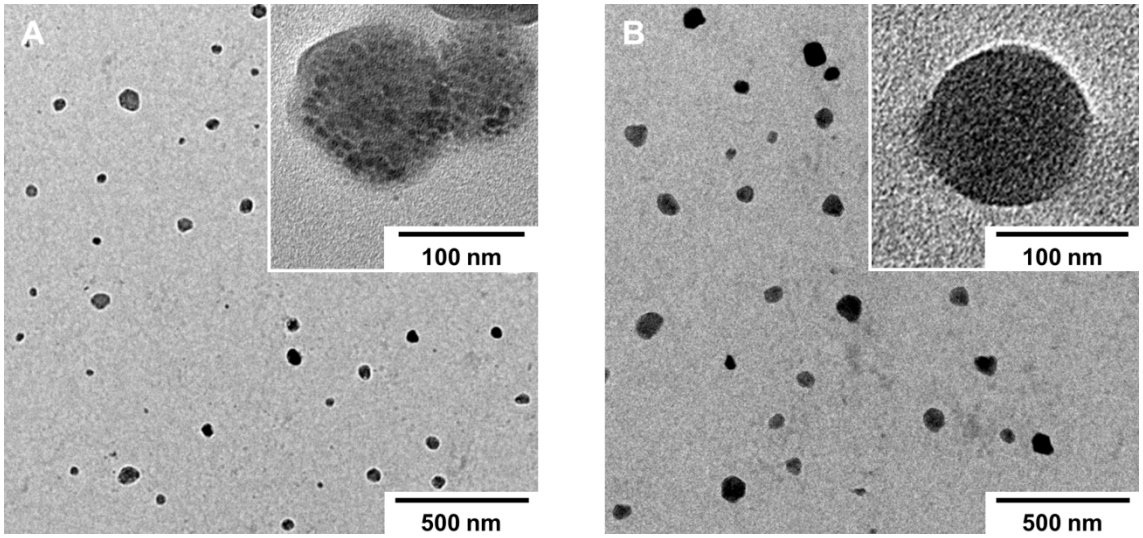

Figure 34. TEM images of empty (A) and DOX-loaded LYZ^{2k} nanoparticles (B). Reprinted from Fach *et al.*[147] Copyright (2016) American Chemical Society.

Doxorubicin Content, Drug Loading and Entrapment Efficiency

As visible in Figure 29, not the entire initial feed of DOX is entrapped into NPs. The amount of DOX entrapped in the resulting NP suspension was determined by comparing the absorption of the drug (λ = 488 nm) to a standard dilution of DOX × HCl ranging from 85 to 3 μM in a similar manner as described by Wu *et al.*[116] The concentration of DOX found in the NP suspension is 33 μM. With the known amount of the protein-PEG conjugate being 2 mg/mL (57 μM), the amount of DOX per protein is 0.58. From the DOX content of 33 μM, the entrapment efficiency (EE) of doxorubicin in NPs was calculated by Equation 3 together with Equation 4. The initial DOX feed ($n_{drug,feed}$) is 920 nmol (0.5 mg of desalted DOX, 543.52 g/mol). The amount of entrapped DOX ($n_{drug,entrapped}$) is 83 nmol (calculated from the resulting DOX concentration (c_{drug}) of 33 μM and the final volume of the NP suspension ($V_{NP\ suspension}$) of 2.5 mL). As a result, the entrapment efficiency of DOX is 9%.

$$EE = \frac{n_{drug,entrapped}}{n_{drug,feed}} \times 100\% \qquad \text{Equation 3}$$

with $$n_{drug,entrapped} = c_{DOX} \times V_{NP\ suspension} \qquad \text{Equation 4}$$

The DOX-loading in weight percentage $wt\%_{DOX}$ is calculated by Equation 5 together with Equation 6. The mass of entrapped DOX ($m_{DOX,entrapped}$) is 0.045 mg (calculated from the

entrapped amount of DOX ($n_{DOX,entrapped}$) of 83 nmol and the mol. wt. of desalted DOX (M_{DOX}) of 543.52 g/mol). The initial mass of the protein feed ($m_{protein}$) is 5.0 mg. As a result, the doxorubicin loading in NPs is 0.9%.

$$wt\%_{DOX} = \frac{m_{drug,entrapped}}{m_{drug,entrapped} + m_{Protein}} \times 100\% \qquad \text{Equation 5}$$

with $$m_{drug,entrapped} = n_{drug,entrapped} \times M_{drug} \qquad \text{Equation 6}$$

Table 8. Weight percentage and entrapment efficiency of doxorubicin in the resulting nanoparticles calculated from the measured concentration of DOX in the NP suspension.

Sample	c_{DOX} / μM	$wt\%_{DOX}$ / %	EE_{DOX} / %
DOX NP	33.0	0.9	9

Catalytic Activity of Empty Nanoparticles

As presented previously, the activity of the protein is retained despite high conjugation of PEG to its surface (see page 34). Since the sonication step has no influence on the protein structure (see page 39) it is expected that the resulting nanoparticle has a catalytic activity, too. Empty nanoparticles fully consist of the protein PEG conjugate that already shows 19 % of the initial protein activity. Additionally, to the sterically hindering of the PEG on the protein surface, the catalytic moieties of some enzymes are now buried in the particle matrix. Proteins with a catalytic pocket facing to the outside of the particle are expected to show the same catalytic activity. As soon as the catalytic center of proteins on the particle surface is faced towards the center of the particle or the proteins are located in the inside, a decrease in their catalytic rate is expected. Also, since the proteins are the embedded by a network-like matrix of PEG chains it is more difficult for the substrate to diffuse to the active site of the protein. In Figure 35, the activity of empty nanoparticles is compared to the same amount of PEGylated LYZ^{2k} in its free form. This time, the enzymatic activity assay was performed over a time period of 7 h (in comparison, 3 h were sufficient for free protein samples) to gain a high turnover of the substrate. The resulting catalytically activity of 14% compared to the LYZ^{2k} material in free form represents the mean over all proteins in the particle matrix. This confirms the

assumption, that not all proteins take part in enzymatic catalysis equally. Compared to the native protein, the nanoparticle represents 3% of the initial enzymatic activity.

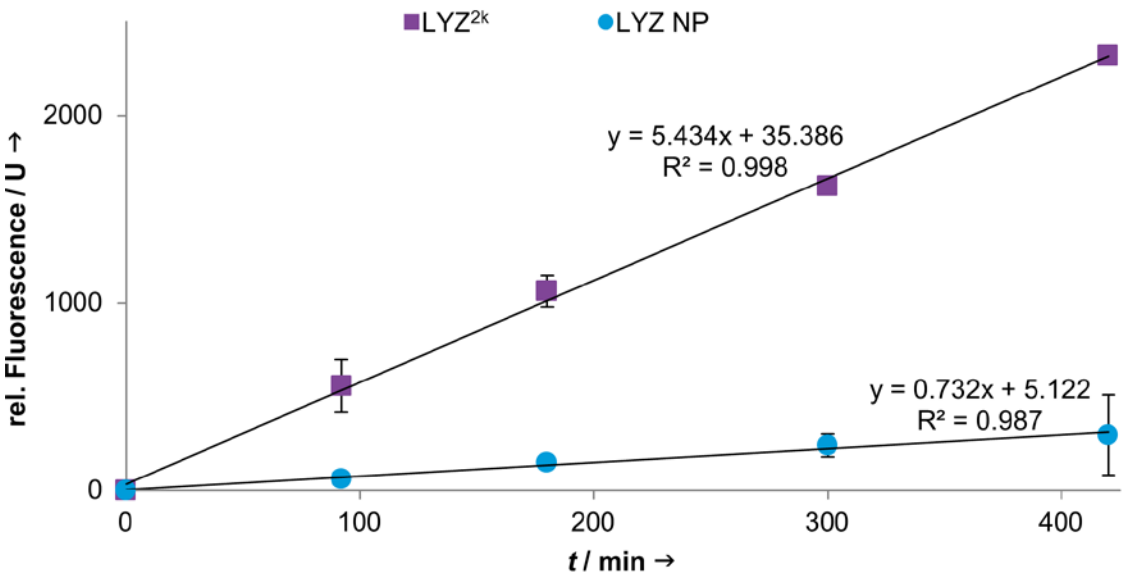

Figure 35. Activity assay of empty LYZ-NPs (●) and LYZ^{2k} (■). The nanoparticles show an activity of 14% compared to the same amount of PEGylated proteins. The overall activity of the nanoparticles is 3% compared to the protein activity of unmodified LYZ. Adapted from Fach *et al.*[147] Copyright (2016) American Chemical Society.

Particle Stability in Physiologically Relevant Buffer Systems

For an efficient drug delivery system it is necessary to be stable in a physiological environment. The great benefit of nanoparticles is the enhanced circulation time in the blood cycle and by the accumulation in tumor tissues only a localized delivery of the payload. For this, the particles need to be stable until they reach the point of interest. On the other hand, the drug needs to be released after a particle has reached the final destination, e.g. the intracellular environment. Figure 36 shows the stability of the presented NP system under different physiologically relevant buffer conditions. For this, the NP suspension was dialyzed against various buffer systems over a time period of 24 h. The absorption in the range from 350 to 650 nm of samples was determined after 2 h, 4 h, 8 h and 24 h. The absorption signal in the area of λ = 490 nm represents the entrapped drug DOX. The absorption spectra of the initial particle suspensions (after 0 h) were used as reference and the intensity of the local maximum of the absorption was set to 100% representing the complete amount of entrapped drug after particle preparation. A decrease of the signal in this area shows, that the drug is released from

the particle and dialyzed out of the membrane chamber, whereas a stable absorption signal indicates, that the drug is still encapsulated in the nanoparticle matrix.

PBS (A) and DMEM (B) represent buffered model systems for the extracellular environment as present in the blood stream. The absorption measurement shows stable signals of the drug in the suspension over the entire time period of 24 h. Only fluctuations around the initial value of the drug but no time dependent release of the drug is observed. The intracellular environment is simulated by different buffer conditions. In this environment a release of the cargo is desired as the final destination of the drug is reached. Lowering the pH of the buffer solution to pH 5.2 (C) simulates the slightly acidic conditions of intracellular compartments like the lysosomes.[172]

For these buffer conditions a release of the drug over time is observed. After 2 h the drug content is decreased by 5 %, the drug release continues but reaches a plateau after 8 h and no further release is observed. This result is most likely caused by the protonation of DOX. Prior particle preparation, the commercial water soluble hydrochloride salt of DOX was "desalted" by deprotonation of the primary amine of DOX. Under acidic conditions, the amine is returns to its inital protonated state. This form is hydrophilic and prefers the aqueous environment surrounding the protein particle. The plateau of the release after 8 h is explained by the fact, that only the drug is affected by the lowering of the pH and not the particle itself. The deeper the drug is inside of the particle, the harder it is for the drug to exit the particle matrix by diffusion. Therefor it is assumed, that only drug molecules in the outer layers of the particle are released by a decrease of the pH value.

After a cellular uptake, proteins are degraded by proteases in lysosomes. As the particle consists mainly of a protein-polymer conjugate, the protein backbone is expected to undergo degradation by proteases. This effect is suggested to destabilize the NP and therefore drug is released from the particles. To simulate a proteolytic environment, a protease mix was added to the nanoparticle suspension (D). By this, a time dependent decrease of DOX is observed. After 2 h the DOX-concentration is decreased by 4 %. After 24 h the absorbance of the drug in the particle suspension is lowered and a decrease of the intensity by 10 % is observed. It is assumed, that proteases start to cleave the polypeptide backbone on the surface of the NPs. Thereby the particle material is disintegrates starting from the surface and the entrapped drug is released.

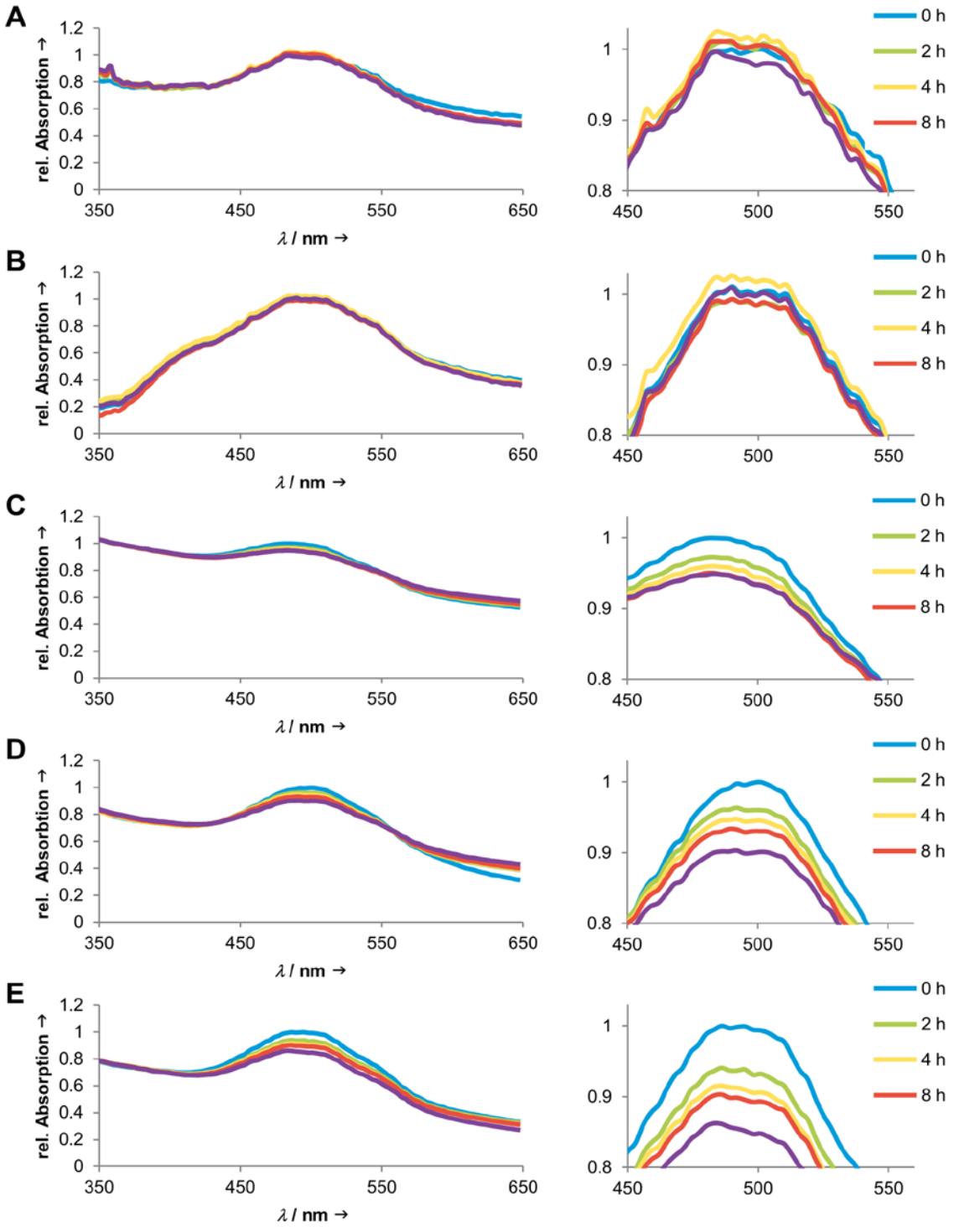

Figure 36. Particle stability in PBS at pH 7.4 (A), DMEM (B), 0.1 M phosphate buffer at pH 5.2 (C), trypsin in PBS (1 mg/mL, D) and glutathione in PBS (10 mM, E). The left spectra show the relative absorbance of the initial particle solution (blue) and the dialyzed particle samples after 2 h (green), 4 h (yellow), 8 h (red) and 24 h (purple) from 350 to 650 nm. The right spectra focus on the area of DOX absorption around 500 nm. Adapted from Fach *et al.*[147] Copyright (2016) American Chemical Society.

The reductive environment in the cytosol of the cell is simulated by a buffer containing glutathione in a concentration of 10 mM (E). Under these conditions, internal disulfide bridges of the proteins are disrupted. This effect is assumed to destabilize the NPs and therefore the entrapped drug is released. By a decrease of the DOX signal by 14% over 24 h, the reductive environment of 10 mM glutathione shows the highest effect on drug release from all tested conditions. Here, a decrease by 7% of the drug signal is already observed after 2 h that lowers over time.

In summary, the data shows that the particles are stable in conditions similar to the extracellular environment. A release of the payload is only observed under acidic conditions, in the presence of proteases or a reductive environment, similar to the cytosol of cells.

3.1.4 In Vitro Effects of Lysozyme Nanoparticles

Cell Association of Nanoparticles by Cell sorting

Fluorescence-activated Cell Sorting (FACS) was used to investigate the association of the nanoparticles with cells of the human carcinoma cell line (HeLa). Therefore, cells were incubated with DOX-loaded NPs. After 1 h and 4 h, the cells were isolated and the fluorescence of the sample was determined (Figure 37). NPs were prepared with fluorescein labeled F_LYZ^{2k} protein material to ensure an individual tracking of the NP matrix material and the encapsulated drug. The channel FL1-H (530/30) was used to determine the green fluorescence of the particle material (F_LYZ^{2k}). FL3-H (650LP) was used to detect the red fluorescence of the encapsulated DOX. Cells incubated without NPs are used as reference and show only a weak auto-fluorescence of the cells. After 1 h of incubation, the fluorescence signals of both, the NP-material and the encapsulated drug were detected, indicating a simultaneous cellular uptake. After 4 h this uptake is further increased as fewer cells show only auto-fluorescence and the intensities of both the DOX and the protein signal is increased. A major disadvantage of FACS analysis is, that it only shows association of the fluorophore with the cell. It is not possible to determine whether a particle is taken up by a cell or just attached to its surface. For this reason, the cellular uptake was further investigated by confocal microscopy.

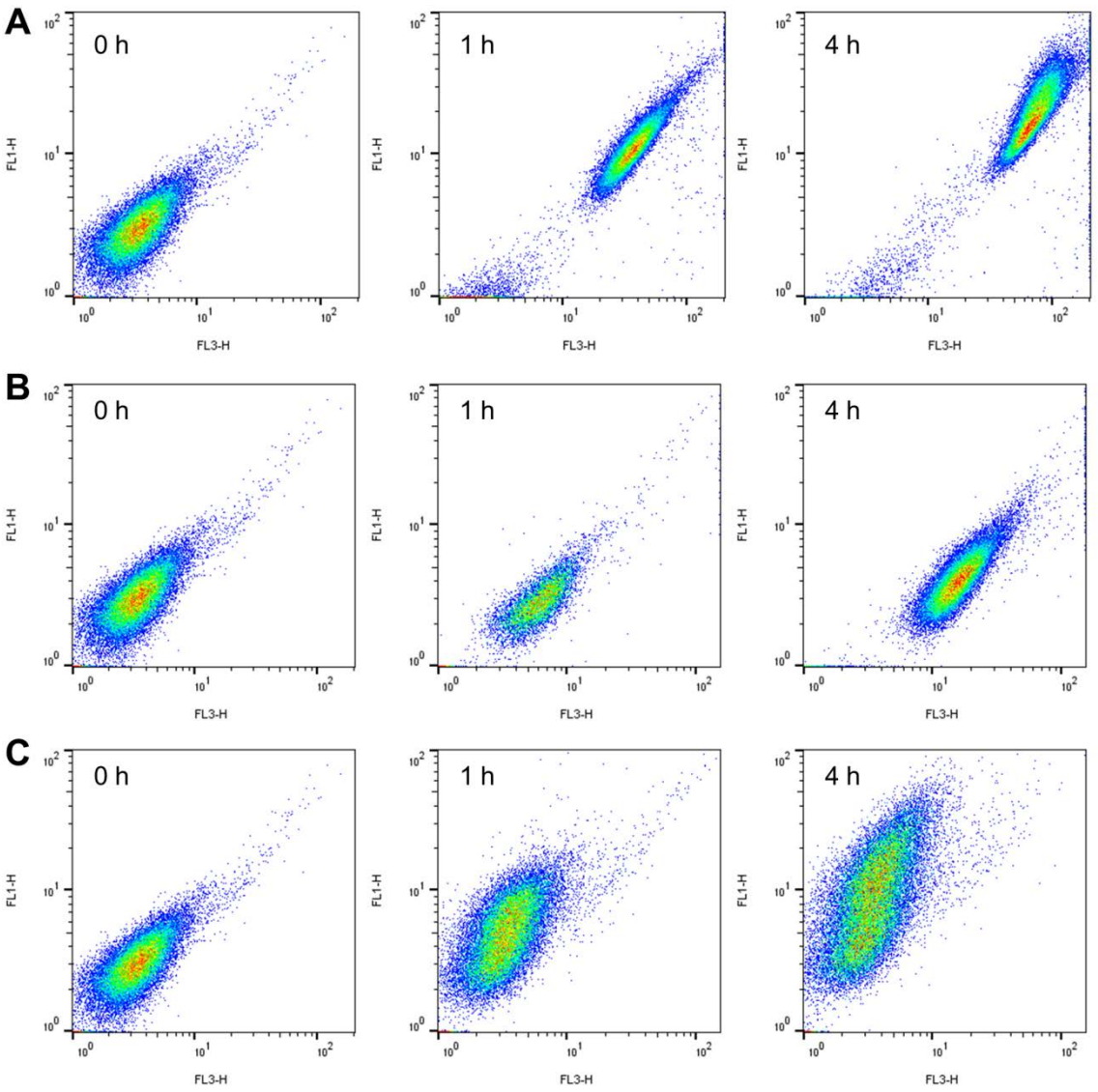

Figure 37. Pseudo-color plots obtained by flow cytometry show the cellular uptake of DOX-loaded NPs with labeled protein matrix (A) in comparison with DOX particles with unlabeled protein matrix (B) and empty particles with labeled protein matrix (C). Only a weak auto-fluorescence of control cells that were not incubated with nanoparticles is observed (0 h). Signals for both the encapsulated drug and particle material are detected after 1 h, indicating a simultaneous cellular uptake. This uptake is further increased after 4 h. FL1-H was used to detect the fluorescence of the particle material (F_LYZ^{2k}). The encapsulated DOX was detected with FL3-H.

Cellular uptake of DOX-loaded Nanoparticles

Confocal laser scanning microscopy (CLSM) was used to further investigate the cellular uptake and drug release of DOX-loaded NPs (Figure 38). Again, nanoparticles were prepared with the fluorescent labeled protein-PEG conjugate (F_LYZ^{2k}) to track the particle material and the encapsulated drug individually. Cells were incubated with NP and fixed after 1, 4 and 24 h, respectively. Co-staining of the nucleus of the cell was performed using blue DAPI. The NPs are readily taken up by the cell after 1 h and localize in intracellular compartments. At this point, the fluorescent signal of the protein and the encapsulated drug are co-localized. This shows that the NP is still fully assembled, after being taken up by the cell. After 4 h, a release of DOX into the cytosol and the start of accumulation in the nucleus are observed. After 24 h of incubation, all doxorubicin can be found in the nucleus of the cell whereas the particle material is spread over the cytosol of the cell. Once the nanoparticles are taken up by the cell, the NP is most likely disassembled by proteases and changes of protein integrity under the reductive conditions in the intracellular environment.

In comparison, the uptake of free DOX was investigated (Figure 39). The drug enters the cell rapidly by passive diffusion through the membrane and is fully localized in the nucleus after 4 h. No change of the uptake or localization of the drug after 4 or 24 h is observed.

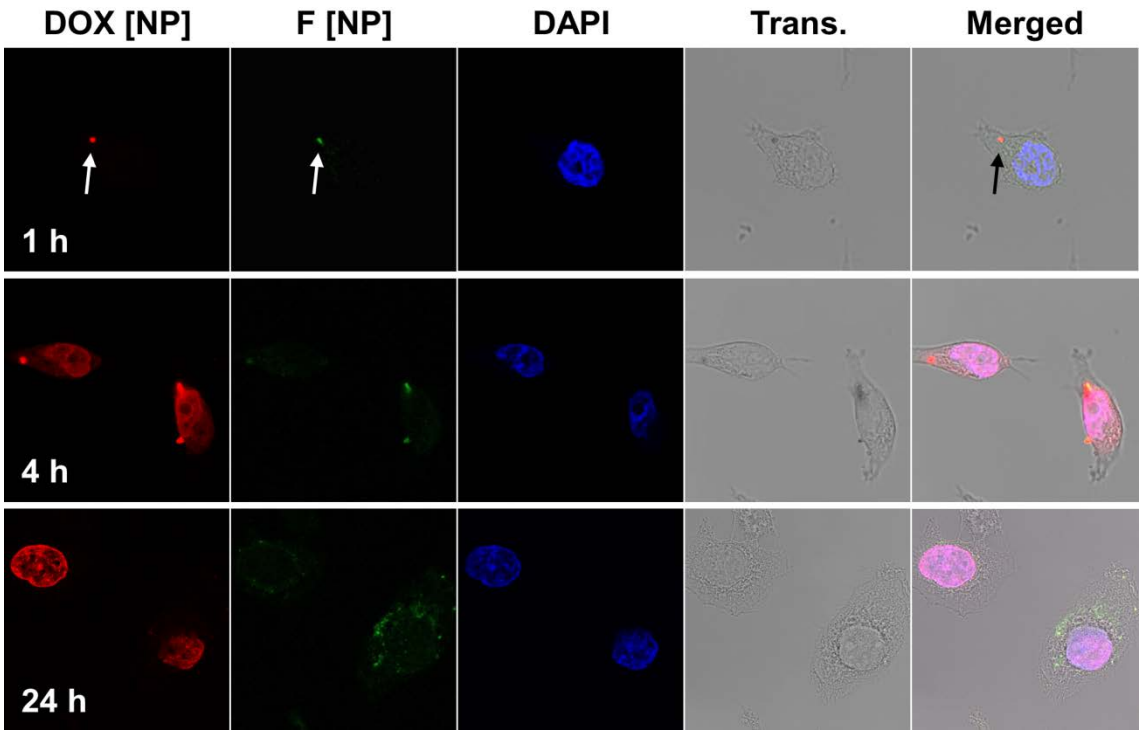

Figure 38. Confocal images of nanoparticle uptake after 1 h, 4 h and 24 h in HeLa-cells. The final concentration of nanoparticle encapsulated DOX was 4 μM (in DMEM). DOX-loaded and fluorescent-labeled NPs are taken up after 1 h and show a colocalization of the red-fluorescent payload [DOX (NP)] and the green-fluorescent protein particle material signal [F (NP)]. The payload is released in the cytosol of the cell after 4 h and the released DOX starts to accumulate in the nucleus. After 24 h, DOX is completely localized in the cell core whereas the PEGylated protein is spread over the cell. Reprinted from Fach *et al.*[147] Copyright (2016) American Chemical Society.

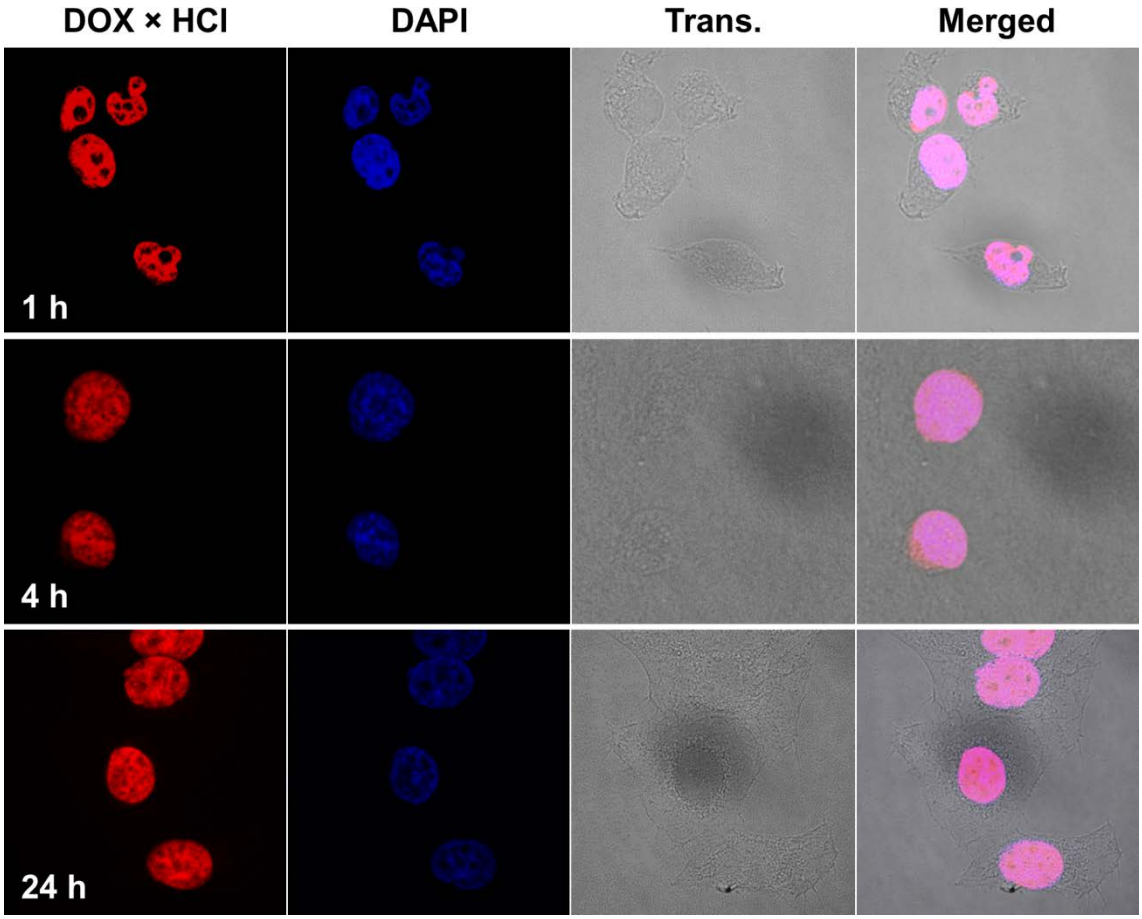

Figure 39. Confocal images of unformulated (free) DOX × HCl uptake after 1 h, 4 h and 24 h. The concentration of free doxorubicin was adjusted to the encapsulated amount in F_LYZ(TsT-mPEG)$_{10}$ nanoparticles (final concentration in DMEM is 4 μM). Free DOX accumulates immediately (already after 1h) in the cell core by passive diffusion across the cell membrane. Reprinted from Fach *et al.*[147] Copyright (2016) American Chemical Society.

Effects on Cell viability of Empty and DOX-loaded Nanoparticles

The toxic effect of drug-loaded nanoparticles on the viability of human cervical cancer cells (HeLa) reflects the successful delivery and release of DOX into the cell. A MTT assay was used to investigate the viability of the cells that are incubated with NPs for 48 h. The cell viability is reflected by the NAD(P)H-dependent cellular oxyreductase enzymes that reduce the tetrazolium salt MTT to its water insoluble formazan (Scheme 8, Page 139). Despite the different uptake mechanism, DOX-loaded nanoparticles show similar therapeutic effects like free DOX × HCl in concentrations up to 10 μM whereas empty NPs show no toxicity (Figure 40).

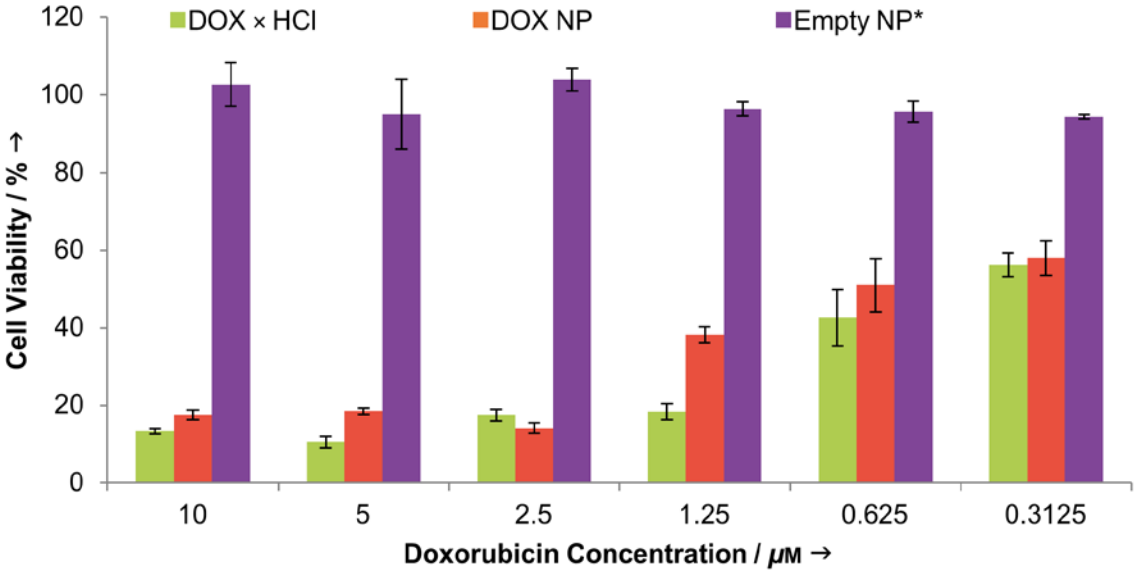

Figure 40. Cell viability of HeLa cells after incubation with free DOX × HCl (green, left), DOX-loaded LYZ(TsT-mPEG)$_{10}$-NP (red, middle) and empty LYZ(TsT-mPEG)$_{10}$-NP (purple, right) (*diluted in the same manner as DOX-loaded particles to achieve the same concentration of particle material). Adapted from Fach *et al.*[147] Copyright (2016) American Chemical Society.

Additionally the materials used for the NP preparation, the native protein LYZ, the activated TsTmPEG2k and the protein-PEG conjugate LYZ^{2k} were tested on their toxic effects towards HeLa cells and did not show significant decrease of the cell viability (Figure 41).

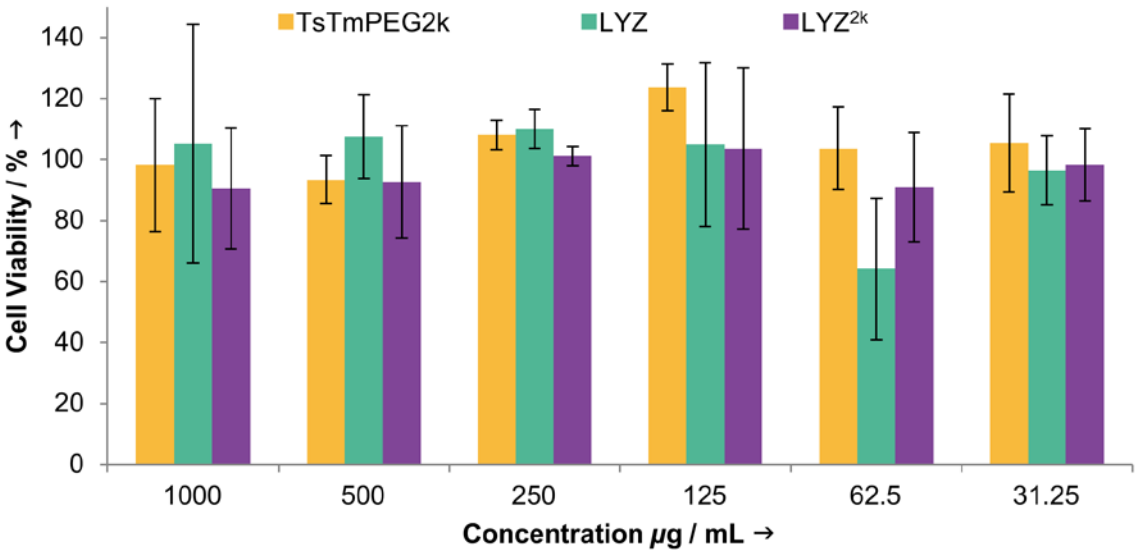

Figure 41. Cell viability of HeLa cells after incubation with Cl-TsT-mPEG (yellow, left) native lysozyme (green, middle) and LYZ(TsT-mPEG)$_{10}$ (purple, right) for 48 h. Adapted from Fach *et al.*[147] Copyright (2016) American Chemical Society.

These results lead to the conclusion that all materials for particle preparation are non-toxic. This is especially important, as the use of TsT as activation agent for mPEG might raise concerns about its toxicity.[173]

Also, empty nanoparticles do not show inhibitory effects on the growth of HeLa cells. Only after entrapment of DOX, the nanoparticles show a decrease of cell viability, similar to the toxicity induced by DOX in its free form as hydrochloride salt. From this it can be concluded, that the particles successfully deliver the payload into the cells without affecting the toxicity of the drug.

The here presented results show the successful development of a novel lysozyme-based nanocarrier system for doxorubicin. High surface PEGylation of lysozyme let to a protein-polymer conjugate that retains its protein structure and activity but is also soluble in organic solvents. This material was the used to prepare empty nanoparticles and DOX-loaded particles and to deliver the drug into cancer cells. These results build a sound basis to expand the nanocarrier system to differend hydrophobic payloads and to investigate whether this particle preparation approach is limited to lysozyme only or transferable to different proteins.

3.2 Transfer of the Model System to Various Proteins

3.2.1 Protein PEGylation

High Surface PEGylation of Various Model Proteins

Section 3.1 described in detail the development of a new of protein-based nanoparticle system, from the surface modification of the enzyme lysozyme to the *in vitro* effects of the obtained NP assemblies. In the following, we transferred/extended this approach to other proteins with varying sizes and properties. This has been done partially in collaboration with Laura Mayer in the course of her bachelor thesis.[174] By the selection of the proteins *β*-lactoglobulin (BLG), ovalbumin (OVA), human serum albumin (HSA) and the protein cage ferritin (FER), the size range of used proteins is extended from 14 kDa to 485 kDa (Figure 42). Instead of doxorubicin, the diarylheptanoid curcumin was used show the applicability of the NP system to delivery other types of drugs.

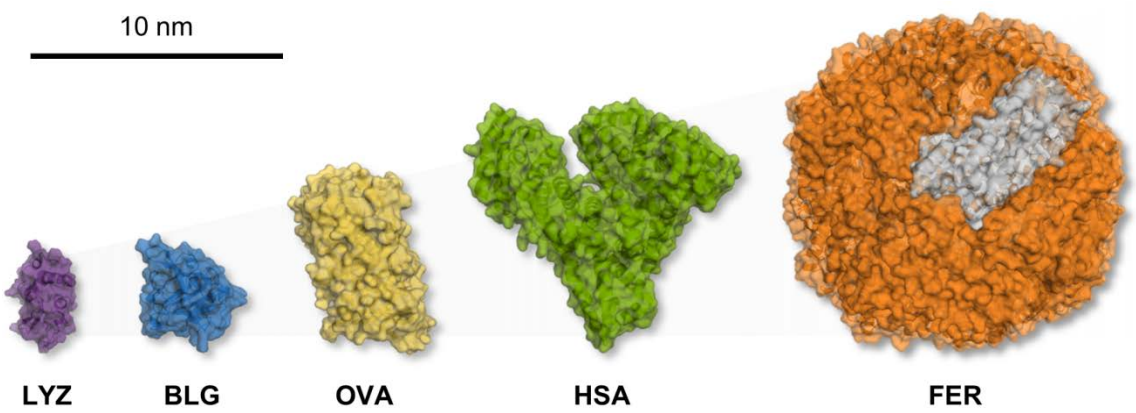

Figure 42. 3-Dimensional structures of the globular proteins lysozyme (LYZ, purple, pdb: 1lyz), *β*-lactoglobulin (BLG, blue, pdb: 1beb), ovalbumin (OVA, yellow, pdb: 1ova), human serum albumin (HSA, green, pdb: 1e7i) and the 24-mer ferritin (FER, orange with a subunit highlighted in grey, 1ier). Scale bar: 10 nm. (Reproduction of Figure 7 to offer the reader a visualization of the size range of the used proteins directly in this section).

Protein PEGylation

The PEGylation of the protein surface of BLG, OVA, HSA and FER was carried out as previously described, by using the same weight of the mPEG to proteins. All proteins were dissolved in a concentration of 10 mg/mL in borate buffer and activated mPEG was added to achieve a concentration of 0.2 g/mL for TsTmPEG2k and 0.5 g/mL for TsTmPEG5k. Again, to stop the reaction, a 1.5-fold excess of phosphate buffer was added to obtain a neutral pH. By this, the reaction procedure was kept simple and easy to transfer to a variety of proteins. Excess mPEG was removed by ultrafiltration using centrifugal devices. A filter with a MWCO of 30 kDa was used for all samples modified with TsTmPEG2k, as well as LYZ and BLG that were modified with TsTmPEG5k. For the relatively large proteins OVA, HSA and FER, a MWCO of 100 kDa was used to remove excess mPEG5k as the final product is expected to be held back by the membrane of the filtration device. The products were freeze dried for further storage at +4 °C.

Molecular Weight Analysis of Protein Conjugates by Gel Electrophoresis

SDS-PAGE was used to determine the surface modification of the various proteins by the PEGylation procedure (Figure 43). For a better comparison, all protein gels show the same layout of lanes from left to right (Marker; corresponding initial protein; protein modified with mPEG2k; protein modified with mPEG5k; corresponding initial protein). The amount of polyacrylamide in the gel matrix was adjusted for each individual initial protein. This gives the opportunity for an optimal running behavior of the protein samples in the gel. The use of the same PA amount for each gel is not suitable as protein bands outside the optimal PA content are compressed in the resulting gel (Figure 43A) or migrate out of the gel (Figure 43B and C). For native BLG the protein band migrates almost to the marker lane of around 15 kDa, which indicates a slightly smaller mol. wt. than the literature value of 18.3 kDa. The BLG^{2k} conjugate starts around 40 kDa whereas the band of the mPEG5k conjugate is located on the top of the gel only and does not further migrate through the gel. Ovalbumin (native 42.8 kDa) also shows with a protein band around 38 kDa a lower mol. wt. than expected for the initial protein. The band for the OVA^{2k} starts at 70 kDa and stretches to the top of the gel. The OVA^{5k} conjugate only enters the separation gel but does not move further. For HSA, the protein band of the initial unmodified protein corresponds to the literature value of 66.5 kDa.

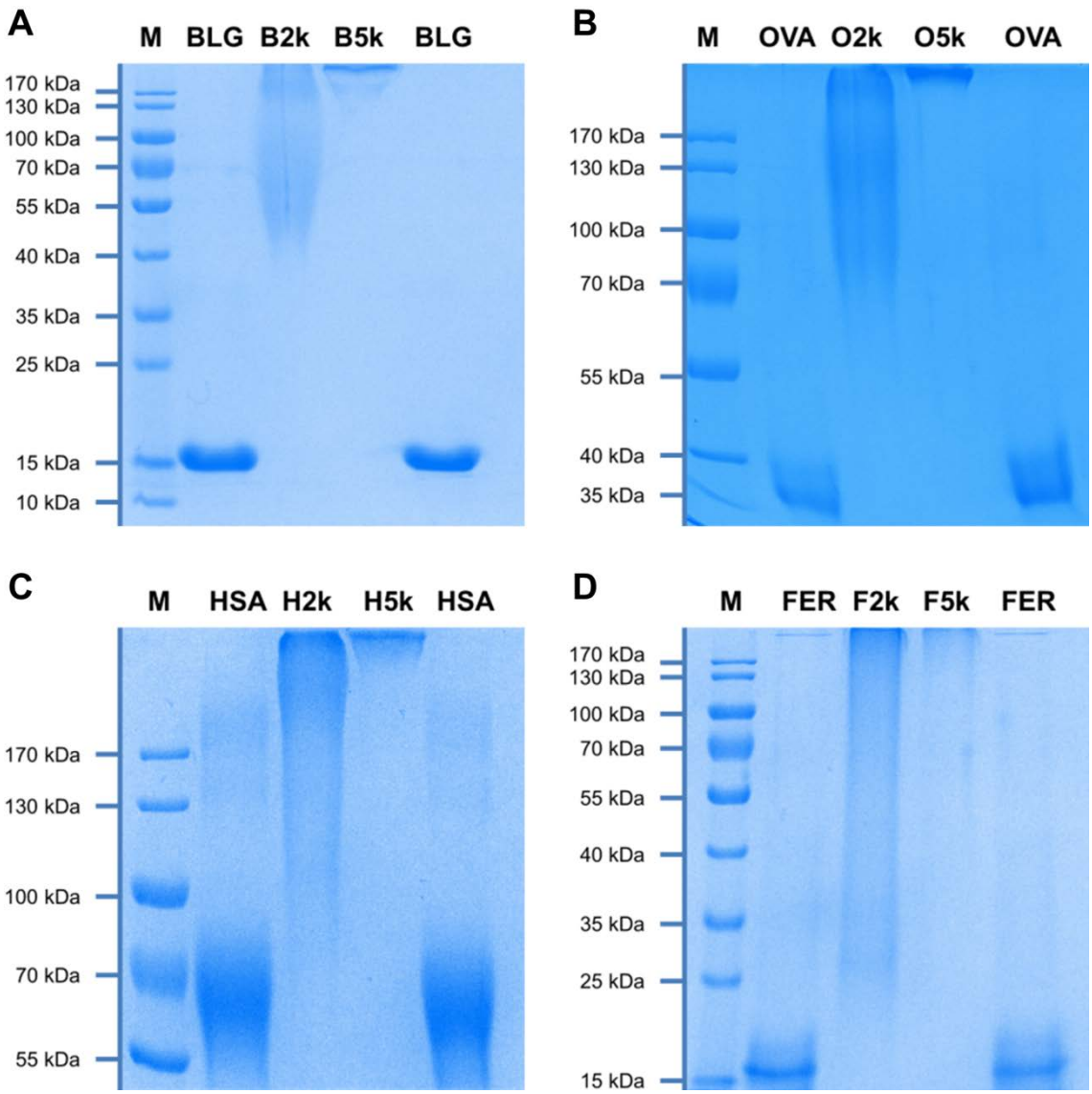

Figure 43. SDS-PAGE of BLG (A), OVA (B), HSA (C) and FER (D) show the conversion of the native proteins to their highly PEGylated conjugates with mPEG2k of mPEG5k attached to the protein. None of the PEGylated samples shows residual unmodified protein.

The HSA^{2k} conjugate shows a protein band from 100 kDa stretching to the top of the gel with the highest intensity above 170 kDa. HSA^{5k} does not migrate through the separation gel and shows only an intense band on the top of the gel. For the case of FER, it has to be taken in consideration that the protein cage is a 24-mer in its intact, fully assembled state. By SDS-PAGE the cage is disrupted and the subunit proteins migrate individually through the gel. The initial protein shows a band at slightly above 15 kDa. Similar to BLG, this does not correspond well with the native mol. wt. of 18.3 kDa. The FER^{2k} derivative shows a band that stretches

almost over the entire separation gel starting from 25 kDa. The mPEG5k conjugate migrates only weakly through the separation gel, showing a protein band that starts around 130 kDa. Table 9 gives an overview of the molecular weight of the PEGylated proteins as determined via SDS-PAGE. The Increase of mol. wt. and the amount of attached mPEG chains is further investigated by MALDI-ToF MS later in this section.

None of the protein-PEG conjugates shows bands of residual protein that are not PEGylated. For proteins, that are smaller than the MWCO of the centrifugal device this was expected, as the unmodified proteins are removed by filtration step. Interestingly, also no residual protein was observed for samples that are filtered with a MWCO that was suitable for the mPEG to pass the membrane but not the initial protein (OVA, HSA and FER).

Hence, it can be concluded that a conversion of the initial proteins to highly PEGylated conjugates occurs regardless of the used protein. As shown in section 3.1.1 the protein bands in the SDS-PAGE do not correspond firmly to the actual mol. wt. of the conjugate, as PEG chains tend to smear in the gel. For the mPEG5k chains this effect turns out to influence the protein bands even more. Here, the high amount of PEG attached to the protein hinders the migration through the gel matrix. The increase of the size of the proteins becomes too large and the proteins are not able to migrate further through the separation gel once they passed the collecting gel.

Table 9. Summary of the molecular weight analysis by SDS-PAGE.

Protein	**mol. wt. / kDa**	**Surfaces Nucleophiles**	**mPEG / kDa**	**max. mol. wt. / kDa**	**mol. wt. by PAGE / kDa**	**mPEG per protein**
BLG	18.3	16	2	~50	40	11
			5	~100	out of range	n/a
OVA	42.8	21	2	~85	70	14
			5	~150	out of range	n/a
HSA	66.5	30-35	2	~125–136	100–top	17–n/a
			5	~215–245	out of range	n/a
FER	20.2	3	2	26	25	3
			5	35	130	n/a

Solubility of Protein-Polymer Conjugates in Dichloromethane

After successful surface modification, the protein-PEG conjugates were tested on their solubility behavior in DCM (Table 10). The solubility was considered as good (+), when the conjugate got dissolved within 15 min at room temperature. This time has been proven to be ideal for an easy particle preparation by the described solvent evaporation method. An extended time period may lead to uncontrolled evaporation of the organic solvent and thereby to unpredictable changes in material concertation and solvent ratios during emulsification.

For LYZ, the attachment of both 2 kDa and 5 kDa PEG chains led to a full solubility in DCM. The same effect was observed for BLG that has a similar size of the native protein. Although OVA^{2k} was somewhat soluble in DCM, a complete dissolution of the material was only observed after 4 h. For this reason, OVA^{2k} was considered as not suitable for particle preparation. However, for OVA^{5k} full solubility within 15 min was observed. In the case of HSA^{2k} and FER^{2k} both proteins were not soluble in DCM after PEGylation. Only the attachment of mPEG5k led to a full solubility in DCM.

Table 10. Solubility of protein-PEG conjugates in DCM. Samples are rated as: in soluble in less than 15 min. at rt. (+), soluble at room temperature after 4 h (+/–) and insoluble in DCM (–).

M_{mPEG}	LYZ	BLG	OVA	HSA	FER
2 kDa	+	+	+/–	–	–
5 kDa	+	+	+	+	+

From these results, it can be concluded, that the chain length of the attached PEGs plays a key role for the enhanced solubility of the protein-polymer conjugates in organic solvents. Large proteins need longer PEG chains attached to the surface to become soluble in DCM. Exemplary, the solubility behavior of FER^{2k} and FER^{5k} is presented in Figure 44. As already mentioned, FER^{5k} is fully soluble in DCM, leading to an orange-colored solution (Figure 44A, right). On the other hand, the attachment of mPEG2k chains to the surface is not sufficient for a solubility of the protein. The FER^{2k} conjugate remains as a solid that precipitates on the bottom of the vial (Figure 44A, left). Next, 500 μL of the DCM were replaced by the same amount of water and the samples were vigorously mixed. After phase separation, FER^{5k} shows the same solubility behavior that was already described for LYZ^{2k}. The PEGylated protein remains in the DCM phase and is not extracted into the aqueous phase (visible for the human

eye by the orange color of the protein cage). Also FER^{2k} is fully dissolved after phase separation. Not in DCM but in the aqueous phase on top of the organic layer. This shows that the attachment of mPEG2k chains does not lead to a solubility switch of the protein towards an organic environment. As a conclusion from these results, only LYZ^{2k}, BLG^{2k}, OVA^{5k}, HSA^{5k} and FER^{5k} were considered as suitable for further preparation of nanoparticles and therefore further characterized.

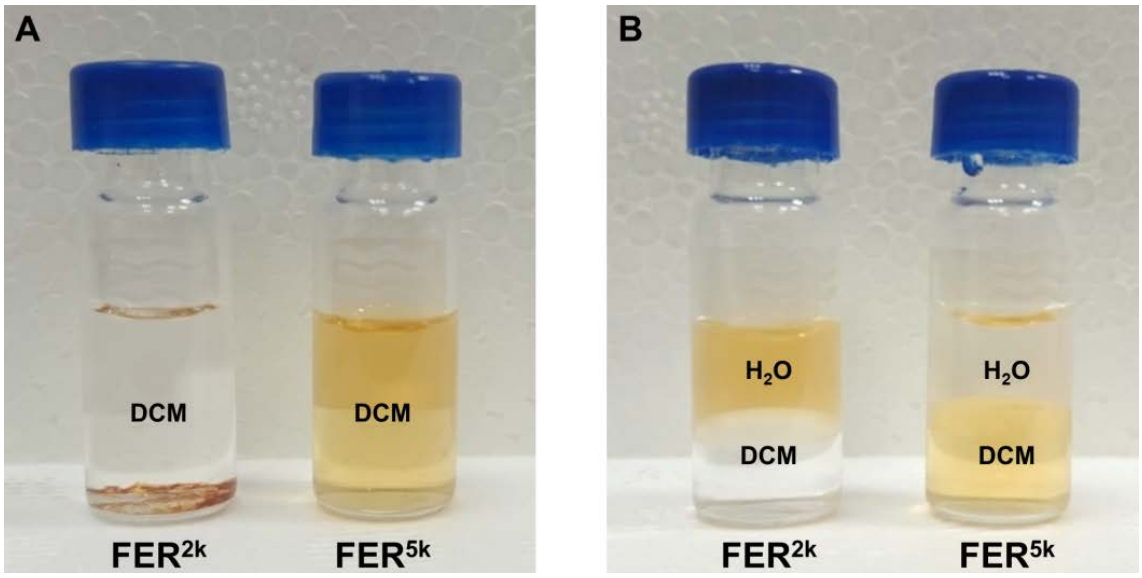

Figure 44. Solubility of protein-PEG conjugates in DCM exemplified on the orange colored ferritin conjugates FER^{2k} and FER^{5k} (A). Addition of water dissolves the FER^{2k} conjugate in the aqueous phase whereas FER^{5k} remains in the organic layer (B).

Size Increase Analysis by Fast Protein Liquid Chromatography (FPLC)

In addition to SDS-PAGE, FPLC was used for the analysis of the protein conjugates that showed a suitable solubility for NP preparation (BLG^{2k}, OVA^{5k} and HSA^{5k}, Figure 45). The BLG^{2k} conjugate shows a V_e of 11.7 mL in comparison to 15.2 mL of native BLG. OVA^{5k} eluates at a V_e of 8.2 mL, whereas the native protein shows a V_e of 15.0 mL. The lowest V_e is observed for HSA^{5k}. Also the native protein shows with 13.9 mL the lowest V_e of all tested native proteins.

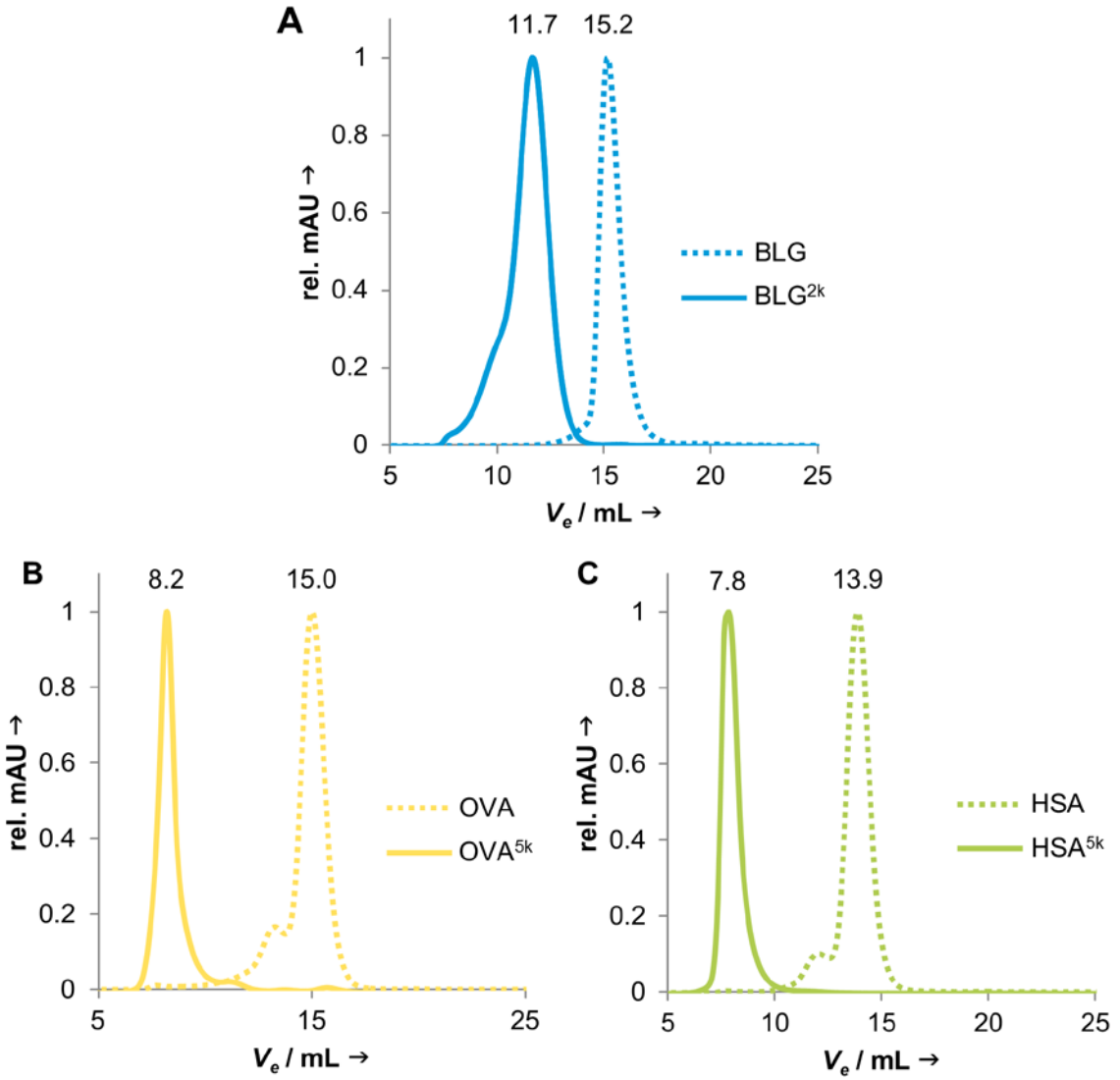

Figure 45. FPLC analysis of the PEGylated conjugates BLG^{2k} (A), OVA^{5k} and HSA^{5k} (C) and their corresponding native proteins. The PEGylated proteins are presented as solid lines, whereas the corresponding native proteins are shown as dotted lines.

None of the protein conjugates shows any trace of unmodified protein and no indications of cross linking of the proteins. The V_e of initial BLG is relatively large compared to the similar sized LYZ (see Figure 18). It has to be considered that the protein is known to form dimers under neutral and alkaline conditions. Therefore the V_e at 15.2 of native BLG and also the V_e of 11.7 mL for BLG^{2k} most likely corresponds to the dimeric form of the protein. FER and its conjugates are too large (with a size of 485 kDa for the native protein) for the analysis by FPLC and only suitable for analysis methods like SDS-PAGE where the protein cage is disassembled.

Molecular Weight Analysis by MALDI-ToF MS

MALDI-ToF mass spectroscopy was used to determine the molecular weight of the PEGylated proteins BLG^{2k}, OVA^{5k} and HSA^{5k} (Figure 46 and Table 11). For BLG^{2k}, a mol. wt. of 42 kDa was detected. With the initial mol. wt. of around 18 kDa for native BLG this means that 12 mPEG2k chains are attached to the protein surface to the available 16 nucleophilic groups on the protein surface. In comparison to the similar in sized LYZ (14.3 kDa) this appears to be incomplete. Though, it has to be considered that BLG is in a dimeric state under neutral to alkaline conditions as present during the reaction. Therefore, not all amino acids on the protein might available for surface modification.

As the conjugates of OVA^{5k} and HSA^{5k} are expected to be outside of the detection limits of MALDI-ToF MS only their M^{2+} ionization states were detected. As already observed for LYZ (see Figure 19), the M^{2+} state appears at half the weight of the M^{+} signal that represents the actual molecular weight. OVA^{5k} shows a signal around m/z of 70, representing a mol. wt. of around 140 kDa. This means that approx. 20 mPEG5k chains are attached to the surface of OVA (42.8 kDa). Compared to the 21 nucleophilic amino groups that are presented on the OVA surface, this corresponds well to the previously obtained high surface PEGylation of LYZ. For HSA^{5k} a broad signal is detected around 100 m/z. This represents a mol. wt. of 200 kDa and indicates that approx. 30 mPEG5k chains are attached to the surface of HSA (65 kDa). HSA offers 60 nucleophilic groups on its surface. It is assumed that only around 30 to 35 are available to for surface modifications of the protein, as reported for the structurally alike BSA.[173] With 25 to 30 attached mPEG5k chains a high surface modification was obtained. FER and its conjugates are not suitable for an analysis by MALDI-ToF MS as already the initial protein with a mol. wt. of 485 kDa is too large for this analysis method and PEGylation increases the mass additionally. At this point, the PEGylation of FER was not further investigated. Here, the solubility in org. solvents (as presented in Figure 43 and Figure 44) was considered as sufficient for particle preparation. Nonetheless, further research needs to be done to fully determine the extent of PEGylation when using FER.

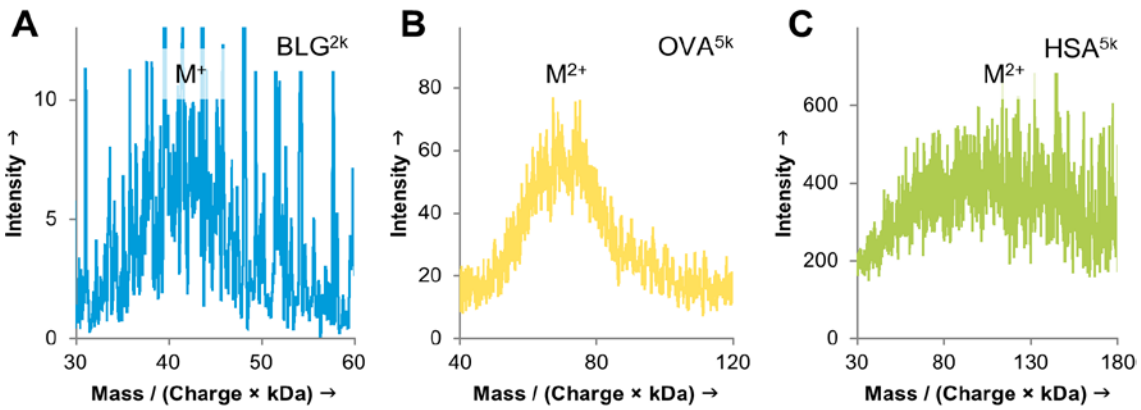

Figure 46. MALDI-ToF MS measurements of the protein-PEG conjugates BLG^{2k} (A), OVA^{5k} (B) and HSA^{5k} (C).

Table 11. Mol. wt. determination and calculation of mPEG chains attached to the surface of the protein-PEG conjugates BLG^{2k}, OVA^{5k} and HSA^{5k}.

Sample	m/z	z	mol. wt.	n_{PEG} / protein	Name
BLG^{2k}	~42 kDa	1	42 kDa	12	BLG(TsTmPEG2k)$_{12}$
OVA^{5k}	~70 kDa	2	140 kDa	20	OVA(TsTmPEG5k)$_{20}$
HSA^{5k}	~100 kDa	2	~200 kDa	25–30	HSA(TsTmPEG5k)$_{25–30}$

Structural Integrity of Protein-Polymer conjugates

The effect of the PEGylation on the integrity of the secondary structure of the proteins was investigated by CD-spectroscopy (Figure 47). Here, only the conjugates used for further particle preparation – BLG^{2k}, OVA^{5k}, HSA^{5k} and FER^{5k} – were investigated. The experiment was performed as described for LYZ^{2k}. Proteins are incubated under reaction conditions, with activated mPEG, hydroxyl mPEG or without mPEG. An unheated sample and a heat denaturated sample (heating to 80 °C) were used as reference for each protein. For BLG (A) a slight decrease in the helical segments is observed compared to the native protein. This structural change already occurs, when the protein is incubated under reaction conditions with non-activated and even without mPEG. OVA (B) does not undergo structural changes when PEGylated with TsTmPEG5k under the described reaction conditions. Only heat denaturation leads to a change in the secondary structure of the protein. HSA (C) shows the same protein stability towards the reaction conditions as already seen for LYZ and OVA. Neither PEGylation nor the treatment under reaction conditions affects the protein structure. Also for

HSA[5k], a change in the secondary structure of the protein can only be detected when the protein is heated to 80 °C.

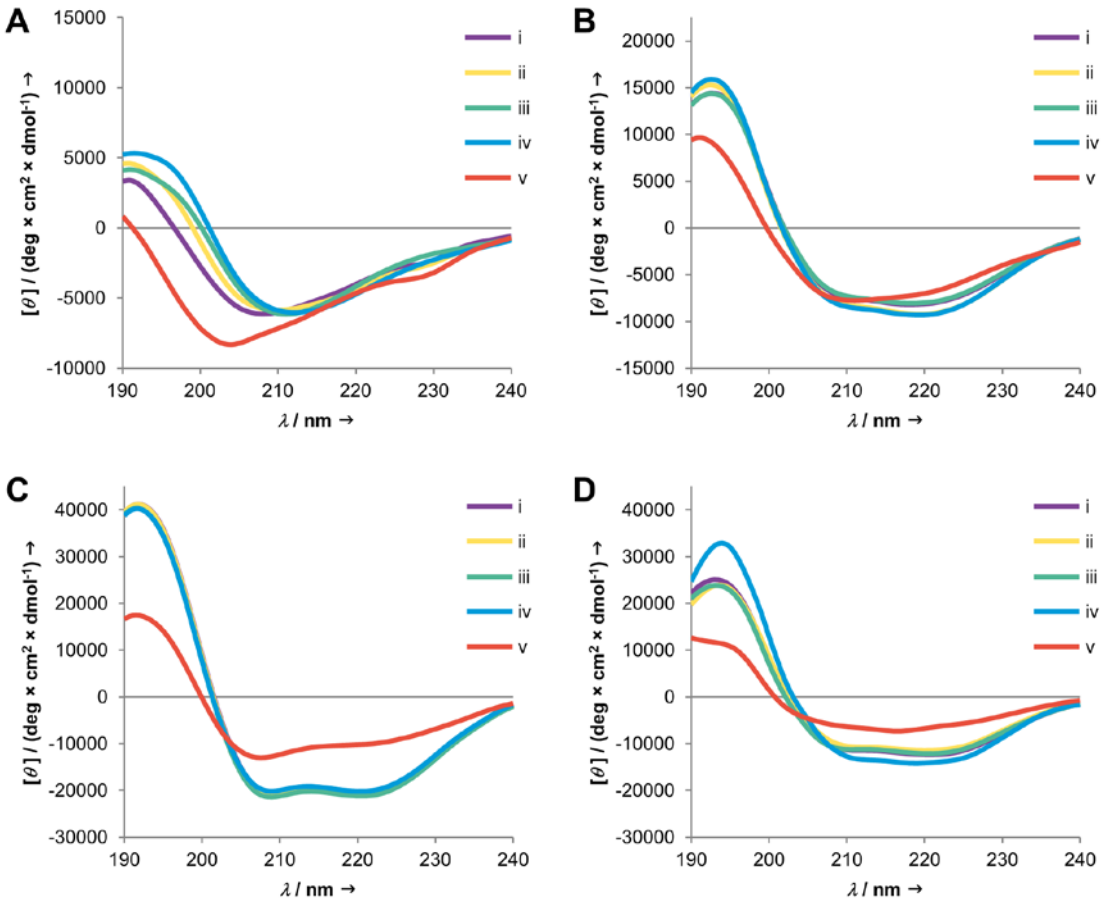

Figure 47. CD-Spectra of the protein PEGylation of BLG (A), OVA (B), BSA (C) and FER (D) respectively. The spectra show PEGylated protein (i, purple), mixture of protein and mPEG-OH (ii, yellow) and protein only (iii, green) incubated for 2 h under reaction conditions. For comparison, an untreated protein sample (iv, blue) and an untreated sample measured at 80 °C (v, red) causing thermal denaturation.

Similar for FER (D), the heat denaturation leads to a heavy change in the protein structure. Additionally, FER shows slight changes in the helical structure when the protein gets PEGylated similar as seen for BLG, too. The changes for FER occur in the same manner on samples incubated with activated mPEG, with unreactive hydroxyl mPEG and when the protein is treated under reaction conditions without the addition of mPEG. This shows that the attached PEG chains do not have effects on the structure of FER. However, it appears that the reaction conditions for the attachment of TsT activated mPEG leads to a decrease of

the structural order of the protein. For this reason the activation of mPEG with TsT does not seem to be the perfect solution to obtain highly PEGylated protein-polymer conjugates from all proteins by fully retaining their structure. As demonstrated for LYZ, OVA and HSA this method is very successful for robust proteins. On the other hand, BLG and FER show that not all proteins withstand the required modification conditions (40 °C and pH 10 over 2 h) without structural changes. For this kind of proteins, alternative activated mPEGs should be considered for the surface modification.

Protein PEGylation with NHS-activated PEG

To reduce the effect of unfavorable reaction conditions during the surface PEGylation, an alternative method for the attachment of mPEG was investigated in collaboration with Carina Ade in the course of her bachelor thesis[175] *N*-hydroxysuccinimide-esters (NHS) are known to be highly reactive towards nucleophilic groups. They are often used for the attachment of small molecules or polymers to macromolecules, as they are highly reactive and stable enough under aqueous conditions (see also section 3.1.1). NHS-ester activated mPEGs can react with amines on the proteins forming an amide bond between protein and polymer. For this study commercially available NHS-activated mPEG (NHSmPEG) was used. Applying this, the reaction temperature was lowered from 40° to room temperature. Additionally, the pH of the used buffer was lowered from pH 10.0 to pH 8.5, representing only a weak alkaline environment. However, in order to secure a high surface PEGylation of the protein, the reaction time was extended to 16 h. Comparing the five presented proteins, the highest change in protein structure was observed for BLG, this protein was chosen as model to test if the new PEGylation method is an improvement. For this, a fully DCM-soluble protein-PEG conjugate BLG^{NHS2k} was synthesized. Also Nanoparticles were successfully prepared from this conjugate.[175]

Enhanced Protein Integrity by PEGylation with NHS-activated PEG

CD-Spectroscopy was again used for the investigation of structural changes that occur under the new reaction conditions (Figure 48). Again, the PEGylated protein is compared to an untreated and a heat-denaturated sample of the protein. As non-activated mPEG does not affect the CD-spectra, hydroxyl mPEG was added to the sole protein under reaction conditions to simulate represent these two references in one sample. For the β-sheet segments of the protein, the amount stays the same for all samples with the exception of the heat denaturated reference. In contrast to the TsT-activated PEG2k where the total amount of helices in the protein is lowered, the reaction with NHS-activated mPEG2k keeps the helices unaffected.

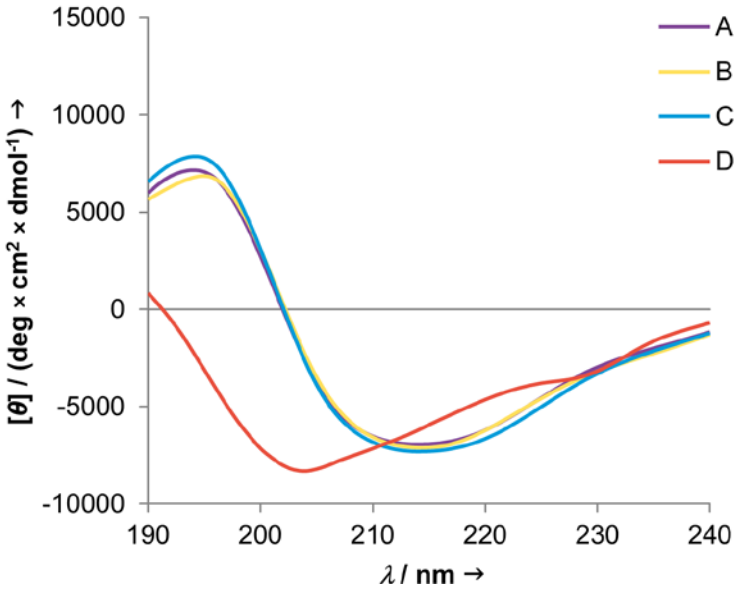

Figure 48. CD Spectra of BLG, PEGylated with NHS activated mPEG2k (A, purple). For comparison, the CD.-spectra of a BLG sample incubated with hydroxyl mPEG2k (B, yellow) an untreated BLG sample (C, blue) and a heat denaturated sample, measured at 80°C (D, red) are shown.

Although, the conjugate prepared with NHS-activated mPEG is milder for the preparation of nanoparticles, the BLG conjugate prepared with TsT-activated mPEG is used for the experiments described in the next section. This ensures a homogeneous sample setup and better comparability between the different proteins.

3.2.2 Cystein Selective Fluorescent Labeling of the Proteins

Site-specific Fluorescence Labeling of *β*-Lactoglobulin

In section 3.1.2, a method for the attachment of fluorophores via carbodiimide mediated amid formation was presented. In that approach free carboxylic groups on the protein surface take part in the reaction with an amine functionalized dye.

Now, a more site-specific reaction is presented. Cysteines are rarely presented on protein surfaces, as these amino acids are mainly responsible for building the three dimensional protein structure via intramolecular disulfide bonds.[150, 173] For example, the here presented proteins LYZ, OVA and FER do not present free thiol groups on their surface. However, HSA (cys35) and BLG (cys121) contains a single free thiol group. Using a selective linker molecule, this unique attribute can be used to address this cysteine on the protein surface. Therefore, a maleimide functionalized fluorescein was used for the selective attachment of the dye to BLG (selected as model protein with a single thiol group on the surface). Experiments were performed in collaboration with Carina Ade in the course of her bachelor thesis.[175]

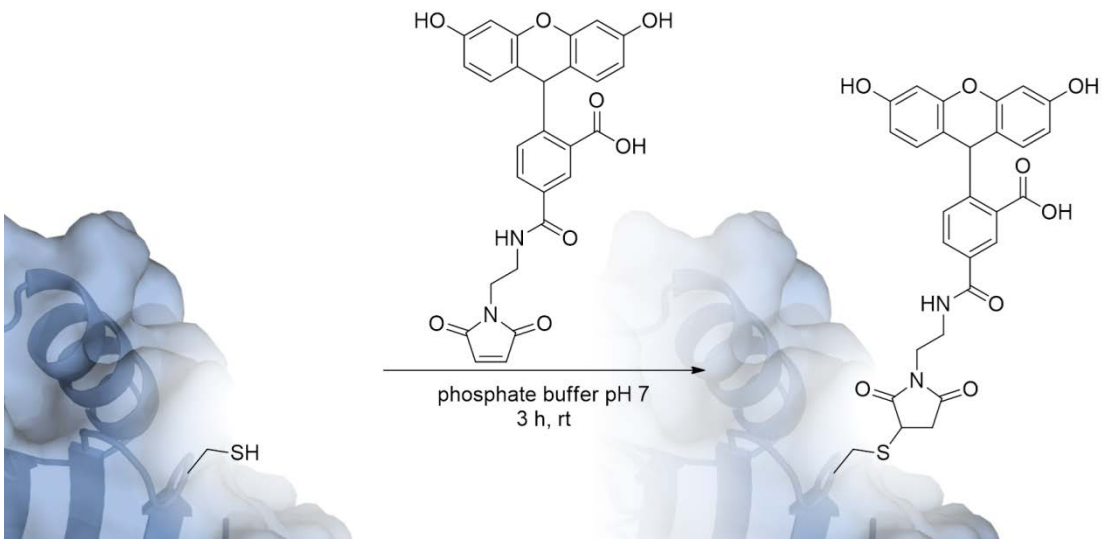

Scheme 5. Site selective attachment of fluorescein maleimide to the free tiol on the surface of BLG.

The reaction was carried out within 3 h at room temperature under neutral buffer conditions. In Figure 49, the fluorescein maleimide modified BLG (F_BLG ≙ F_B) is compared to the native protein (BLG ≙ B) prior and after PEGylation with NHS-activated mPEG. The left side of the image shows the coomassie stained gel, the right side shows the fluorescent image of the gel. Here only the dye-functionalized proteins and the marker lane are visible. In the SDS-Page it can be observed that the increase of the mol. wt. of the protein by the covalent attachment of fluorescein slightly influences the running behavior of the protein in the gel. Interestingly, the protein band of non-labeled protein (BLG^{NHS2k} ≙ B^{2k}) appears to have a slightly higher mol. wt. than the fluorescent-labeled protein (F_BLG^{NHS2k} ≙ FB^{2k}). This effect can be explained by the chosen reaction order. For BLG^{NHS2k} all nucleophilic groups of the protein surface are present for the reaction with NHS-activated mPEG. After the selective labeling of the free thiol of cys121, one nucleophilic acid less is available for the attachment of PEG. This is reflected in a slightly lower mol. wt. in the gel. Certainly, further research needs to be done to fully determine the influence of a cys modification before the PEGylation.

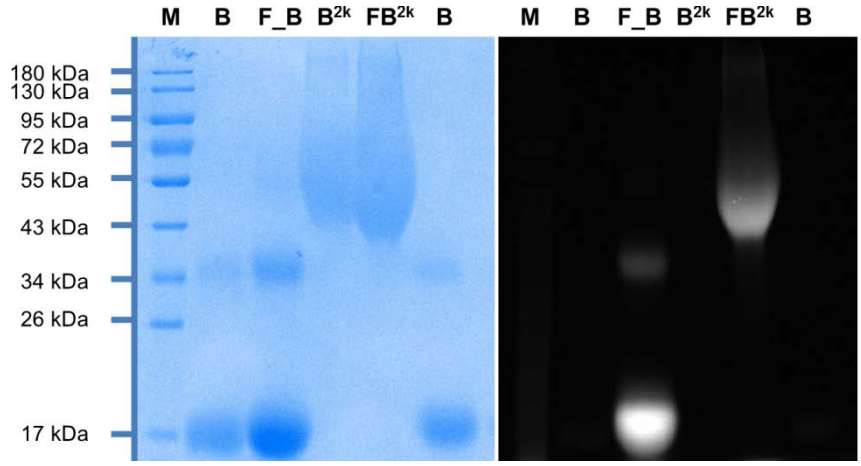

Figure 49. SDS-PAGE of fluorescence labeled BLG as coomassie stained gel (left) and as fluorescence image (right). A protein marker (Lane M) and native BLG (Lane B) are used as reference. Fluorescence labeled BLG (Lane F_B) shows a fluorescence signal in unlike the native protein. After PEGylation the size of both proteins increase significantly leading to the unlabeled BLG^{2k} conjugate (Lane B^{2k}) and the fluorescent conjugate (Lane FB^{2k}). Here, F_B shows a slightly lower mol.wt. than unlabeled B^{2k}. The polyacrylamide content was 12% with a thickness of 0.75 mm (first 90 V, 60 min; then 180 V, 60 min). Adapted from Carina Ades bachelor thesis.[175]

Fluorescein Content of Cys-selective Labeled BLG

The amount of fluorescein attached to the protein conjugate was determined using a standard dilution of free fluorescein ranging from 200 to 13 nM (Figure 61). The protein sample with a concentration of 270 nM shows a fluorescence that is equal of a concentration of 69.3 nM free fluorescein. With a fluorescein per F_BLG ratio of 0.26, every fourth BLG protein has a fluorescein molecule attached to its free thiol group of cys121. In comparison to the attachment of fluorescein amine to the surface of LYZ as described in section 3.1.2, the amount of fluorophore is increased by 2.5-times. Especially for CLSM imaging, this increase of the dye attached to the protein can lead to a significant improvement of the signal to noise ratio when the protein is spread over a large area and not concentrated on a single spot like an endosome (see Figure 38).

Table 12. The amount of attached cysteine selective fluorescein per BLG was calculated from the measured fluorescein concentration and the protein concentration used in the fluorescence assay. Based on this, approx. every fourth protein was modified with fluorescein.

Sample	c_{F_BLG} / nM	$c_{Fluorescein}$ / nM	Fluorescein per F_BLG
F_BLG	270	69.3	0.26

3.2.3 Preparation of Empty and Curcumin-loaded Nanoparticles

Particle preparation

The conjugates LYZ^{2k}, BLG^{2k}, OVA^{5k}, HSA^{5k} and FER^{5k} were used to produce empty and drug loaded nanoparticles. This time the potential anti-cancer drug curcumin (CUR) was used as alternative model drug with similar hydrophobic properties as doxorubicin. As described in detail for LYZ^{2k}, the protein-conjugates were dissolved in DCM. Here, CUR was added to the DCM solution instead of DOX. The organic solvent was layered with PBS and sonication forms a stable emulsion of DCM droplets in the aqueous buffer. Evaporation of the solvent and dialysis led to a suspension of CUR-loaded and empty NPs. Figure 50 presents empty (–) and yellow colored CUR-loaded NPs (+) using LYZ^{2k}, BLG^{2k}, OVA^{5k}, HSA^{5k} and FER^{5k} as particle material. The orange color of FER NPs is caused by the iron ions entrapped in the protein cage.

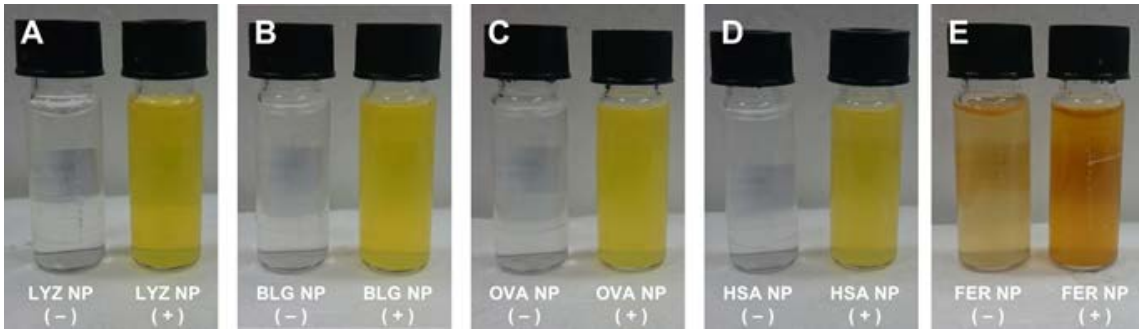

Figure 50. Nanoparticle suspensions of empty (–) and yellow CUR-loaded (+) particles obtained from nano-emulsion procedure. The CUR content was adjusted to 100 μM and the empty particles diluted in the same manner. The FER NPs show an orange color due to the iron entrapped in the FER protein cage.

Curcumin Content of Drug-loaded Nanoparticles

The CUR content of the drug-loaded NPs was determined by measuring the absorbance (λ = 488 nm) of the particle suspensions in comparison to a solution of free CUR (Figure 64). As free CUR is not soluble in water, a mixture of DMSO and water in the ratio of 9:1 was used to ensure a complete solubility of the drug. Also, for the NP samples the high amount of DMSO leads to a dissolution of the particle material and the release of the entrapped drug. From the measured CUR content, the entrapment efficiency of curcumin in NPs (EE_{CUR}) was calculated by Equation 3 together with Equation 4. The drug loading in weight percentage $wt\%_{CUR}$ is calculated by Equation 5 together with Equation 6. The drug content ranges from 234.5 to 331.0 μM. The entrapment efficiency of curcumin is thereby between 43 and 61% with the weight percentage of curcumin in the NPs ranging from 4.1 to 5.8%. This is approx. four to six times higher as previously reported for DOX (see section 3.1.3).

Table 13. Entrapment efficiency (EE) and weight percentage (wt%) were calculated from the CUR concentration (c_{CUR}) by Equation 3 and Equation 5.

Nanoparticle Sample	c_{CUR} / μM	$wt\%_{CUR}$ / %	EE_{CUR} / %
LYZ NP (+)	331.0	5.8	60.9
BLG NP (+)	234.5	4.1	43.2
OVA NP (+)	314.2	5.5	57.8
HSA NP (+)	245.2	4.3	45.2
FER NP (+)	310.3	5.4	57.2

Size Determination by Nanoparticle Tracking Analysis

The size of CUR-loaded and empty NPs was determined via Nanoparticle Tracking Analysis (NTA). After NP preparation, samples of the NP suspensions were diluted and the size was determined as described for DOX-loaded NPs. The size distribution curves are presented for empty NPs in Figure 51 and for CUR-loaded NPs in Figure 52. The mean and modal diameter as well as the standard deviation (SD) is presented in detail in Table 14. The mean size of the particles ranges from 187.2 to 267.2 nm, whereas the modal size, that represents the size of the highest population of NPs ranges from 113.0 to 117.4 nm. In general result particles prepared from LYZ^{2k} and BLG^{2k} in smaller mean diameters. Here, both proteins also carry the smaller mPEG2k chains on the surface. In addition, the attachment of small PEG chains also results in a higher protein to PEG ratio (both in the conjugate and also in the resulting particles). Since the particles are held together mainly by hydrophobic interactions between the protein conjugates, these interactions are expected to be higher when the surface shielding mPEG chain are smaller. Hence, the resulting particles as in general a bit smaller than particles made from larger proteins. Additionally, after the complete evaporation of the DCM during the NP preparation, the polymer starts swelling in the aqueous environment. For the longer mPEG5k chains this effect is expected to be higher than for mPEG2k chains.

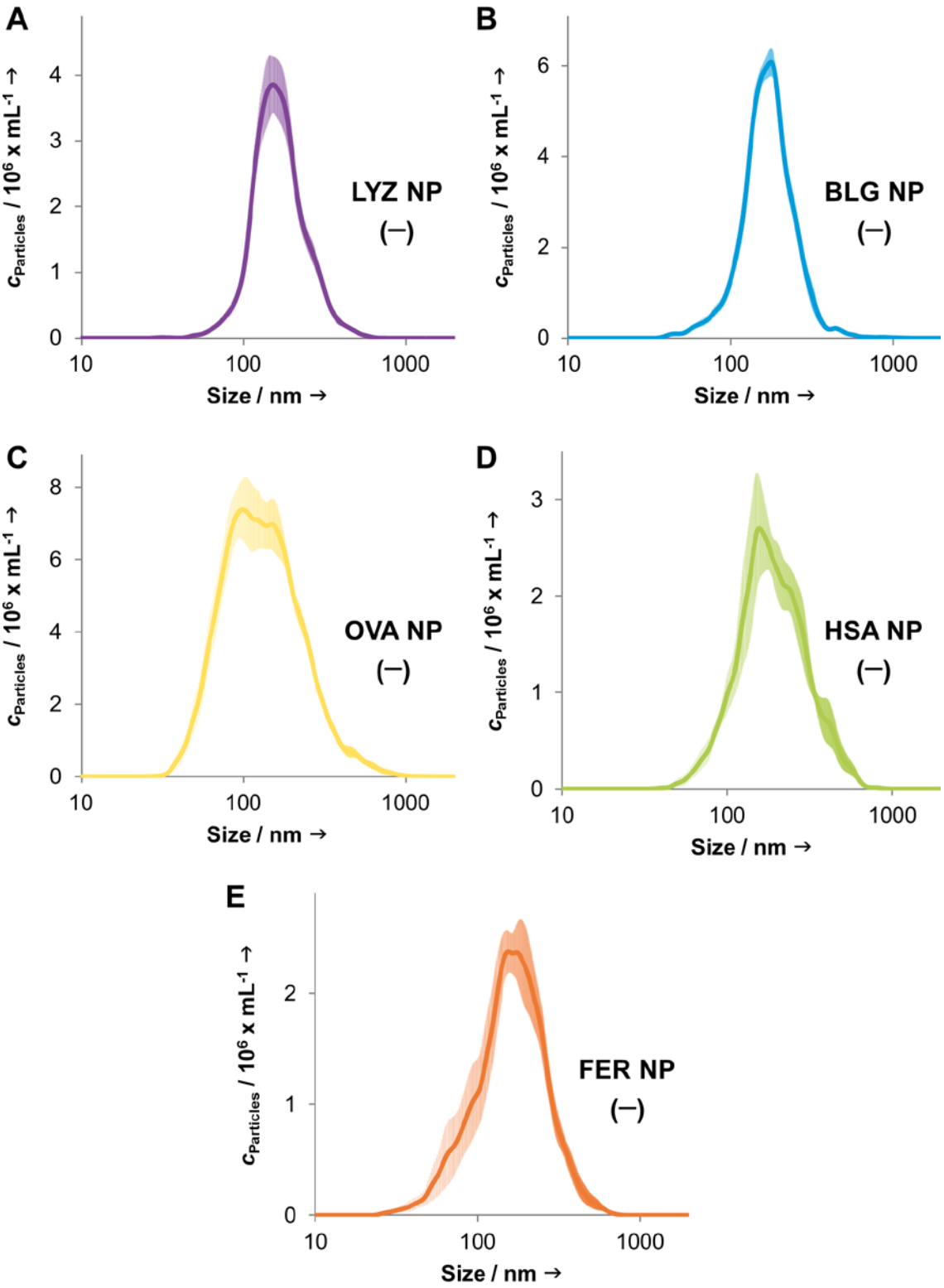

Figure 51. Nanoparticle Tracking Analysis of empty nanoparticles prepared via single emulsion from LYZ^{2k} (A), BLG^{2k} (B), OVA^{5k} (C), HSA^{5k} and FER^{5k}. The modal size of the empty particles ranges from 121 to 177 nm.

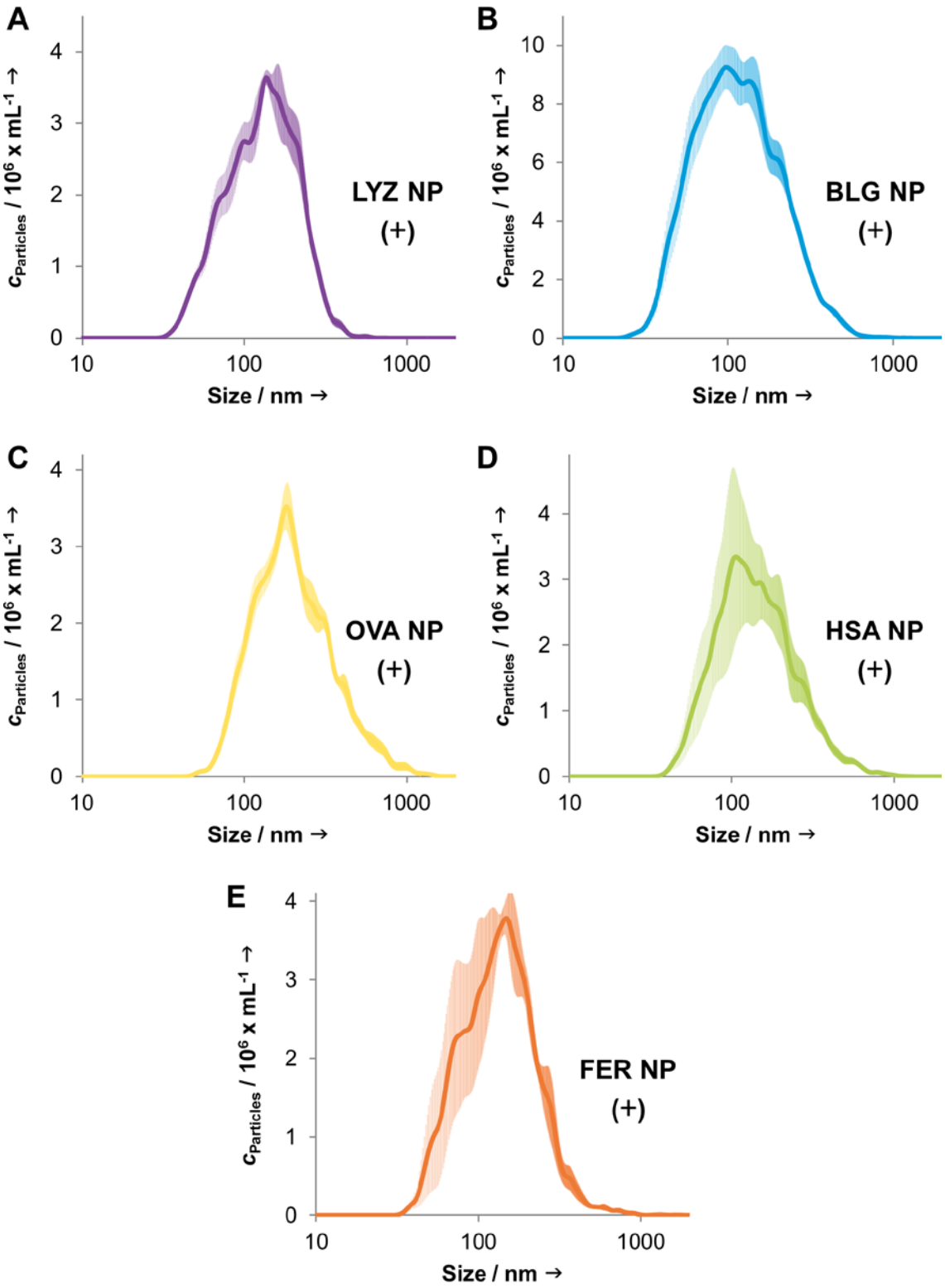

Figure 52. Nanoparticle Tracking Analysis of CUR-loaded nanoparticles prepared via single emulsion from LYZ^{2k} (A), BLG^{2k} (B), OVA^{5k} (C), HSA^{5k} and FER^{5k}. The modal size of the empty particles ranges from 113 to 149 nm.

Table 14. Detailed size distribution of empty and CUR-loaded NPs obtained by nano emulsion. The protein conjugates LYZ^{2k}, BLG^{2k}, OVA^{5k}, HSA^{5k} and FER^{5k} were used as material. Data was obtained by NTA. Mean size and SD (standard deviation) correspond to the arithmetic values calculated based on the sizes of all particles detected in the NTA measurement. Mode values describe the average size of the main particle population.

Nanoparticle Sample	d_{mean} **/ nm**	d_{mode} **/ nm**	**SD / nm**	D_{90} **/ nm**	D_{50} **/ nm**	D_{10} **/ nm**
LYZ NP (–)	203.7 ± 3.7	148.1 ± 6.0	85.8 ± 4.5	316.5 ± 8.1	181.9 ± 4.9	118.7 ± 1.5
LYZ NP (+)	174.9 ± 4.0	149.3 ± 6.4	78.4 ± 3.1	274.0 ± 5.9	163.5 ± 3.9	83.5 ± 2.5
BLG NP (–)	211.9 ± 6.5	167.2 ± 6.4	102.1 ± 14.3	303.1 ± 9.3	188.2 ± 4.4	125.7 ± 4.2
BLG NP (+)	187.2 ± 7.5	113.0 ± 17.2	112.3 ± 3.6	331.0 ± 14.9	158.5 ± 5.7	74.0 ± 5.4
OVA NP (–)	217.2 ± 12.1	121.3 ± 19.0	144.0 ± 13.7	411.1 ± 35.6	176.6 ± 9.5	83.3 ± 3.9
OVA NP (+)	267.2 ± 23.5	123.5 ± 21.6	227.4 ± 25.1	700.4 ± 51.5	291.5 ± 22.9	132.5 ± 4.9
HSA NP (–)	257.1 ± 20.1	176.5 ± 15.8	119.0 ± 10.9	419.3 ± 33.7	226.6 ± 24.0	133.4 ± 10.9
HSA NP (+)	248.0 ± 20.4	135.7 ± 12.4	163.2 ± 20.1	475.3 ± 53.9	196.4 ± 15.5	98.6 ± 8.9
FER NP (–)	223.4 ± 12.9	177.4 ± 15.4	102.2 ± 10.4	360.6 ± 28.8	199.4 ± 12.4	113.9 ± 11.5
FER NP (+)	210.4 ± 06.3	129.1 ± 13.6	148.2 ± 4.7	353.9 ± 9.6	173.6 ± 4.7	90.5 ± 9.9

Electron Microscopy Images of CUR-loaded NPs

Transmission electron microscopy (TEM) was used to visualize the CUR-loaded NPs. Figure 53 shows that the TEM images represent the size distribution of the NPs detected by NTA. It has to be mentioned, that the particle samples are measured in a dry state. Under these conditions, the mPEG starts to crystalize that leads to a change in the size of the nanoparticles which is not representative for the particles in solution. For this reason, the TEM images were not used for further size determination.

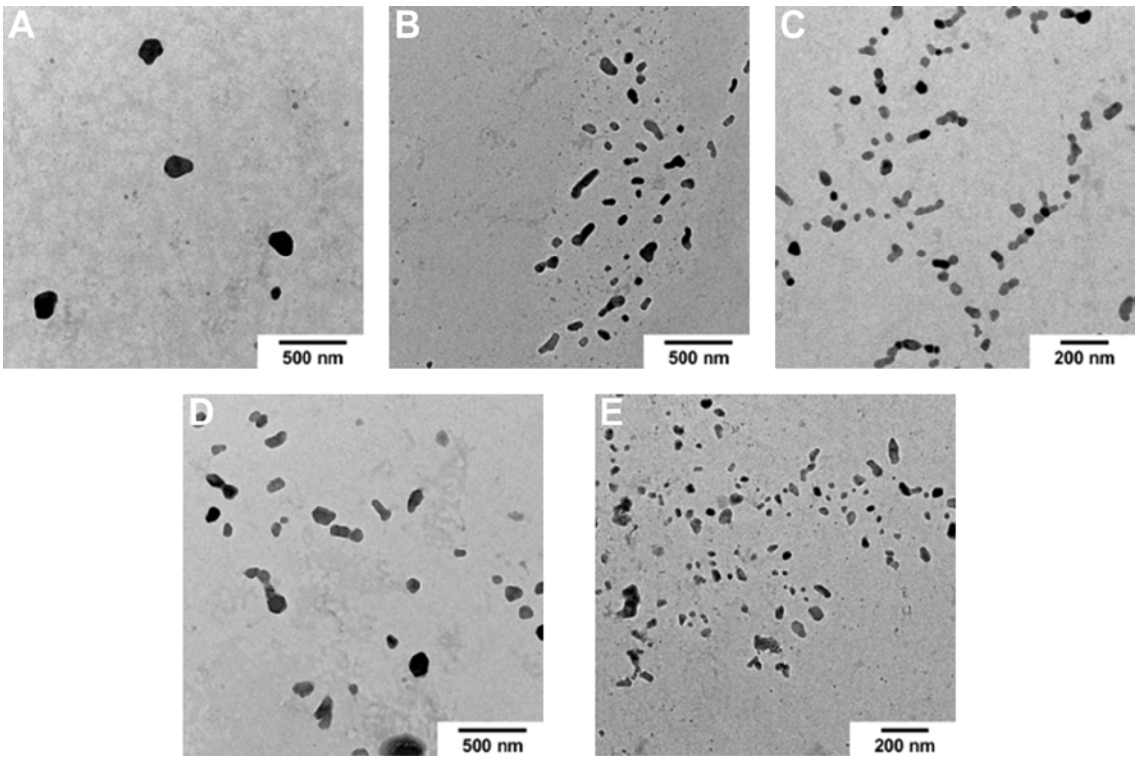

Figure 53. TEM images of CUR-loaded (+) LYZ (A), BLG (B), OVA (C), HSA (D) and FER (E) NPs obtained from nano-emulsion procedure. The NPs show similar size distributions as observed by nanoparticle tracking analysis.

Surface Charge of Protein Nanoparticles

The ζ-potential, representing the surface charge of the NPs, of the particle suspensions was determined with the help of a Zetasizer (Table 15). Overall, the ζ-potential of the particles ranges from –1.4 to –17.6 mV. As already observed, the charge of the particle surface is negative for all samples. Again, the reason for this is the attachment of mPEG to the amines on the protein surface, leaving mainly carboxylic groups as negatively charged groups on the protein surface. The particles prepared from the conjugates with mPEG2k (LYZ^{2k} and BLG^{2k}) show more negative values for the surface charge than the particles prepared from proteins that are modified with mPEG5k chains. It can be assumed that the higher density of the linear extended mPEG chains shields the charges on the protein surface (see section 3.1.1) and thereby leads to a more neutral surface charge. The entrapment of CUR into the NPs does not change the ζ-potential of the particle suspensions for all particles prepared from proteins modified with mPEG5k. For the particles resulting from proteins modified with mPEG2k, the ζ-potential is increased when curcumin is encapsulated.

Table 15. ζ-potential of empty and CUR-loaded nanoparticles determined by DLS. The surface charge is negative for all obtained samples. Proteins PEGylated with shorter mPEG chains lead to a more negative surface charge.

Nanoparticle Sample	**ζ-Potential / mV**
LYZ^{2k} NP (–)	– 17.56 ± 1.75
LYZ^{2k} NP (+)	– 8.92 ± 0.11
BLG^{2k} NP (–)	– 16.37 ± 0.35
BLG^{2k} NP (+)	– 9.91 ± 0.63
OVA^{5k} NP (–)	– 1.99 ± 0.03
OVA^{5k} NP (+)	– 1.40 ± 0.57
HSA^{5k} NP (–)	– 2.00 ± 0.43
HSA^{5k} NP (+)	– 1.95 ± 0.38
FER^{5k} NP (–)	– 4.86 ± 0.65
FER^{5k} NP (+)	– 5.51 ± 0.66

3.2.4 *In Vitro* Effects of Protein Nanoparticles

Effects on Cell Viability of Empty and CUR-loaded Nanoparticles

The toxic effects towards human carcinoma cells (HeLa) were tested using the MTT method, as previously described for DOX-loaded NPs. Cells were incubated with CUR-loaded nanoparticles with a final CUR concentration ranging from 1.5 to 50 μM. Empty NPs – diluted in the same manner to achieve the same concentration of the particle material – were used as reference. Empty NPs do not show any toxic effects towards HeLa cells. For all dilutions, no difference between the used protein material was observed. However, CUR-loaded NPs induce a decrease of the cell viability of HeLa cells. This inhibitory effect on the cell growth starts at CUR concentrations of 6 μM and enhances when the CUR content in the sample increases. The effect on the cell viability is lower than previously reported for free CUR (IC_{50} = 8 μM[176]), but the here presented particle system does not require ethanol or DMSO in the medium to dissolve the drug.

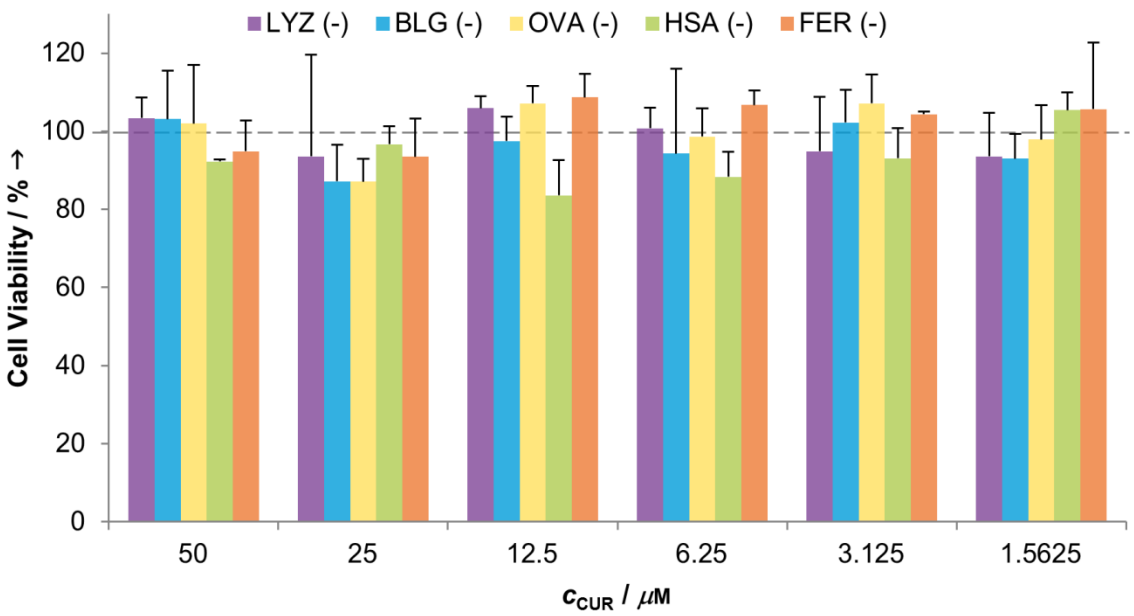

Figure 54. Cell viability of HeLa cells after incubation with empty (–) NPs after incubation for 48 h. No decrease of cell viability is observed at any concentration. Samples were diluted in the same manner as CUR-loaded particles to achieve the same amount of particle material on the cells.

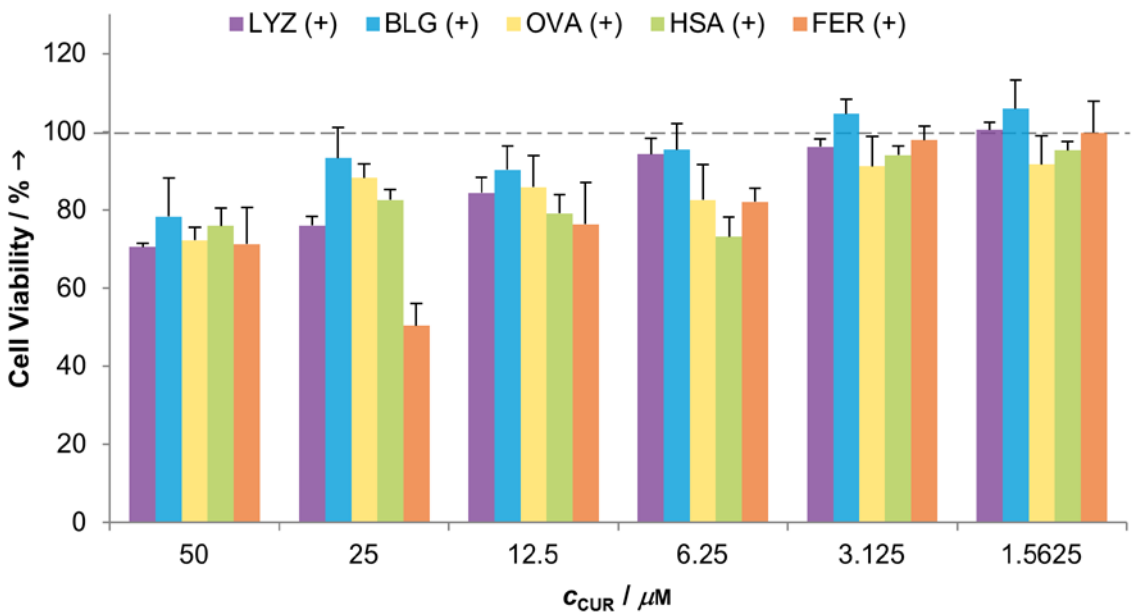

Figure 55. Cell viability of HeLa cells after incubation with CUR-loaded (+) NPs (B) after incubation for 48 h. A decrease of cell viability is observed from a concentration of CUR of 6 μM.

In summary in can be stated that our nanoparticles – consisting of various surface PEGylated proteins – are non-toxic regardless of the initial protein that was used for the particle preparation. When looking at drug-loaded particles, it can be concluded, that all proteins are suitable to stabilize CUR and by that induce a decrease in cell viability. Here, no significant difference between the different proteins in observed.

In this section, it was shown that it is possible to transfer the presented nanoparticle preparation procedure to different hydrophobic payloads and proteins in a broad size range. This can be used to transfer this carrier system to a variety of hydrophobic drugs to optimize their therapeutic effects. Benefits from the transfer to different proteins can be taken in the future by the use of this procedure to prepare nanoparticles from more therapeutically relevant proteins (e.g. asparaginase) than the ones presented here.

3.3 Particle Preparation for Hydrophilic Payloads

In this section, the modified proteins are used for a different type of emulsification method that allows the entrapment of hydrophilic (macro)molecules. To entrap hydrophilic drugs like nucleic acids, it is necessary to surround the water-soluble payload with the lipophilic protein material to achieve an accumulation of the payload in the core area of the nanoparticles. The drugs have to be shielded (and in some cases even protected) from their surrounding environment, preventing them from mixing them with the water phase. Therefore, a double emulsification method from Cohen *et al.*[137] was adapted for the protein-polymer conjugates. Here, the lipophilic protein material is dissolved in DCM and layered with a minimal amount of an aqueous solution containing the hydrophilic payload.

3.3.1 Entrapment of Rhodamine-labeled Dextran

Double Emulsion Method

The double emulsion method is stepwise illustrated in Figure 56. A first sonication step forms an emulsion of water droplets – here, containing a labeled dextran as hydrophilic model drug – in the DCM solution. At this point the protein conjugates are still spread evenly in the DCM phase. This water-in-oil (w/o) emulsion is then layered with a five-fold amount of PBS buffer. Now, a second sonication step forms a water-in-oil-in-water (w/o/w) emulsion. In this state, the water droplets – still containing the hydrophilic drug – are surrounded by a layer of DCM that is containing the desired lipophilic particle material. These DCM-layered water droplets are spread evenly in the PBS buffer without the need off additional stabilizer or surfactant. Again, the protein-pendant PEG chains act as stabilizer of the emulsion. Similar to the single emulsion procedure (see section 3.1.3), evaporation of the highly volatile DCM leads to self-assembly of the proteins and a particle matrix of tightly packed individual proteins is formed. Thereby the lipophilic protein-material entraps the hydrophilic molecules between the individual proteins and shield the payload from the outer aqueous phase. Again, due to their lipophilic character, the protein-PEG conjugates prefer the hydrophobic intermolecular interactions in the solid particles and do not diffuse into the surrounding water. The particles are stable without additional cross-linking of the particle surface.

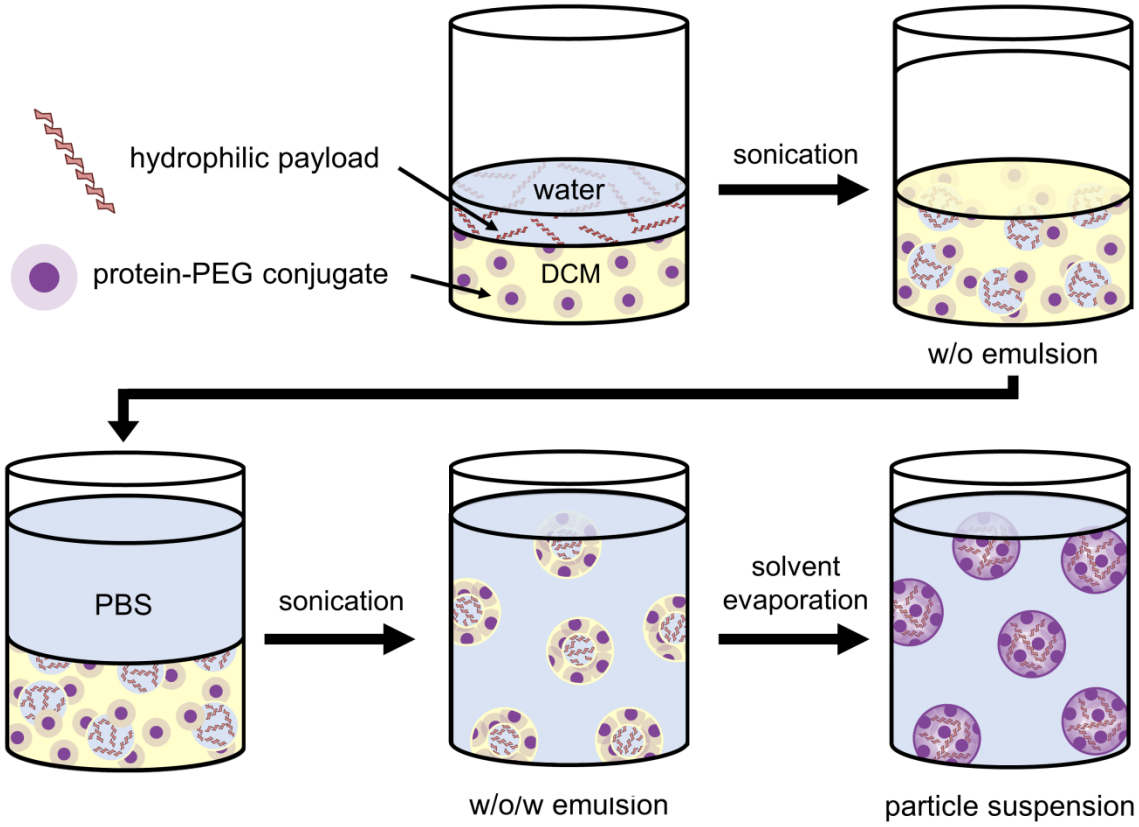

Figure 56. Schematic entrapment of hydrophilic molecules by double emulsion. The hydrophobic payload is dissolved in water and the particle material in DCM. A fist sonication step forms a water-in-oil (w/o) emulsion. After layering the emulsion with PBS, a second sonication step forms a water-in-oil-in-water (w/o/w) emulsion. Evaporation of the organic solvent leads to a stable suspension of nanoparticles in the PBS buffer.

Encapsulation of Rhodamine-labeled Dextran as Hydrophilic Model Drug

As proof of principle, that a hydrophilic payload can be entrapped by this method, the system was evaluated by using rhodamine-labeled dextran (RhoDEX). The mol. wt. of RhoDEX (10 kDa) is similar to the mol. wt. of common nucleic acids like siRNA (13 to 14 kDa).[177] Additionally, the fluorescent label allows the determination of the drug content and entrapment efficiency. For this approach, the albumin conjugates OVA^{5k} and BSA^{5k} were used to form the lipophilic particle material (The modification of BSA is not presented in detail previously, but highly corresponds to the sequentially similar HSA; for further information, see Appendix). The first emulsion was prepared with 100 μL water containing RhoDEX and 800 μL DCM containing the protein material. For the second emulsion, 2.5 mL PBS buffer was added. After solvent evaporation, the particles were dialyzed (MWCO 100 kDa) to remove non-entrapped RhoDEX. The size distribution of the obtained particles was determined by NTA and is shown in Figure 57 and Table 16. The mean sizes of the particles prepared by double emulsion are with an average diameter of around 240 nm for BSA NPs and around 300 nm for OVA NPs slightly larger compared to particles obtained by single emulsion. A reason for this might be the ratio of the solvents in the second emulsification step. The ratio for single emulsion was 1:5 (DCM:PBS), here a ratio of around 1:3 was used. This might lead to larger oil droplets during the emulsification step and therefore to larger assemblies of proteins. The entrapment of the hydrophilic RhoDEX into the particle matrix did not show any significant influence on the particle size compared to empty particles (Figure 57 and

Table 16. Detailed size distribution of empty (–) and RhoDEX-loaded (+) nanoparticles prepared by a double emulsion procedure. OVA^{5k} and BSA^{5k} were used as particle matrix material. Data was obtained by NTA. Mean size and SD (standard deviation) correspond to the arithmetic values calculated based on the sizes of all particles detected in the NTA measurement. Mode values describe the average size of the main particle population.

Nanoparticle Sample	d_{mean} / nm	d_{mode} / nm	SD / nm	D_{90} / nm	D_{50} / nm	D_{10} / nm
OVA NP (–)	307.3 ± 2.7	253.3 ± 16.9	141.4 ± 6.0	482.5 ± 18.6	227.2 ± 3.9	162.4 ± 6.3
OVA NP (+)	290.1 ± 8.9	226.9 ± 11.3	114.1 ± 8.4	476.7 ± 22.2	262.9 ± 5.4	148.1 ± 2.1
BSA NP (–)	235.7 ± 7.2	147.9 ± 6.7	126.4 ± 9.7	405.6 ± 22.0	201.4 ± 4.0	112.5 ± 1.4
BSA NP (+)	238.0 ± 11.8	152.7 ± 10.0	137.4 ± 6.8	401.8 ± 19.6	199.9 ± 11.1	111.0 ± 4.5

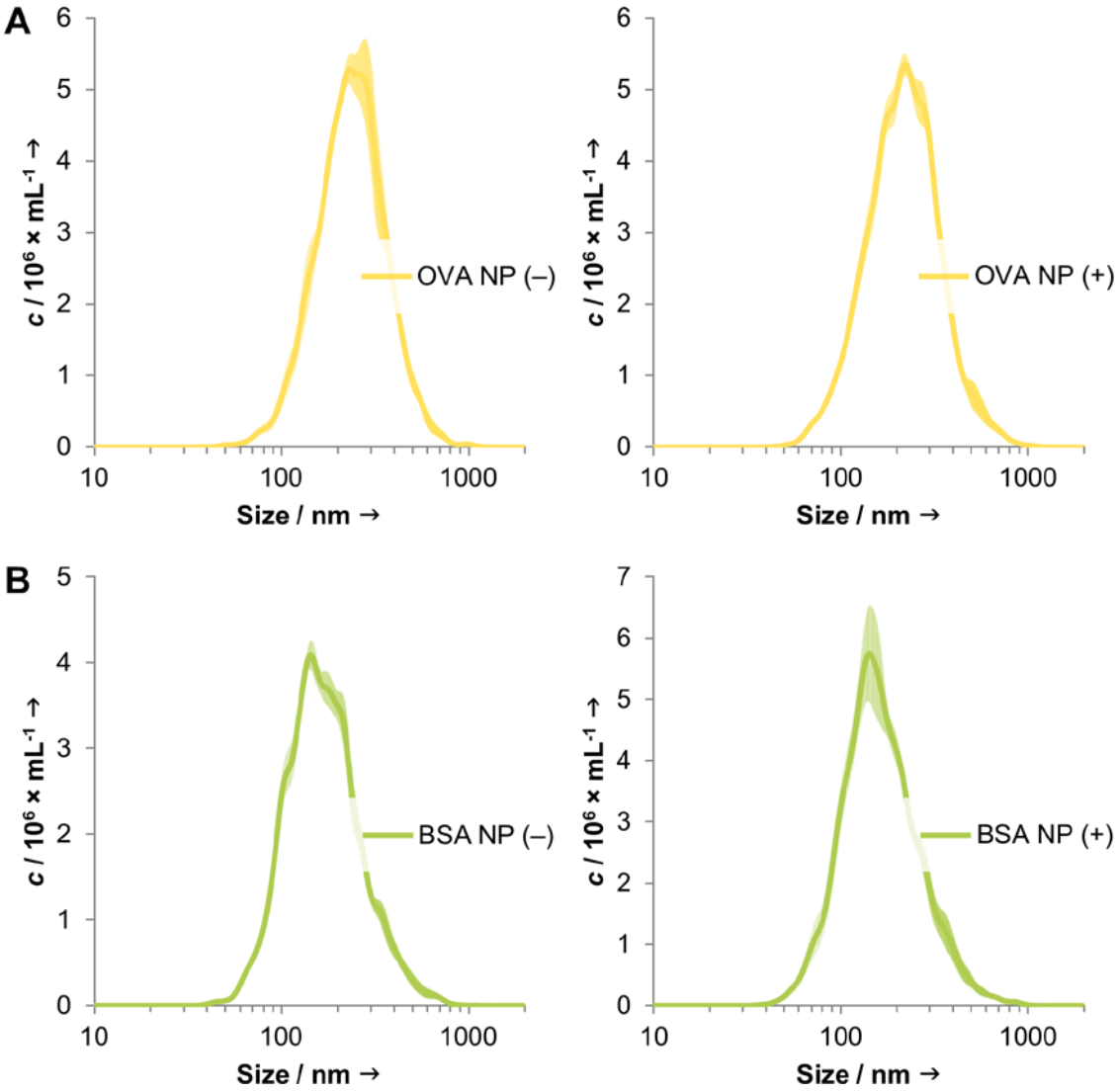

Figure 57. Size distribution of empty (–) and RhoDEX-loaded (+) nanoparticles prepared by a double emulsion procedure. OVA^{5k} (A) and BSA^{5k} (B) were used as particle matrix material. Data were obtained by NTA.

Rho-DEX content of Drug-loadedNanoparticles

The content of dextran entrapped in the protein particles was determined by comparing the fluorescence of the nanoparticles to a standard dilution of RhoDEX in free form ranging from 25 to 600 ng/mL (Figure 65). A successful entrapment of RhoDEX is possible with both protein conjugates. Interestingly, the amount of entrapped RhoDEX in the OVA^{5k} protein matrix is around 7.5-times higher than the amount of RhoDEX entrapped in BSA^{5k} particles. It shows an entrapment efficiency of around 54 %, whereas only 7.2 % of the payload feed was entrapped in the BSA^{5k} matrix. A reason for this might be, that the intrinsic hydrophobic surface characteristic of BSA obstructs the entrapment of hydrophilic payloads. Further research needs to be done in this regard, to clarify the influence of different proteins for the efficient entrapment of hydrophilic drugs.

Table 17. RhoDEX content of loaded nanoparticles prepared by double emulsion.

Nanoparticle Sample	c_{RhoDEX} **/ ng mL^{-1}**	**EE / %**
OVA NP (+)	216.6	54.1
BSA NP (+)	28.6	7.2

3.3.2 Size Reduction of Particles Prepared by Double Emulsion

For the proof of principle experiments, the size of the obtained nanoparticles in a range between 240 and 300 nm are acceptable. However, for an efficient drug delivery by passive targeting, the optimal particle size should be below 200 nm (see section 1.1). For this reason, it was attempted to decrease the size of the particles, prepared by double emulsion. The same amount of PBS (2.5 mL, volume ratio DCM/PBS = 1:3) as used for the single emulsion procedure led to larger particles than obtained during single emulsion experiments. As discussed before, the main factor for the particles sizes might be the ratio of aqueous to oil phase during the second emulsification step.

Here, this ratio was changed and the same volume ratio of PBS referred to DCM (4 mL, volume ratio DCM/PBS = 1:5) was used. Again, the protein conjugates OVA^{5k} and HSA^{5k} were used. As LYZ^{2k} previously showed smaller particle diameters than OVA^{5k} and HSA^{5k} during single emulsion (see section 3.2), this protein conjugate was used in addition to investigate whether this effect occurs during double emulsion, too. The particle size distribution is shown in Figure 58 and presented detailed in Table 18.

Particles obtained by this optimized volume ratio show a similar size distribution as previously presented for particles prepared by the single emulsion experiments (Table 5 and Table 14). This leads to the conclusion that the ratio of PBS to DCM in the second sonication step is crucial for the size of the resulting nanoparticles. This information offers the opportunity to vary the particle size by changing the volume ratios of organic and aqueous solvents.

Table 18. Detailed size distribution of empty nanoparticles prepared by a double emulsion procedure. LYZ^{2k} (A), OVA^{5k} (B) and HSA^{5k} (C) were used as particle matrix material. Data were obtained by NTA.

Nanoparticle Sample	d_{mean} / nm	d_{mode} / nm	SD / nm	D_{90} / nm	D_{50} / nm	D_{10} / nm
LYZ NP (–)	123.2± 2.2	101.7 ± 2.9	56.1 ± 1.8	190.1 ± 5.6	111.5 ± 1.6	65.5 ± 1.1
OVA NP (–)	160.1 ± 1.8	137.3 ± 2.9	69.0 ± 1.6	239.3 ± 3.9	148.5 ± 1.1	87.9 ± 1.2
HSA NP (–)	165.0 ± 1.7	141.3± 6.1	68.1 ± 2.8	245.0 ± 4.3	153.9 ± 2.1	91.7 ± 1.0

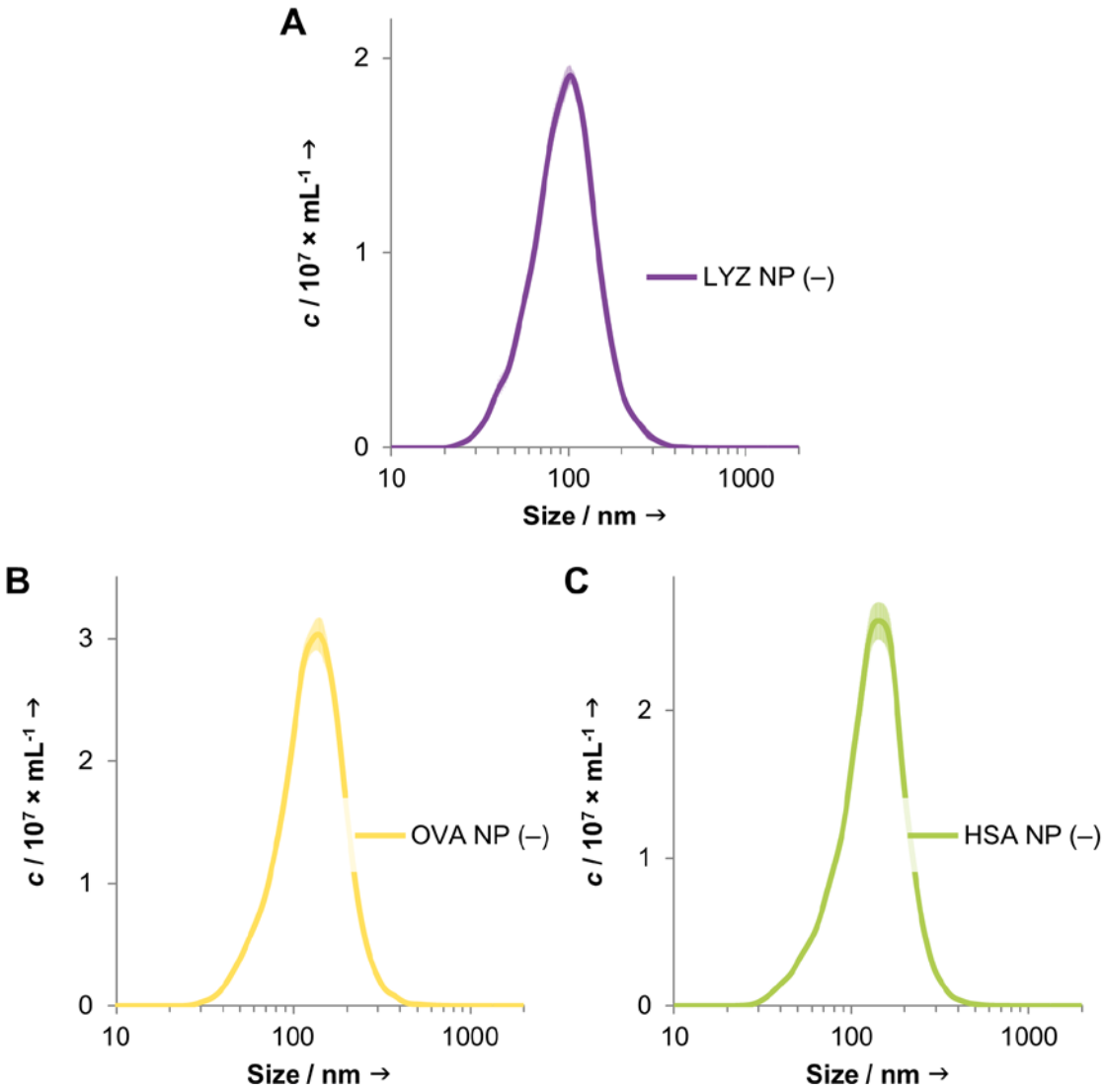

Figure 58. Size distribution curves of empty nanoparticles prepared by a double emulsion procedure. LYZ^{2k} (A), OVA^{5k} (B) and HSA^{5k} (C) were used as particle matrix material. Distribution curves were obtained by NTA.

It can be concluded, that the double emulsion method is in principle suitable for the entrapment of hydrophilic payloads, e.g. RhoDEX. This successfully expands the possible applications of nanoparticles based on protein-PEG conjugates for the delivery of hydrophilic drugs. In future experiments, therapeutic relevant payload such as RNA or DNA should be evaluated, in particular in terms of loading efficiency and *in vitro* functionality.

4 CONCLUSION AND OUTLOOK

In summary of this work, a novel method for the preparation of protein-based nanoparticles for drug delivery applications was established. Hereby, the focus was on the development and the evaluation of the nanocarrier system for hydrophobic payloads. By showing that it is possible to apply this procedure to proteins of various sizes, it should be possible to produce nanoparticles from any protein of choice. Additionally, it was shown in first tests that this system can also be transferred for the delivery of hydrophilic payloads.

4.1 Lysozyme Nanoparticles for Doxorubicin-Delivery

Lysozyme PEGylation

By using lysozyme as model protein, the PEGylation procedure was investigated in detail. Trichloro-*s*-triazine was successfully used to activate the unreactive hydroxyl group of the polymer for reactions with nucleophilic amino acids on the protein. The attachment of the polymer to the protein surface resulted in a protein-polymer conjugate with increased size compared to the native protein. Qualitatively, the conjugation with mPEG led to a loss of primary amines on the protein surface. This leads to a change in the surface charge (pI), as only carboxylic groups remain on the protein surface. The remaining carboxylic acid groups on the protein were afterwards used to attach a fluorescent dye (6-fluoresceinamine) for further *in vitro* studies. The attachment of the polymer also increases the hydrodynamic diameter. Light scattering measurements showed a growth from 3.6 nm for the native to 10.8 nm for the PEGylated protein. Additionally, the PEG conjugation is even visible in electron microscopy images, that indicate a faint PEG corona around the protein core. Quantitatively, the PEGylation increases of the mol. wt. of the resulting conjugate to 34.9 kDa. This means that 10 mPEG chains with a mol. wt. of 2 kDa are attached to the protein surface. Therefore, it can be stated that PEGylation of LYZ with TsT activated mPEG led to a complete modification of nucleophilic groups on the protein surface. Additionally, a conclusion of the PEG morphology on the protein surface is drawn. By the grafting density of 0.25 mPEG2k chains per nm^2 on the protein surface it can be assumed, that the PEG chains form an extended mushroom to brush-like structure. In the case of mPEG5k the grafting density on the surface is with 5–8 chains markedly lower, however the likelihood of a brush-like orientation is

increased. Despite the high surface modification, the protein integrity is preserved. This is on one hand confirmed by investigating the secondary structural elements via CD spectroscopy and on the other by the retained enzymatic glycosidase activity of lysozyme. The loss in protein activity for LYZ^{2k} to 19% and for LYZ^{5k} to 7% can be explained by the high density of the mPEG chains around the protein as the polymer layer most likely hinders the substrate to reach the catalytic site of the enzyme. The high surface PEGylation also leads to a transfer of the solubility behavior of mPEG to the resulting protein PEG conjugate. By this, the conjugate is soluble in organic solvents like chloroform, dichloromethane, and toluene without precipitation. Furthermore, it was shown in extraction experiments that the protein-PEG conjugates prefer an organic DCM environment over an aqueous.

Preparation of Empty and Doxorubicin-loaded Nanoparticles

After the successful preparation of the lysozyme-PEG conjugate, the enhanced solubility behavior allowed the use in a – for proteins unique – single emulsification technique. Here, the protein is dissolved in the organic phase along with the desired payload. In this case, the anti-cancer drug doxorubicin was used. By layering the organic phase with aqueous buffer and sonication, an oil-in-water nanoemulsion is prepared. It was found out, that the resulting emulsion was stable without the need of stabilizers as the protein-PEG conjugate works as stabilizing agent itself. Evaporation of the organic solvent and subsequent dialysis leads to a suspension of stable nanoparticles that do not require further cross-linking for stability. Particles can be prepared by this method either with, or without entrapped payload. The size of the resulting particles was determined by NTA and DLS. Both methods show sizes around 100 nm for empty as well as for drug-loaded NPs. Furthermore, it was presented that these particle sizes do not change upon storage for 6 months at +4°C. TEM images helped to obtain a visual representation of the particle morphology and showed that the nanocarrier consist of multiple individual protein conjugates forming a larger particle. Doxorubicin was entrapped into the protein particle matrix with an efficiency of around 9% leading to a weight percentage in the final particle of around 1% which is indeed on the lower end compared with other literature known nanocarriers – a typically range is between 1 and 10%[22] – and leaves room for further improvement. The particles are stable in the physiologically relevant buffers PBS and DMEM that represent an extracellular environment. Incubation of the particles at low pH

(pH 5.2), in the presence of proteases (trypsin) and a reductive environment (10 mM GSH) led to a release of the drug. These conditions represent the intracellular environment as present after particle uptake by cells. Furthermore, empty nanoparticles were tested on their retained glucosidase activity and remained 14% of the activity of the PEGylated protein (3% of native protein).

In Vitro Effects of Lysozyme Nanoparticles

To gain first information of an association of the nanoparticles with HeLa cells, FACS was used. Here, the cell association of both, the drug and the particles increased over time. CLSM was performed to ensure a cellular uptake in HeLa cells on one hand, but also whether the particles and the drug are taken up simultaneously. Here, it is presented that particles and payload are taken up as a unit, showing that the particles are still intact. Additionally a slow release of the drug inside of the cells and a final accumulation of the drug in the nucleus can be observed. These results confirm the previously gained results that the particles are stable in an extracellular environment and only release the entrapped drug once inside the cells. A cell viability assay with HeLa cells showed no loss in toxicity of the drug. Furthermore, empty nanoparticles and all materials used for the NP preparation did not show any toxic effects. This leads to the conclusion that the here presented nanocarrier system can successfully deliver and release a hydrophobic payload into cancer cells without inhibition of the therapeutic effect of the drug. This is a promising starting point for the extension of the particle system to other proteins and payloads.

4.2 Transfer of the Model System to Various Proteins

Protein PEGylation

The idea of performing a lipohphilic switch was successfully transferred to proteins ranging from 18 to around 500 kDa. Namely, *β*-lactoglobulin, ovalbumin, human serum albumin, bovine serum albumin and ferritin. Here it is observed, that the length of the attached mPEG chain is decisive whether the protein-PEG conjugate becomes soluble in DCM or not. Small proteins like LYZ and BLG become soluble after PEGylation with mPEG2k. HSA, BSA and FER conjugates, however, are only soluble when PEGylated with mPEG5k. OVA – with its native size of 43 kDa – appears to represent the threshold from which larger mPEG chains are required. Although it becomes soluble in DCM after 4 h at room temperature, its solubility behavior was not considered to be sufficient enough for further particle preparation. Generally, protein conjugates obtained from the smaller proteins BLG and LYZ were easier to handle and investigate as conjugates from large proteins were not suitable for all analysis methods. When transferring the PEGylation procedure to the various proteins, it was observed that the secondary structure was not fully preserved for all proteins – mainly BLG showed structural changes. However, the use of NHS-activated PEG for BLG also led to a high surface PEGylation whilst retaining the secondary structure elements. Therefore, this could represent a promising improvement of the protein conjugation, especially when using with fragile proteins. Additionally, it was shown that the free thiol of BLG can be selectively labeled with a fluorophore (fluorescein maleimide) for further potential *in vitro* applications.

Preparation of Empty and Curcumin-loaded Nanoparticles

Selected protein-PEG conjugates were further used for the preparation of empty and CUR-loaded nanoparticles. The switch from DOX to CUR exemplifies that the preparation procedure can be transferred to other hydrophobic drugs. Here, the obtained nanoparticles show a modal size distribution from 113.0 to 177.4 nm. The entrapment efficiency of curcumin ranges from 43% to 61% leading to a weight percentage of 4.1% to 5.8%. Here, no difference between the used proteins was observed but compared to DOX the drug content was increased by four to six times.

In vitro Effects of Protein Nanoparticles

Empty nanoparticles show no inhibitory effects on the growth of HeLa cells in a cell viability assay (MTT) proving that nanoparticles prepared by the described method are non-toxic by themselves. Entrapment of curcumin into nanoparticles leads to an inhibition of the growth of the cancer cells starting from drug concentrations of 6 μM. Again, no difference between the nanocarriers was observed regardless which protein was used as particle material. This shows that all of the here presented nanoparticle systems are suitable to deliver the water insoluble drug successfully into cancer cells. From these results it can be expected, that a change of the protein does not affect the drug delivery potential.

In summary, it was possible to prepare nanoparticles that are suitable for the delivery of curcumin using all the here presented proteins. The variation of the proteins did neither influence the entrapment efficiency nor the toxic effects of the entrapped payload towards cancer cells.

4.3 Particle Preparation for Hydrophilic Payloads

By using rhodamine-labeled dextran, a hydrophilic model drug was successfully entrapped into the protein-based particle matrix via a double emulsion procedure. Here, a water-in-oil-in-water emulsion was prepared with the hydrophilic payload inside of the protein containing oil droplets. This method produced particles with a mean size of around 240 to 300 nm. The encapsulation efficiency of the payload was 7% for BSA and 54.1% for OVA. These results provide a proof of principle for the entrapment of hydrophilic drugs. As the particles were above the optimal size of 200 nm, a first optimization regarding the particle size was successfully performed by changing the ratio of organic to aqueous phase. With this, the size of the particles was decreased to around 150 nm, yielding a similar size as previously observed for single emulsion experiments. These first experiments are a promising basis for the further development of this particle preparation approach towards the delivery of hydrophilic drugs like RNA and DNA.

4.4 Outlook

The presented methods have the potential to expand the pool of protein-based nanoparticles to any protein of choice and a broad pool of payloads. A graphical overview of potential further development of this nanoparticle system is presented in Figure 59.

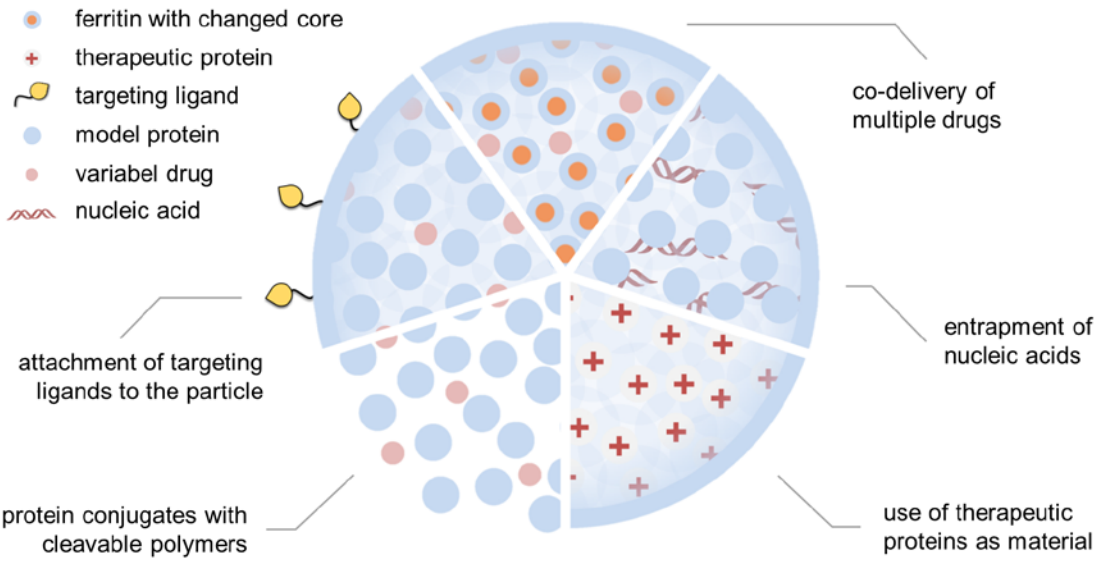

Figure 59. Further perspectives for protein-based nanoparticles prepared by the described emulsification technique.

The closest application to the here presented approach is to vary the encapsulated hydrophobic payload. Also, the use of ferritin as protein material could allow the preparation of nanocarriers with two payloads entrapped by two different mechanisms. The iron core of ferritin can be replaced by other small molecules. This modified carrier protein can thereafter entrap another molecule by the method described in this PhD work. This would allow co-delivery of different payloads or different release kinetics of the same drug.

The possibility to entrap hydrophilic payloads into the particle matrix further extends the use of these protein nanocarriers. More research needs to be done to optimize the system, but especially the opportunity to deliver small nucleic acids like siRNA or therapeutic proteins as payload makes this system very interesting for further applications e.g. in immunotherapy. First approaches are recently presented in the master thesis of Elena Steiert in our group.[178]

Based on the presented results, it might be possible to extend the protein-particle system to one where the protein not only functions as biodegradable material, but in addition can also be

active and perform for example catalytic functions. For example, this could be applied in the future to entrap prodrugs that are only therapeutically active when the drug is released by a catalytically active protein after cellular uptake of the particle. Here a naturally present activation of the protein (e.g. for lysozyme high activity at lysosomal pH levels but not at neutral pH) can be used. In addition, a transfer of this system to proteins with a more therapeutically relevant function than the proteins presented here has the potential to benefit from the catalytic activity of the nanoparticle itself. For example, nanoparticles formed of cytochrome c as protein material have the potential to induce apoptosis after a cellular uptake. The use of peroxidases as particle material has the potential to obtain a nanoparticle that leads to a decreased peroxidase level in cells as present under cellular stress

A different perspective is to attach cleavable polymer chains onto the protein surface. By this, a cellular uptake can lead to a full recovery of the native protein. By losing of the shielding polymer corona, also the full activity is regained. Additionally, an erosion of the polymer would leads to a controlled release of the entrapped payload.

Currently, the particles are only suitable to accumulate in a tumor by passive targeting that relies on the size of the particles. Attachment of active targeting moieties – like folic acid or antibodies – would lead to a preferred binding of the particles to the surface of tumor cells presenting the corresponding receptors. This has the potential to enhance a selective cellular uptake and increase a therapeutic effect *in vitro* and *in vivo*.

In contrast to the only commercially available drug delivery system based on proteins (Abraxane®) the here presented nanocarrier system is not limited to serum albumins as nanocarrier material. Furthermore, using this new particle preparation procedure, proteins are no longer restricted to serve just as a biodegradable polymer. As the protein function is preserved – even in the resulting particles – they can now be used as both, carrier and functional nano-sized catalyst. Especially the preservation of the enzymatic activity opens up the opportunity for new pharmaceutical and technological innovations in the field of drug delivery.

5 EXPERIMENTAL PART

5.1 Materials

5.1.1 Equipment

Absorption Measureme1nts

Equipment: Victor X5 Multilabel Plate Reader, Perkin Elmer, Waltham, Massachusetts, USA. Analysis was carried out using the software WorkOut 2.5.
Infinite® Pro M200 Plate Reader, Tecan Group Ltd., Switzerland. Analysis was carried out using the software i-control 1.7.
V-650 Photometer. JASCO International co., LTD., Hachioji, Tokyo, Japan.

Absorption measurements to determine protein concentrations and the TNBS Assay were performed with clear 96-well microplates (flat bottom) on the Victor X5. For protein absorption (λ = 280 nm), UV-Star plates (Greiner) were used. All other absorption based assays were performed on the Infinite® Pro M200 using clear polystyrene flat bottom 96-well plates (Sarsted).

The comparison of the solubility behavior of LYZ^{2k} was performed using the Jasco V-650 in clear quartz cuvettes (pathlength: 10 mm).

Bath Sonicator

Equipment: Sonorex RK 102 H, Bandelin electronic GmbH & Co. KG, Berlin, Germany.

Biological Safety Cabinet

Equipment: Herasafe™, Kendro Laboratory Products, Langenselbold, Germany.

All experiments involving cell culture were performed under this biological safety cabinet.

Camera

Equipment: Xperia™ Z1 Compact Smartphone, Sony Corporation, Tokio, Japan.

Centrifuge

Equipment: Heraeus™ Multifuge™ X3R, ThermoFischer Scientific, Waltham, Massachusetts, USA.

Circular Dichroism (CD)

Equipment: J-815 Circular Dichroism Spectrometer, JASCO International co., LTD., Hachioji, Tokyo, Japan.
Analysis was carried out using the software Spectra Manager 2.12 00.

If not mentioned elsewise, measurements were performed at 20 °C in 1 mm path length quartz cuvettes (Hellma Analytics).

Confocal Laser Scanning Microscopy

Equipment: TCS SP5 Confocal Microscope, Leica Microsystems, Wetzlar, Germany.
Images were taken using the software LAS AF Lite and further processed with the software ImageJ 1.49m.

The TCS SP5 is an inverted microscope with four photomultipliers (PMT), four laser lines (λ = 405 nm, 488 nm, 561 nm and 635 nm), six objectives (10×/0.3 dry; 20×/0.7 dry; 20×/0.7 multi-immersion objective; 40×/1.3 oil; 63×/1.4 oil; 63×/1.2 water) and a fast resonance scanner. Here the 63×/1.4 oil objective was used.

Dialysis

Equipment: Spectra/Por R Float-A-Lyzer R G2, molecular weight cut off (MWCO) 100 kDa, Spectrum Labs, Rancho Dominguez, California, USA.
Slide-A-Lyzer™ Dialysis Cassettes, MWCO 10 kDa, ThermoFischer Scientific, Waltham, Massachusetts, USA.
ZelluTrans/Roth Mini Dialyzer MD300, MWCO 6–8 kDa

Dynamic Light Scattering

Equipment: Malvern Zetasizer Nano ZS, Malvern Instruments GmbH, Herrenberg, Germany.

Electronic Data Processing

Microsoft Word 2010 was used for writing.

Microsoft PowerPoint 2010 was used for graphical illustrations and presentations.

Microsoft Excel 2010 was used for data processing.

EndNote X7.2 (Thomson Reuters) was used for reference management.

PyMOL Molecular Graphics System, Version 1.8 Schrödinger, LLC was used for the visualization of proteins.

Crystall structures were taken from the RCSB protein data bank.

ChemBioDraw Ultra Version 12.0, Cambridgesoft, was used for drawing chemical structures.

Fast Protein Liquid Chromatography

Equipment: Äkta™ FPLC System, GE Healthcare, Little Chalfont, UK.
Column: Superdex 200 10/300 GL.

Fluorescence-activated Cell Sorting

Equipment: BD FACSCalibur™, Beckton Dickinson GmbH, Heidelberg, Germany. Obtained data were analyzed using FlowJo v10.1 software.

Fluorescence Measurements

Equipment: Infinite® Pro M200 Plate Reader, Tecan Group Ltd., Switzerland. Analysis was carried out using the software i-control 1.7.

Fluorescence measurements were performed with black 96-well microplates (flat bottom).

The excitation and emission wavelengths of the used fluorophores are presented in Table 19.

Table 19. Excitation and emission maxima of the used fluorescent samples.

Fluorescent Dye or Drug	λ_{EX} / nm	λ_{EM} / nm
Fluorescein	490	520
4-Methylumbelliferone	380	460
Doxorubicin	490	560

Gel Permeation Chromatography

Equipment: Agilent 1100 Series, Agilent Technologies, Santa Clara, USA. Polymer Standards Service was used as external standard. A HEMA 300/100/40 column (l: 95.0 cm; d: 0.8 cm) was used with a flow rate of 1 mL/min at 50.0 °C. A refractive index detector (Agilent G1362A) and an UV detector (Agilent G1314A) were used for detection and the results were obtained with the Fa. PSS WinGPC Unity software.

Incubator

Equipment: Heraeus® BB 15 FUNCTION Line, Thermo Scientific, Waltham, Massachusetts, USA.

Inert Gas

Equipment: Argon gas bomb in 99.998% purity N46, Air Liquide Deutschland GmbH, Germany.

Lyophilisator

Equipment: ALPHA 1- 2 LD plus, Martin Christ Gefriertrocknungsanlagen GmbH, Osterode am Harz, Germany.

Mass Spectrometry

Equipment: Shimadzu Axima CFR MALDI-ToF mass spectrometer, Columbia, Maryland, USA

Nanoparticle Tracking Analysis

Equipment: NanoSight LM 14, NanoSight Ltd., Amesbury, Wiltshire, United Kingdom. Analysis was carried out using Nanosight NTA 3.1 software.

Particle Sonicator

Equipment: Bandelin Ultrasonic Homogenisator Sonoplus UW 70 (v220-240w), microtip MS 73 SH70G Stufenhorn 20 kHz, BANDELIN electronic GmbH & CO. KG, Berlin, Germany.
(Settings: power 75%, cycle 70% MS 72/D)

pH Measurements

Equipment: SevenCompact™ pH/Ion S220 with InLab® Micro special electrode, Mettler-Toledo Ltd., Beaumont Leys, Leicester, United Kingdom.

Pipettes

Equipment: Eppendorf Research® plus, one channel, 0.1–2.5 µL
Eppendorf Research® plus, one channel, 2–20 µL
Eppendorf Research® plus, one channel, 20–200 µL
Eppendorf Research® plus, one channel, 100–1000 µL
Eppendorf Research®, 8 channel, 30–300 µL
Eppendorf Xplorer® plus, 12 channel, 15–300 µL

Protein Purification by Ultrafiltration

Different centrifugal devices for protein purification (see list of disposables) were used as suggested by the supplier. Centrifugation was carried out in the Heraeus™ Multifuge™.

Sample Denaturation and Incubation

Equipment: Thermomixer pro, CellMedia, Elsteraue, Germany

Scales

Equipment: Equipment: Mettler Toledo Excellence Plus.
Sartorius™ M-Prove™ Scales AY303, Sartorius, Göttingen, Germany

Samples below 200 mg were weighted on the balance from Mettler Toledo- All samples above 200 mg were weighted on the balance from Satorius.

SDS Gel Electrophoresis

Equipment: Mini Vertical Ectrophoresis Unit Hoefer SE260, Hoefer Inc., Holliston, Massachusetts, USA.
GelDoc XR$^+$ with Image LabTM Software, Bio-Rad Laboratories Inc., Hercules, California, USA.

Transmission Electron Microscopy (TEM)

Equipment: Philips transmission electron microscope EM-420 (Acceleratiovoltage: 120 kV, Electronsource: LaB6 Cathode), FEI, Hillsboro, Oregon, USA. Slow Scan CCD Camera, Tietz Video and Image Processing Systems GmbH, Gauting, Germany.

Water Purification

Equipment: Direct-Q® 5 UV Remote Water Purification System, Merck Millipore, Germany.

If not mentioned elsewise, purified water was used in all preparation and analysis steps.

Zeta Potential

Equipment: Malvern Zetasizer Nano ZS, Malvern Instruments GmbH, Herrenberg, Germany.

5.1.2 Disposables

Amicon® Ultra 15 mL, MWCO 10 kDa	Merck Millipore
CELLSTAR® cell culture flasks 25 cm^2, 75 cm^2	Greiner Bio One
Coverslips (thickness: 0.17 ±0.005 mm, borosilicate glass)	Carl Roth
Disposable cuvettes, polystyrene	Carl Roth
Disposable hypodermic needles (size: 21 G)	B. Braun
Disposable pipettes 2 mL, 5 mL, 10 mL, 20 mL	Sarstedt
Disposable syringes 1 mL, 2 mL, 5 mL, 10 mL, 20 mL	B. Braun
Filtropur S 0.2 (sterile, non-pyrogenic)	Sarstedt
ZelluTrans/Roth Mini Dialyzer MD300 (MWCO 6000-8000 Da)	Carl Roth
Macrosep™ Advance Centrifugal Devices (MWCO 100 kDa)	PALL
Microplate 12-well, flat bottom, clear, sterile	Greiner Bio-One
Microplate 96-well, flat bottom, clear, sterile	Greiner Bio-One
Microplate 96-well, flat bottom, clear	Sarstedt
Microplate 96-well, flat bottom, clear, UV-Star®	Greiner Bio-One
Microplate 96-well, flat bottom, black	Greiner Bio-One
Microscopy slides	Carl Roth
Microsep™ Advance Centrifugal Devices (MWCO 30 kDa)	PALL
Pipette tips 2 μL, 250 μL, 1000 μL	Sarstedt
Slide-A-Lyzer™ Dialysis Cassettes (MWCO 10 kDa)	ThermoFischer Scientific
Spectra/Por R Float-A-Lyzer R G (MWCO 100 kDa)	Spectrum Labs
Tubes 13 mL, 100×16 mm, polypropylene	Sarstedt
Tubes 15 mL, 120×17 mm, polypropylene	Sarstedt
Tubes 50 mL, 114x28 mm, polypropylene	Sarstedt

5.1.3 Reagents and Solvents

Chemical	Supplier	CAS
Acetic acid	Sigma Aldrich	64-19-7
Albumin from chicken egg, grade V (OVA)	Sigma Aldrich	9006-59-1
Albumin from human serum (HSA)	Sigma Aldrich	7024-90-7
6-Aminofluorescein	Sigma Aldrich	51649-83-3
Ammoniumperoxodisulfat	Carl Roth	7727-54-0
β-lactoglobulin (BLG)	Sigma Aldrich	9045-23-2
Boronic Acid	Sigma Aldrich	10043-35-3
Bovine albumin fraction V (BSA)	Carl Roth	90604-29-8
Curcumin	TCI	458-37-7
Dako mounting medium	Agilent	
Dichloromethane (anhydrous, ≥99.8%, containing 40–150 ppm amylene as stabilizer)	Sigma-Aldrich	75-09-2
Dimethylsulfoxide	Sigma-Aldrich	67-68-5
DMEM GlutaMAX™	Sigma-Aldrich	
Doxorubicin × HCl	Promochem	25316-40-9
1-Ethyl-3-(3-dimethylaminopropyl)carbodiimide	Alfa Aeser	25952-53-8
Ferritin from equine spleen (FER)	Sigma Aldrich	9007-73-2
Fetal Calf Serum (FCS)	Life Technologies	
Fluorescein	Fluka	2321-07-5
Fluorescein maleimide	Linaris	
Glycine	Sigma Aldrich	56-40-6
Hydrochloric acid	Carl Roth	7647-01-0
Lysozyme from chicken egg white (LYZ)	Sigma Aldrich	12650-88-3

Chemical	Supplier	CAS
4-Methylumbelliferyl *β*-D-*N*,*N*',*N*''-triacetylchitotrioside	Sigma Aldrich	53643-13-3
N-hydroxysuccinimide, 98%	Sigma Aldrich	6066-82-6
PageRuler Prestained Protein Ladder (SM0671)	Thermo Scientific	
Penicillin-streptomycin (5,000 U/mL) Gibco™	Thermo Scientific	
Phosphate buffered saline	Sigma Aldrich	
Polyethylenglycol (2000) monomethylether	Sigma Aldrich	9004-74-4
Polyethylenglycol (5000) monomethylether	Sigma Aldrich	9004-74-4
Polyethylenglycol (2000) *α*-methoxy-*ω*-NHS ester	Rapp Polymere	
Roti®-Histofix 4% acid free (pH 7)	Carl Roth	
Rotiload	Carl Roth	
Rotiphoresegel Gel30	Carl Roth	
Sodium chloride	Carl Roth	7647-14-5
Sodium dihydrogen phosphate	Amresco	7558-80-7
Sodium dodecyl sulfate	Carl Roth	151-21-3
Sodium hydroxide	Carl Roth	1310-73-2
Tetramethylenediamine	Sigma Aldrich	110-60-1
Thiazolyl Blue Tetrazolium Bromide	Sigma Aldrich	298-93-1
Toluene (anhydrous)	Sigma Aldrich	108-88-3
Trichloro-*s*-triazine	Sigma Aldrich	108-77-0
Trypsin from bovine pancreas	Sigma Aldrich	9002-07-7

HeLa Cells

The carcinoma cell line was derived from a cervical cancer tissue sample of Henrietta Lacks on February 8 in 1951. Cells were a kind gift from the group of Prof. Dr. Bernd Epe (Johannes Gutenberg University of Mainz).

5.1.4 Buffers and Media

Purified water (Direct-Q®) was used for all buffers and media.

Borate Buffer (0.1 M, pH 10.0)

6.18 g boric acid (mol. wt.: 61.83 g/mol) were dissolved in water (1 L) and adjusted with NaOH to pH 8.5.

Coomassie Staining Solution

250 mg Coomassie Brillant Blue R-250 were dissolved in a mixture of water (45 mL), ethanol (45 mL) and acetic acid (10 mL).

Destaining Solution for Coomassie Stained Gels

A mixture of ethanol (450 mL), water (450 mL) and acetic acid (100 mL) was used.

DMEM for HeLa cells

DMEM GlutaMAX™ with phenol red was mixed with 10% FCS, 1% pyruvate and 1% penicillin-streptomycin.

Glycine Buffer (0.5 M, pH 10.0)

37.5 g glycine (mol. wt.: 75.07 g/mol) and 5.8 g sodium chloride (mol. wt.: 58.44 g/mol) were dissolved in water and adjusted with NaOH to pH 10.0.

Glycine Buffer (0.5 M, pH 12.0)

37.5 g glycine (mol. wt.: 75.07 g/mol) and 5.84 g sodium chloride (mol. wt.: 58.44 g/mol) were dissolved in water (1 L) and adjusted to with NaOH to pH 12.0.

HEPES Buffer (10 M, pH 7.4) for FPLC

2.38 g 4-(2-hydroxyethyl)-1-piperazineethanesulfonic acid (mol.wt.: 238.30 g/mol) and 29.22 g sodium chloride (mol. wt.: 58.44 g/mol) were dissolved in water (1 L) and the pH was adjusted with NaOH to pH 7.5 and filtered (poresize: 0.2 μm).

Phosphate Buffer (0.1 M, pH 6.0)

12 g sodium dihydrogen phosphate (mol. wt.: 119.98 g/mol) were dissolved in water and the pH was adjusted with NaOH to pH 5.2.

Phosphate Buffer (0.1 M, pH 6.0)

12 g sodium dihydrogen phosphate (mol. wt.: 119.98 g/mol) were dissolved in water (1 L) and the pH was adjusted with NaOH to pH 6.0.

Phosphate buffer (0.1 M, pH 7.4)

12 g sodium dihydrogen phosphate (mol. wt.: 119.98 g/mol) were dissolved in water (1 L) and the pH was adjusted with NaOH to pH 7.4.

Phosphate Buffer (5%, pH 8.5)

50 g sodium dihydrogen phosphate (mol. wt.: 119.98 g/mol) were dissolved in water (1 L) and the pH was adjusted to with NaOH to pH 8.5.

Running Buffer for Gel Electrophoresis (5x concentrated)

15.1 g Tris and 94 g glycine and a solution of SDS in water (20%, 25 mL) were dissolved with water to final volume of 1 L.

SDS 20% in water

20 g sodium dodecyl sulfate were dissolved in water to a final volume of 100 mL.

5.2 Protein PEGylation

5.2.1 Preparation of TsT-activated mPEG

TsT-activated mPEG2k

TsT-activated mPEG2k was synthesized similar to Abuchowski *et al.*[145] *a*-methoxy-*ω*-hydroxy polyethylene glycol (mol.wt.: 2000 g/mol) (2 g, 1 mmol), molecular sieve (4 Å, 1 g), sodium carbonate (1 g, 9.4 mmol) and trichloro-*s*-triazine (550 mg, 3 mmol) were dissolved in anhydrous benzene (40 mL) and stirred at room temperature for 16 h. The mixture was centrifuged (15000 × *g*, 15 min.) and the supernatant was added dropwise with vigorous stirring to petroleum ether (60 mL). The crude product was isolated by centrifugation (15000 × *g*, 15 min). The resulting pellet was redissolved in benzene and re-precipitated in petrol ether (60 mL). The washing step was repeated five times to remove excess triazine. The product (1756 mg, 84%) was dried under reduced pressure and stored under argon atmosphere at -20 °C. Elemental analysis was performed to determine the nitrogen content (found: C, 53.19%; H, 8.39%; N, 1.26%; calculated: C, 52.21%; H, 8.53%; N, 1.94%) indicating a PEG modification of 65%.

TsT-activated mPEG5k

TsT-activated mPEG5k was synthesized in a similar manner to the procedure described above. *a*-methoxy-*ω*-hydroxy polyethylene glycol (mol.wt.: 5000 g/mol) (1 g, 0.2 mmol), molecular sieve (4 Å, 0.1 g), sodium carbonate (594 mg, 5.6 mmol) and trichloro-*s*-triazine (184 mg, 1 mmol) were dissolved in anhydrous benzene (10 mL) and stirred at room temperature for 16 h. The mixture was centrifuged (15000 × *g*, 15 min) and the supernatant was added dropwise with vigorous stirring to petroleum ether (30 mL). The crude product was isolated by centrifugation (15000 × *g*, 15 min). The resulting pellet was redissolved in benzene and re-precipitated in petrol ether (60 mL). The washing step was repeated five times to remove excess triazine. The product (703 mg, 68%) was dried under reduced pressure and stored under argon atmosphere at -20 °C. Elemental analysis was performed to determine the nitrogen content (found: C, 54.14%; H, 12.45%; N, 0.51%; calculated: C, 54.07%; H, 8.91%; N, 0.82%) indicating a PEG modification of 62%.

Size Exclusion Chromatography (SEC)

Size exclusion chromatography measurements of activated PEG were performed in DMF containing 0.25 g/L lithium bromide as additive on an Agilent 1100 Series as an integrated instrument using PSS (Polymer Standards Service). A HEMA 300/100/40 column (l: 95.0 cm; d: 0.8 cm) was used with a flow rate of 1 mL/min at 50.0 °C. A refractive index detector (G1362A RID) was used for detection. This analysis was performed by Monika Schmelzer of the working group of Prof. Dr. H. Frey (JGU Mainz, Germany).

5.2.2 Protein PEGylation with TsT-activated mPEG

The desired protein (100 mg) was dissolved in 0.1 M borate buffer pH 10.0 (20 mL). TsT-activated mPEG (2055 mg for TsTmPEG2k; 5055 mg for TsTmPEG5k) was added and the mixture was stirred for 2 h at 40 °C. The reaction was stopped by the addition of 0.1 M phosphate buffer pH 6.0, (30 mL). Excess mPEG was removed with Microsep™ centrifugal devices. (MWCO 30 kDa). The resulting solution was freeze dried for further storage.

5.2.3 BLG PEGylation with NHS-activated mPEG

BLG (15 mg) was dissolved in phosphate buffer (0.1 M, pH 8.5) and NHS-activated mPEG (244.7 mg, 122.4 μmol) was added. The reaction mixture was stirred over night at room temperature. Excess mPEG was removed with Microsep™ centrifugal devices. (MWCO 30 kDa). The resulting solution was freeze dried for further storage. BLG^{NHS2k} was obtained as colorless solid (49.1 mg).

5.2.4 Fluorescence Labeling of Proteins

Coupling of Aminofluoresceine to Carboxylic Acids

LYZ^{2k} (30 mg, 0.86 μmol, bearing 10 carboxylic-groups per protein) was dissolved in 0.1 M phosphate buffer (pH 7.4, 4 mL). Similar buffered solution of *N*-(3-dimethylaminopropyl)-*N*'-ethylcarbodiimide hydrochloride (EDC, 1 mL, 2 mg/mL, 10.4 μmol) and *N*-hydroxysuccinimid (NHS, 1 mL, 1 mg/mL, 8.6 μmol) were added, followed by 100 μL of a fluorescein-6-amine stock solution (36 mg/mL in DMSO, 10.4 μmol). The reaction mixture

was stirred for 16 h at room temperature in the dark. Excess dye was removed using Amicon™ centrifugal devices (MWCO 10 kDa). F_LYZ(TsT-mPEG)$_{10}$ (16.1 mg, 54% of the origin mass) was obtained as a yellow powder after freeze-drying.

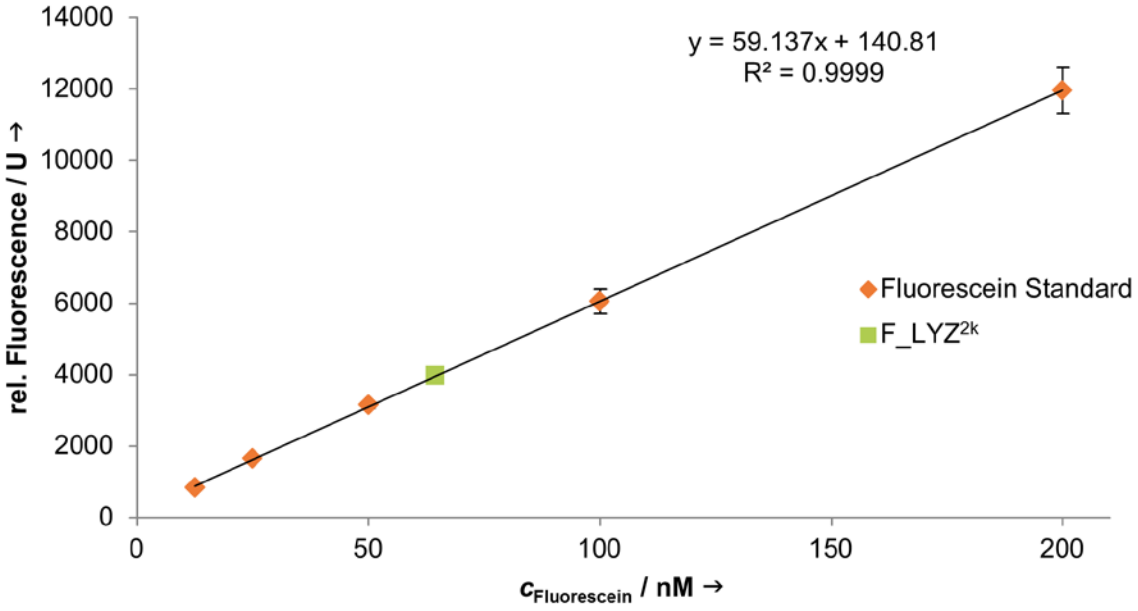

Figure 60. Determination of the fluorescein content of F_LYZ^{2k} (■) by using a dilution of fluorescein (◆). The protein sample (573 nM) shows a fluorescein content of 64.5 nM. This leads to a fluorescein/protein ratio of 0.113:1.

Site-specific Coupling to Cysteine Residues

Protein labeling was performed as suggested by the supplier (Vector Laboratories). BLG (30 mg) was dissolved in 0.1 M phosphate buffer (pH 7.5, 6 mL) and the dye fluorescein maleimide (25 μL, stock solution 20 mg/mL in DMSO) was added. The reaction mixture was incubated for 3 h at room temperature. Excess dye was removed using Amicon™ centrifugal devices (MWCO 10 kDa) and the resulting solution was freeze-dried for further storage. F_BLG was obtained as a yellow powder (25.5 mg, 85%)

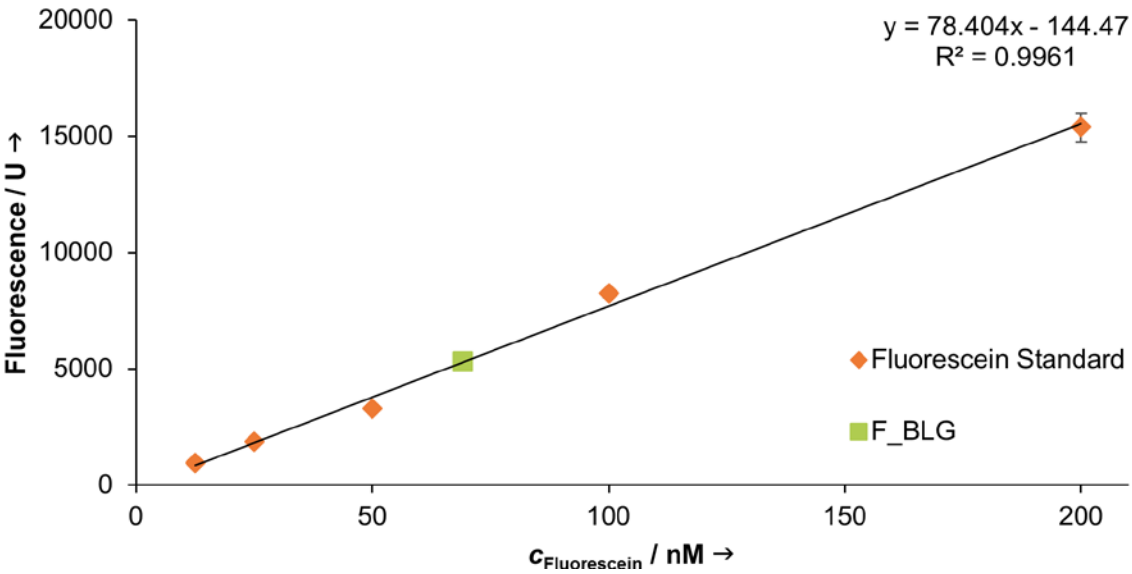

Figure 61. The fluorescein content of the protein was determined by measuring the fluorescence (λ_{EX}: 490 nm / λ_{EM}: 520 nm) of the labeled protein (c = 270 nM) in comparison to a standard dilution of free fluorescein.

5.2.5 Analysis of Protein Polymer Conjugates

SDS Gel Electrophoresis

SDS-PAGE was performed as described elsewhere[179] using a polyacrylamide gel (Rothiphorese® 30 gel mix) with a thickness of 0.75 mm (Hoefer) (For composition see Table 20 and Table 21) and stained with Coomassie Brilliant Blue R-250. 5 μL of PageRuler Pre-Stained Protein Ladder (10–170 kDa) was used as marker. Protein samples were dissolved in water in a concentration of 1 mg/mL for non-PEGylated and 2 mg/mL for PEGylated proteins. The proteins were denatured by addition of 5 μL of Roti®-Load 1 (Carl Roth) to 15 μL of the protein solution and heating in a boiling water bath for 10 min. Images were taken with a Gel DOC™ XR+ Imager (Bio-Rad) using standard protocols for Coomassie Brilliant Blue. Fluorescence images for detection of fluorescein labeled proteins were taken with a standard protocol for ethidium bromide (λ_{EX} = 240 nm). Fluorescent images were taken prior to staining with Coomassie Brilliant Blue.

Table 20. Composition of the collecting gel with a total volume of 2 mL for SDS-PAGE.

H_2O / mL	Rothiphorese® 30 / mL	1 M Tris (pH 6.8) / mL	20% SDS / mL	10% APS / mL	TEMED / mL
1.37	0.34	0.26	0.01	0.02	0.002

Table 21. Composition of separation gels with a total volume of 5 mL for SDS-PAGE.

PA Content / %	H_2O / mL	Rothiphorese® 30 / mL	1,5 M Tris (pH 8.8) / mL	20% SDS / mL	10% APS / mL	TEMED / mL
6	2.625	1.0	1.3	0.025	0.05	0.004
8	2.325	1.3	1.3	0.025	0.05	0.003
10	1.925	1.7	1.3	0.025	0.05	0.002
12	1.625	2.0	1.3	0.025	0.05	0.002
15	1.125	2.5	1.3	0.025	0.05	0.002

Fast Protein Liquid Chromatography

Fast Protein Liquid Chromatography (FPLC) was performed on an ÄKTA FPLC System equipped with a Superdex 200 10/300 GL column. The volume of each sample was 500 μL with a concentration of 2 mg/mL. Buffer conditions were 10 mM HEPES pH 7.5, 0.5 M NaCl with a flow rate of 0.5 mL/min.

Matrix-assisted Laser Desorption/Ionization

Matrix-assisted laser desorption/ionization time-of-flight mass spectrometry (MALDI-ToF MS) measurements were recorded on a Shimadzu Axima CFR MALDI-ToF mass spectrometer, equipped with a pulsed nitrogen laser (λ = 337 nm, 3 ns). Sinapic acid was used as a matrix. The analytes were dissolved in methanol at a concentration of 1 g/L. An aliquot (5 μL) was added to 25 μL of a matrix solution (10 g/L). Acetonitril/TFA 0.1% 1:1 was used as solvent. This analysis was performed by Dr. Elena Berger-Nicoletti of the working group of Prof. Dr. H. Frey (JGU Mainz, Germany).

Enzymatic Activity of PEGylated Lysozyme

LYZ^{2k} was dissolved in 0.1 M phosphate buffer (pH 5.2) and diluted to a final protein concentration of 2 μM. A solution of 4-methylumbelliferyl β-D-*N*,*N*',*N*''-triacetylchitotrioside ($(GlcNAc)_3MeU$, 20 μM in the same buffer) was preheated to 42 °C for 5 min. 200 μL of each solution were combined and further incubated in the dark at 42 °C in a Thermomixer pro (CellMedia, Germany). Samples of the reaction mixture were taken every 30 min (50 μL) and transferred to ice-cold 0.5 M glycine buffer (pH 12.0, 300 μL) to stop the catalytic activity of the protein and enhance the fluorescence intensity of methylumbelliferone. The fluorescence of the released MeU (Scheme 6) was determined in triplets (100 μL) on a black 96-well plate (Greiner) with an Infinite® 200 PRO plate reader (λ_{EX}: 380 nm / λ_{EX}: 460 nm).[180] The fluorescence intensity at t_0 was subtracted from every sample as background fluorescence. A solution of native lysozyme (2 μM) treated under the same conditions was used as reference.

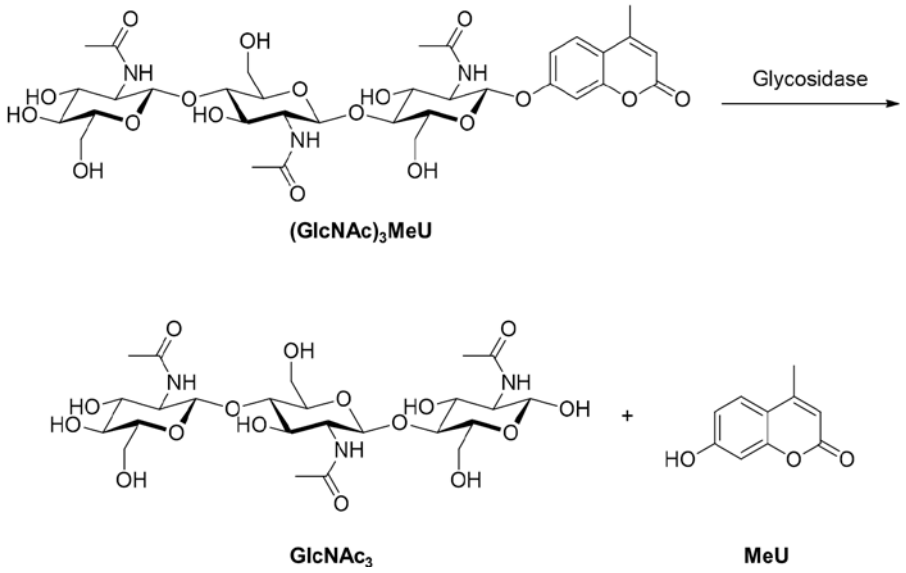

Scheme 6. Enzymatic cleavage of 4-methylumbelliferone from the triacetylchitotrioside $(GlcNAc)_3MeU$ by a glycosidase (e.g. lysozyme).

Circular Dichroism

CD spectra were recorded on a J-815 spectropolarimeter at 20 °C on a continuous scan mode using 1 mm path length quartz cells (Hellma Analytics). Data points were collected as triplets at a resolution of 0.1 nm and accumulated using Spectra Manager (Version 2.12 00) software.

Influence of Surface PEGylation on the Protein Structure. The protein modification procedure was performed according to the procedure described for protein PEGylation with a protein concentration of 0.5 mg/mL (150 μL). Either 150 μL of activated mPEG (A), ω-hydroxyl-mPEG (B) (10.5 mg/mL in borate buffer) or only buffer (C) were added to the protein solution and incubated for 2 h. After incubation, 450 μL of phosphate buffer were added. Additionally a solution containing only LYZ without heating (D) and with heating to 80 °C (E) were used as reference samples. CD spectra were measured with a final protein concentration of 0.1 mg/mL. The buffer background was subtracted from each measurement. Secondary structure content was calculated with DICHROWEB[156, 157] using the CONTIN-LL method (reference set 7[152]).

Influence of Sonication on the Protein Structure. A Solution of LYZ^{2k} (0.1 mg/mL in buffer containing 10 mM potassium phosphate, 50 mM sodium sulfate) was cooled to 4 °C. The sample was sonicated for 45 s on ice using a probe sonicator (Bandelin Ultrasonic Homogenisator Sonoplus UW 70, Power MS 72/D, Cycle 70%) placing the sonicator tip in the middle of the aqueous solution. A sample of untreated LYZ^{2k} was used as reference. CD spectra were measured and the buffer background signal was subtracted from each measurement and smoothed using the Savitzky-Golay (convolution width 13) method.

TNBS Assay

An aqueous solution of LYZ^{2k} (100 μL, 0.625 mg/mL), phosphate buffer (100 μL, 5% w/v, pH 8.5) and TNBS working solution (200 μL, 0.01% w/v) were combined and mixed well. The mixture was incubated for 2 h in the dark at 40 °C. The reaction (Scheme 7) was stopped by adding 1 M HCl (100 μL) to the reaction mixture. Triplets of 100 μL were added to a 96-well plate (Sarsted) and the absorption of the sample was measured with a VICTOR^{TM} X5 microplate reader at 405 nm. The absorption of the background containing only water instead of a sample was subtracted from each measurement. A dilution of glycine was used as standard and native lysozyme (0.25 mg/mL) as reference.

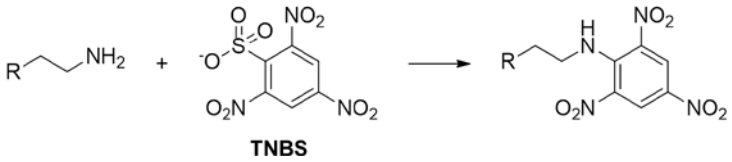

Scheme 7. Reaction of trinitrobenzoesulfonic acid (TNBS) with primary amines e.g. on the surface of proteins.

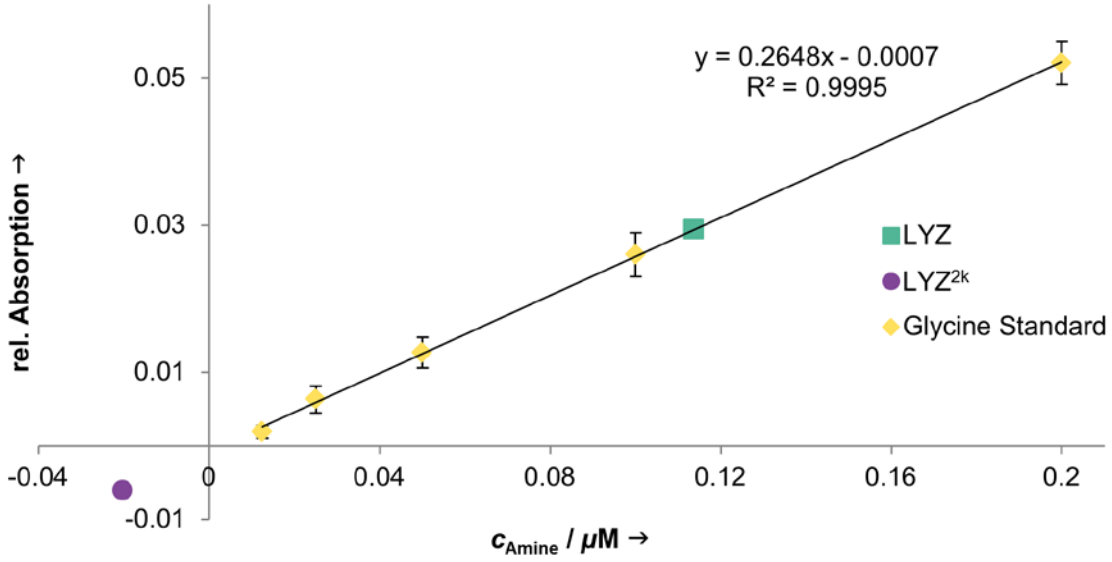

Figure 62. TNBS assay of native LYZ (■) and LYZ(TsTmPEG2k) (●). A solution of glycine (◆) was used as standard. The amount of amines in detected for LYZ corresponds to seven free amines on the protein. For the surface of PEGylated LYZ, no free amines were detected.

Determination of the Isoelectric Point

The PEGylated or native protein is dissolved in 0.05 M phosphate buffer (0.2 mg/mL) with pH values ranging from pH 2 to 11.6. The ζ-potential of the resulting solution is measured on a Zetasizer Nano ZS instrument (Malvern) using a clear disposable capillary cell. Three measurements with fifteen individual runs were performed. The refractive index (RI) of the dispersant (preset: water) was set to 1.330 and the viscosity to 0.8872 cP, respectively. The RI of the sample was set to 1.45 with a dielectric constant of 78.5.

Hydrodynamic Diameter of Proteins (DLS)

Dynamic light scattering experiments were performed on a Malvern Zetasizer Nano ZS in disposable polystyrene micro cuvettes using 110 μL of freshly prepared sample solution (1 mg/mL). Generally, after equilibration to 25 °C three measurements were performed with the instrument optimizing the number of runs for each measurement. The refractive index (RI) of the dispersant (preset: water) was set to 1.330 and the viscosity to 0.8872 cP, respectively. The RI of the particle was set to 1.45. The absorption of the protein was set to 0.00, both attenuator and measurement position were controlled by the instrument and all measurements were performed at a scattering angle of 173°.

Solubility of LYZ^{2k} in Organic Solvents

A qualitative analysis of the solubility behavior of highly PEGylated lysozyme was performed by adding LYZ^{2k} (0.5 mg) to different organic solvents (1 mL).

Extraction Experiment for PEGylated LYZ^{2k} in Dichloromethane/Water

LYZ^{2k} (2 mg) was dissolved in DCM (2 mL) and the organic phase was extracted with water (2 mL) under vigorous mixing for 24 h. The two layers were separated and the absorbance of each phase was measured from 250 to 400 nm with a V-650 Photometer. The background signal of the solvent was subtracted from each sample measurement.

5.3 Nanoparticle Preparation

5.3.1 General Preparation Procedures

General Procedure for Empty Nanoparticles

Protein-based particles were prepared using a single emulsion oil/water (o/w) solvent evaporation method similar to a procedure described previously.[137] The PEGylated protein (5 mg) was dissolved in ice-cold DCM (0.5 mL). The mixture was covered with a layer of PBS (pH 7.4, 2.5 mL) in a 13 mL round bottom tube and placed in an ice bath. The mixture was sonicated for 45 s on ice using a probe sonicator (Bandelin Ultrasonic Homogenisator Sonoplus UW 70, power MS 72/D, cycle 70%) placing the sonicator tip slightly above the DCM layer. The emulsion was stirred in a fume hood overnight, to evaporate the DCM. The solution was dialyzed against double distilled water (Spectra/Por® Float-A-Lyzer®G2, MWCO 100 kDa) resulting in a suspension of stable nanoparticles with a protein concentration of 2 mg/mL.

Desalting of Doxorubicin

Doxorubicin hydrochloride (10 mg, 17.2 mmol) was dissolved in 1.5 mL water and triethylamine (3 μL, 21.6 mmol) was added. The aqueous solution was extracted five times with DCM (2 mL). The organic layers were combined and the solvent was removed under reduced pressure leading to 8 mg of desalted doxorubicin.

General Procedure for DOX-loaded Nanoparticles

Protein-based particles containing doxorubicin were prepared using a single emulsion oil/water (o/w) solvent evaporation method similar to a procedure described previously.[137] The PEGylated protein (5 mg) was dissolved in ice-cold DCM (0.25 mL) and added to 250 μL of a solution of desalted doxorubicin (0.5 mg) in ice-cold DCM (0.25 mL). The mixture was covered with a layer of PBS (pH 7.4, 2.5 mL) in a 13 mL round bottom tube and placed in an ice bath. The mixture was sonicated for 45 s on ice using a probe sonicator (Bandelin Ultrasonic Homogenisator Sonoplus UW 70, power MS 72/D, cycle 70%) placing the sonicator tip slightly above the DCM layer. The emulsion was stirred in a fume hood

overnight, to evaporate the DCM. The solution was dialyzed against double distilled water (Spectra/Por® Float-A-Lyzer®G2, MWCO 100 kDa) resulting in a suspension of stable nanoparticles with a protein concentration of 2 mg/mL.

General Procedure for CUR-loaded Nanoparticles

Protein-based particles containing curcumin were prepared using a single emulsion oil/water (o/w) solvent evaporation method similar to a procedure described previously.[137] The PEGylated protein (5 mg) was dissolved in ice-cold DCM (0.25 mL) and added to 250 μL of a solution of curcumin (0.5 mg) in ice-cold DCM (0.25 mL). The mixture was covered with a layer of PBS (pH 7.4, 2.5 mL) in a 13 mL round bottom tube and placed in an ice bath. The mixture was sonicated for 45 s on ice using a probe sonicator (Bandelin Ultrasonic Homogenisator Sonoplus UW 70, power MS 72/D, cycle 70%) placing the sonicator tip slightly above the DCM layer. The emulsion was stirred in a well-ventilated hood overnight, to evaporate the DCM. The solution was dialyzed against double distilled water with Slide-A-Lyzer® dialysis cassettes, MWCO 10 kDa) resulting in a suspension of stable nanoparticles with a protein concentration of 2 mg/mL.

General Procedure for Double Emulsion Particles

Protein-based particles were prepared using a double emulsion water/oil/water (w/o/w) solvent evaporation method similar to a procedure described previously.[68] The PEGylated protein (5 mg) was dissolved in ice-cold DCM (0.8 mL). A small amount of water (100 μL) was added in a 13 mL round bottom tube and placed in an ice bath for empty NPs. For RhoDEX-loaded NPs, the aqueous layer contained 10 μg of RhoDEX. The mixture was sonicated for 15 s on ice using a probe sonicator (Bandelin Ultrasonic Homogenisator Sonoplus UW 70, power MS 72/D, cycle 70%) placing the sonicator tip in the DCM layer. The resulting emulsion was covered with a layer of PBS (pH 7.4, 2.5 or 4 mL) and again sonicated for additional 30 s placing the sonicator tip slightly above the DCM layer. The emulsion was stirred in a well-ventilated hood overnight, to evaporate the DCM. The solution was dialyzed against double distilled water (Spectra/Por® Float-A-Lyzer®G2, MWCO 100 kDa) resulting in a suspension of stable nanoparticles with a protein concentration of 2 mg/mL (V = 2.5 mL) or 1.25 mg/mL (V = 4 mL).

5.3.2 Nanoparticle Analysis

Size Determination using Nanoparticle Tracking Analysis (NTA)

Nanoparticle tracking analysis was performed on a NanoSight LM 10 equipped with a green laser (532 nm) and a marlin charged coupled device (CCD) camera. NTA has high sensitivity and accuracy for soft materials with low scattering properties. Samples were diluted in a ratio of 1:100 with filtered water and loaded into the measurement cell using a 1 mL syringe. Movements of particles in the samples were recorded as videos for 30 seconds at 23.3 °C. The videos were analyzed with the nanoparticle tracking analysis (NTA) 3.1 analytical software version build 3.1.54.

Size Determination using Dynamic Light Scattering (DLS)

Dynamic light scattering experiments were performed on a Malvern Zetasizer Nano ZS in disposable polystyrene micro cuvettes using 110 μL of freshly prepared sample solution (protein nanoparticle content: 2 mg/mL). Generally, after equilibration to 25 °C, three measurements were performed, with the instrument optimizing the number of runs for each measurement. The refractive index (RI) of the dispersant (preset: water) was set to 1.330 and the viscosity to 0.8872 cP, respectively. The RI of the particle was set to 1.45. The absorption of the protein was set to 0.00, both attenuator and measurement position were controlled by the instrument and all measurements were performed at a scattering angle of 173°.

Transmission Electron Microscopy (TEM)

Samples were prepared by adding one drop of particle or protein solution (2 mg/mL) on a 300 mesh copper grid (Science Service) and removing excess sample with a filter paper after one minute. Images were prepared in cooperation with Lydia Radi and Kristina Wichmann.

PEGylated Protein. The images were taken with a Philips EM-420 transmission electron microscope (acceleration voltage: 120 kV, angular resolution: up to 3.3 nm, electron source: LaB_6-cathode, image acquisition: slow-scan CCD-Camera (1k × 1k)).

Protein Nanoparticles. Images were taken with a Tenchai T12 (FEI) electron microscope (acceleration voltage: 120 kV, electron source: LaB6-twin cathode, image acquisition: 4k CCD camera).

Determination of Drug Content

Doxorubicin Content. Similar to Wu *et al.*,[116] the doxorubicin content of the particles was determined by measuring the absorbance (λ = 488 nm) of the particle solution in comparison to DOX × HCl in triplets of 100 μL on a 96-well plate (Sarsted)using an Infinite® 200 PRO (Tecan) plate reader. The absorbance of the background signal was subtracted from each measurement (water for DOX × HCl and empty protein NPs in the same concentration for DOX-loaded particles). The doxorubicin content of the particle solution was 33 μM, leading to DOX per protein ratio of 0.58:1.

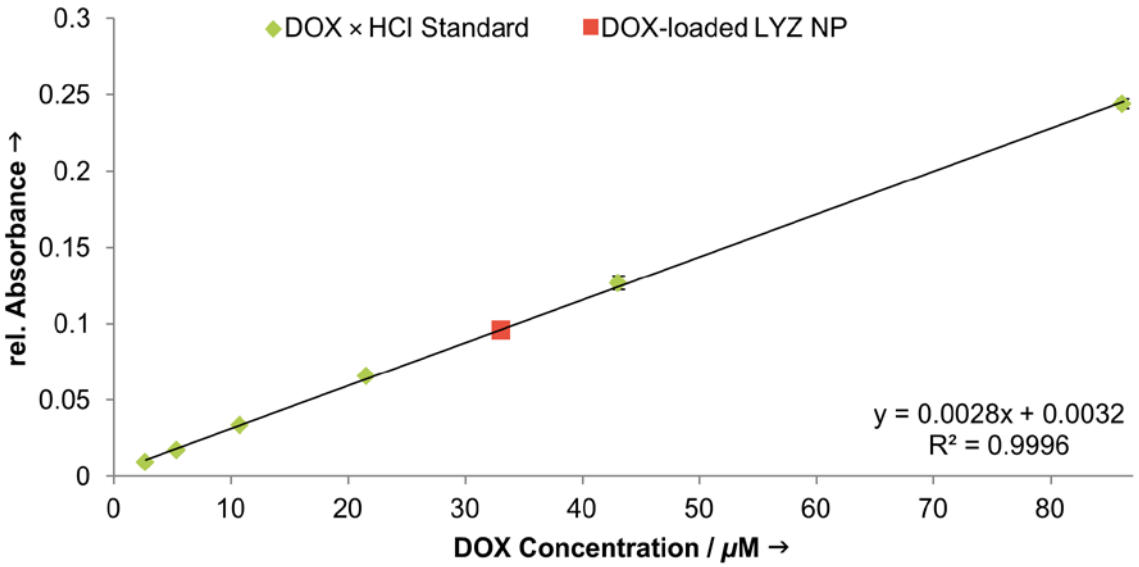

Figure 63. Determination of the doxorubicin content of DOX-loaded LYZ^{2k} nanoparticles (■) by using a dilution of doxorubicin hydrochlorid (◆).

Curcumin Content. The amount of entrapped curcumin in nanoparticles was determined by measuring the absorbance (λ = 440 nm) of the particle solution in comparison to free CUR. The particle suspension (50 μL) was diluted with DMSO (450 μL) to dissolve the particles and the entrapped payload. The resulting solution was measured in triplets of 100 μL on a 96-well plate (Sarsted) using an Infinite® 200 PRO plate reader. The absorbance of the background signal was subtracted from each measurement (DMSO/water mix for free curcumin and empty protein NPs in the same concentration for CUR-loaded particles).

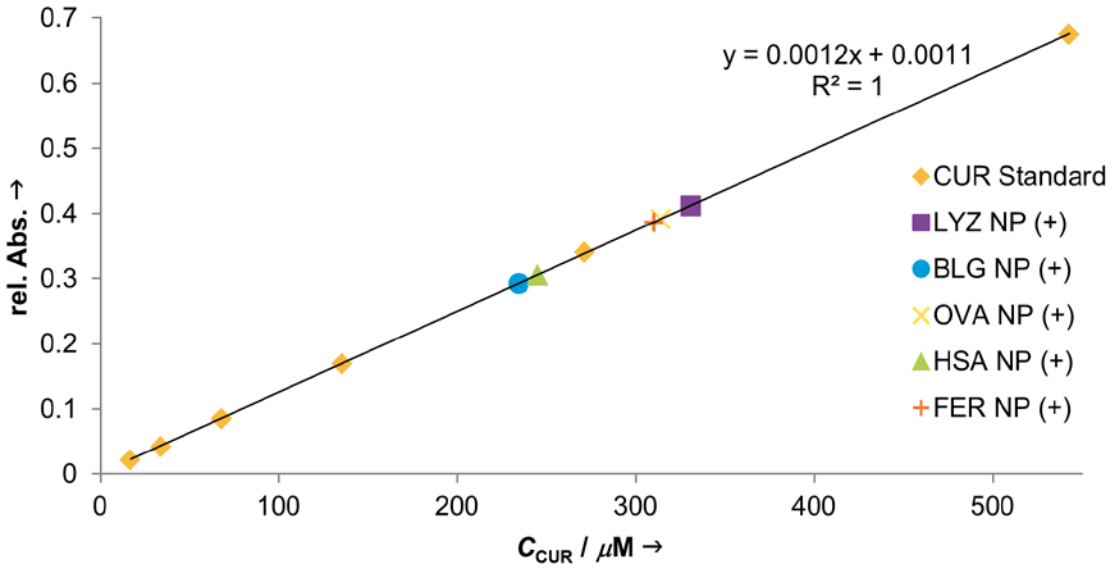

Figure 64. The CUR content of drug-loaded nanoparticles was determined by measuring the absorption (λ = 440 nm) of the nanoparticle samples. The CUR content of the particle suspension ranges from 235 to 331 μM after preparation.

RhoDEX Content. The RhoDEX content of the particles was determined by measuring the fluorescence (λ_{EX}: 500 nm / λ_{EM}: 590 nm) of the particle solution in comparison to free RhoDEX in triplets of 100 μL ranging from 25 to 600 ng/mL to in a black 96-well plate (Greiner) using an Infinite® 200 PRO plate reader. The fluorescence of the background signal was subtracted from each measurement (water for RhoDEX and empty protein NPs in the same concentration for RhoDEX-loaded particles).

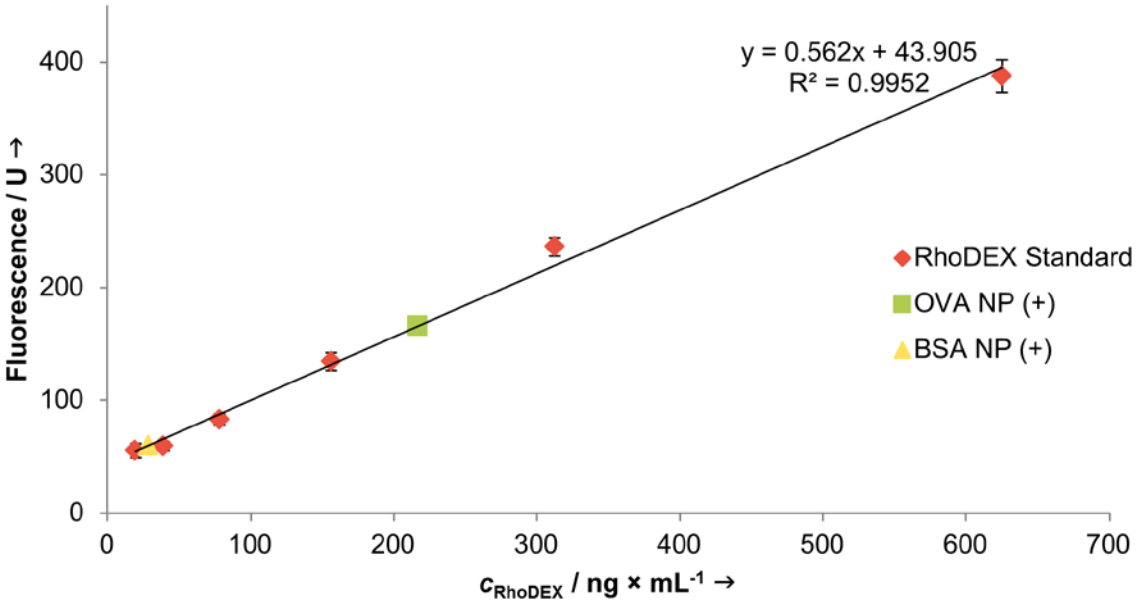

Figure 65. Determination of the RhoDEX content of nanoparticles prepared from double emulsion method.

Entrapment Efficiency

The entrapment efficiency (EE) of drugs in NPs was calculated by equation 1 together with equation 2. The initial DOX feed ($n_{DOX,feed}$) is 920 nmol (0.5 mg of desalted DOX, 543.52 g/mol). The amount of entrapped DOX ($n_{DOX,entrapped}$) is 83 nmol (calculated from the resulting DOX concentration (c_{DOX}) of 33 μM and the final volume of the NP suspension ($V_{NP\ suspension}$) of 2.5 mL). As a result, the entrapment efficiency of DOX is 9%.

$$EE = \frac{n_{drug,entrapped}}{n_{drug,feed}} \times 100\% \qquad \text{(eq. 1)}$$

with $$n_{drug,entrapped} = c_{drug} \times V_{NP\ suspension} \qquad \text{(eq. 2)}$$

Particle Stability Dialysis Assay

Particle stability under various physiological conditions was analyzed by dialysis of DOX-loaded LYZ nanoparticles against PBS (pH 7.4), DMEM, 0.1 M phosphate buffer (pH 5.2), a protease containing solution (trypsin) and a solution mimicking the reductive intracellular environment (glutathione, GHS, 10 mM)[9]. Therefore, the particle solutions (300 μL) were

placed in a ZelluTrans/Roth Mini Dialyzer MD300 (MWCO 6000-8000 Da) and dialyzed against PBS, DMEM and PBS containing 10 mM glutathione. For the stability in a protease solution, trypsin (23.3 kDa) was added directly to the particle suspension inside of the dialyzer to obtain a protease concentration of 1 mg/mL. The dialysis was stopped after 2, 4, 8 or 24 h, respectively. The absorbance spectrum of the initial particle solution and each dialyzed sample was recorded as triplet (3 × 80 μL on 96-well UV-Star® microplate) on an Infinite® 200 PRO (Tecan) plate reader. The blank signal of PBS, DMEM or phosphate buffer pH 5.2 was subtracted from each measurement.

Enzymatic Activity

Empty LYZ^{2k} NPs were dissolved in 0.1 M phosphate buffer (pH 5.2) and diluted to a final concentration of 3.5 μM. SingleLYZ^{2k} in free form was tested in the same concentration as the protein-NP. A solution of 4-methylumbelliferyl β-D-*N*,*N*',*N*''-triacetylchitotrioside ($(GlcNAc)_3MeU$, 20 μM in the same buffer) was preheated to 42 °C for 5 min. 200 μL protein containing and 200 μL substrate containing solution were combined and further incubated in the dark at 42 °C in a Thermomixer pro. Samples of the reaction mixture (50 μL) were taken over a period of 7 h and transferred to ice-cold 0.5 M glycine buffer (pH 12.0, 300 μL) to stop the catalytic activity of the protein and enhance the fluorescence intensity of methylumbelliferon. The fluorescence of the samples was determined in triplets (100 µL) on a black 96-well plate (Greiner)with an Infinite® 200 PRO plate reader (λ_{EX}: 380 nm / λ_{EX}: 460 nm).[180] The fluorescence intensity signal at t_0 was subtracted as background signal from each sample.

5.4 *In Vitro* Effects of Nanoparticles

HeLa cell lines were grown in Dulbecco's Modified Eagle Medium (DMEM) supplemented with 10% (v/v) fetal calf serum (FCS), 1% glutamine, 1% pyruvate, 1% penicillin/streptomycin. Cell incubations were performed in a humidified incubator at 37 °C with 5% CO_2 atmosphere. All used buffers were either autoclaved, sterile filtered or already sterile when supplied and preheated to 37 °C. Cells were grown in 75 cm^2 standard cell culture flasks.

Fluorescence-activateded Cell Sorting

Cells were seeded at a density of 2×10^5 cells per well in a 12-well plate (Greiner Bio-One) and allowed to attach overnight. The cells were incubated with DOX-loaded F_LYZ^{2k}-NPs in DOX concentrations of 4 μM (1 mL) (37 °C, 5% CO_2). The sample containing medium was replaced after 1 h and 4 h. Cells were detached, isolated and washed three times with PBS. Cells were fixed for 30 min at 4 °C in Rotifix® (PBS + 4% Formaldehyde) and washed three times with PBS afterwards. Analysis by flow cytometry was performed using a BD FACSCalibur™ and FlowJo v10.1 software. A sample of untreated cells was used as reference. FL1-H (530/30) was used to determine the green fluorescence of the particle material (F_LYZ^{2k}). FL3-H (650LP) was used to detect the red fluorescence of the encapsulated DOX.

Confocal Laser Scanning Microscopy

Cells were seeded at a density of 8×10^4 cells per well on untreated coverslips (borosilicate, 0.17 mm, Carl Roth, Germany) in a 12-well plate (Greiner Bio-One) and allowed to attach overnight. The cells were incubated with DOX-loaded F_ LYZ^{2k} -NP or free DOX × HCl in equivalent DOX concentrations of 4 μM (1 mL) (37 °C, 5% CO_2). The sample containing medium was replaced after 1 h, 4 h or 24 h. Cells were then washed three times with PBS, fixed for 30 min at 4 °C in Rotifix® (PBS + 4% formaldehyde) and washed three times with PBS afterwards. Co-staining of the nucleus was performed with DAPI (1 μg/mL in methanol). The fixed cells were washed once with DAPI/methanol and afterwards incubated for 15 min with DAPI/methanol (1 mL) at 37 °C. Cells were washed three times with methanol and mounted on microscope slides using Dako mounting medium for fluorescence microscopy.

Confocal laser scanning microscopy was performed on a Leica TCS SP-5 confocal fluorescence microscope, equipped with 405 nm, 488 nm, 561 nm and 635 nm laser lines. A 63×/1.4 oil objective was used.

Cell Viability by MTT method

The cell viability of human HeLa cells in presence of activated mPEG, native lysozyme, LYZ^{2k}, free DOX × HCl, empty nanoparticles and doxorubicin-loaded nanoparticles was determined using the MTT method (Scheme 8).[10] Cells were seeded in a 96-well plate with a density of 1.5×10^4 cells per well. 100 μL of different sample dilutions in culture media were added as triplets to the well plate. The cells were incubated (37 °C, 5% CO_2) and after 48 h a solution of 3-(4,5-dimethyl-2-thiazolyl)-2,5-diphen-yl-2H-tetrazolium bromide (MTT) in medium (40 μL, 3.0 mg/mL) was added directly to each well and the plate was incubated for additional 30 min. The medium was then replaced with DMSO (200 μL/well) and 0.1 M glycine buffer (25 μL/well, pH 10.0). 50 μL/well of the resulting purple DMSO solution was added to another clear-bottom 96-well assay plate containing a mixture of glycine buffer (17 μL/well, pH 10.0) and DMSO (133 μL/well). The absorbance signal at 570 nm was measured using an Infinite® 200 PRO plate reader the absorbance signal at 690 nm was subtracted as background signal. Cell viability was normalized to the absorbance signal measured from untreated cells.

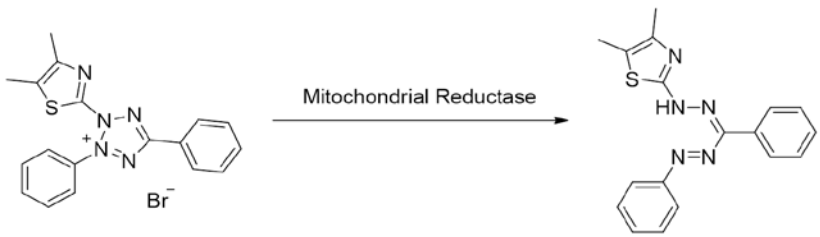

Tetrazine **Formazan**

Scheme 8. Conversion of MTT (3-(4,5-dimethylthiazol-2-yl)-2,5-diphenyltetrazolium bromide) to formazan ((E,Z)-5-(4,5-dimethylthiazol-2-yl)-1,3-diphenylformazan) by a mitochondrial reductase.

6 APPENDIX

6.1 Abbreviations

Abs.	absorption
AIDS	acquired immune deficiency syndrome
approx.	approximately
ATRP	atom-transfer radical-polymerization
BLG	*β*-lactoglobulin
BLG^{2k}	*β*-lactoglobulin, PEGylated with mPEG2k
BLG^{5k}	*β*-lactoglobulin, PEGylated with mPEG5k
BLG^{NHS2k}	*β*-lactoglobulin, PEGylated with NHS activated mPEG2k
BSA	bovine serum albumin
BSA^{2k}	bovine serum albumin, PEGylated with mPEG2k
BSA^{5k}	bovine serum albumin, PEGylated with mPEG5k
c	concentration
CCD	marlin charged coupled device
CD	circular dichroism
CRC	collaborative research centre
CUR	curcumin
cys	cysteine
d	diameter
D	Germany
d_{hyd}	hydrodynamic diameter
dd	double distilled
Da	dalton (1 Da equals 1 g/mol)
DAPI	4',6-diamidino-2-phenylindole
DCM	dichloromethane
DLS	dynamic light scattering
DMMA	dimethylmaleic anhydride
DMSO	dimethyl sulfoxide

DNA	deoxyribonucleic acid
DOX	doxorubicin
EE	entrapment efficiency
EDC	*N*-(3-dimethylaminopropyl)-*N*'-ethylcarbodiimide
e.g.	exempli gratia
EGFP	enhanced green fluorescent protein
em.	emission
eq.	equation
et al.	et alii
EtOAc	ethyl acetate
EtOH	ethanol
FACS	fluorescence-activated cell sorting
F_BLG^{NHS2k}	fluorescence-labeled *β*-lactoglobulin, PEGylated with NHS activated mPEG2k
FCS	fetal calf serum
FDA	food and drug administration
FER	ferritin
FER^{2k}	ferritin, PEGylated with mPEG2k
FER^{5k}	ferritin, PEGylated with mPEG5k
F_LYZ^{2k}	fluorescence-labeled lysozyme, PEGylated with mPEG2k
FPLC	fast protein liquid chromatography
g	acceleration by gravity of the earth (9.81 m/s^2)
GlcNAc	*N*-acetylglucosamine
GSH	glutathione
h	hour(s)
HEPES	4-(2-hydroxyethyl)-1-piperazineethanesulfonic acid
his	histidine
hMPV	human metapneumovirus
HSA	human serum albumin
HSA^{2k}	human serum albumin, PEGylated with mPEG2k
HSA^{5k}	human serum albumin, PEGylated with mPEG5k

JGU	Johannes Gutenberg-University
λ	wavelength
λ_{EM}	emission wavelength
λ_{EX}	excitation wavelength
LCST	lower critical solution temperature
lys	lysine
LYZ	lysozyme
LYZ^{2k}	lysozyme, PEGylated with mPEG2k
LYZ^{5k}	lysozyme, PEGylated with mPEG5k
m	mass
M	molar (1 M equals 1 mol/L)
MALDI ToF	matrix-assisted laser desorption/ionization time of flight
MeU	methylumbelliferone
min.	minute(s)
mo.	months
mol. wt.	molecular weight
mPEG	monomethoxy poly(ethylene glycol)
mPEG2k	monomethoxy poly(ethylene glycol) 2000 g/mol
mPEG5k	monomethoxy poly(ethylene glycol) 5000 g/mol
MS	mass spectroscopy
MTT	3,(4,5-dimethylthiazol-2-yl)-2,5-diphenyl-tetrazoliumbromide
MWCO	molecular weight cut-off
n	amount
NAD(P)H	Nicotinamide adenine dinucleotide phosphate
nBSA	nanoparticular BSA
NHS	*N*-hydroxysuccinimide
NP	nanoparticle
NTA	nanoparticle tracking analysis
OVA	ovalbumin
OVA^{2k}	ovalbumin, PEGylated with mPEG2k
OVA^{5k}	ovalbumin, PEGylated with mPEG5k

PAA	poly(amidoamine)
PBS	phosphate buffered saline
pdb	protein data bank
PDI	polydispersity index
PDMA	poly(dimethylacryl-amide)
pDNA	plasmid deoxyribonucleic acid
PEG	poly(ethylene glycol)
PGA	poly(glycolic acid)
PLA	poly(lactic acid)
PLGA	poly(lactic-*co*-glycolic acid)
PMMA	poly(methyl methacrylate)
PNIPAM	poly(*N*-isopropylacrylamide)
PPEGMA	poly(oligo (ethylene glycol) methyl ether methacrylate)
R	radius of gyration
RAFT	reversible addition-fragmentation chain transfer
rel.	relative
RGD	Amino acid sequence arginine-glycine-asparagine
RhoDEX	rhodamine-labeled dextran
RI	refractive index
rt.	room temperature
SD	standard deviation
SDS-PAGE	sodium dodecyl sulfate polyacrylamide gel electrophoresis
SE	Sweden
SEC	size exclusion chromatography
sfGFP	super folder green fluorescent protein
SLN	solid lipid nanoparticle
tat	trans-activator of transcription
TEM	transmission electron microscopy
TMED	tetramethylethylenediamine
TFA	trifluoroacetic acid
TsT	trichloro-*s*-triazine

tyr	tyrosine
U	units
UK	United Kingdom
USA	United States of America
UV	ultra violet
V	Volume
V_e	elution volume
wt%	weight percentage
z	charge

6.2 Supplemental Data

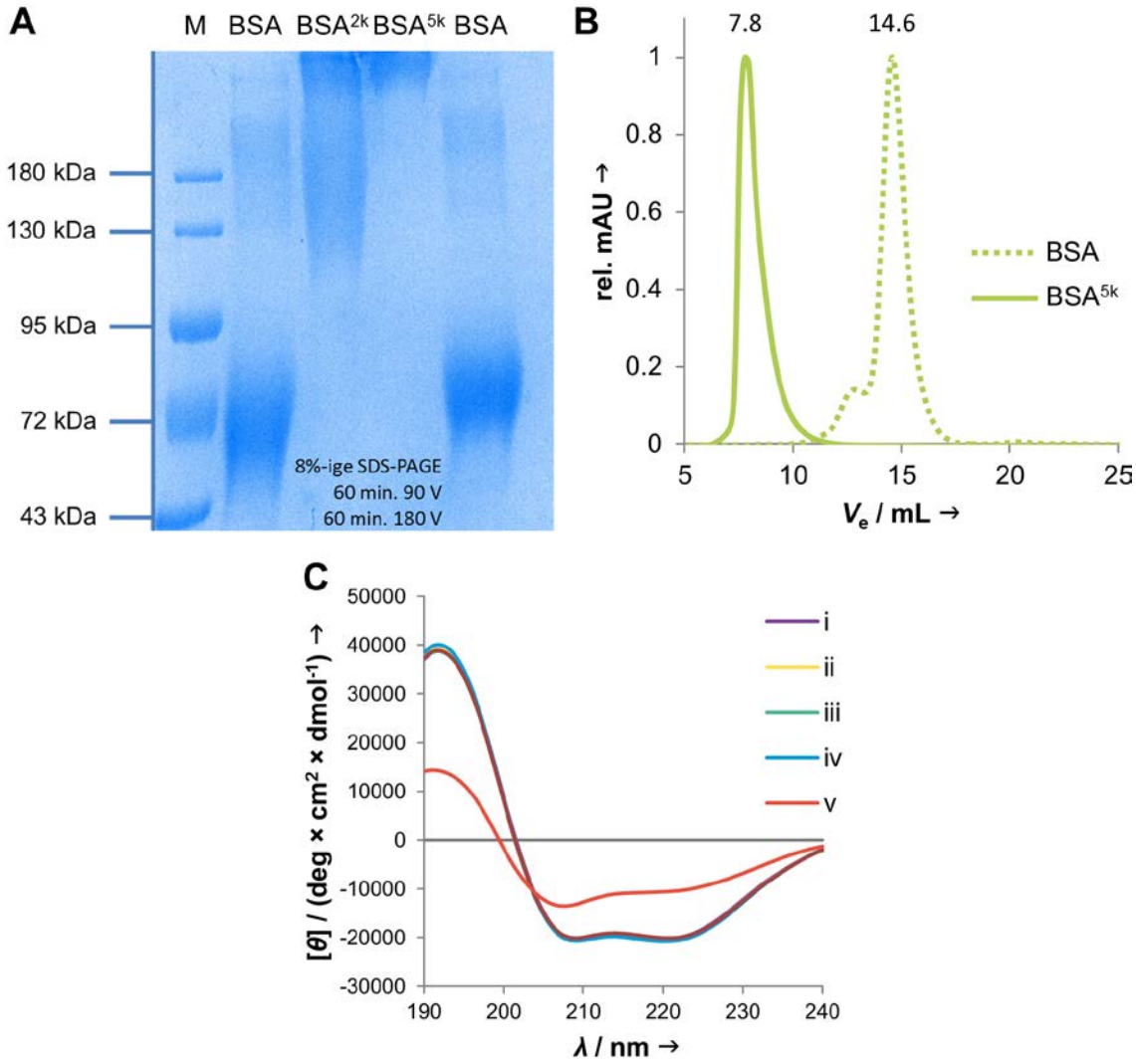

Figure 66. Analytical data of BSA PEGylation. SDS-PAGE of BSA, BSA^{2k} and BSA^{5k} compared to a standard marker (A). FPLC analysis of BSA and BSA^{5k} (B) and analysis of the protein integrity by CD-spectrometry of the PEGylation process(C). The CD-spectra show PEGylated protein (i, purple), mixture of protein and mPEG-OH (ii, yellow) and protein only (iii, green) incubated for 2 h under reaction conditions. For comparison, an untreated protein sample (iv, blue) and an untreated sample measured at 80 °C (v, red) causing thermal denaturation.

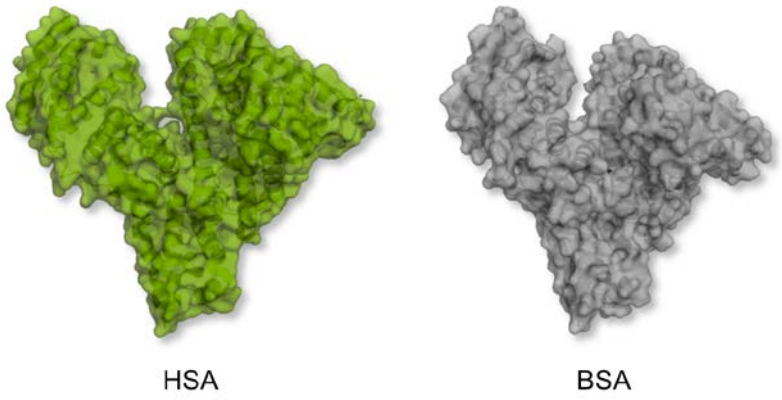

Figure 67. Structural comparison between human serum albumin (HSA, green, pdb: 1e71) and bovine serum albumin (BSA, grey, pdb: 3v03)

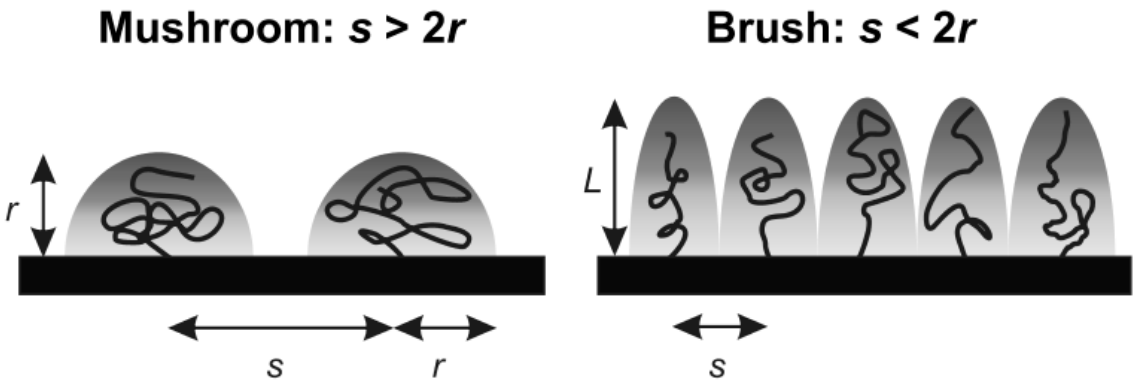

Figure 68. Illustration of different conformations of surface-tethered polymer chains. Depending on how closely packed the polymer chains are, they form either "mushroom" -like or "brush"-like conformations. If the distance between neighboring chains s is larger than twice the radius of the polymer, a mushroom regime occurs The brush conformation is observed when s is smaller than $2r$. Here the polymers chains are extended away from the surface at a height of L. The shaded areas emphasize the stochastic nature of the polymer chains where each chain has a high probability to occupy all positions within a given volume. Reprinted from Backmann *et al.*[163] (Open Access article under the terms of the Creative Commons Attribution License).

Table 22. Results summary of structural elements calculated with DICROWEB using the CONTIN-LL method (reference Set 7[5]) for BLG using 5 kDa mPEG.

Sample	$a_{regular}$	$a_{disordered}$	a_{total}	$\beta_{regular}$	$\beta_{disordered}$	β_{total}	Turns	Unordered	Total
BLG (i)	0.034	0.069	0.103	0.182	0.116	0.298	0.223	0.375	0.999
BLG (ii)	0.034	0.061	0.095	0.206	0.119	0.325	0.219	0.361	1.000
BLG (iii)	0.039	0.070	0.109	0.209	0.225	0.434	0.335	0.288	0.999
BLG (iv)	0.048	0.081	0.129	0.192	0.117	0.309	0.224	0.339	1.001
BLG (v)	0.028	0.078	0.106	0.131	0.098	0.229	0.205	0.461	1.001

Table 23. Results summary of structural elements calculated with DICROWEB using the CONTIN-LL method (reference Set 7[5]) for OVA using 5 kDa mPEG.

Sample	$a_{regular}$	$a_{disordered}$	a_{total}	$\beta_{regular}$	$\beta_{disordered}$	β_{total}	Turns	Unordered	Total
OVA (i)	0.129	0.093	0.222	0.173	0.086	0.259	0.161	0.356	0.998
OVA (ii)	0.142	0.093	0.235	0.172	0.090	0.262	0.168	0.335	1.000
OVA (iii)	0.132	0.098	0.230	0.166	0.092	0.258	0.172	0.341	1.001
OVA (iv)	0.140	0.094	0.234	0.170	0.091	0.261	0.172	0.333	1.000
OVA (v)	0.085	0.072	0.157	0.178	0.096	0.274	0.176	0.394	1.001

Table 24. Results summary of structural elements calculated with DICROWEB using the CONTIN-LL method (reference Set 7[5]) for HSA using 5 kDa mPEG.

Sample	$a_{regular}$	$a_{disordered}$	a_{total}	$\beta_{regular}$	$\beta_{disordered}$	β_{total}	Turns	Unordered	Total
HSA (i)	0.409	0.213	0.622	0.000	0.025	0.025	0.133	0.219	0.999
HSA (ii)	0.410	0.210	0.620	0.000	0.024	0.024	0.133	0.223	1.000
HSA (iii)	0.410	0.215	0.625	0.000	0.022	0.022	0.128	0.225	1.000
HSA (iv)	0.396	0.206	0.602	0.000	0.027	0.027	0.136	0.235	1.000
HSA (v)	0.211	0.144	0.355	0.069	0.056	0.125	0.157	0.364	1.001

Table 25. Results summary of structural elements calculated with DICROWEB using the CONTIN-LL method (reference Set 7[5]) for FER using mPEG5k.

Sample	$\alpha_{regular}$	$\alpha_{disordered}$	α_{total}	$\beta_{regular}$	$\beta_{disordered}$	β_{total}	Turns	Unordered	Total
FER (i)	0.234	0.146	0.380	0.111	0.073	0.184	0.174	0.261	0.999
FER (ii)	0.231	0.153	0.384	0.108	0.074	0.182	0.178	0.257	1.001
FER (iii)	0.223	0.143	0.366	0.102	0.070	0.172	0.172	0.290	1.000
FER (iv)	0.295	0.177	0.472	0.098	0.064	0.162	0.169	0.197	1.000
FER (v)	0.111	0.090	0.201	0.159	0.088	0.247	0.170	0.383	1.001

Table 26. Results summary of structural elements calculated with DICROWEB using the CONTIN-LL method (reference Set 7[5]) for BSA using mPEG5k.

Sample	$\alpha_{regular}$	$\alpha_{disordered}$	α_{total}	$\beta_{regular}$	$\beta_{disordered}$	β_{total}	Turns	Unordered	Total
BSA (i)	0.393	0.206	0.599	0.007	0.037	0.044	0.162	0.194	0.999
BSA (ii)	0.389	0.193	0.582	0.014	0.029	0.043	0.138	0.238	1.001
BSA (iii)	0.392	0.203	0.595	0.000	0.031	0.031	0.146	0.228	1.000
BSA (iv)	0.393	0.208	0.601	0.000	0.032	0.032	0.15	0.217	1.000
BSA (v)	0.190	0.138	0.328	0.062	0.06	0.122	0.165	0.386	1.001

Table 27. Results summary of structural elements of BLG when PEGylated with NHSmPEG2k, calculated with DICROWEB using the CONTIN-LL method (reference set 7[152]).

Sample	$\alpha_{regular}$	$\alpha_{disordered}$	α_{total}	$\beta_{regular}$	$\beta_{disordered}$	β_{total}	**Turns**	**Unordered**	**Total**
BLG (A)	0.077	0.081	0.158	0.198	0.113	0.311	0.211	0.321	1.001
BLG (B)	0.081	0.063	0.144	0.250	0.118	0.368	0.197	0.290	0.999
BLG (C)	0.088	0.077	0.165	0.208	0.115	0.323	0.211	0.302	1.001
BLG (D)	0.104	0.000	0.104	0.340	0.099	0.439	0.085	0.372	1.000

LITERATURE

[1] http://apps.who.int/gho/data/node.main.CODWBINC?lang=en
Global Health Observatory data repository, a service of the World Health Organization, Accessed: 02/01/2016.

[2] Global cancer facts & figures 3rd edition
American Cancer Society **2015**.

[3] Global surveillance of cancer survival 1995-2009: analysis of individual data for 25676887 patients from 279 population-based registries in 67 countries (CONCORD-2)
C. Allemani, H. K. Weir, H. Carreira, R. Harewood, D. Spika, X.-S. Wang, F. Bannon, J. V. Ahn, C. J. Johnson, A. Bonaventure, R. Marcos-Gragera, C. Stiller, G. Azevedo e Silva, W.-Q. Chen, O. J. Ogunbiyi, B. Rachet, M. J. Soeberg, H. You, T. Matsuda, M. Bielska-Lasota, H. Storm, T. C. Tucker, M. P. Coleman, *Lancet* **2015**, *385*, 977.

[4] Strategies to address low drug solubility in discovery and development
H. D. Williams, N. L. Trevaskis, S. A. Charman, R. M. Shanker, W. N. Charman, C. W. Pouton, C. J. Porter, *Pharmacol. Rev.* **2013**, *65*, 315.

[5] Development and characterization of a novel Cremophor® EL free liposome-based paclitaxel (LEP-ETU) formulation
J. A. Zhang, G. Anyarambhatla, L. Ma, S. Ugwu, T. Xuan, T. Sardone, I. Ahmad, *Eur. J. Pharm. Biopharm.* **2005**, *59*, 177.

[6] Abraxane in the treatment of ovarian cancer: The absence of hypersensitivity reactions
J. P. Micha, B. H. Goldstein, C. L. Birk, M. A. Rettenmaier, J. V. Brown, III, *Gynecol. Oncol.* **2006**, *100*, 437.

[7] Anthracyclines in the treatment of cancer. An overview
G. N. Hortobágyi, *Drugs* **1997**, *54*, 1.

[8] Anthracycline cardiotoxicity: Prevalence, pathogenesis and treatment
M. Volkova, R. Russell, *Curr. Cardiol. Rev.* **2011**, *7*, 214.

[9] Nanomedicine in cancer therapy: Challenges, opportunities, and clinical applications
A. Wicki, D. Witzigmann, V. Balasubramanian, J. Huwyler, *J. Controlled Release* **2014**, *200*, 138.

[10] http://www.clinicaltrials.gov
A service of the U. S. National Institute of Health, Accessed: 01/10/2016.

[11] nab-paclitaxel in the treatment of metastatic breast cancer: a comprehensive review
A. J. Montero, B. Adams, C. M. Diaz-Montero, S. Glück, *Expert Rev. Clin. Pharmacol.* **2011**, *4*, 329.

[12] Reduced cardiotoxicity and comparable efficacy in a phase III trial of pegylated liposomal doxorubicin HCl (CAELYX™/Doxil®) versus conventional doxorubicin for first-line treatment of metastatic breast cancer
M. E. R. O'Brien, N. Wigler, M. Inbar, R. Rosso, E. Grischke, A. Santoro, R. Catane, D. G. Kieback, P. Tomczak, S. P. Ackland, F. Orlandi, L. Mellars, L. Alland, C. Tendler, *Annals of Oncology* **2004**, *15*, 440.

[13] Liposomal daunorubicin as treatment for Kaposi's sarcoma
C. E. Petre, D. P. Dittmer, *Int. J. Nanomed.* **2007**, *2*, 277.

[14] Pharmacology of drugs formulated with DepoFoam™
M. S. Angst, D. R. Drover, *Clin. Pharmacokinet.* **2006**, *45*, 1153.

[15] Doxil?? - The first FDA-approved nano-drug: Lessons learned
Y. Barenholz, *J. Controlled Release* **2012**, *160*, 117.

[16] Polymeric micelles in anticancer therapy: Targeting, imaging and triggered release
C. Oerlemans, W. Bult, M. Bos, G. Storm, J. F. W. Nijsen, W. E. Hennink, *Pharm. Res.* **2010**, *27*, 2569.

[17] Marqibo® (vincristine sulfate liposome injection) improves the pharmacokinetics and pharmacodynamics of vincristine
J. A. Silverman, S. R. Deitcher, *Cancer Chemother. Pharmacol.* **2013**, *71*, 555.

[18] Liposomal doxorubicin in the treatment of breast cancer patients: A review
J. Lao, J. Madani, T. Puértolas, M. Álvarez, A. Hernández, R. Pazo-Cid, Á. Artal, A. Antón Torres, *J. Drug Delivery* **2013**, *2013*, 456409.

[19] FDA drug approval summary: Pegaspargase (Oncaspar®) for the first-line treatment of children with acute lymphoblastic leukemia (ALL)
P. A. Dinndorf, J. Gootenberg, M. H. Cohen, P. Keegan, R. Pazdur, *The Oncologist* **2007**, *12*, 991.

[20] Macromolecular therapeutics
K. Greish, J. Fang, T. Inutsuka, A. Nagamitsu, H. Maeda, *Clin. Pharmacokinet.* **2003**, *42*, 1089.

[21] Engineered nanoparticles for drug delivery in cancer therapy
T. Sun, Y. S. Zhang, B. Pang, D. C. Hyun, M. Yang, Y. Xia, *Angew. Chem. Int. Ed.* **2014**, *53*, 12320.

[22] Design, functionalization strategies and biomedical applications of targeted biodegradable/biocompatible polymer-based nanocarriers for drug delivery
J. Nicolas, S. Mura, D. Brambilla, N. Mackiewicz, P. Couvreur, *Chem. Soc. Rev.* **2013**, *42*, 1147.

[23] Nanoparticles - a historical perspective
J. Kreuter, *Int. J. Pharm.* **2007**, *331*, 1.

[24] Polymer conjugates as anticancer nanomedicines
R. Duncan, *Nat. Rev. Cancer* **2006**, *6*, 688.

[25] Taylor dispersion analysis compared to dynamic light scattering for the size analysis of therapeutic peptides and proteins and their aggregates
A. Hawe, W. L. Hulse, W. Jiskoot, R. T. Forbes, *Pharm. Res.* **2011**, *28*, 2302.

[26] Polymer–drug conjugates: towards a novel approach for the treatment of endrocine-related cancer
R. Duncan, M. J. Vicent, F. Greco, R. I. Nicholson, *Endocr. Relat. Cancer* **2005**, *12*, S189.

[27] Liposomal-entrapped doxorubicin: an active agent in AIDS-related Kaposi's sarcoma
M. Harrison, D. Tomlinson, S. Stewart, *J. Clin. Oncol.* **1995**, *13*, 914.

[28] Abraxane, a novel Cremophor-free, albumin-bound particle form of paclitaxel for the treatment of advanced non-small-cell lung cancer
M. R. Green, G. M. Manikhas, S. Orlov, B. Afanasyev, a. M. Makhson, P. Bhar, M. J. Hawkins, *Annals of Oncology* **2006**, *17*, 1263.

[29] nab-Paclitaxel (Abraxane®): an albumin-bound cytotoxic exploiting natural delivery mechanisms into tumors
J. Iglesias, *Breast Cancer Res.* **2009**, *11*, S21.

[30] Macromolecular therapeutics in cancer treatment: The EPR effect and beyond
H. Maeda, *J. Controlled Release* **2012**, *164*, 138.

[31] A new concept for macromolecular therapeutics in cnacer chemotherapy: mechanism of tumoritropic accumulatio of proteins and the antitumor agents Smancs
Y. Matsumura, H. Maeda, *Cancer Res.* **1986**, *46*, 6387.

[32] Biologically optimized nanosized molecules and particles: more than just size
M. R. Longmire, M. Ogawa, P. L. Choyke, H. Kobayashi, *Bioconjugate Chem.* **2011**, *22*, 993.

[33] Clearance properties of nano-sized particles and molecules as imaging agents: considerations and caveats
M. Longmire, P. L. Choyke, H. Kobayashi, *Nanomedicine* **2008**, *3*, 703.

[34] Chapter 12 - Nanoparticles in cancer chemotherapy
D. Banerjee, S. Sengupta, in *Progress in Molecular Biology and Translational Science, Vol. Volume 104* (Ed.: V. Antonio), Academic Press, **2011**, pp. 489.

[35] Nanoparticle delivery systems for cancer therapy: advances in clinical and preclinical research
S. P. Egusquiaguirre, M. Igartua, R. M. Hernández, J. L. Pedraz, *Clin. Transl. Oncol.* **2012**, *14*, 83.

[36] Nanoparticles for drug delivery in cancer treatment
B. Haley, E. Frenkel, *Urol. Oncol.* **2008**, *26*, 57.

[37] Vascular permeability in a human tumor xenograft: Molecular size dependence and cutoff size
F. Yuan, M. Dellian, D. Fukumura, M. Leunig, D. A. Berk, V. P. Torchilin, R. K. Jain, *Cancer Res.* **1995**, *55*, 3752.

[38] Nanoparticle delivery of cancer drugs
A. Z. Wang, R. Langer, O. C. Farokhzad, *Annu. Rev. Med.* **2012**, *63*, 185.

[39] Strategies in the design of nanoparticles for therapeutic applications
R. A. Petros, J. M. DeSimone, *Nat. Rev. Drug Discovery* **2010**, *9*, 615.

[40] Delivering nanomedicine to solid tumors
R. K. Jain, T. Stylianopoulos, *Nat. Rev. Clin. Oncol.* **2010**, *7*, 653.

[41] Ligand-targeted liposome design: challenges and fundamental considerations
G. T. Noble, J. F. Stefanick, J. D. Ashley, T. Kiziltepe, B. Bilgicer, *Trends Biotechnol.* **2014**, *32*, 32.

[42] Extracellularly activated nanocarriers: a new paradigm of tumor targeted drug delivery
E. Gullotti, Y. Yeo, *Mol. Pharm.* **2009**, *6*, 1041.

[43] Toxicology of engineered nanomaterials: Focus on biocompatibility, biodistribution and biodegradation

A. Kunzmann, B. Andersson, T. Thurnherr, H. Krug, A. Scheynius, B. Fadeel, *Biochim. Biophys. Acta, Gen. Subj.* **2011**, *1810*, 361.

[44] Immunological properties of engineered nanomaterials
M. A. Dobrovolskaia, S. E. McNeil, *Nat. Nanotechnol.* **2007**, *2*, 469.

[45] Endocytic mechanisms for targeted drug delivery
L. M. Bareford, P. W. Swaan, *Adv. Drug Delivery Rev.* **2007**, *59*, 748.

[46] Regulated portals of entry into the cell
S. D. Conner, S. L. Schmid, *Nature* **2003**, *422*, 37.

[47] Nanomedicine and drug delivery: a mini review
A. Z. Mirza, F. A. Siddiqui, *Int. Nano Lett.* **2014**, *4*, 94.

[48] Cancer nanomedicine: progress, challenges and opportunities
J. Shi, P. W. Kantoff, R. Wooster, O. C. Farokhzad, *Nat. Rev. Cancer* **2016**, *advance online publication*.

[49] Doxorubicin: an update on anticancer molecular action, toxicity and novel drug delivery systems
O. Tacar, P. Sriamornsak, C. R. Dass, *J. Pharm. Pharmacol.* **2013**, *65*, 157.

[50] Curcumin as "Curecumin": From kitchen to clinic
A. Goel, A. B. Kunnumakkara, B. B. Aggarwal, *Biochem. Pharmacol.* **2008**, *75*, 787.

[51] 19th WHO model list of essential medicines
W. H. Organisation, **2015**.

[52] Effect of adriamycin on DNA, RNA, and protein synthesis in cell-free systems and intact cells
R. L. Momparler, M. Karon, S. E. Siegel, F. Avila, *Cancer Res.* **1976**, *36*, 2891.

[53] Interference by doxorubicin with DNA unwinding in MCF-7 breast tumor cells
F. A. Fornari, J. K. Randolph, J. C. Yalowich, M. K. Ritke, D. A. Gewirtz, *Mol. Pharmacol.* **1994**, *45*, 649.

[54] Turmeric and curcumin: Biological actions and medical applications (Review)
C. Ishita, B. Khaushik, *Curr. Sci.* **2004**, *87*, 44.

[55] Role of curcumin in cancer therapy
S. Shishodia, M. M. Chaturvedi, B. B. Aggarwal, *Curr. Probl. Cancer* **2007**, *31*, 243.

[56] Is curcumin a chemopreventive agent for colorectal cancer?
B. Uzzan, R. Benamouzig, *Curr. Colorectal Cancer Rep.* **2016**, *12*, 35.

[57] Curcumin as an anti-cancer agent: review of the gap between basic and clinical applications
G. Bar-Sela, R. Epelbaum, M. Schaffer, *Curr. Med. Chem.* **2010**, *17*, 190.

[58] Potential anticancer properties and mechanisms of action of curcumin
N. G. Vallianou, A. Evangelopoulos, N. Schizas, C. Kazazis, *Anticancer Res.* **2015**, *652*, 645.

[59] Polymeric nanoparticle-encapsulated curcumin ("nanocurcumin"): a novel strategy for human cancer therapy
S. Bisht, G. Feldmann, S. Soni, R. Ravi, C. Karikar, A. Maitra, A. Maitra, *J. Nanobiotechnol.* **2007**, *5*, 3.

[60] Albumin–polymer conjugate nanoparticles and their interactions with prostate cancer cells in 2D and 3D culture: comparison between PMMA and PCL
Y. Jiang, H. Lu, A. Dag, G. Hart-Smith, M. H. Stenzel, *J. Mater. Chem. B* **2016**, *4*, 2017.

[61] Pharmacokinetic study of nanoparticulate curcumin: Oral formulation for enhanced bioavailability
R. Ravichandran, *J. Biomater. Nanobiotechnol.* **2013**, *04*, 291.

[62] Mathematical modeling and simulation of drug release from microspheres: Implications to drug delivery systems
D. Y. Arifin, L. Y. Lee, C.-H. Wang, *Adv. Drug Delivery Rev.* **2006**, *58*, 1274.

[63] Nanoparticles - a review
V. J. Mohanraj, Y. Chen, *Trop. J. Pharm. Res.* **2006**, *5*, 561.

[64] Co-assembled hybrids of proteins and carbon dots for intracellular protein delivery
J. Zhang, M. Zheng, Z. Xie, *J. Mater. Chem. B* **2016**, *4*, 5659.

[65] Synthesis of amphiphilic block copolypept(o)ides by bifunctional initiators: Making PeptoMicelles redox sensitive
R. Holm, K. Klinker, B. Weber, M. Barz, *Macromol. Rapid Commun.* **2015**, 2083.

[66] Mechanisms of polymer degradation and erosion
A. Göpferich, *Biomaterials* **1996**, *17*, 103.

[67] Acetalated dextran is a chemically and biologically tunable material for particulate immunotherapy
K. E. Broaders, J. A. Cohen, T. T. Beaudette, E. M. Bachelder, J. M. J. Fréchet, *Proc. Natl. Acad. Sci. U. S. A.* **2009**, *106*, 5497.

[68] Acetal-derivatized dextran: An acid-responsive biodegradable material for therapeutic applications
E. M. Bachelder, T. T. Beaudette, K. E. Broaders, J. Dashe, J. M. J. Fréchet, *J. Am. Chem. Soc.* **2008**, *130*, 10494.

[69] Acetal-modified dextran microparticles with controlled degradation kinetics and surface functionality for gene delivery in phagocytic and non-phagocytic cells
J. a. Cohen, T. T. Beaudette, J. L. Cohen, K. E. Broaders, E. M. Bachelder, J. M. J. Fréchet, *Adv. Mater.* **2010**, *22*, 3593.

[70] Chemoselective ligation in the functionalization of polysaccharide-based particles
T. T. Beaudette, J. A. Cohen, E. M. Bachelder, K. E. Broaders, J. L. Cohen, E. G. Engleman, J. M. J. Fréchet, *J. Am. Chem. Soc.* **2009**, *131*, 10360.

[71] Desolvation process and surface characterisation of protein nanoparticles
C. Weber, C. Coester, J. Kreuter, K. Langer, *Int. J. Pharm.* **2000**, *194*, 91.

[72] Functionalizing nanoparticles with biological molecules: Developing chemistries that facilitate nanotechnology
K. E. Sapsford, W. R. Algar, L. Berti, K. B. Gemmill, B. J. Casey, E. Oh, M. H. Stewart, I. L. Medintz, *Chem. Rev.* **2013**, *113*, 1904.

[73] Biopolymer-based nanoparticles for drug/gene delivery and tissue engineering
S. K. Nitta, K. Numata, *Int. J. Mol. Sci.* **2013**, *14*, 1629.

[74] Nanoparticles - a new colloidal drug delivery system
J. J. Marty, R. C. Oppenheim, P. Speiser, *Pharm. Acta Helv.* **1978**, *53*, 17.

[75] Multifunctional materials through modular protein engineering
R. L. Dimarco, S. C. Heilshorn, *Adv. Mater.* **2012**, *24*, 3923.

[76] Albumin as a drug carrier: Design of prodrugs, drug conjugates and nanoparticles
F. Kratz, *J. Controlled Release* **2008**, *132*, 171.

[77] Impact of albumin on drug delivery - New applications on the horizon
B. Elsadek, F. Kratz, *J. Controlled Release* **2012**, *157*, 4.

[78] The extraordinary ligand binding properties of human serum albumin
M. Fasano, S. Curry, E. Terreno, M. Galliano, G. Fanali, P. Narciso, S. Notari, P. Ascenzi, *IUBMB Life* **2005**, *57*, 787.

[79] Gp60 activation mediates albumin transcytosis in endothelial cells by tyrosine kinase-dependent pathway
C. Tiruppathi, W. Song, M. Bergenfeldt, P. Sass, A. B. Malik, *J. Biol. Chem.* **1997**, *272*, 25968.

[80] The effect of solution properties on the morphology of ultrafine electrospun egg albumen-PEO composite fibers
S. Wongsasulak, K. M. Kit, D. J. McClements, T. Yoovidhya, J. Weiss, *Polymer* **2007**, *48*, 448.

[81] The chemistry of lysozyme and its use as a food preservative and a pharmaceutical
V. a. Proctor, F. E. Cunningham, D. Y. C. Fung, *Crit. Rev. Food Sci. Nutr.* **1988**, *26*, 359.

[82] Lysozymes in the animal kingdom
L. Callewaert, C. W. Michiels, *J. Biosci.* **2010**, *35*, 127.

[83] Lysozyme in human body fluids
J. Hankiewicz, E. Swierczek, *Clin. Chim. Acta* **1974**, *57*, 205.

[84] The properties of lysozyme and its action on microorganisms
M. R. J. Salton, *Bacteriol. Rev.* **1957**, *21*, 82.

[85] Use of whey proteins for encapsulation and controlled delivery applications
S. Gunasekaran, S. Ko, L. Xiao, *J. Food Eng.* **2007**, *83*, 31.

[86] Preparation of sub-100-nm β-lactoglobulin (BLG) nanoparticles
S. Ko, S. Gunasekaran, *J. Microencapsul.* **2006**, *23*, 887.

[87] Antibody-drug conjugates: targeting melanoma with cisplatin encapsulated in protein-cage nanoparticles based on human ferritin
E. Falvo, E. Tremante, R. Fraioli, C. Leonetti, C. Zamparelli, A. Boffi, V. Morea, P. Ceci, P. Giacomini, *Nanoscale* **2013**, *5*, 12278.

[88] Improved doxorubicin encapsulation and pharmacokinetics of ferritin-fusion protein nanocarriers bearing proline, serine, and alanine elements
E. Falvo, E. Tremante, A. Arcovito, M. Papi, N. Elad, A. Boffi, V. Morea, G. Conti, G. Toffoli, G. Fracasso, P. Giacomini, P. Ceci, *Biomacromolecules* **2016**, *17*, 514.

[89] Albumin-based nanoparticles as potential controlled release drug delivery systems
A. O. Elzoghby, W. M. Samy, N. A. Elgindy, *J. Controlled Release* **2012**, *157*, 168.

[90] Nanogels prepared by self-assembly of oppositely charged globular proteins
S. Yu, P. Yao, M. Jiang, G. Zhang, *Biopolymers* **2006**, *83*, 148.

[91] Albumin-micelles via a one-pot technology platform for the delivery of drugs
Y. Jiang, M. Liang, D. Svejkar, G. Hart-Smith, H. Lu, W. Scarano, M. H. Stenzel, *Chem. Commun.* **2014**, *50*, 6394.

[92] PEGylated albumin-based polyion complex micelles for protein delivery
Y. Jiang, H. Lu, F. Chen, M. Callari, M. Pourgholami, D. L. Morris, M. H. Stenzel, *Biomacromolecules* **2016**, *17*, 808.

[93] Nano spray drying: a novel method for preparing protein nanoparticles for protein therapy
S. H. Lee, D. Heng, W. K. Ng, H.-K. Chan, R. B. H. Tan, *Int. J. Pharm.* **2011**, *403*, 192.

[94] Optimization of the preparation process for human serum albumin (HSA) nanoparticles
K. Langer, S. Balthasar, V. Vogel, N. Dinauer, H. Von Briesen, D. Schubert, *Int. J. Pharm.* **2003**, *257*, 169.

[95] Albumin nanoparticles with predictable size by desolvation procedure
B. von Storp, A. Engel, A. Boeker, M. Ploeger, K. Langer, *J. Microencapsul.* **2012**, *29*, 138.

[96] Protein-based nanoparticles as a drug delivery system: Chances, risks, perspectives
S. Fuchs, C. Coester, *J. Drug Delivery Sci. Technol.* **2010**, *20*, 331.

[97] pH-dependent anticancer drug release from silk nanoparticles
F. P. Seib, G. T. Jones, J. Rnjak-Kovacina, Y. Lin, D. L. Kaplan, *Adv. Healthcare Mater.* **2013**, *2*, 1606.

[98] PEGylated silk nanoparticles for anticancer drug delivery
T. Wongpinyochit, P. Uhlmann, A. J. Urquhart, F. P. Seib, *Biomacromolecules* **2015**, *16*, 3712.

[99] An engineered spider silk protein forms microspheres
U. K. Slotta, S. Rammensee, S. Gorb, T. Scheibel, *Angew. Chem. Int. Ed.* **2008**, *47*, 4592.

[100] Recombinant spider silk particles as drug delivery vehicles
A. Lammel, M. Schwab, M. Hofer, G. Winter, T. Scheibel, *Biomaterials* **2011**, *32*, 2233.

[101] Improvement of nanoprecipitation technique for preparation of gelatin nanoparticles and potential macromolecular drug loading
S. A. Khan, M. Schneider, *Macromol. Biosci.* **2013**, *13*, 455.

[102] Doxorubicin-loaded human serum albumin nanoparticles surface-modified with TNF-related apoptosis-inducing ligand and transferrin for targeting multiple tumor types
S. Bae, K. Ma, T. H. Kim, E. S. Lee, K. T. Oh, E.-S. Park, K. C. Lee, Y. S. Youn, *Biomaterials* **2012**, *33*, 1536.

[103] Glutaraldehyde: behavior in aqueous solution, reaction with proteins, and application to enzyme crosslinking
I. Migneault, C. Dartiguenave, M. J. Bertrand, K. C. Waldron, *BioTechniques* **2004**, *37*, 790.

[104] Ligand-modified human serum albumin nanoparticles for enhanced gene delivery
J. Look, N. Wilhelm, H. von Briesen, N. Noske, C. Günther, K. Langer, E. Gorjup, *Mol. Pharm.* **2015**, *12*, 3202.

[105] Albumin hydrogels formed by electrostatically triggered self-assembly and their drug delivery capability
K. Baler, R. Michael, I. Szleifer, G. A. Ameer, *Biomacromolecules* **2014**, *15*, 3625.

[106] Human serum albumin (HSA) nanoparticles stabilized with intermolecular disulfide bonds
W. Wang, Y. Huang, S. Zhao, T. Shao, Y. Cheng, *Chem. Commun.* **2013**, *49*, 2234.

[107] Preparation of surface-modified albumin nanospheres.
W. Lin, M. C. Garnett, M. C. Davies, F. Bignotti, P. Ferruti, S. S. Davis, L. Illum, *Biomaterials* **1997**, *18*, 559.

[108] Nanoparticles with dextran/chitosan shell and BSA/chitosan core - doxorubicin loading and delivery
J. Qi, P. Yao, F. He, C. Yu, C. Huang, *Int. J. Pharm.* **2010**, *393*, 176.

[109] Green preparation process, characterization and antitumor effects of doxorubicin-BSA-dextran nanoparticles
W. Deng, J. Li, P. Yao, F. He, C. Huang, *Macromol. Biosci.* **2010**, *10*, 1224.

[110] Controlled self assembly of collagen nanoparticle
M. Papi, V. Palmieri, G. Maulucci, G. Arcovito, E. Greco, G. Quintiliani, M. Fraziano, M. De Spirito, *J. Nanopart. Res.* **2011**, *13*, 6141.

[111] Nanoparticle technologies for cancer therapy
F. Alexis, E. M. Pridgen, R. Langer, O. C. Farokhzad, *Handb. Exp. Pharmacol.* **2010**, 55.

[112] Preparation, characterization and biodistribution of the lactone form of 10-hydroxycamptothecin (HCPT)-loaded bovine serum albumin (BSA) nanoparticles
L. Yang, F. Cui, D. Cun, A. Tao, K. Shi, W. Lin, *Int. J. Pharm.* **2007**, *340*, 163.

[113] Targeted brain delivery of AZT via transferrin anchored pegylated albumin nanoparticles
V. Mishra, S. Mahor, A. Rawat, P. N. Gupta, P. Dubey, K. Khatri, S. P. Vyas, *J. Drug Target.* **2006**, *14*, 45.

[114] Novel ionically crosslinked casein nanoparticles for flutamide delivery: formulation, characterization, and in vivo pharmacokinetics
A. O. Elzoghby, M. W. Helmy, W. M. Samy, N. A. Elgindy, *Int. J. Nanomed.* **2013**, *8*, 1721.

[115] Biodegradable protein nanocontainers
K. Piradashvili, M. Fichter, K. Mohr, S. Gehring, F. R. Wurm, K. Landfester, *Biomacromolecules* **2015**, *16*, 815.

[116] Nano-sized albumin-copolymer micelles for efficient doxorubicin delivery
Y. Wu, E. K. Shih, A. Ramanathan, S. Vasudevan, T. Weil, *Biointerphases* **2012**, *7*, 5.

[117] DNA-Mediated cellular delivery of functional enzymes
J. D. Brodin, A. J. Sprangers, J. R. McMillan, C. A. Mirkin, *J. Am. Chem. Soc.* **2015**, *137*, 14838.

[118] Site-specific conjugation of RAFT polymers to proteins via expressed protein ligation
Y. Xia, S. Tang, B. D. Olsen, *Chem. Commun.* **2013**, *49*, 2566.

[119] Protein-polymer hybrid nanoparticles for drug delivery
J. Ge, E. Neofytou, J. Lei, R. E. Beygui, R. N. Zare, *Small* **2012**, *8*, 3573.

[120] Protein−nolymer nanoparticles for nonviral gene delivery
J. Zhang, Y. Lei, A. Dhaliwal, Q. K. T. Ng, J. Du, M. Yan, Y. Lu, T. Segura, *Biomacromolecules* **2011**, *12*, 1006.

[121] Protein–polymer conjugates: synthetic approaches by controlled radical polymerizations and interesting applications
G. N. Grover, H. D. Maynard, *Curr. Opin. Chem. Biol.* **2010**, *14*, 818.

[122] PEGylation and its impact on the design of new protein-based medicines
C. Ginn, H. Khalili, R. Lever, S. Brocchini, *Future Med. Chem.* **2014**, *6*, 1829.

[123] Mechanical Reinforcement of Proteins with Polymer Conjugation
E. P. Debenedictis, E. Hamed, S. Keten, *ACS Nano* **2016**, *10*, 2259.

[124] Therapeutic protein–polymer conjugates: advancing beyond PEGylation
E. M. Pelegri-O'Day, E.-W. Lin, H. D. Maynard, *J. Am. Chem. Soc.* **2014**, *136*, 14323.

[125] PEG–peptide conjugates
I. W. Hamley, *Biomacromolecules* **2014**, *15*, 1543.

[126] Protein-polymer conjugates: Synthetic approaches by controlled radical polymerizations and interesting applications
G. N. Grover, H. D. Maynard, *Curr. Opin. Chem. Biol.* **2010**, *14*, 818.

[127] Well-defined protein−polymer conjugates via in situ RAFT polymerization
C. Boyer, V. Bulmus, J. Liu, T. P. Davis, M. H. Stenzel, C. Barner-Kowollik, *J. Am. Chem. Soc.* **2007**, *129*, 7145.

[128] The developing story of Sprouty and cancer
S. Masoumi-Moghaddam, A. Amini, D. L. Morris, *Cancer Metastasis Rev.* **2014**, *33*, 695.

[129] Degradable PEGylated protein conjugates utilizing RAFT polymerization
C. G. Decker, H. D. Maynard, *Eur. Polym. J.* **2015**, *65*, 305.

[130] Bioengineered protein-based nanocage for drug delivery
E. J. Lee, N. K. Lee, I. S. Kim, *Adv. Drug Delivery Rev.* **2016**.

[131] Dual pH- and temperature-responsive protein nanoparticles
N. M. Matsumoto, G. W. Buchman, L. H. Rome, H. D. Maynard, *Eur. Polym. J.* **2015**, *69*, 532.

[132] Self-assembly of temperature-responsive protein-polymer Bioconjugates
D. Moatsou, J. Li, A. Ranji, A. Pitto-Barry, I. Ntai, M. C. Jewett, R. K. O'Reilly, *Bioconjugate Chem.* **2015**, *26*, 1890.

[133] Application of polyethylene glycol-modified enzymes in biotechnological processes: organic solvent-soluble enzymes
Y. Inada, K. Takahashi, T. Yoshimoto, *TIBTECH* **1986**, *1*, 190.

[134] Targeted albumin-based nanoparticles for delivery of amphipathic drugs
R. Xu, M. Fisher, R. L. Juliano, *Bioconjugate Chem.* **2011**, *22*, 870.

[135] Transiently responsive protein-polymer conjugates via a 'grafting-from' RAFT approach for intracellular co-delivery of proteins and immune-modulators
N. Vanparijs, R. De Coen, D. Laplace, B. Louage, S. Maji, L. Lybaert, R. Hoogenboom, B. G. De Geest, *Chem. Commun.* **2015**, *51*, 13972.

[136] Protein - Polymer Nanoparticles for Nonviral Gene Delivery
J. Zhang, Y. Lei, A. Dhaliwal, Q. K. T. Ng, J. Du, M. Yan, Y. Lu, T. Segura, *Biomacromolecules* **2011**, 1006.

[137] Acid-degradable cationic dextran particles for the delivery of siRNA Therapeutics
J. L. Cohen, S. Schubert, P. R. Wich, L. Cui, J. A. Cohen, J. L. Mynar, J. M. J. Fréchet, *Bioconjugate Chem.* **2011**, *22*, 1056.

[138] Aerosolized antimicrobial agents based on degradable dextran nanoparticles loaded with silver carbene complexes
C. Ornelas-Megiatto, P. N. Shah, P. R. Wich, J. L. Cohen, J. a. Tagaev, J. a. Smolen, B. D. Wright, M. J. Panzner, W. J. Youngs, J. M. J. Frechet, C. L. Cannon, *Mol. Pharm.* **2012**, *9*, 3012.

[139] Review : Polyethylene glycol(PEG)-protein conjugates: Application to biomedical and biotechnological processes
Y. Inada, a. Matsuswma, Y. Kodera, H. Nishimura, *J. Bioact. Compat. Polym.* **1990**, *5*, 343.

[140] Ester synthesis catalyzed by polyethylene glycol-modified lipase in benzene
Y. Inada, H. Nishimura, K. Takahashi, *Biochem. Biophys. Res. Commun.* **1984**, *122*, 845.

[141] Modification of e.coli asparaginase with 2,4-bis(o-methoxypolyethylene glycol)-6-chloro-s-triazine(activated PEG2); Disappearence of binding ability towards anti-serum and tetention of enzymatic activity
A. Matsushima, H. Nishimura, Y. Ashihara, Y. Yokota, Y. Inada, *Chem. Lett.* **1980**, *9*, 773.

[142] Modification of batroxobin with activated polyethylene glycol: Reduction of binding ability towards anti-batroxobin antibody and retention of defibrinogenation activity in circulation of preimmunized dogs
H. Nishimura, K. Takahashi, K. Sakurai, K. Fujinuma, Y. Imamura, M. Ooba, Y. Inada, *Life Sci.* **1983**, *33*, 1467.

[143] Selective synthesis of 2,4-bis(O-methoxypolyethylene glycol)-6-chloro-s-triazine as a protein modifier
K. Ono, Y. Kai, H. Maeda, F. Samizo, K. Sakurai, H. Nishimura, Y. Inada, *J. Biomater. Sci. Polym. Ed.* **1991**, *2*, 61.

[144] Tolerogenic capacity of poly(ethylene glycol) (PEG)-modified ovalbumins in relation to their immunoreactivity towards anti-ovalbumin antibody
T. Saito, H. Nishimura, T. Sekine, T. Urushibara, Y. Kodera, M. Hiroto, A. Matsushima, Y. Inada, *J. Biomater. Sci. Polym. Ed.* **1997**, *8*, 311.

[145] Alteration of immunological properties of bovine serum albumin by covalent attachment of polyethylene Glycol
A. Abuchowski, T. van Es, N. C. Palczuk, F. F. Davis, *J. Biol. Chem.* **1977**, *252*, 3578.

[146] Alteration of the circulating life and antigenic properties of bovine adenosine deaminase in mice by attachment of polyethylene glycol
S. Davis, A. Abuchowski, Y. K. Park, F. F. Davis, *Clin. Exp. Immunol.* **1981**, *46*, 649.

[147] Nanoparticle assembly of surface-modified proteins
M. Fach, L. Radi, P. R. Wich, *J. Am. Chem. Soc.* **2016**, *138*, 14820.

[148] Cyanuric acid and cyanuric chloride
K. L. H. Uthmacher, D. Ag, F. Republic, D. I. M. Ost, *Ullmann's Encyclopedia of Industrial Chemistry* **2012**, *11*, 1.

[149] Native PAGE eliminates the problem of PEG-SDS interaction in SDS-PAGE and provides an alternative to HPLC in characterization of protein PEGylation
C. Zheng, G. Ma, Z. Su, *Electrophoresis* **2007**, *28*, 2801.

[150] Biochemistry
J. M. Berg, J. L. Tymoczko, L. Stryer, **2002**.

[151] Using circular dichroism spectra to estimate protein secondary structure.
N. J. Greenfield, *Nature: Protocols* **2006**, *1*, 2876.

[152] Estimation of protein secondary structure from circular dichroism spectra: comparison of CONTIN, SELCON, and CDSSTR methods with an expanded reference set
N. Sreerama, R. W. Woody, *Anal. Biochem.* **2000**, *287*, 252.

[153] The ultraviolet circular dichroism of polypeptides
G. Holzwarth, P. Doty, *J. Am. Chem. Soc.* **1965**, *87*, 218.

[154] Computed circular dichroism spectra for the evaluation of protein conformation
N. Greenfield, G. D. Fasman, *Biochemistry* **1969**, *8*, 4108.

[155] Circular dichroic analysis of denatured proteins: inclusion of denatured proteins in the reference set
S. Y. Venyaminov, I. A. Baikalov, Z. M. Shen, C. S. Wu, J. T. Yang, *Anal. Biochem.* **1993**, *214*, 17.

[156] DICHROWEB, an online server for protein secondary structure analyses from circular dichroism spectroscopic data
L. Whitmore, B. A. Wallace, *Nucleic Acids Res.* **2004**, *32*, W668.

[157] Protein secondary structure analyses from circular dichroism spectroscopy: methods and reference databases.
L. Whitmore, B. A. Wallace, *Biopolymers* **2008**, *89*, 392.

[158] The spectrophotometric determination of amine, amino acid and peptide with 2, 4, 6-trinitrobenzene 1-sulfonic acid
K. Satake, T. Okuyama, *J. Biochem.* **1960**, *47*, 654.

[159] Optimization of PEGylation conditions for BSA nanoparticles using response surface methodology
H. Kouchakzadeh, S. A. Shojaosadati, A. Maghsoudi, E. Vasheghani Farahani, *AAPS PharmSciTech* **2010**, *11*, 1206.

[160] Surface modification of protein nanocontainers and their self-directing character in polymer blends
M. Sengonul, J. Ruzicka, A. B. Attygalle, M. Libera, *Polymer* **2007**, *48*, 3632.

[161] Structure of hen egg-white lysozyme. A three-dimensional Fourier synthesis at 2 Angstrom resolution
C. C. Blake, D. F. Koenig, G. A. Mair, A. C. North, D. C. Phillips, V. R. Sarma, *Nature* **1965**, *206*, 757.

[162] Polyethylene glycol density and length affects nanoparticle uptake by cancer cells
D. B. Chithrani, *J. Nanomed. Res.* **2014**, *1*, 1.

[163] Sensing surface PEGylation with microcantilevers
N. Backmann, N. Kappeler, T. Braun, F. Huber, H.-P. Lang, C. Gerber, R. Y. H. Lim, *Beilstein J. Nanotechnol.* **2010**, *1*, 3.

[164] Synthesis and characterization of hydrophobic ferritin proteins
K. K. W. Wong, H. Cölfen, N. T. Whilton, T. Douglas, S. Mann, *J. Inorg. Biochem.* **1999**, *76*, 187.

[165] Hydrophobic proteins: synthesis and characterisation of organic-soluble alkylated ferritins
K. K. W. Wong, N. T. Whilton, T. Douglas, S. Mann, H. Cölfen, *Chem. Commun.* **1998**, 1621.

[166] Nanoparticles produced by emulsifier-free emulsion
S. H. I. C. Yang, H. A. I. X. Ge, Y. Hu, X. I. Q. U. N. Jiang, C. Z. Yang, *Polymer* **1999**, 517.

[167] PLGA Nanoparticles formed by single- or double-emulsion with vitamin E-TPGS
R. L. McCall, R. W. Sirianni, *J. Visualized Exp.* **2013**, *82*, 51015.

[168] Nanoemulsions: formation, properties and applications
A. Gupta, H. B. Eral, T. A. Hatton, P. S. Doyle, *Soft Matter* **2016**, *12*, 2826.

[169] Increased antitumor activity, intratumor paclitaxel concentrations, and endothelial cell transport of cremophor-free, albumin-bound paclitaxel, ABI-007, compared with cremophor-based paclitaxel
N. Desai, V. Trieu, Z. Yao, L. Louie, S. Ci, A. Yang, C. Tao, T. De, B. Beals, D. Dykes, P. Noker, R. Yao, E. Labao, M. Hawkins, P. Soon-Shiong, *Clin. Cancer Res.* **2006**, *12*, 1317.

[170] Critical evaluation of nanoparticle tracking analysis (NTA) by NanoSight for the measurement of nanoparticles and protein aggregates
V. Filipe, A. Hawe, W. Jiskoot, *Pharm. Res.* **2010**, *27*, 796.

[171] Characterization of Turbid Colloidal Suspensions Using Light Scattering Techniques Combined with Cross-Correlation Methods
C. Urban, P. Schurtenberger, *J. Colloid Interface Sci.* **1998**, *207*, 150.

[172] Lysosomal pH and analysis of the counter ion pathways that support acidification
J. E. DiCiccio, B. E. Steinberg, *J. Gen. Physiol.* **2011**, *137*, 385.

[173] Bioconjugate Techniques
G. T. Hermansson, **2013**.

[174] Nanopartikelherstellung basierend auf lipophiler Oberflächenmodifikation von Proteinen
L. Mayer, Bachelor Thesis, Supervisor: M. Fach, P. R. Wich, Johannes Gutenberg-Universität Mainz, **2015**.

[175] Fluoreszenzmarkierung von Proteinen zur Herstellung von Nanopartikeln
C. Ade, Bachelor Thesis, Supervisor: M. Fach, P. R. Wich, Johannes Gutenberg-Universität Mainz, **2016**.

[176] Curcumin-mediated decrease in the expression of nucleolar organizer regions in cervical cancer (HeLa) cells
A. Lewinska, J. Adamczyk, J. Pajak, S. Stoklosa, B. Kubis, P. Pastuszek, E. Slota, M. Wnuk, *Mutation Research - Genetic Toxicology and Environmental Mutagenesis* **2014**, *771*, 43.

[177] Hydrogel-siRNA for cancer therapy
S. Ramakrishnan, *Cancer Biol. Ther.* **2011**, *11*, 849.

[178] Protein-basierte Nanopartikel für den Transport von hydrophilen Wirkstoffen
E. Steiert, Master Thesis, Supervisor: P. R. Wich, Johannes Gutenberg-Universität Mainz, **2016**.

[179] Cleavage of structural proteins during the assembly of the head of bacteriophage T4
U. Laemmli, *Nature* **1970**, *227*, 680.

[180] Kinetic analysis of barley chitinase.
T. Hollis, Y. Honda, T. Fukamizo, E. Marcotte, P. J. Day, J. D. Robertus, *Arch. Biochem. Biophys.* **1997**, *344*, 335.

CURRICULUM VITAE

not available in electronical version

not available in electronical version

LIST OF PUBLICATIONS

not available in electronical version